Impacts of Changes in Winter Precipitation on C Stocks and Fluxes in Arctic Tussock Tundra

BY

MARIA ELENA BLANC BETES
B.A., University of Barcelona, Barcelona, Spain, 2003
M.S., Catalan Institute of Technology, Barcelona, Spain, 2004

THESIS

Submitted as partial fulfillment of the requirements
for the degree of Doctor of Philosophy in Biological Sciences
in the Graduate College of the
University of Illinois at Chicago, 2017

Chicago, Illinois

Defense Committee:

Dr. Miquel A. Gonzalez-Meler, Chair and Advisor
Dr. Jeffrey M. Welker, Univ. Of Alaska, Anchorage
Dr. Neil C. Sturchio, Univ. of Delaware
Dr. Jean E. Bogner, Earth and Environmental Sciences
Dr. Emily S. Minor, Biological Sciences

ACKNOWLEDGEMENTS

I would like to thank my thesis advisor, Prof. Miquel Gonzalez-Meler, for the opportunity of joining his lab, giving me the freedom and trust to follow my interests wherever they would take me, and his continuous support throughout my endeavors. I would also like to express my sincere gratitude to my committee members. Thank you, Jeffrey Welker, Neil Sturchio, Jean Bogner and Emily Minor for your kind guidance, motivation and enthusiasm. I firmly believe that the critical thinking and the "out-of-the-box" perspective you have encouraged over these years will shape the way I approach science in the future.

My lab mates and friends at UIC, thank you for so many scientific discussions, and more importantly for being a constant source of encouragement and companionship. Special thanks to Lina Shea for that first push that introduced me into Arctic research against all odds, and for selflessly offering support when needed. I would also like to extend my gratitude to Niccole Van Hoey, Benjamin Thurnhoffer, Linnea Heraty, Jessica Rucks, Andy Anderson-Smith and Matthew Rogers, whose field and technical assistance have been crucial for the completion of this thesis.

This research would not have been possible without the generous financial support from the Department of Energy (Terrestrial Ecosystem Science Program), the University of Illinois at Chicago (Elmer Hadley Research Award), NSF AON grants, the International Tundra Experiment, and the International Polar Year. Support from the Toolik Lake Field Station staff is greatly appreciated, as it is the logistical support of CH2MHill Polar Services. This research has been presented in several international conferences with the support from the College of Liberal Arts and Sciences, the Department of Biological Sciences, the Graduate College and the

Graduate Student Council at the University of Illinois at Chicago.

Finally, my deep and sincere gratitude to my family for their unwavering love and support. To my extended family, my friends, for keeping me sane over the years. To my parents, Julio and Santina, for encouraging the endless curiosity and appreciation of life that made me who I am. To my sister, Maria, for always walking by my side, without condition, proving true the relativity of distance. And to my partner, Nuri, for sharing every bit of the journey, for the unending scientific debates over breakfast, for your amazing ability to turn bad into good and good into better, and for making sure that I always feel at home.

EBB

CONTRIBUTION OF AUTHORS

Chapter 1 is a review of the current state of knowledge regarding climate/C-cycle feedbacks from the Arctic region under current and future climate scenarios, and places my research in the context of recent literature.

Chapter 2 is an unpublished manuscript investigating the rate at which permafrost C will become available for decomposition and will be released relative to ecosystem C inputs under future precipitation scenarios.

Chapter 3 is an unpublished manuscript investigating the long-term impacts of altered winter precipitation patterns on the magnitude, form and direction of climate/C-cycle feedbacks from Arctic tundra.

Chapter 4 is a published manuscript for which I was first author. The research contained therein investigated the regulation mechanisms of winter precipitation on methane dynamics in Arctic tundra. In this thesis, this work is reprinted in its entirety with permission from: **Blanc-Betes, E.**, Welker, J. M., Sturchio, N. C., Chanton, J. P. and Gonzalez-Meler, M. A. (2016) Winter precipitation and snow accumulation drive the methane sink or source strength of Arctic tussock tundra. *Glob Change Biol*, **22**, 2818–2833. doi:10.1111/gcb.13242. (*See* Appendix A, Copyright clearance statement from publisher). **EB-B** conceived and designed the study, collected, processed and analyzed data, and wrote the manuscript. **JMW** designed the study and wrote the manuscript. **NCS** wrote the manuscript. **JPC** wrote the manuscript. **MAG-M** designed the study and wrote the manuscript.

Chapters 5 is an unpublished opinion that elaborates on findings from Chapters 2, 3 and 4 to reconcile discrepancies among existing literature and reconsiders current line of thought on

the mechanisms driving the Arctic tundra C budget and radiative forcing on the climate system.

Chapter 6 synthesizes my research, concisely addresses the significance of the findings presented herein, and point to research directions that would improve quantitative predictions of climate/C-cycle feedbacks from the Arctic region.

TABLE OF CONTENTS

TABLE OF CONTENTS (continued)

TABLE OF CONTENTS (continued)

TABLE OF CONTENTS (continued)

LIST OF TABLES

LIST OF TABLES (continued)

LIST OF TABLES (continued)

LIST OF FIGURES

LIST OF FIGURES (continued)

LIST OF FIGURES (continued)

LIST OF FIGURES (continued)

LIST OF FIGURES (continued)

SUMMARY

Projected increases in winter precipitation strongly affect carbon (C) cycling in Arctic tundra systems whose large stocks of soil organic carbon (SOC) make them critical to future climate trends. Warming and thawing of permafrost under deeper winter snow represents a potential positive feedback on climate warming, as long-term preserved SOC becomes available for decomposition. This response may be either mitigated or enhanced by associated increases in nutrient availability and changes in plant community structure and productivity. The derived climate/C-cycle forcing feedbacks remain largely unresolved due to uncertainties in the strength, form (CO_2 and CH_4) and timing of C fluxes under future precipitation scenarios.

Critical to the fate of Arctic tundra SOC pools is the rate at which permafrost C will become vulnerable and released relative to ecosystem C inputs. We investigated both biological and physical impacts of short- (2yr) and long-term (14yr and 18yr) snow additions on permafrost dynamics and SOC pools in Alaskan Arctic tundra. Enhanced winter snow accelerated soil warming and permafrost thawing above climate-driven trends in the area of study, and increased the vulnerable SOC pool over time. As a result, deeper winter snow led to a fast depletion of the SOC pool at an annual scale and to a gradual recovery of the SOC pool at a decadal time scales, suggesting the potential of Arctic tundra to act as an additional C sink under future precipitation scenarios. We note that neglecting to incorporate soil physical processes and time dependent non-linearities may result in strong biases in both empirical and model observations of climate-driven permafrost degradation and its impacts on the Arctic tundra C budget.

To evaluate the structural and functional changes driving long-term responses of the Arctic tundra C budget and derived forcing on climate to changes in precipitation, we

investigated how 18 years of experimental snow depth increases and decreases affect the magnitude, direction and global warming potential (GWP) of ecosystem C fluxes. Deeper winter snow reduced the C source strength but increased the GWP of Arctic tundra over the growing season. Our results further indicate that the enhanced Arctic tundra C sink strength resulted mainly from impacts on the predominant microbial function and activity rather than from enhanced plant productivity. Moreover, our results suggest certain resistance of net plant productivity to long-term changes in winter precipitation, and that this resistance responded to metabolic adjustments at the canopy level mediated by shifts in plant community structure rather than by the acclimation of physiological processes. Importantly, by stimulating CH_4 emissions, deeper snow increased the GWP of Arctic tundra C emissions, therefore representing a potentially strong positive feedback on climate change despite reducing ecosystem C losses. These results indicate a key role of the CH_4 metabolism in driving C fluxes and GWP of Arctic tundra under future precipitation scenarios.

Given the potential of Arctic CH_4 emissions to act as a significant climate forcing feedback under future precipitation scenarios, we measured ecosystem CH_4 fluxes, and soil CH_4 and CO_2 concentration and ^{13}C composition to investigate the predominant metabolic pathways and transport mechanisms driving the response of Arctic tundra CH_4 fluxes after 18 years of experimental snow depth increases and decreases. Our results reveal a synergistic effect of soil moisture and temperature on net ecosystem CH_4 production and oxidation under near water-saturated (more anoxic) and drier (more oxic) soil conditions respectively. Therefore, changes in winter precipitation, by influencing both soil parameters may impact CH_4 fluxes beyond what may be predicted by Arctic warming alone. Moreover, changes in plant community structure

associated to persistent changes in snow accumulation critically defined the predominant CH_4 transport mechanism, largely contributing to the ecosystem CH_4 sink or source strength.

Taken together, our results provide empirical support to a growing body of literature that suggest that future climate/C-cycle feedbacks from Arctic regions may depend more strongly on future precipitation scenarios than currently considered in Earth system models. We suggest that an improved representation of the sensitivity of both physical and biotic processes to changes in precipitation at different time-scales will probably help reconcile empirical- and model-based discrepancies and reduce uncertainties on climate-forcing feedbacks from Arctic systems.

1. INTRODUCTION

The rate of accumulation of greenhouse gases (GHGs) in the atmosphere has been increasing since the industrial revolution reaching 2 ppm CO_2 yr^{-1} and 6 ppb CH_4 yr^{-1} over the last decade. Together, atmospheric CO_2 and CH_4 represent about 90% of current Global Warming Potential (i.e. GWP; CO_2 equivalents) (Nisbet *et al.*, 2014). Under business as usual scenario (RCP8.5), global temperatures are projected to increase by 4.5^{o}C by the end of this century (Stocker *et al.*, 2013, 2014). To lessen the effects of future climate change, attempts have been made to stabilize atmospheric GHGs concentrations at levels that will limit warming to 2^{o}C above pre-industrial temperatures by 2100 (UNEP, 2013). At present, photosynthetic CO_2 uptake of terrestrial ecosystems exceeds respiratory carbon (C) losses, mitigating anthropogenic C emissions by up to 30% (Le Quéré *et al.*, 2015). Projected climate warming and associated changes in precipitation patterns may critically affect the C sink strength of terrestrial ecosystems, exerting a strong control on future atmospheric C concentrations and climate (Carvalhais *et al.*, 2014; Le Quéré *et al.*, 2015). Generating realistic GHGs emission targets requires the understanding and reliable quantification of the positive and negative climate/C-cycle feedbacks from terrestrial systems.

The permafrost region (area underlined by permanently frozen soils) has been, on average, a sink of C throughout the Holocene (Hicks Pries *et al.*, 2011; Walter Anthony *et al.*, 2014), as limited decay of organic matter within pervasive cold and wet soils allowed for the long-term protection of highly labile soil organic carbon (SOC) (Uhlířová *et al.*, 2007; Waldrop *et al.*, 2010). In recent decades, the permafrost region has removed between 0.5 and 0.8 PgC yr^{-1} from the atmosphere, which represents 25% to 40% of the global net terrestrial CO_2 sink and about 10% to 15% of total anthropogenic C emissions (McGuire *et al.*, 2009; Hayes *et al.*, 2011;

Le Quéré *et al.*, 2015). As a result, with just 15% of the global area cover, the permafrost region contains up to 50% of the global SOC pool, twice as much C as the global atmosphere (Tarnocai *et al.*, 2009; Hugelius *et al.*, 2014). Any environmental change that affects the stability of even a fraction of this large C pool may lead to large emissions of CO_2 and CH_4, thereby amplifying climate change (DeConto *et al.*, 2012; Harden *et al.*, 2012; Elberling *et al.*, 2013; Jorgenson *et al.*, 2013). The latest simulations indicate that the permafrost region will become a C source to the atmosphere by the end of the century regardless of the emissions scenario considered (Abbott *et al.*, 2016). The derived climate/C-cycle feedback is projected to increase global mean temperatures by 10–40% above expected warming trends (Crichton *et al.*, 2016), and risks overshooting the 2^{o}C warming target.

Over the last three decades, the Arctic region has warmed 0.06^{o}C yr^{-1}, twice as fast as the global average (Serreze & Barry, 2011; Cohen *et al.*, 2014), and has experienced substantial increases in precipitation, particularly from October to February in the form of snow (Callaghan *et al.*, 2011; Cohen *et al.*, 2012; Mudryk *et al.*, 2014). There is unambiguous evidence of a system-wide response of the Arctic region to recent climate change. The rate of permafrost degradation and thermokarst development has abruptly increased since the 1970s (Romanovsky *et al.*, 2010; Smith *et al.*, 2010), principally affecting the Alaskan tundra that has lost 10–30% of its permafrost area (Jorgenson *et al.*, 2001, 2006; Åkerman & Johansson, 2008). Consistently, process-based models estimate that the seasonally-thawed soil layer (i.e. active layer) has deepened at a rate of 0.2 to 0.6 cm yr^{-1} over the circumpolar region (Hayes *et al.*, 2014; Yi *et al.*, 2015), exposing a total of 10–15 PgC of thawed SOC to decomposition over this same period (Hayes *et al.*, 2014). The consequences are already noticeable in a weakening of the Arctic tundra CO_2 sink strength (Hayes *et al.*, 2011). Both process-based models and field data show a

recent shift from a historical C sink to a C source despite evidence of increased growing season CO_2 uptake over much of the Alaskan Arctic tussock tundra (Hayes *et al.*, 2011; Myers-Smith *et al.*, 2011; Belshe *et al.*, 2013). While 50% of recent permafrost warming and thawing in northern Alaska is linked to a rise in atmospheric temperatures, the other 50% is attributable to increased snowfall and accumulation (Stieglitz *et al.*, 2003; Osterkamp, 2007).

Climate models consistently predict an amplified warming of the Arctic region over the coming decades, with winter temperatures leading annual warming trends (Christensen *et al.*, 2013). Given the strong sensitivity of Arctic precipitation to climate warming (Räisänen, 2008; Rawlins *et al.*, 2010; Bintanja & Selten, 2014), the Arctic region is expected to experience 25–50% increases in precipitation during this century, particularly over winter and fall in the form of snow (Kattsov *et al.*, 2005, 2007; Räisänen, 2008; Collins *et al.*, 2013; Zhang *et al.*, 2013).

Accelerated C losses under future climate scenarios represent a potentially large but highly uncertain feedback to global climate change (Fisher *et al.*, 2014; Schaefer *et al.*, 2014; Crichton *et al.*, 2016) (Table I). About 50% of current model uncertainty on climate/C-cycle feedbacks from Arctic regions corresponds to the emissions scenario considered (Burke *et al.*, 2012); however, even assuming the same scenario predictions of permafrost degradation, the magnitude and global warming potential (i.e. GWP, CO_2-equivalents) of associated C emissions vary widely among models (Table I). Much of the observed spread results from differences in how snow processes and associated effects on soil thermal and hydrological regimes are represented in models (Koven *et al.*, 2012; Schaefer *et al.*, 2014).

TABLE I

Model predictions of permafrost degradation and projections of associated cumulative emissions in the northern hemisphere by 2100 arranged per emission scenario. Adapted from Schaefer *et al*. (2014).

Scenario	Loss of permafrost area (%)	Permafrost C emissions	
		(Gt C)	(CO_2 – Equiv.)[1]
A1B	26 – 85[a]	104[d]	130
A2	30 – 90[b]	37 – 347[e]	46 – 435
RCP 8.5	32 – 65[c]	50 – 218[f]	62 – 273

[1] Permafrost C emissions in CO_2 equivalent calculated assuming CH_4 represents 2.3% of total carbon emissions and has a global warming potential of 33 (Shindell *et al.*, 2009; Schuur *et al.*, 2013).

[a] Euskirchen et al., 2006; Schaefer et al., 2011; Marchenko et al., 2008; Saito et al., 2007; Lawrence et al., 2008.

[b] Koven et al., 2011; Lawrence et al., 2012, Eliseev et al., 2009; Lawrence and Slater, 2005.

[c] Koven et al., 2013; Schuur et al., 2013; McDougall et al., 2012; Schneider von Deimling et al., 2012; Burke et al., 2012.

[d] Schaefer et al., 2011

[e] Zhuang et al., 2006; Koven et al., 2011; Schuur et al., 2009; Raupach and Canadell, 2008.

[f] Burke et al., 2013; Schneider von Deimling et al., 2012; Burke et al., 2012; Schuur et al., 2013; MacDougall et al., 2012; Harden et al., 2012.

Variations in snow accumulation explain as much as 50% to 100% of total soil temperature variability, thereby exerting a strong control on Arctic C balance (McGuire *et al.*, 2000; Lawrence & Slater, 2010). The depth of the snow pack defines ground temperatures over the snow-covered season, as the insulating effect of snow allow for soil temperatures to remain several degrees warmer than atmospheric temperatures (Zhang, 2005; Morgner *et al.*, 2010). Given the high temperature sensitivity of heterotrophic respiration (Mikan *et al.*, 2002; Dorrepaal *et al.*, 2009), soil warming under deeper snow allows for greater SOC mineralization rates during the cold season (Gouttevin *et al.*, 2012; Webb *et al.*, 2016), which may account for up to 70% of annual C emissions from Arctic systems (Welker *et al.*, 2000).

Beyond the direct impacts of soil warming on the Arctic C balance during the snow-covered season, deeper winter snow may result in legacies over the snow-free season with significant implications on growing season C dynamics, annual C budgets, and climate/C-cycle feedbacks from Arctic systems (Fig. 1). Snow-induced increases in soil wetness results in greater soil latent heat and thermal conductivity upon snow-melt, promoting soil warming and thawing over the snow-free season (Qian *et al.*, 2011; Jorgenson *et al.*, 2013; Subin *et al.*, 2013).

Warmer and deeper active layer may enhance SOC availability and decomposition, promoting CO_2 losses from Arctic regions to the atmosphere (Trucco *et al.*, 2012; Elberling *et al.*, 2013; Xue *et al.*, 2016) (Fig. 1). Alternatively, greater mineralization rates may promote nutrient availability (Schimel *et al.*, 2004; Semenchuk *et al.*, 2015; Salmon *et al.*, 2016), which in turn could stimulate plant productivity and shrub expansion, mitigating or offsetting ecosystem CO_2 losses (Bret-Harte *et al.*, 2002; Elmendorf *et al.*, 2012b; DeMarco *et al.*, 2014) (Fig. 1).

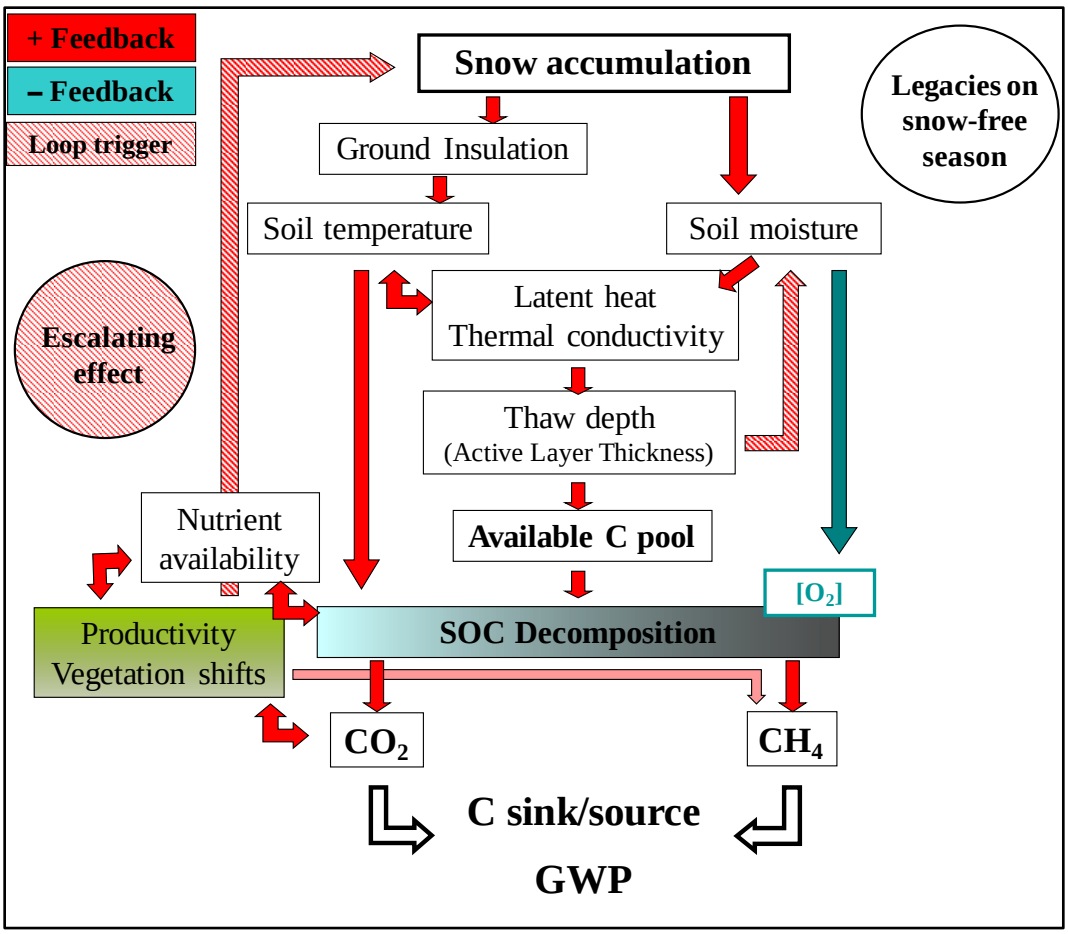

Figure 1: Diagram depicting the physical and biological impacts of snow accumulation over the snow-free period.

In addition, snow- and thaw-induced increases in soil wetness may decrease oxygen availability and promote anaerobic decomposition (i.e. methanogenesis) above the aerobic decomposition of SOC (Fig. 1). The slower metabolism of methanogenesis could contribute to reduce ecosystem C losses but strengthen the positive forcing on climate owing to the greater GWP of CH_4 emissions (Shindell *et al.*, 2009; Myhre *et al.*, 2013). Arctic CH_4 emissions under deeper winter snow could be further fueled by greater substrate availability (e.g. newly available SOC and/or enhanced ecosystem productivity), and by facilitated emissions through plant-

mediated transport aided by the expansion of tall graminoids accompanying the initial stages of thermokarst development (Chowdhury & Dick, 2013; Johansson *et al.*, 2013; Hodgkins *et al.*, 2014; McCalley *et al.*, 2014) (Fig. 1).

Notably, these processes are likely to be amplified over time, setting the system into a continuously degrading state (Osterkamp & Romanovsky, 1999) bolstered primarily by (i) thaw-induced increases in soil wetness, which in turn promotes further permafrost warming and thawing (Fan *et al.*, 2011; Subin *et al.*, 2013), and by (ii) favoring the expansion of shrubs that favors snow trapping and accumulation (Sturm *et al.*, 2001) (Fig. 1).

Therefore, the potential magnitude of climate/C-cycle feedbacks derived from altered snow fall and accumulation patterns suggests that projected changes in winter precipitation may be as relevant as climate warming in driving climate/C-cycle radiative forcing from Arctic regions (Carvalhais *et al.*, 2014; Yi *et al.*, 2015), with its effects on the Arctic tundra C balance continuing for decades or even centuries after warming stops (Schaefer *et al.*, 2011).

Our ability to accurately predict climate forcing feedbacks from Arctic systems is currently limited by the stepwise addition of uncertainties in three major unresolved questions: (i) how much and how fast will the Arctic SOC pool become vulnerable and change in response to changes in climate?; (ii) what is the magnitude, form and direction of ecosystem C fluxes and derived climate forcing feedbacks?; and (iii) which are the mechanisms underlying such changes? (Burke *et al.*, 2012; Schuur *et al.*, 2013, 2015; Schaefer *et al.*, 2014; McGuire *et al.*, 2016). To address these overarching questions, we investigated the impacts of altered winter precipitation patterns on Arctic tundra C budget and fluxes. The moist acidic tussock tundra represents 40% of the Alaskan tundra – 20% of the Arctic tundra, globally – and contains 15% of the global SOC pool (Hugelius *et al.*, 2014; Forbes, 2015). This research was performed in moist

acidic tundra near Toolik Lake in the northern foothills of the Brooks Range, Alaska (Fig. 2) (Walker *et al.*, 1999).

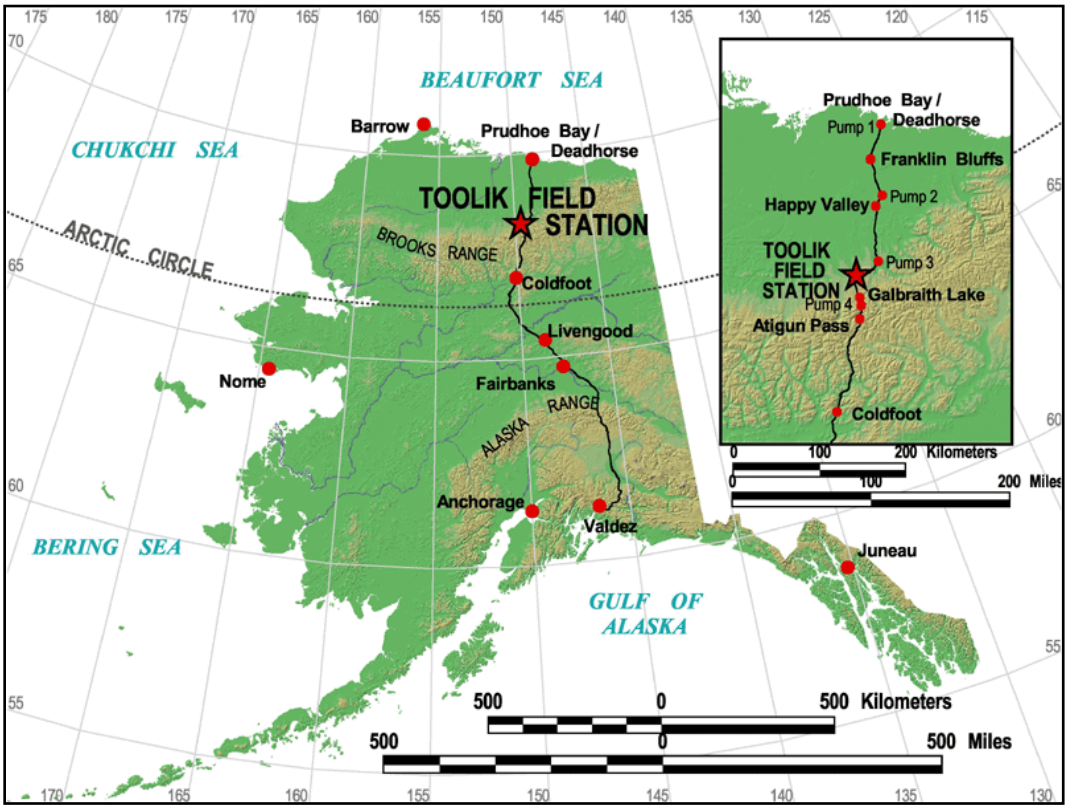

Figure 2: Location map of the Toolik Field Station (68°38'N, 149°38'W). The inset shows the study area in relation to the northern coast of Alaska (Courtesy of the GIS & Remote Sensing Service Center, Toolik Field Station).

Specifically, we used a long-term snow manipulation experiment to investigate (Fig. 3):

(a) Short- and long-term impacts of increased winter precipitation on the Arctic tundra SOC budget (Chapter 2; Winter snow drives transient modulations in Arctic tundra soil carbon budget).

(b) Impacts of snow accumulation on C fluxes and climate/C-cycle forcing from Arctic tundra (Chapter 3; Winter precipitation drives ecosystem C fluxes (CO_2 and CH_4) and climate/C-cycle feedbacks from Arctic tundra).

(c) Regulation mechanisms of winter precipitation on CH_4 dynamics in Arctic tundra (Chapter 4; Winter precipitation and snow accumulation drive the CH_4 sink or source strength of Arctic tussock tundra).

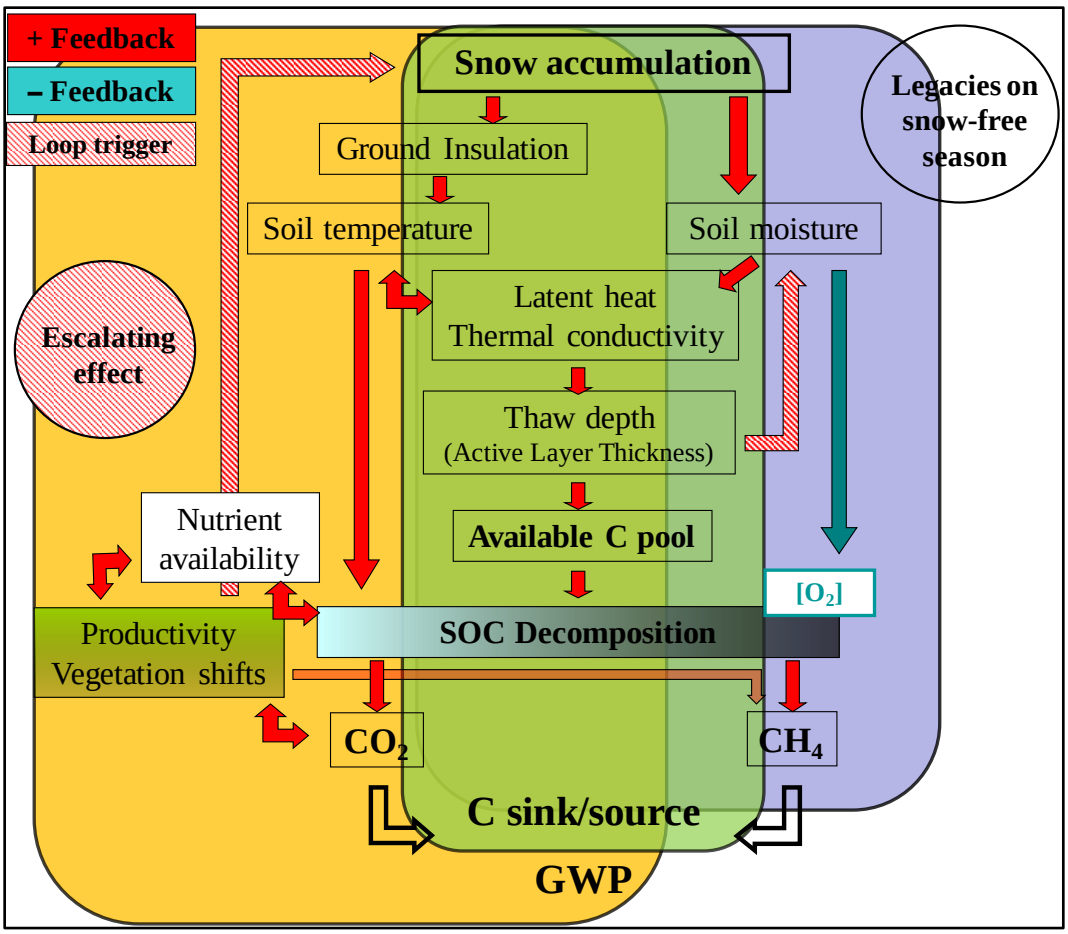

Figure 3: Schematic of the three major questions that conform this research: (a) Short- and long-term impacts of increased winter precipitation on the Arctic tundra SOC budget (*in green*, Chapter 2); (b) Impacts of snow accumulation on C fluxes and climate/C-cycle forcing from Arctic tundra (*in orange*, Chapter 3); and (c) Regulation mechanisms of winter precipitation on CH_4 dynamics in Arctic tundra (*in purple*, Chapter 4).

We further capitalized on this system-wide, multi-year and multi-level approach to reconcile discrepancies among studies and reconsider the mechanisms driving the Arctic tundra C budget and radiative forcing on the climate system (Chapter 5; Discussion: Reshaping our understanding of Arctic tundra carbon dynamics). Finally, we concisely address the significance of the findings presented herein, and point to research directions that would improve quantitative predictions of climate/C-cycle feedbacks from the Arctic region (Chapter 6; Broader impacts).

1.1 Cited Literature

Abbott BW, Jones JB, Schuur EAG et al. (2016) Biomass offsets little or none of permafrost carbon release from soils, streams, and wildfire: an expert assessment. *Environmental Research Letters*, **11**, 034014.

Åkerman HJ, Johansson M (2008) Thawing permafrost and thicker active layers in sub-arctic Sweden. *Permafrost and Periglacial Processes*, **19**, 279–292.

Belshe EF, Schuur E a. G, Bolker BM (2013) Tundra ecosystems observed to be CO_2 sources due to differential amplification of the carbon cycle. *Ecology Letters*, **16**, 1307–1315.

Bintanja R, Selten FM (2014) Future increases in Arctic precipitation linked to local evaporation and sea-ice retreat. *Nature*, **509**, 479–482.

Bret-Harte MS, Shaver GR, Chapin FS (2002) Primary and secondary stem growth in Arctic shrubs: implications for community response to environmental change. *Journal of Ecology*, **90**, 251–267.

Burke EJ, Hartley IP, Jones CD (2012) Uncertainties in the global temperature change caused by carbon release from permafrost thawing. *The Cryosphere*, **6**, 1063–1076.

Callaghan TV, Johansson M, Brown RD et al. (2011) The Changing Face of Arctic Snow Cover: A Synthesis of Observed and Projected Changes. *AMBIO*, **40**, 17–31.

Carvalhais N, Forkel M, Khomik M et al. (2014) Global covariation of carbon turnover times with climate in terrestrial ecosystems. *Nature*, **514**, 213–217.

Chowdhury TR, Dick RP (2013) Ecology of aerobic methanotrophs in controlling methane fluxes from wetlands. *Applied Soil Ecology*, **65**, 8–22.

Christensen JH, Kanikicharla KK, Marshall GJ, Turner J (2013) Climate phenomena and their relevance for future regional climate change. In: *Climate Change 2013: The physical science basis. Contribution of Working Group I to the fifth Assessment of the Intergovernmental Panel on Climate Change* (eds Stocker TF, Qin D, Plattner G-K, Tignor MMB, Allen SK, Boschung J, Nauels A, Xia Y, Bex V, Midgley PM), pp. 1217–1308. Cambridge University Press, Cambridge.

Cohen JL, Furtado JC, Barlow MA, Alexeev VA, Cherry JE (2012) Arctic warming, increasing snow cover and widespread boreal winter cooling. *Environmental Research Letters*, **7**, 014007.

Cohen J, Screen JA, Furtado JC et al. (2014) Recent Arctic amplification and extreme mid-latitude weather. *Nature Geoscience*, **7**, 627–637.

Collins M, Knutti R, Arblaster J et al. (2013) Climate change 2013: the physical science basis. Contribution of Working Group I to the Fifth Assessment Report of the Intergovernmental Panel on Climate Change. *Long-term Clim. Chang. Proj. Commitments Irreversibility, Cambridge Univ. Press. Cambridge, UK, New York*.

Crichton KA, Bouttes N, Roche DM, Chappellaz J, Krinner G (2016) Permafrost carbon as a missing link to explain CO_2 changes during the last deglaciation. *Nature Geoscience*, **9**, 683–686.

DeConto RM, Galeotti S, Pagani M et al. (2012) Past extreme warming events linked to massive carbon release from thawing permafrost. *Nature*, **484**, 87–91.

DeMarco J, Mack MC, Bret-Harte MS, Burton M, Shaver GR (2014) Long-term experimental warming and nutrient additions increase productivity in tall deciduous shrub tundra. *Ecosphere*, **5**, 1–22.

Dorrepaal E, Toet S, van Logtestijn RSP, Swart E, van de Weg MJ, Callaghan TV, Aerts R (2009) Carbon respiration from subsurface peat accelerated by climate warming in the subarctic. *Nature*, **460**, 616–619.

Elberling B, Michelsen A, Schädel C et al. (2013) Long-term CO_2 production following permafrost thaw. *Nature Climate Change*, **3**, 890–894.

Elmendorf SC, Henry GHR, Hollister RD et al. (2012a) Plot-scale evidence of tundra vegetation change and links to recent summer warming. *Nature Climate Change*, **2**, 453–457.

Elmendorf SC, Henry GHR, Hollister RD et al. (2012b) Global assessment of experimental climate warming on tundra vegetation: heterogeneity over space and time. *Ecology Letters*, **15**, 164–175.

Fan Z, Neff JC, Harden JW et al. (2011) Water and heat transport in boreal soils: Implications for soil response to climate change. *Science of The Total Environment*, **409**, 1836–1842.

Fisher JB, Sikka M, Oechel WC et al. (2014) Carbon cycle uncertainty in the Alaskan Arctic. *Biogeosciences Discuss.*, **11**, 2887–2932.

Forbes BC (2015) Arctic Vegetation Cover: Patterns, Processes and Expected Change. In: *The New Arctic* (eds Evengård B, Larsen JN, Paasche Ø), pp. 117–132. Springer International Publishing.

Gouttevin I, Menegoz M, Dominé F et al. (2012) How the insulating properties of snow affect soil carbon distribution in the continental pan-Arctic area. *Journal of Geophysical Research: Biogeosciences*, **117**, G02020.

Harden JW, Koven CD, Ping C-L et al. (2012) Field information links permafrost carbon to physical vulnerabilities of thawing. *Geophysical Research Letters*, **39**, L15704.

Hayes DJ, McGuire AD, Kicklighter DW, Gurney KR, Burnside TJ, Melillo JM (2011) Is the northern high-latitude land-based CO_2 sink weakening? *Global Biogeochemical Cycles*, **25**, GB3018.

Hayes DJ, Kicklighter DW, McGuire AD et al. (2014) The impacts of recent permafrost thaw on land–atmosphere greenhouse gas exchange. *Environmental Research Letters*, **9**, 045005.

Hicks Pries CE, Schuur EAG, Crummer KG (2011) Holocene Carbon Stocks and Carbon Accumulation Rates Altered in Soils Undergoing Permafrost Thaw. *Ecosystems*, **15**, 162–173.

Hodgkins SB, Tfaily MM, McCalley CK et al. (2014) Changes in peat chemistry associated with permafrost thaw increase greenhouse gas production. *Proceedings of the National Academy of Sciences*, 201314641.

Hugelius G, Strauss J, Zubrzycki S et al. (2014) Improved estimates show large circumpolar stocks of permafrost carbon while quantifying substantial uncertainty ranges and identifying remaining data gaps. *Biogeosciences Discussions*, **11**, 4771–4822.

Johansson M, Callaghan TV, Bosiö J, Åkerman HJ, Jackowicz-Korczynski M, Christensen TR (2013) Rapid responses of permafrost and vegetation to experimentally increased snow cover in sub-arctic Sweden. *Environmental Research Letters*, **8**, 035025.

Jorgenson MT, Racine CH, Walters JC, Osterkamp TE (2001) Permafrost Degradation and Ecological Changes Associated with a Warming Climate in Central Alaska. *Climatic Change*, **48**, 551–579.

Jorgenson MT, Shur YL, Pullman ER (2006) Abrupt increase in permafrost degradation in Arctic Alaska. *Geophysical Research Letters*, **33**, L02503.

Jorgenson MT, Harden J, Kanevskiy M et al. (2013) Reorganization of vegetation, hydrology and soil carbon after permafrost degradation across heterogeneous boreal landscapes. *Environmental Research Letters*, **8**, 035017.

Kattsov VM, Källén E, Cattle HP et al. (2005) Future climate change: modeling and scenarios for the Arctic. In: *Arctic Climate Impact Assessment (ACIA)*. Cambridge University Press, Cambridge, UK, pp. 99–150.

Kattsov VM, Walsh JE, Chapman WL, Govorkova VA, Pavlova TV, Zhang X (2007) Simulation and Projection of Arctic Freshwater Budget Components by the IPCC AR4 Global Climate Models. *Journal of Hydrometeorology*, **8**, 571–589.

Koven CD, Riley WJ, Stern A (2012) Analysis of Permafrost Thermal Dynamics and Response to Climate Change in the CMIP5 Earth System Models. *Journal of Climate*, **26**, 1877–1900.

Lawrence DM, Slater AG (2010) The contribution of snow condition trends to future ground climate. *Climate Dynamics*, **34**, 969–981.

Le Quéré C, Moriarty R, Andrew RM et al. (2015) Global carbon budget 2014. *Earth Syst. Sci. Data*, **7**, 47–85.

McCalley CK, Woodcroft BJ, Hodgkins SB et al. (2014) Methane dynamics regulated by microbial community response to permafrost thaw. *Nature*, **514**, 478–481.

McGuire AD, Melillo JM, Randerson JT et al. (2000) Modeling the effects of snowpack on heterotrophic respiration across northern temperate and high latitude regions: Comparison with measurements of atmospheric carbon dioxide in high latitudes. *Biogeochemistry*, **48**, 91–114.

McGuire AD, Anderson LG, Christensen TR et al. (2009) Sensitivity of the carbon cycle in the Arctic to climate change. *Ecological Monographs*, **79**, 523–555.

McGuire AD, Koven C, Lawrence DM et al. (2016) Variability in the sensitivity among model simulations of permafrost and carbon dynamics in the permafrost region between 1960 and 2009. *Global Biogeochemical Cycles*, 2016GB005405.

Mikan CJ, Schimel JP, Doyle AP (2002) Temperature controls of microbial respiration in Arctic tundra soils above and below freezing. *Soil Biology and Biochemistry*, **34**, 1785–1795.

Morgner E, Elberling B, Strebel D, Cooper EJ (2010) The importance of winter in annual ecosystem respiration in the High Arctic: effects of snow depth in two vegetation types. *Polar Research*, **29**, 58–74.

Mudryk LR, Kushner PJ, Derksen C (2014) Interpreting observed northern hemisphere snow trends with large ensembles of climate simulations. *Climate Dynamics*, **43**, 345–359.

Myers-Smith IH, Forbes BC, Wilmking M et al. (2011) Shrub expansion in tundra ecosystems: dynamics, impacts and research priorities. *Environmental Research Letters*, **6**, 045509.

Myhre G, Shindell D, Bréon FM et al. (2013) Anthropogenic and natural radiative forcing. *Climate change*, 658–740.

Nisbet EG, Dlugokencky EJ, Bousquet P (2014) Methane on the Rise—Again. *Science*, **343**, 493–495.

Osterkamp TE (2007) Causes of warming and thawing permafrost in Alaska. *Eos, Transactions American Geophysical Union*, **88**, 522–523.

Osterkamp TE, Romanovsky VE (1999) Evidence for warming and thawing of discontinuous permafrost in Alaska. *Permafrost and Periglacial Processes*, **10**, 17–37.

Qian B, Gregorich EG, Gameda S, Hopkins DW, Wang XL (2011) Observed soil temperature trends associated with climate change in Canada. *Journal of Geophysical Research: Atmospheres*, **116**, D02106.

Räisänen J (2008) Warmer climate: less or more snow? *Climate Dynamics*, **30**, 307–319.

Rawlins MA, Steele M, Holland MM et al. (2010) Analysis of the Arctic System for Freshwater Cycle Intensification: Observations and Expectations. *Journal of Climate*, **23**, 5715–5737.

Romanovsky VE, Smith SL, Christiansen HH (2010) Permafrost thermal state in the polar Northern Hemisphere during the international polar year 2007–2009: a synthesis. *Permafrost and Periglacial Processes*, **21**, 106–116.

Salmon VG, Soucy P, Mauritz M, Celis G, Natali SM, Mack MC, Schuur EAG (2016) Nitrogen availability increases in a tundra ecosystem during five years of experimental permafrost thaw. *Global Change Biology*, **22**, 1927–1941.

Schaefer K, Zhang T, Bruhwiler L, Barrett AP (2011) Amount and timing of permafrost carbon release in response to climate warming. *Tellus B*, **63**, 165–180.

Schaefer K, Lantuit H, Romanovsky VE, Schuur EAG, Witt R (2014) The impact of the permafrost carbon feedback on global climate. *Environmental Research Letters*, **9**, 085003.

Schimel JP, Bilbrough C, Welker JM (2004) Increased snow depth affects microbial activity and nitrogen mineralization in two Arctic tundra communities. *Soil Biology and Biochemistry*, **36**, 217–227.

Schuur E a. G, Abbott BW, Bowden WB et al. (2013) Expert assessment of vulnerability of permafrost carbon to climate change. *Climatic Change*, **119**, 359–374.

Schuur E a. G, McGuire AD, Schädel C et al. (2015) Climate change and the permafrost carbon feedback. *Nature*, **520**, 171–179.

Semenchuk PR, Elberling B, Amtorp C, Winkler J, Rumpf S, Michelsen A, Cooper EJ (2015) Deeper snow alters soil nutrient availability and leaf nutrient status in high Arctic tundra. *Biogeochemistry*, **124**, 81–94.

Serreze MC, Barry RG (2011) Processes and impacts of Arctic amplification: A research synthesis. *Global and Planetary Change*, **77**, 85–96.

Shindell DT, Faluvegi G, Koch DM, Schmidt GA, Unger N, Bauer SE (2009) Improved Attribution of Climate Forcing to Emissions. *Science*, **326**, 716–718.

Smith S l., Romanovsky V e., Lewkowicz A g. et al. (2010) Thermal state of permafrost in North America: a contribution to the international polar year. *Permafrost and Periglacial Processes*, **21**, 117–135.

Stieglitz M, Déry SJ, Romanovsky VE, Osterkamp TE (2003) The role of snow cover in the warming of Arctic permafrost. *Geophysical Research Letters*, **30**, 1721.

Stocker TF, Qin D, Plattner G-K et al. (2013) Long-term Climate Change: Projections, Commitments and Irreversibility. In: *Climate Change 2013: The Physical Science Basis. Contribution of Working Group I to the Fifth Assessment Report of the Intergovernmental Panel on Climate Change.*

Stocker TF, Qin D, Plattner G-K et al. (2014) *Climate change 2013: The physical science basis*. Cambridge University Press Cambridge, UK, and New York.

Sturm M, Holmgren J, McFadden JP, Liston GE, Chapin FS, Racine CH (2001) Snow–Shrub Interactions in Arctic Tundra: A Hypothesis with Climatic Implications. *Journal of Climate*, **14**, 336–344.

Subin ZM, Koven CD, Riley WJ, Torn MS, Lawrence DM, Swenson SC (2013) Effects of Soil Moisture on the Responses of Soil Temperatures to Climate Change in Cold Regions. *Journal of Climate*, **26**, 3139–3158.

Tarnocai C, Canadell JG, Schuur E a. G, Kuhry P, Mazhitova G, Zimov S (2009) Soil organic carbon pools in the northern circumpolar permafrost region. *Global Biogeochemical Cycles*, **23**, GB2023.

Trucco C, Schuur EAG, Natali SM, Belshe EF, Bracho R, Vogel J (2012) Seven-year trends of CO_2 exchange in a tundra ecosystem affected by long-term permafrost thaw. *Journal of Geophysical Research: Biogeosciences*, **117**, G02031.

Uhlířová E, Šantrůčková H, Davidov SP (2007) Quality and potential biodegradability of soil organic matter preserved in permafrost of Siberian tussock tundra. *Soil Biology and Biochemistry*, **39**, 1978–1989.

UNEP UNEP (2013) *Global environment outlook 2000: The emissions gap report*, Vol. 1. Routledge.

Waldrop MP, Wickland KP, White Iii R, Berhe AA, Harden JW, Romanovsky VE (2010) Molecular investigations into a globally important carbon pool: permafrost-protected carbon in Alaskan soils. *Global Change Biology*, **16**, 2543–2554.

Walker MD, Walker DA, Welker JM et al. (1999) Long-term experimental manipulation of winter snow regime and summer temperature in Arctic and alpine tundra. *Hydrological Processes*, **13**, 2315–2330.

Walter Anthony KM, Zimov SA, Grosse G et al. (2014) A shift of thermokarst lakes from carbon sources to sinks during the Holocene epoch. *Nature*, **511**, 452–456.

Webb EE, Schuur EA, Natali SM et al. (2016) Increased wintertime CO_2 loss as a result of sustained tundra warming. *Journal of Geophysical Research: Biogeosciences*.

Welker JM, Fahnestock JT, Jones MH (2000) Annual CO_2 Flux in Dry and Moist Arctic Tundra: Field Responses to Increases in Summer Temperatures and Winter Snow Depth. *Climatic Change*, **44**, 139–150.

Xue K, M. Yuan M, J. Shi Z et al. (2016) Tundra soil carbon is vulnerable to rapid microbial decomposition under climate warming. *Nature Climate Change*, **6**, 595–600.

Yi Y, Kimball JS, Rawlins MA, Moghaddam M, Euskirchen ES (2015) The role of snow cover affecting boreal-arctic soil freeze–thaw and carbon dynamics. *Biogeosciences*, **12**, 5811–5829.

Zhang T (2005) Influence of the seasonal snow cover on the ground thermal regime: An overview. *Reviews of Geophysics*, **43**, RG4002.

Zhang X, He J, Zhang J, Polyakov I, Gerdes R, Inoue J, Wu P (2013) Enhanced poleward moisture transport and amplified northern high-latitude wetting trend. *Nature Climate Change*, **3**, 47–51.

2. WINTER SNOW ACCUMULATION DRIVES TRANSIENT MODULATIONS IN ARCTIC TUNDRA SOIL CARBON BUDGET

2.1 ABSTRACT

Projected increases in winter precipitation strongly affect carbon (C) cycling in Arctic tundra systems whose large stocks of soil organic carbon (SOC) make them critical to future climate trends. Warming and thawing of permafrost under deeper winter snow represents a potential positive feedback on climate warming, as long-term preserved SOC becomes available for decomposition. This response may be either mitigated or enhanced by associated increases in nutrient availability and plant productivity. Related climate-forcing feedbacks remain largely unresolved due to uncertainties in their strength and timing. Critical to the fate of Arctic tundra SOC pools is the rate at which permafrost C will become vulnerable and released relative to ecosystem C inputs. Here we report both biological and physical impacts of short- (2yr) and long-term (14yr and 18yr) snow additions on permafrost dynamics and SOC pools in Alaskan Arctic tundra. We provide evidence of ongoing warming and deepening of the active layer that has turned Arctic tundra into a net C source at the study site. Deeper winter snow accelerated the rate of soil warming and deepening of the active layer above climate-driven trends, increasing the vulnerable SOC pool to 1.2, 3.0 and 5.2 kgC m^{-2} after 2, 14 and 18yr. SOC dynamics were markedly non-linear and evolved over the course of progressive degradation, leading to a fast initial SOC loss (34% of the original SOC pool) and to a 40% SOC gain over the following decades that mitigated up to 61.5% of climate-driven C losses from Arctic tundra. Our results emphasize the potential of Arctic tundra to become a transient C source under future precipitation scenarios contributing to reduce the overall global terrestrial C sink, but also to act as an additional long-term C sink with persistent increases in winter precipitation. We further note that observing soil physical processes and time-dependent non linearities may help reduce

current uncertainty predictions of climate/C-cycle feedbacks from Arctic regions.

2.2 INTRODUCTION

There is growing evidence of a climate-driven shift of Arctic tundra from a historical C sink to a C source in recent decades – largely attributed to enhanced C losses during the cold season – raising great concern over the fate of the vast permafrost SOC stock under future climate scenarios (Belshe *et al.*, 2013; Hayes *et al.*, 2014; Oechel *et al.*, 2014; Crichton *et al.*, 2016; McGuire *et al.*, 2016). Warmer winters have been observed and are projected for most of the Arctic region along with increases in annual precipitation, particularly as snow (Kattsov *et al.*, 2005). Snow fall and accumulation are critical determinants of the C cycle in terrestrial Arctic systems (Fig. 1) (Walker *et al.*, 1999; Blanc-Betes *et al.*, 2016). Deeper snow, by increasing ground thermal insulation, promotes soil warming during the cold season (Lawrence & Slater, 2010) sustaining greater C mineralization (Nobrega & Grogan, 2007) and increasing winter contributions to annual C losses (Fig. 1) (Welker *et al.*, 2000; Xue *et al.*, 2016). Moreover, greater latent heat and thermal conductivity upon snowmelt promote soil warming over the growing season with strengthening effects on permafrost degradation (Johansson *et al.*, 2013), SOC decomposition (Xue *et al.*, 2016), nutrient cycling (Schimel *et al.*, 2004; Xue *et al.*, 2016), plant productivity (Natali *et al.*, 2011; Xue *et al.*, 2016) and shrub expansion (Leffler *et al.*, 2016) beyond the impacts of winter warming alone (*see* Chapters 3 and 4) (Blanc-Betes *et al.*, 2016).

The net impact of deeper snow cover on Arctic SOC pools integrates the individual responses of a variety of competing ecosystem C processes that operate at different time scales and at different rates. For example, deeper winter snow may affect Arctic SOC pools rapidly (years) via C and nutrient mineralization rates (Xue *et al.*, 2016), and more slowly (decades) via

SOC redistribution (Klaminder *et al.*, 2009), alterations of the SOC quantity and quality (Hodgkins *et al.*, 2014), and changes in the productivity and composition of the supported vegetation (*see* Chapters 3 and 4) (Johansson *et al.*, 2013; Leffler *et al.*, 2016; Xue *et al.*, 2016). Moreover, these processes respond to the intensity of a disturbance whose effects amplify over time. Through thaw-induced increases in soil wetness and heat transfer, deeper snow further accelerates warming and thawing triggering a hardly reversible positive feedback on permafrost degradation (Fig. 1) (Osterkamp *et al.*, 2009; Fan *et al.*, 2011; Subin *et al.*, 2013). In addition, associated shrub expansion enhances snow accumulation further amplifying the impacts of increased winter precipitation over time (Fig. 1) (Sturm *et al.*, 2005; Leffler *et al.*, 2016). The Arctic tundra C budget therefore responds to non-stationary dynamics that unfold over the course of progressive permafrost degradation.

Thaw-induced settlement of ice-rich permafrost under deeper winter snow may lead to soil consolidation, and hence the subsidence of the ground surface and progressive deformation of the active layer over relatively short timescales (years to decades) (Jorgenson *et al.*, 2006; Osterkamp, 2007; Osterkamp *et al.*, 2009). Overlooking this physical disturbance may lead to underestimation of the impact of changes in winter precipitation patterns on the rate of permafrost degradation and hence SOC availability, leading to biased predictions of C-climate forcing feedbacks from Arctic regions (Koven *et al.*, 2012; Streletskiy *et al.*, 2012).

At present, discrepancies remain on the magnitude and direction of climate-driven impacts on Arctic C balance. Arctic tundra SOC pools have been suggested to substantially decrease (Hicks Pries *et al.*, 2011; Natali *et al.*, 2014) or remain unaltered (Lamb *et al.*, 2011; Sistla *et al.*, 2013) with enhanced winter warming and precipitation, and model projections lead to a wide range of potential climate forcing feedbacks scenarios from Arctic regions (Table I)

(Schaefer *et al.*, 2014). This uncertainty results from inaccurate estimates of the rate of permafrost degradation determining the size of the SOC pool available for decomposition, and the lack of a time-hierarchical assessment of the vulnerability of C in Arctic soils to changes in climate (Burke *et al.*, 2012; Schuur *et al.*, 2013; Schaefer *et al.*, 2014; McGuire *et al.*, 2016).

We investigated the short- (years) and long-term (decades) impacts of increases in snow accumulation on permafrost thaw and the SOC budget in Arctic tundra.

2.3 METHODS

2.3.1 Site description

The experimental sites are located in moist acidic tussock tundra near Toolik Lake (68º38'N, 149º38'W; 760 m) at the Long Term Ecological Research Site in the northern foothills of the Brooks Range, Alaska (Fig. 2) (Jones *et al.*, 1998; Welker *et al.*, 2000; Pattison & Welker, 2014). Mean annual air temperature is –8ºC, with summer temperatures averaging 10.5ºC. The active layer thickness averages ~30cm during the growing season and reaches a maximum thaw depth of 45–50 cm by late August (Welker, Arctic LTER). Annual precipitation is around 350 mm, 50% of which falls as snow (Deslippe & Simard, 2011). Snow accumulation is 45–80cm, the snow-covered season typically running from mid-September to late-May. Soils are classified as acidic, coarse-loamy, mixed, Ruptic-Histic Pergelic Cryaquept (Michaelson *et al.*, 1996). The area is characterized by poorly drained soils, with relatively shallow organic layers (10–15cm; 20–45 %C) progressively grading into organic-enriched mineral layers (5–20%C) and into mineral layers (1–3 %C) with depth (Ping *et al.*, 1997). Vegetation is dominated by tussock forming sedges (*Eriophorum vaginatum*), and interspaced shrubs (*Betula nana, Salix pulchra*) and mosses (*Sphagnum sp.*) characteristic of moist acidic tundra across the Alaskan North Slope (Walker *et al.*, 1994; Wahren *et al.*, 2005).

2.3.2 Experimental design

Two snow fences were built near Toolik Lake, AK, one in 1994 (ITEX, International Tundra Experiment) and the other in 2006 (IPY), to artificially increase snow accumulation (Walker *et al.*, 1999; Welker *et al.*, 2000). At each fence, we identified two distinct snow accumulation regimes: (i) ambient snow accumulation (CTL; 45–80cm snow depth), and (ii) Snow Addition treatment (SA) with 20–45% more snow than CTL. In 2008, we measured soil environmental variables, and soil profile SOC, radiocarbon (^{14}C) abundance and ^{137}Cs activity within the active layer in both sites (IPY and ITEX) at CTL (CTL_{2008}) and treatment plots, after 2yr (SA_2) and 14yr (SA_{14}) of persistent snow additions. Control plots in both sites were found similar in all measured and estimated parameters, and were therefore considered together for statistical purposes. The oldest fence (ITEX) was resampled (soil environmental variables, and SOC content and distribution) in 2012, at both CTL (CTL_{2012}) and treatment (SA_{18}) plots, after 18yr of snow additions. Direct comparison of control plots sampled in different years (CTL_{2008} and CTL_{2012}) allowed evaluation of current trends of permafrost and SOC dynamics in Arctic tundra underlying the snow treatment effect. Vegetation in the area of study is characteristic of moist acidic tundra across the Alaskan North Slope (Walker *et al.*, 1994). A visible expansion of deciduous shrubs consistent with initial permafrost degradation (Johansson *et al.*, 2013) was observed after two decades of experimental snow additions (SA_{14} and SA_{18}) (*see* Chapters 3 and 4) but not after two years of treatment (SA_2).

2.3.3 Soil environment

Soil environmental variables were monitored over the growing seasons of 2008 and 2012. Soil temperature at 10cm depth was measured using a portable temperature probe (OMEGA Engineering Inc., CT, USA). Thaw depth was monitored using a metal depth rod. Replicates

(n=5) are averaged values of 8 pseudo-replicates per plot. Mean active layer thickness (ALT) was calculated at each plot and sampling year as the seasonal average of the depth to the permafrost table to integrate permafrost dynamics over the growing season. Measured ALT, uncorrected for physical distortion of the active layer, was regarded as apparent ALT.

2.3.4 Soil sampling and processing

Soil cores (4.8cm diameter) were collected at each plot and sampling year to mean active layer thickness (n=2–3). Cores were sectioned into 1-cm depth increments and air-dried to a constant weight for the direct determination of soil water content and bulk density (ρb; soil mass per unit of volume, g cm^{-3}).

2.3.5 Soil carbon and nitrogen content and isotopic analyses

Total C and N content (%) and stable isotopic composition ($\delta^{13}C$ and $\delta^{15}N$) were determined at each sampling year, plot and depth interval by dry combustion with a continuous flow Thermo Finnigan Delta-Plus XL equipped with Conflo III (Bremen, Germany) and zero-blank Elemental Analyzer (Costech Analytical, EC4010; Valencia, CA, USA).

Total C represents organic C as the presence of carbonates was negligible. The density of soil organic C (SOC; kgC m^{-2}) at each depth section, plot and sampling year was calculated as:

(Eq. 2.1) $$SOC_n = (\rho b_n \times \%C_n \times T_n)/10$$

where ρb_n is the soil bulk density (g cm^{-3}), %C is the carbon content (%) and T_n is the thickness (cm) of the soil section considered (Bockheim & Hinkel, 2007).

Inventories of SOC within the active layer at each plot and sampling year were calculated as the sum of the SOC density of the soil sections to target depth (Z), and error biases resulted from the propagation of the variance accumulated with depth.

(Eq. 2.2) $$cSOC_Z = \sum_{i=1}^{n}(\rho b_n \times \%C_n \times T_n)/10$$

Radiocarbon content (^{14}C) was analyzed from a subset of samples collected in 2008 within and below the ^{137}Cs activity peak (see below). Radiocarbon analyses were performed at Center for Accelerator Mass Spectometry facility at Lawrence Livermore National Laboratory (Van de Graaff FN accelerator mass spectrometer) following procedures described in Vogel *et al.* (1984). Measured $\delta^{13}C$ values were used to correct for mass-dependent fractionation. Radiocarbon data reported in $\Delta^{14}C$ notation had an average AMS precision of 3‰, and were corrected for ^{14}C decay since the year of sampling (2008). Negative $\Delta^{14}C$ values denote C fixed prior to nuclear weapons testing and the onset of fossil fuel expansion, old enough for significant radioactive decay to have occurred. Atmospheric $\Delta^{14}C$ increased to +900‰ during the peak activity of nuclear testing in 1963–1964, and has declined thereafter at a rate of 6–10‰ yr^{-1} reaching +120‰ and +45‰ in 1994 and 2008, respectively (Hua *et al.*, 2013).

2.3.6 Assessment of physical disturbance and physical corrections on the active layer thickness and soil organic carbon inventories

Physical processes and the associated distortion of the active layer were identified and quantified using three different approaches: (i) ^{137}Cs depth distribution; (ii) equivalent soil mass (ESM); and (iii) ρb-predictive model. We further used assessments of physical disturbance to perform corrections in the active layer thickness and distribution of SOC inventories therein, allowing for direct comparisons between equivalent depths.

2.3.6.1 ^{137}Cs distribution approach

^{137}Cs is a bomb-derived fallout radionuclide that had a global maximum deposition in 1963–1964, strongly adsorbing to clay and organic matter after deposition (Staunton *et al.*, 2002). Because ^{137}Cs – with a half-life of 30.2 yr – is largely immobilized by its strong physical adsorption and is biologically inert, the vertical distribution of ^{137}Cs within the soil column reflects deposition time and mechanical movement only, therefore allowing the investigation of physical processes (i.e. soil accrual, compaction, erosion, leaching and/or mixing) operating at annual to decadal time-scales (Staunton *et al.*, 2002; Harden *et al.*, 2008; Klaminder *et al.*, 2014).

Samples collected in 2008 were analyzed for ^{137}Cs content (Bq kg^{-1}) using a high-purity Ge gamma spectrometer (Model GR3020-Reverse electrode, University of Illinois at Chicago, UIC) calibrated against standard ocean sediment NIST4357 (standard reference material 4357, 1994; National Institute of Standards and Technology, Gaithersburg, Maryland, USA) with reference activities adjusted for decay since certification date. Potential interferences to the ^{137}Cs measurement (photopeak at 661.6 keV) from trace contents of natural decay-series radionuclides were evaluated and found to be below the detection limit.

Measured ^{137}Cs activities (Bq_i) were normalized to the date of collection (Bq_0) to account for decay lag-times between collection and analysis dates using the following equation:

(Eq. 2.3) $$Bq_0 = Bq_i / e^{-\lambda t}$$

where λ is the ^{137}Cs decay constant (0.023 yr^{-1}) calculated as:

(Eq. 2.4) $$\lambda = Ln2 \; / \; (^{137}Cs \; halflife)$$

and t is the time elapsed between sample collection and analysis in years.

The ^{137}Cs inventory within the active layer was calculated from the sum of depth-increment ^{137}Cs content within the soil column. Cumulative ^{137}Cs inventories at both control and

treatment plots fell within the deposition range reported for Arctic tundra in the vicinities of Toolik Lake (from 657.7 to 1044.5 Bq m^{-2}, decay corrected to collection date; Cooper *et al.*, 1991), indicating that losses of ^{137}Cs in the area of study are negligible. Snow additions did not affect total ^{137}Cs inventories (Fig. 4). Therefore, alterations of the ^{137}Cs profile responded to the redistribution of material within the soil column with snow additions (Fig. 4).

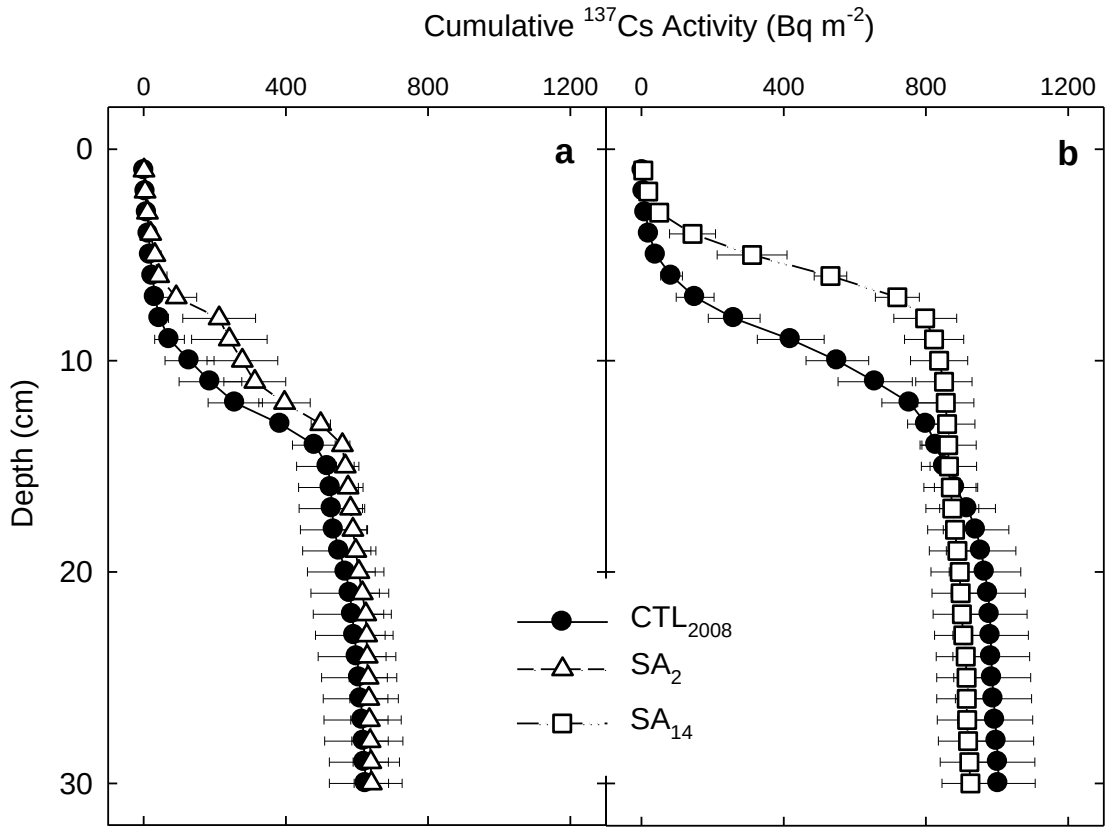

Figure 4: Vertical distribution of cumulative ^{137}Cs activity within the active layer after **(a)** 2yr (CTL_{2008}, SA_2) and **(b)** 14yr (CTL_{2008} and SA_{14}) of experimental snow additions. Values shown are depth averages within site (±SE). ^{137}Cs inventories at both short- and long-term sites fall within the reported range of ^{137}Cs deposited across Alaskan Arctic tundra (~851.1 ± 193.4 Bq m^{-2}) (Cooper *et al.*, 1991) accounting for radioactive decay since deposition. Snow additions resulted in significantly altered cumulative ^{137}Cs distribution within the soil profile at both SA_2 and SA_{14} relative to CTL_{2008} (K-S test: $P<0.05$).

^{137}Cs-equivalent depths were determined from the proportion of cumulative ^{137}Cs activity at a given depth relative to the total ^{137}Cs inventory (%).

We used the Kolmogorov-Snirnov test (K-S test) to evaluate treatment effects on the vertical distribution of ^{137}Cs with in the soil profile. The vertical displacement of the ^{137}Cs distribution in response to treatment was calculated statistically using a Fourier-type cross correlation function analysis applying the extensively used principles of lag-time analyses to estimate lag-distances between control and treatment distributions (White *et al.*, 2003; Gomez-Casanovas *et al.*, 2012).

Soil compaction relative to control plots was then calculated as:

(Eq. 2.5) $$\%Compaction = \Delta Z / {}^{137}Cs_{max}$$

where ΔZ is the estimated displacement between treatment and control and ${}^{137}Cs_{max}$ is the depth of maximum ^{137}Cs activity at control plots.

Estimates of SOC inventories at ^{137}Cs-equivalent depths, extracting the effect of soil compaction and/or consolidation relative to their corresponding controls were then calculated as:

(Eq. 2.6) $$cSOC_{Z_{Cs}} = \sum_{i=1}^{Z_{Cs}} \left(\rho b_{Z_{Cs}} \times \%C_{Z_{Cs}}\right) / 10$$

where $cSOC_{Z_{Cs}}$ (kg m^{-2}) is the cumulative SOC pool integrating all depth intervals down to the depth of equal %^{137}Cs than that at 10-cm depth at the plot of reference (Z_{Cs}; ^{137}Cs-equivalent depth), and ρb_n and $\%C_n$ are interval-specific bulk densities (g cm^{-3}) and %C (%) of the 1-cm soil intervals included within the section considered.

2.3.6.2 Equivalent Soil Mass (ESM) approach

Assuming that changes in soil mass within the soil section considered are negligible, equivalent depths (ESM-depth) may be defined as a function of soil mass instead of distance from the soil surface, therefore avoiding error biases inherent to fixed-depth procedures (Kimble *et al.*, 2000; Gifford & Roderick, 2003; Lee *et al.*, 2009).

The mass of soil, defined as total dry mass of soil per unit of ground area, may be calculated for each depth interval as:

(Eq. 2.7) $$Msoil = \frac{DW}{\pi r^2} \times 10$$

where $Msoil$ is soil mass per unit area (kg m^{-2}), DW is the dry mass of the sample (g) and r is the radius of the soil section under evaluation (cm) (Lee *et al.*, 2009; Wendt & Hauser, 2013).

Similarly, the mass of soil organic carbon per unit area in each soil depth interval is calculated as follows:

(Eq. 2.8) $$Msoc = Msoil \times Csoc$$

where $Msoc$ is defined as SOC mass per unit area (kg m^{-2}) and $Csoc$ is the organic carbon concentration per unit mass of dry soil (g kg^{-1}) within that soil depth interval (Lee *et al.*, 2009; Wendt & Hauser, 2013) (Fig. 5).

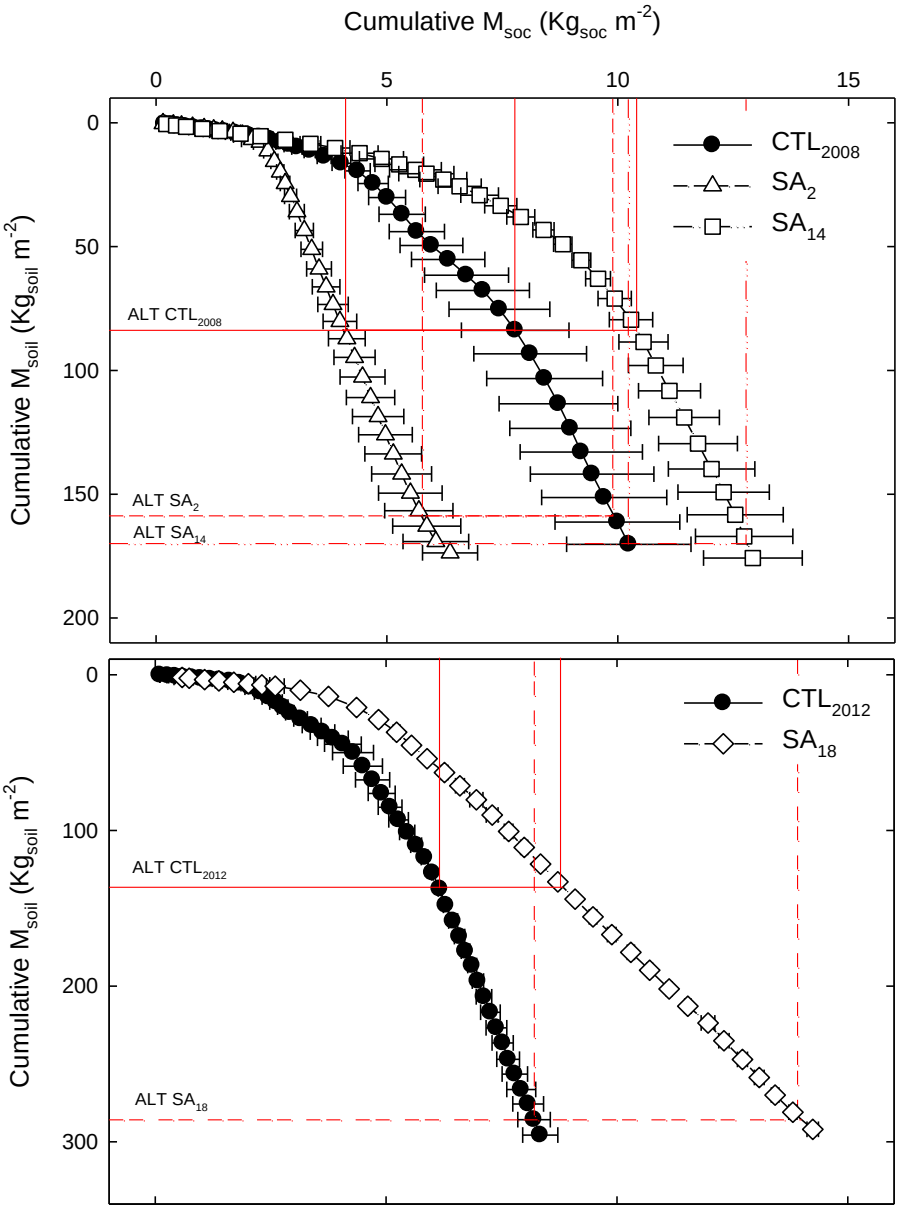

Figure 5: Cumulative soil mass (*cMsoil*) versus soil organic carbon content (*cMsoc*) profile from both control (CTL) and treatment (SA) plots sampled in **(a)** year 2008 (CTL_{2008}, SA_2 and SA_{14}), and **(b)** year 2012 (CTL_{2012} and SA_{18}). Values shown are mean *cMsoc* (±SE) at given *cMsoil* within plot. Red lines indicate comparable SOC inventories at equal *cMsoil* corresponding to mean ALT at **(a)** CTL_{2008} (continuous line), SA_2 (dashed line) and SA_{14} (dashed-dotted line) in samples taken in 2008, and **(b)** CTL_{2012} (continuous line) and SA_{18} (dash-dash line) in samples taken in 2012.

Then, cumulative $Msoil$ ($cMsoil$) and cumulative $Msoc$ ($cMsoc$) within a given soil section may be calculated as the sum of the mass of bulk soil and SOC of the depth intervals (n) integrating the soil column to the target depth (Z; cm):

(Eq. 2.9) $$cMsoil_z = \sum_{i=1}^{n} Msoil_n$$

(Eq. 2.10) $$cMsoc_z = \sum_{i=1}^{n} Msoc_n$$

If $cMsoil$ within a given soil section is maintained among plots, $cMsoil$ at any given plot will be equal to the $cMsoil$ of the plot of reference at equivalent depths (Z_{Eq}).

(Eq. 2.11) $$cMsoil_z = cMsoil_{ZEq}$$

where $cMsoil_z$ is the soil mass per unit area to target depth at the plot of reference and $cMsoil_{ZEq}$ is the soil mass per unit area of the plot of interest to a depth equivalent to that considered in the plot of reference.

Linear interpolation was used to estimate the Z_{Eq} at $cMsoil_z$ considering the depth distribution of $Msoil$ at the plot of interest, and error biases were calculated from the propagation of the variance across plots and with depth (Gifford & Roderick, 2003).

Then, the % compaction of the soil column at a given plot relative to the plot of reference may be then calculated as:

(Eq. 2.12) $$\%Compaction = \frac{Z_{Eq} - Z_{ref}}{Z_{ref}} \times 100$$

where Z_{Eq} is the thickness of the soil section of the plot of interest equivalent to that at the plot of reference, and Z_{ref} is the target depth at the plot of reference.

Implicit to the ESM approach is the attribution of apparent changes in soil mass to mechanical stress, considering the soil column as a closed system with negligible movement of material in or out the soil section under evaluation. If this assumption is invalid, comparisons of

SOC pools in contrasting soils must be based on soil masses that differ according to the amount of redistributed material (Kimble *et al.*, 2000). Both biotic (i.e. gross photosynthesis and respiration) and geomorphic processes (i.e. soil redistribution) may result in detectable changes in soil mass causing a systematic over- and underestimation of soil compaction in areas subject to substantial mineralization and accrual of organic matter, or erosion and sedimentation respectively, therefore leading to biases in SOC budget estimates (Kimble *et al.*, 2000). The ^{137}Cs vertical distribution and budget within the active layer showed no appreciable leaching or erosion in response to treatment but indicated net accrual of material, and previous results from the study site have revealed substantial biotic alterations with treatment (Welker *et al.*, 2000; Blanc-Betes *et al.*, 2016; Leffler *et al.*, 2016).

2.3.6.3 ρb-predictive model approach

Differences in ρb among plots reflect variations in biotic (i.e. level of decomposition) (Bockheim *et al.*, 2003) and physical (i.e. soil compaction and/or consolidation) (Ruehlmann & Körschens, 2009) processes in response to treatment.

The percentage organic carbon (%C) integrates the level of decomposition of the soil organic matter, explaining up to 90% of the variability in ρb at shallow horizons, with particularly good prediction efficiency at highly organic, undisturbed soils (Saini, 1966; Bockheim *et al.*, 2003; Heuscher *et al.*, 2005; Steller *et al.*, 2008).

Therefore, we used an empirical regression model to express ρb as a function of %C, and hence integrating ongoing biotic processes within the soil column (Saini, 1966; Bockheim *et al.*, 2003; Heuscher *et al.*, 2005; Steller *et al.*, 2008; Ruehlmann & Körschens, 2009).

(Eq. 2.13) $$\rho b = a \times exp^{(-b \times \%C)}$$

where the intercept term (a) represents the theoretical ρb of organic C-free mineral soil, and the slope term (b) is the expression for the nonlinear relation between %C and ρb (Table II).

TABLE II

Model parameterization describing soil bulk density (ρb) as a function of soil organic carbon content (%C) at each site and sampling year. Values with different letter denote statistical differences between snow treatment (P<0.05).

	CTL_{2008}	CTL_{2012}	SA_2	SA_{14}	SA_{18}
Intercept (a)	0.897 ± 0.057[a]	0.908 ± 0.002[ab]	0.908 ± 0.045[ab]	1.081 ± 0.029[b]	1.333 ± 0.016[c]
Slope (b)	–0.078 ± 0.003[a]	–0.079 ± 0.002[a]	–0.070 ± 0.002[a]	–0.068 ± 0.002[a]	–0.077 ± 0.002[a]
F-value	1272.4	1180.6	2663.0	875.5	1569.8
P-value	<0.0001	<0.0001	<0.0001	<0.0001	<0.0001
Corr. coef	–0.95	–0.97	–0.99	–0.95	–0.98
r^2	0.91	0.95	0.98	0.91	0.97

Given that the relationship between soil ρb and %C was maintained (b; Table II), deviations of the intercept (a) reflect the theoretical ρb of organic C-free mineral soil and mechanical stress exerted on the soil profile, and can be represented as follows:

(Eq. 2.14) $a = \tau + \beta$

where the coefficient τ represents the value of maximum theoretical ρb of organic C-free mineral soil and β expresses the compaction of the soil column integrating both the compactness inherent to the soil texture and structure (ε) and physical stress (μ) (Ruehlmann & Körschens, 2009).

Given that most of the variability in soil texture defining ε is integrated in %C and hence included in the model description (Ruehlmann & Körschens, 2009), and that shared geological history suggest constant τ across the area of study, alterations of a may be used as a proxy for the compaction of the active layer relative to the plot of reference:

(Eq. 2.15) $\Delta a = \Delta \mu$

Notably, warming and thawing of the active layer could result in alterations in the extent and distribution of organic and mineral horizons affecting ε and hence introducing biases in the measure of compaction. However, the depth and distribution of soil horizons was not affected by either treatment or underlying environmental changes (ANOVA; P=0.8), suggesting minimal or no effect of changes in soil texture on measures of relative soil compaction. Therefore, changes in ρb were the result of relative compaction and or consolidation due to treatment and may be estimated as follows:

(Eq. 2.16) $\%\, Compaction = \frac{a_i - a_{ref}}{a_{ref}} \times 100$

We used paired ρb and %C values from CTL_{2008} plots to parameterize the ρb-predictive model (Table II). The regression of observed- against predicted- ρb values for 6 randomly selected depth measurements per each CTL_{2008} replicated plot revealed an unbiased relationship (R^2=0.96; slope=0.97, intercept=0.003). Therefore, we used plot- and depth-specific %C from SA and CTL_{2012} plots to estimate a theoretical vertical distribution of ρb as affected by biotic processes alone (predicted-ρb). Deviations between observed- (affected by biotic and geophysical processes) and predicted-ρb (affected by biotic processes) reflected the magnitude and extent of soil compaction due to the impact of treatment (SA_2 and SA_{14}) and/or ongoing environmental change (CTL_{2012} and SA_{18}) on physical processes alone.

We estimated the mean deviation of predicted- with respect to the observed- values (RMSD; root mean squared deviation) as:

(Eq. 2.17) $$\text{RMSD} = \sqrt{\frac{1}{n-1}\sum_{i=1}^{n}(pred_i - obs_i)^2}$$

and evaluated the source of deviation by evaluating the relative contribution of Theil's partial inequality coefficients, that partitions the square sum of predictive error (SSPE) into U_{bias} (differences between observed and predicted values), U_{slope} (proportion of variance associated with the slope fitted model and the 1:1 line, and Ue (unexplained variance) (Piñeiro *et al.,* 2008) (Table III).

(Eq. 2.18) $$U_{bias} = \frac{n\,(obs_{Mean} - pred_{Mean})^2}{SSPE}$$

(Eq. 2.19) $$U_{slope} = \frac{(b-1)^2\ \sum_{i=1}^{n}(pred_i - pred_{Mean})^2}{SSPE}$$

(Eq. 2.20) $$U_e = \frac{\sum_{i=1}^{n}(a+(b \times pred_i) - obs_i)^2}{SSPE}$$

(Eq. 2.21) $$SSPE = \sum_{i=1}^{n}(pred_i - obs_i)^2$$

TABLE III

Evaluation of the goodness-of-fit of observed- versus predicted-ρb. Model describes theoretical ρb at each site and sampling year normalized to CTL_{2008} parameterization (a = 0.897; b =0.057). Theil's partial inequality coefficients and root mean squared deviations are shown for the assessment of the source of variance contributing to total error of the predictions, being U_{bias} the proportions associated with mean differences between observed and predicted values, U_{slope} the proportion associated with the slope of the fitted model and the 1:1 line, and U_e the proportion associated with the unexplained variance. Minor contributions from U_{slope} and greater contributions from U_{bias} indicate maintained relationship between ρb and %C, deviations of observed-ρb from predicted values being primarily associated to geophysical alterations of the active layer.

	CTL_{2008}	CTL_{2012}	SA_2	SA_{14}	SA_{18}
R^2	0.98	0.97	0.99	0.94	0.96
SSPE	0.062	0.140	0.234	1.855	2.549
U_{bias}	0.00	0.29	0.78	0.63	0.69
U_{slope}	0.05	0.08	0.00	0.17	0.19
U_e	0.98	0.63	0.22	0.19	0.12
RMSD	0.046	0.070	0.090	0.197	0.296

Negligible deviation between observed- and predicted-ρb at CTL_{2008} indicated that the model successfully reproduced variations in ρb across the area of study. Mean deviation progressively increased at CTL_{2012}, and with time of experimental snow additions suggesting increasing importance of physical alterations in defining ρb relative to CTL_{2008} (Table III). Most of the uncertainty at CTL_{2008} was unexplained (U_e) further supporting the robustness of the model, whereas U_{bias} increased in prediction estimates of ρb at CTL_{2012} and SA plots, with minor contributions from U_{slope} to total predictive error, attributing deviations between observed- and predicted- ρb to Δa, alterations of the ρb-%C relationship being negligible (Table III).

Estimates of inventories and distribution of SOC extracting the effect of relative soil compaction and/or consolidation were then calculated as:

(Eq. 2.22) $$cSOC_z = \sum_{i=1}^{n}(predicted\text{–}\rho b_n \times \%C_n \times T_n)/10$$

where $cSOC_z$ is the cumulative SOC pool (kgC m^{-2}) integrating all depth intervals down to target depth (Z), predicted-ρb_n is the depth-specific model-estimated ρb considering biotic changes only, $\%C_n$ is the depth-specific %C, and T_n is the thickness of the depth interval considered.

Thaw-induced increases in the SOC pool available for decomposition, SOC inventories and relative changes on SOC pools due to treatment and/or underlying environmental change using model-based physical corrections are shown in Figure 7 and Table V.

2.3.7 Approach comparison

Approach comparisons and associated biases are shown in Tables IV and V. Model estimates of soil compaction and variations on SOC pools in response to treatment were in agreement with ^{137}Cs-distribution estimated values indicating that the model was successful in reproducing physical and biotic responses to snow additions (Table IV). ESM estimates showed similar response trends of the ALT, the available SOC pool and SOC inventories to snow additions compared to modelled results, further validating model estimated values. However, the mass dependent method tended to over- and underestimate compaction in plots subject to substantial mineralization and net accrual of organic matter respectively, therefore leading to biases relative to model results (Tables IV and V).

TABLE IV

Estimates of physical compaction (%) of the shallow horizon (0–10cm) and equivalent depths (Z_{Eq}; cm) at each plot and sampling year estimated by ^{137}Cs distribution, ρb-predictive model and equivalent soil mass approaches. Compared to model estimates, the ESM approach over- and underestimated physical impacts at plots subject to substantial decomposition and accrual of soil organic matter respectively, likely by attributing changes in soil mass derived from biotic processes to mechanical stress.

	^{137}Cs activity		ρb-predictive model		Equivalent soil mass	
	%Compaction	Z_{Eq}	%Compaction	Z_{Eq}	%Compaction	Z_{Eq}
CTL_{2008}	ref	10	ref	10	ref	10
CTL_{2012}	-	-	5.9±1.6%	9.4±0.2	10.1±2.4%	9.0±0.2
SA_2	8.7±2.9%	9.1±0.3	12.7±3.1%	8.7±0.3	17.4±4.4%	8.3±0.4
SA_{14}	43.3±4.7%	5.7±0.5	45.3±3.8 %	5.5±0.4	58.8±8.8%	4.1±0.9
SA_{18}	-	-	50.3±4.3%	5.0±0.4	57.8±9.2%	4.2±0.9

TABLE V

Mean active layer thickness (ALT; cm), SOC availability[1] (kgC m^{-2}), and SOC inventories[2] (kgC m^{-2}) at each plot and sampling year as measured by **(A)** the fixed-depth approach (apparent), or estimated by **(B)** ρb-predictive model and **(C)** equivalent soil mass approaches. Error biases represent the % deviation from either model- or ESM- estimates to fixed-depth measures of change, corresponding to the over- or underestimation of the effect size derived from the fixed-depth method. Values in regular font use CTL_{2008} as reference plot. Values in *italic* use CTL_{2012} as reference plot. Direct comparisons of SA_2, SA_{14} and SA_{18} to their corresponding controls reflect the impacts of snow additions on the considered variables, whereas the direct comparison of CTL_{2008} to CTL_{2012} reflects the impact of ongoing environmental change on the considered variables. (*) Denotes statistical significance (ANOVA; $P<0.05$).

	CTL_{2008}	CTL_{2012}	SA_2	SA_{14}	SA_{18}
(A) Fixed-depth approach (Apparent)					
ALT (ΔALT)	30.0±0.4 (ref)	31.9±0.3 (+1.9)	33.3±0.5 (+3.3*)	35.3±0.6 (+5.3*)	36.4±0.6 (+6.4*) *(+4.6*)*
SOC Availability[1] (ΔSOC_{av})	7.8±1.2 (ref)	8.4±1.3 (+0.6)	8.8±1.3 (+1.0)	9.3±1.2 (+1.5)	9.6±1.3 (+1.8) *6.8±0.1 (–1.0)*
SOC Inventory[2] (ΔSOC_{inv})	7.8±1.2 (ref)	6.1±0.0 (–2.3*)	5.4±0.9 (–3.4*)	12.8±1.1 (+3.5)	13.0±0.1 (+4.4*) *(+6.2*)*
(B) ρb-predictive model approach					
% Compaction	(ref)	1.2±0.2%	1.1±0.4%	20.4±3.1%*	48.5±1.8%* *46.8±1.7%**
ALT (ΔALT)	30.0±0.2 (ref)	32.3±0.3 (+2.3*)	34.2±0.4 (+4.2*)	42.5±0.7 (+12.5*)	54.1±0.9 (+24.1*) *(+21.8*)*
ΔALT Bias		1.2%	2.9%	24.0%	58.9% *53.4%*
SOC Availability[1] (ΔSOC_{av})	7.8±0.0 (ref)	8.6±0.1 (+0.8*)	9.1±0.1 (+1.3*)	10.9±0.1 (+3.1*)	13.0±0.4 (+5.2*) *11.9±0.2 (+3.3*)*
ΔSOC_{av} Bias		1.5%	2.5%	19.2%	43.2% *52.5%*
SOC Inventory[2] (ΔSOC_{inv})	7.8±0.0 (ref)	7.3±0.1 (–1.3*)	6.0±0.5 (–3.1*)	11.1±0.5 (+0.2)	12.5±0.7 (–0.5*) *(+0.6*)*
ΔSOC_{inv} Bias		12.3%	3.9%	35.8%	39.3% *86.1%*

TABLE V (continued)

	CTL_{2008}	CTL_{2012}	SA_2	SA_{14}	SA_{18}
(C) Equivalent soil mass approach (ESM)					
% Compaction	(ref)	11.7±24.4%	13.2±3.6%*	10.3±21.4%	43.1±3.6% *34.4±15.2%*
ALT (ΔALT)	30.0±4.0 (ref)	35.4±7.8 (+5.4)	37.7±1.2 (+7.7)	39.0±7.6 (+9.0)	52.1±1.3 (+22.1) *(+16.7)*
ΔALT Bias		11.7%	14.7%	12.1%	52.3% *33.0%*
SOC Availability[1] (ΔSOC_{av})	7.8±1.2 (ref)	9.3±1.3 (+1.5)	9.9±1.4 (+2.1)	10.2±1.3 (+2.4)	13.1±1.3 (+5.3*) *8.8±0.8 (–0.5)*
ΔSOC_{av} Bias		11.8%	14.4%	12.1%	46.1% *26.0%*
SOC Inventory[2] (ΔSOC_{inv})	7.8±1.2 (ref)	6.2±1.0 (–3.1*)	5.7±1.5 (–4.2*)	12.6±2.1 (+2.4)	12.9±0.7 (–0.2) *(+4.1*)*
ΔSOC_{inv} Bias		6.0%	3.8%	14.1%	36.9% *44.6%*

[1] SOC availability (kgC m^{-2}) corresponds to the SOC pool available for decomposition within the mean active layer thickness (ALT) of each plot and sampling year assuming homogeneity in the distribution of the SOC inventory across the area of study. Control plots integrate a shared geophysical and biological history underlying the treatment effect. Therefore, the pool of available SOC unaffected by treatment and/or ongoing environmental change is considered equal to that of the plot of reference at depths corresponding to plot-specific ALT, and ΔSOC_{av} is the estimate of thaw-induced increases in the available SOC pool (newly available SOC; increases in the SOC pool relative to that contained in the ALT of the plot of reference).

[2] SOC inventory (kgC m^{-2}) corresponds to the SOC pool contained within the active layer thickness (ALT) as affected by treatment and/or ongoing environmental change, calculated as cumulative SOC within plot-specific active layer thickness. ΔSOC_{inv} is the net impact of snow additions and/or ongoing environmental change on SOC inventories calculated as the change in the SOC pool of each plot relative to their corresponding SOC availability[1].

2.3.8 Statistical analyses

Repeated measures analyses of variance were used to examine the effects of treatment and/or ongoing climate change on soil environmental variables (i.e. soil temperature, active layer thickness). Soil content and depth distribution of ^{137}Cs, SOC and C and N content and isotopic composition were analyzed with multivariate analysis of variance using soil depth as a fixed factor within plot for the evaluation of alterations in response to short and long-term snow additions (SA_2, SA_{14} and SA_{18}) and/or to underlying environmental change (CTL_{2012}) relative to CTL_{2008}. Significance levels of the distribution differences between each plot and the plot of reference were evaluated with Kolmogorov-Smirnov test (K-S test) on pairs of mean cumulative values of the considered variables. Displacements of the vertical distribution of ^{137}Cs within the soil column were assessed with a Fourier-type cross-correlation function analysis (Mystat v.12; Systat Software, Inc., Chicago, IL, USA). Differences among plots in ^{137}Cs and SOC inventories and mean C/N ratios, $\delta^{13}C$ and $\delta^{15}N$ values among plots at equivalent depths or within given soil sections were examined with simple analysis of variance (ANOVA). All residuals were checked for normality and homogeneity of variances to ensure that the assumptions of ANOVA were met, and the statistical significance was determined at the $P<0.05$ level. Statistical analyses were performed with Statgraphics Centurion XVI software (Statistical Graphics Corp., MD, USA) unless otherwise stated.

2.4 Results and Discussion

Snow additions resulted in higher soil temperatures during the cold season (Oct–Apr; +5.1±0.3ºC), and a warmer (+0.6±0.2ºC, +1.1±0.1ºC and +1.3±0.1ºC at SA_2, SA_{14} and SA_{18} respectively; $P<0.05$) and deeper (+3.3±0.4cm, +5.3±0.6cm and +6.4±0.7cm at SA_2, SA_{14} and SA_{18} respectively; $P<0.05$) active layer over the snow-free season (May–Sep) relative to the

corresponding control. The effect size increased over time, likely due to thaw-induced increases in soil wetness (Fan *et al.*, 2011; Subin *et al.*, 2013; Blanc-Betes *et al.*, 2016). However, thaw-induced settlement may result in underestimates of the apparent active layer thickness (ALT) in subsided areas, underestimating the rate of permafrost thaw (Shiklomanov *et al.*, 2013).

To correct error biases derived from fixed-depth characterizations of the ALT and SOC pools, physical alterations in response to short- (2yr) and long-term (14yr) snow additions were investigated by examining variations in soil ^{137}Cs distribution. ^{137}Cs displayed a regular peak-shape distribution within the soil profile that recorded its depositional history from above-ground nuclear weapons testing fallout across Alaskan Arctic regions during the 1950s and early 1960s. Inventories of ^{137}Cs within the active layer indicated no significant losses at both control and treatment plots suggesting that Arctic tundra is an upward accreting system with negligible vertical mixing, lateral translocation or leaching of material within ^{137}Cs distribution depths (10–15cm) (Fig. 4). Snow additions resulted in the vertical compression of the depth profile of ^{137}Cs activity (Fig. 6a and 6b), but did not affect its distribution when normalized to cumulative dry soil mass. These results indicate that thaw-induced consolidation and compaction of the active layer was a more dominant geomorphological agent under deeper snow than in controls (Fig. 6c and 6d). Analyses of ^{137}Cs-equivalent depths showed 8.7±2.9% and 43.3±4.7% compaction of the shallow organic layer (0–10cm) at SA_2 and SA_{14} relative to CTL_{2008} respectively (Table IV), revealing an intensification over time of thaw settlement and consolidation of the active layer under deeper snow consistent with the initial stages of thermokarst development (thaw-induced subsidence of the ground surface) (Johansson *et al.*, 2013).

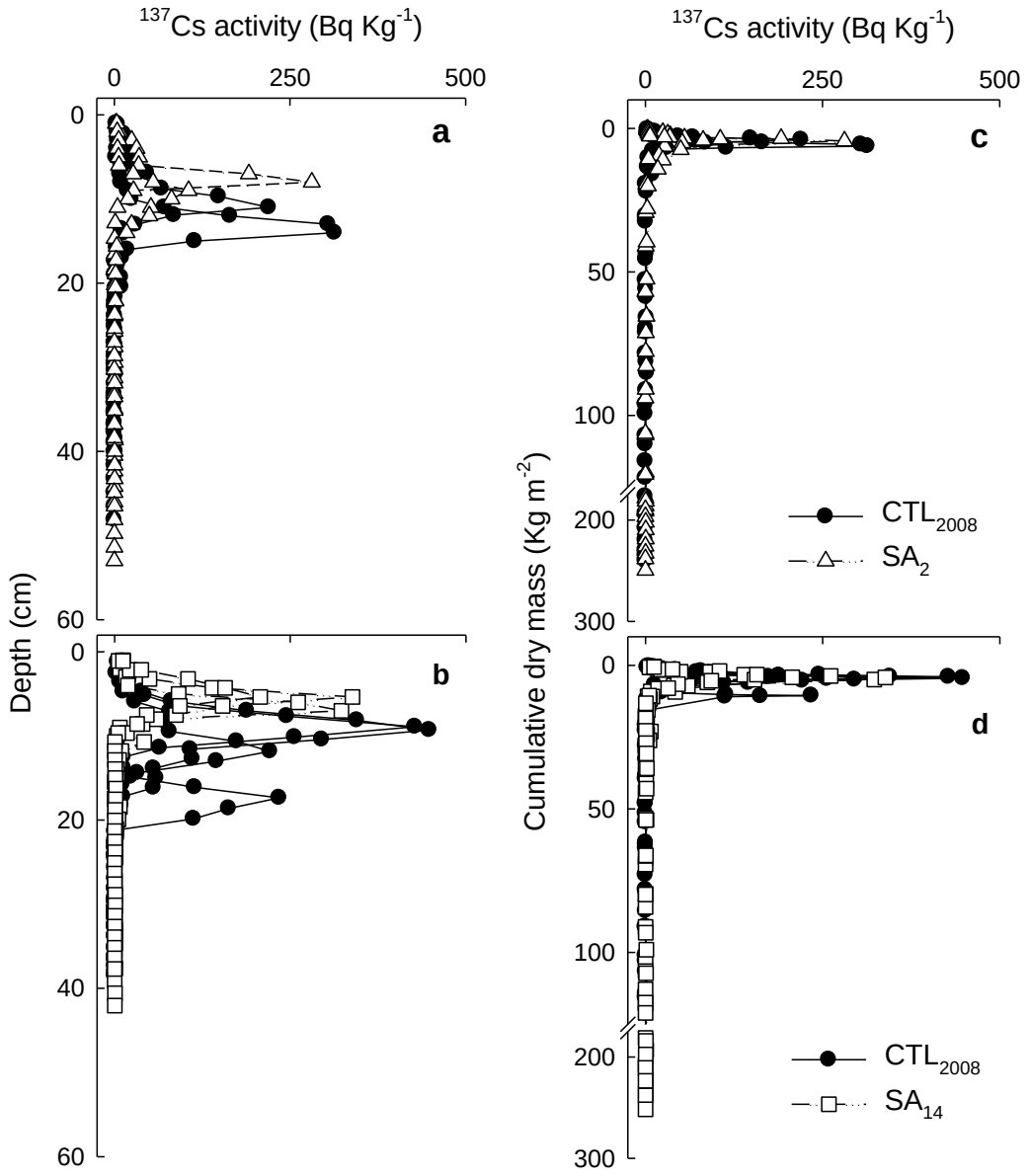

Figure 6: Profile distribution of ^{137}Cs activity (Bq kg^{-1}) at control (CTL_{2008}) and snow addition treatment (SA_2 and SA_{14}) plots expressed by **(a)**, **(b)** depth and **(c)**, **(d)** by cumulative dry mass (kg m^{-2}). Snow additions caused a moderate displacement of the ^{137}Cs distribution by depth at (a) SA_2 (CCFs: 0.9±0.3cm, R^2=0.73; K-S test: *P*=0.07, DN=0.36), that intensified at (b) SA_{14} (CCFs 4.3±0.5cm, R^2=0.87; K-S test, *P*=0.007, DN=0.43) relative to CTL_{2008}. No statistical differences were detected between CTL_{2008} and (c) SA_2 or (d) SA_{14} in the vertical distribution of ^{137}Cs expressed by cumulative dry mass (K-S test>0.5).

The distribution of ^{137}Cs is constrained by its deposition time and the active layer accretion rate, limiting its detection to near-surface (i.e. <10–15 cm depth) material. To effectively evaluate physical alterations integrating the entire active layer, ESM and model approaches were used to normalize SOC storage at equivalent depths across treatments and sampling times against their corresponding controls. Considering the entire active layer, deeper winter snow resulted in 1.3% compaction of the soil column at SA_2 relative to CTL_{2008}, suggesting that observed increases in ρ_b after 2yr of snow additions were almost entirely associated with greater level of decomposition of the organic material, physical compaction being largely limited to shallow organic layers (Fig. 7; Tables IV and V). At decadal scales, however, snow additions resulted in 20.4±3.1% and 46.8±1.7% compaction of the soil column at SA_{14} and SA_{18} relative to their corresponding controls and the impact of soil consolidation extended to the entire active layer. These results further support ^{137}Cs evidence of an intensification of thaw-induced mechanical deformation over time (Fig. 7; Tables IV and V).

The progressive consolidation of the active layer resulted in a mean surface subsidence of 0.9±0.1cm, 7.3±0.4cm and 17.7±0.5cm after 2yr, 14yr and 18yr of snow addition, respectively (Fig. 7). Physical corrections revealed that deeper winter snow increased the ALT by 4.2±0.6cm, 12.5±1.0cm and 21.8±1.2cm at SA_2, SA_{14} and SA_{18} relative to their corresponding controls, exposing a total of 1.2±0.1, 3.0±0.2 and 4.6±0.4 kgC m^{-2} of additional thawed SOC to decomposition after 2yr, 14yr and 18yr of snow additions respectively (Fig. 7; Table V).

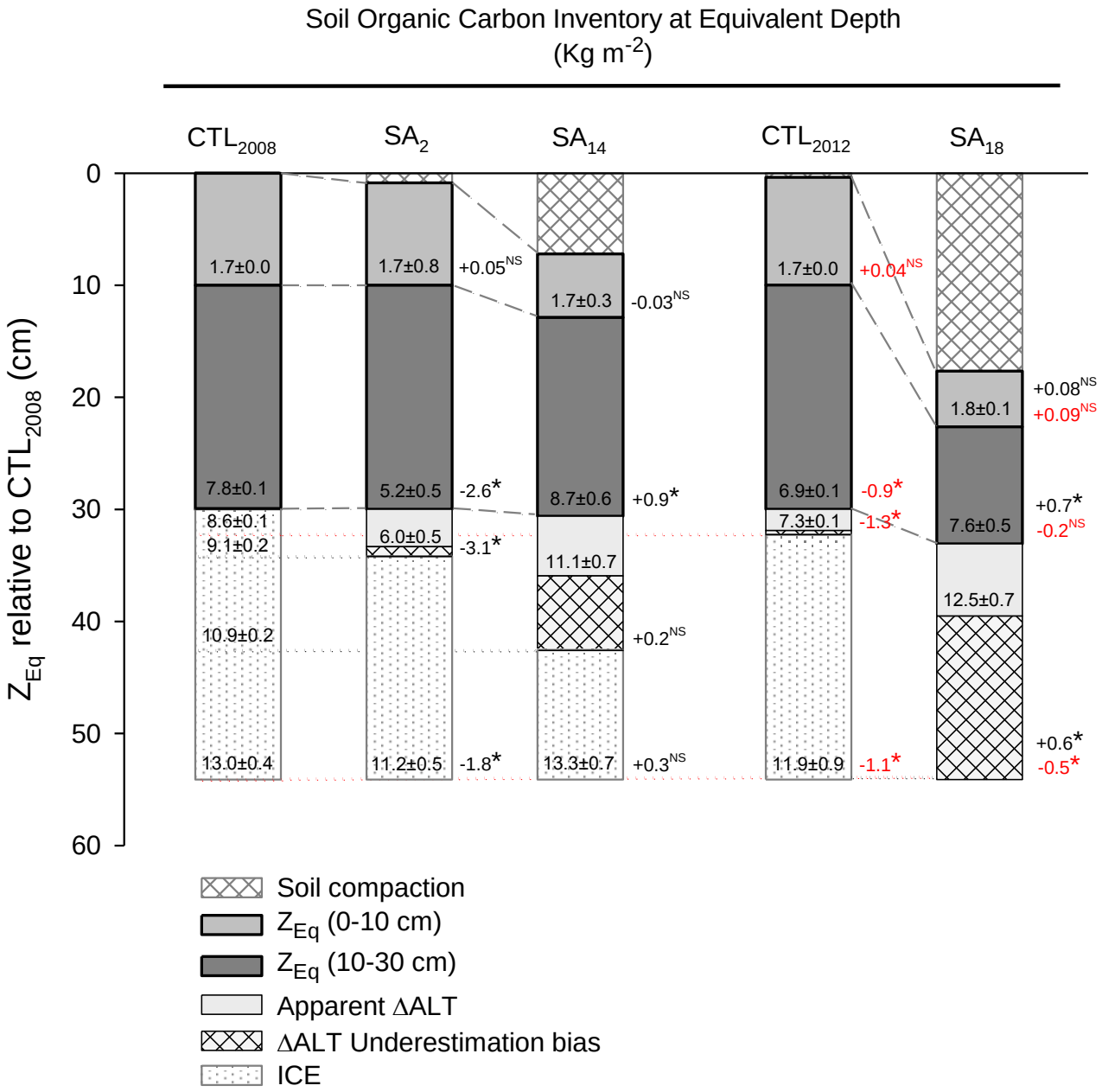

Figure 7: Diagram depicting mean active layer thickness (ALT), soil compaction and SOC inventories and distribution in all plots and sampling years, at model estimated equivalent depths (Z_{Eq}) relative to CTL_{2008}. Within column values correspond to model estimated SOC inventories (±SE) at shallow depths (Z_{Eq} = 10cm), and depths equivalent to ALT at each plot and sampling year. Side values indicate net changes in SOC pools in response to (black) snow additions, and (red) in response to underlying environmental changes. (*) Denotes statistical significance (ANOVA; $P<0.05$).

Based on current understanding of SOC dynamics, the Arctic tundra C source strength is expected to increase proportionally to progressive soil warming and thaw-induced increases in the vulnerable SOC pool under deeper winter snow (Crichton *et al.*, 2016; Hicks Pries *et al.*, 2016). However, the Arctic tundra SOC pool was depleted by 34±7.2% at SA_2 but increased by 2±0.9% and 5±1.4% at SA_{14} and SA_{18} respectively relative to their corresponding controls (Fig. 7; Table V). These results reveal a marked non-linear in the response of the ecosystem C budget to projected changes in precipitation patterns over time, presumably defined by transitions in the controlling variables over the course of progressive permafrost degradation. These observations reconcile discrepancies across studies investigating the impacts of warming in Arctic C, reported responses ranging from enhanced C losses (Hicks Pries *et al.*, 2011; Natali *et al.*, 2014) to no change to experimental warming (Lamb *et al.*, 2011; Sistla *et al.*, 2013). The SOC pool increased by ~40% above SA_2 levels over the years following initial SOC losses, indicating that in apparent contradiction with the above mentioned studies, deeper winter snow converted Arctic tundra into a significant long-term C sink despite substantial warming and deepening of the active layer. Therefore, the assumption of linearity may lead to substantial inaccuracies of the effect size of environmental changes on the Arctic tundra C budget (Fig. 7; Table V).

Snow additions turned Arctic tundra into a transient C source likely by the combined effect of the high decomposability of permafrost SOC, the high temperature sensitivity of microbial activity within the active layer, and the rapid shift in microbial functional structure and abundance following permafrost thaw that allowed for greater mineralization rates (Waldrop *et al.*, 2010; Mackelprang *et al.*, 2011; Xue *et al.*, 2016). Accelerated SOC losses at SA_2 were consistent with increases in $\Delta^{14}C$ relative to CTL_{2008} at ^{137}Cs-equivalent depths (Fig. 8), which coupled to a substantial SOC loss suggest aging of the SOC pool due to the fast depletion of

post-bomb SOC above the potential increases in primary productivity generally associated with warming trends (Welker *et al.*, 2000; Natali *et al.*, 2011).

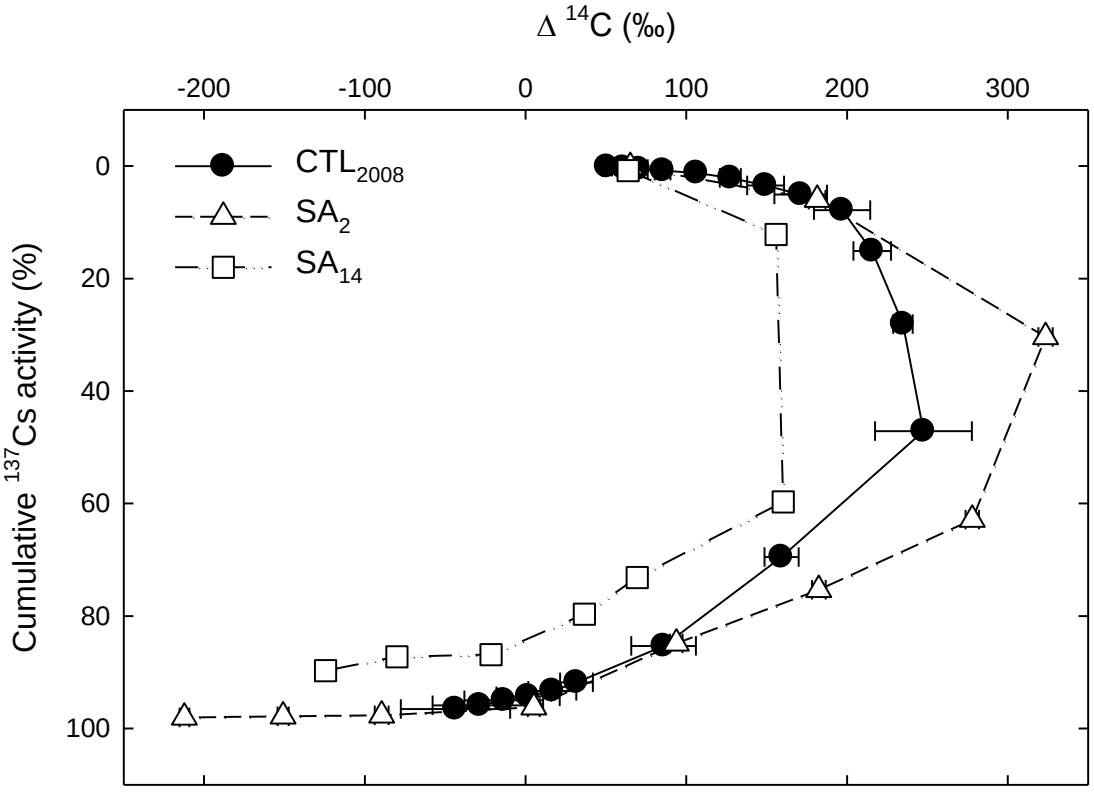

Figure 8: Radiocarbon content (‰) normalized by cumulative ^{137}Cs activity (%) at CTL_{2008}, and SA_2 and SA_{14} treatment plots. Bulk soil $\Delta^{14}C$ increased at SA_2 but decreased at SA_{14} at ^{137}Cs equivalent depths. Error bars correspond to the error propagation of the standard error of the mean and analytical error for CTL_{2008} (n=2) and to analytical error for SA_2 and SA_{14} (n=1).

Notably, deeper snow did not alter surface SOC pools (0–10cm) at SA_2 significantly compared to CTL_{2008}, the greatest losses occurring at subsurface depths roughly corresponding with C-enriched mineral horizons (5–20%C) (Fig. 7). This is consistent with the greater temperature sensitivity of the organic-enriched mineral horizons than the organic surface at subzero temperatures, and agrees with observations of shifts in the preferred substrate towards more recalcitrant compounds with increasing temperatures reported for Arctic tundra soils (Michaelson & Ping, 2003; Biasi *et al.*, 2005).

Observed decreases of C/N ratios and enrichment of $\delta^{13}C$ and $\delta^{15}N$ at SA_2 relative to CTL_{2008} matching subsurface soil layers indicated a greater degree of decomposition of remaining soil organic matter within the organic-rich mineral horizon (Kuhry & Vitt, 1996; Boström *et al.*, 2007; Hobbie & Ouimette, 2009) (Fig. 9). This suggests that warmer soils under deeper snow promoted winter mineralization largely contributing to SOC losses at the annual scale (Welker *et al.*, 2000; Nobrega & Grogan, 2007; Natali *et al.*, 2014). In addition, increases in the availability of SOC and N with enhanced plant productivity and allocation of plant-derived organic compounds in deeper soil layers may have favored a transient priming effect in subsoil horizons contributing to the strong short-term response of subsurface SOC to snow additions during the snow-free season (Berg, 2000; Lavoie *et al.*, 2011; Wild *et al.*, 2014). These observations are consistent with reports of enhanced contributions from old SOC pools to ecosystem C losses following thaw in Arctic and subarctic regions (Nowinski *et al.*, 2010; Hicks Pries *et al.*, 2016).

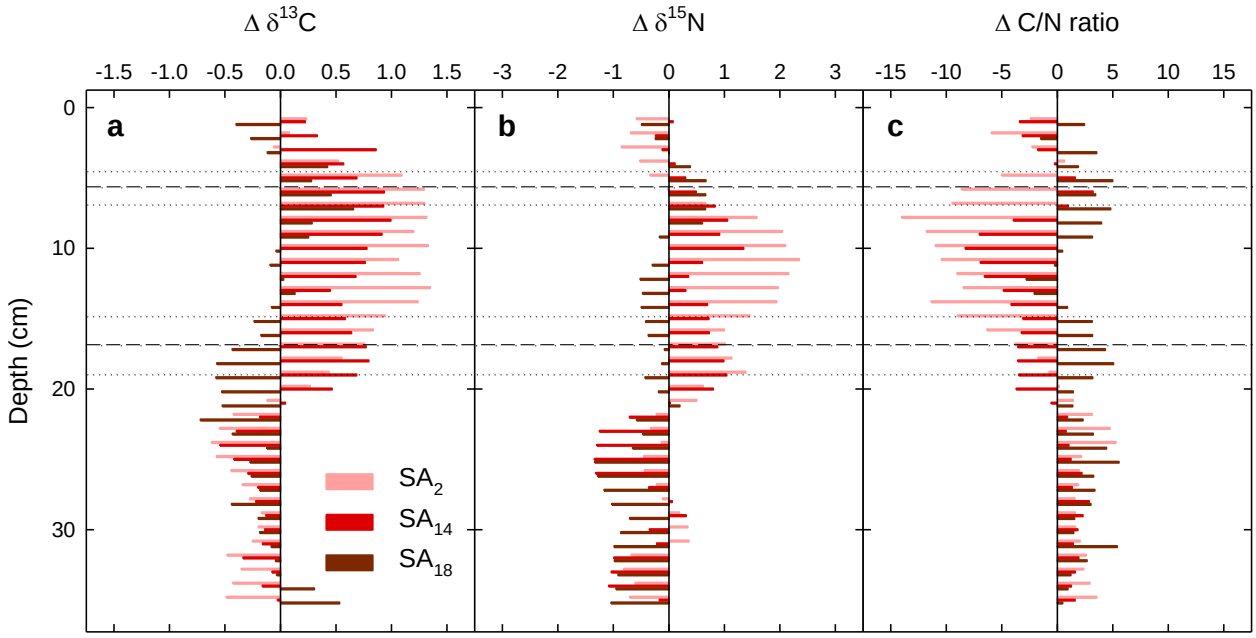

Figure 9: Depth profile distribution of the effect size of snow additions after 2yr (SA_2–CTL_{2008}), 14yr (SA_{14}–CTL_{2008}) and 18yr (SA_{18}–CTL_{2012}) of snow additions on $\delta^{13}C$, $\delta^{15}N$ and the C/N ratio. Each bar represents the difference between depth-specific averages at treatment plots and their corresponding controls. Dashed and dotted lines delimit average soil depths (±SE) corresponding to organic horizon (>20%C; upper section), organic-enriched mineral horizon (5–20 %C; mid-section), and mineral horizon (<5%C; lower section). No detectable treatment effect was detected on $\delta^{13}C$, $\delta^{15}N$ and C/N ratios considering the entire ALT (two-way ANOVA, site effect, $P>0.1$), but there were significant differences between treatment plots and their corresponding controls within the soil section corresponding to the organic-rich mineral layer ($P<0.05$).

At a decadal time-scales however, initial SOC losses were gradually recovered likely by the combined effect of enhanced gross primary productivity matching the observed expansion of deciduous shrubs and suppressed SOC mineralization with long-term snow additions (Fig. 7; Table V). This was supported by lower $\Delta^{14}C$ at SA_{14} relative to CTL_{2008} and SA_2 at ^{137}Cs-equivalent depths (Fig. 8), which indicated the net incorporation of recently fixed C into the soil column at SA_{14} with respect to SA_2 and CTL_{2008}. In agreement with these results, the effect size of deeper winter snow on C/N ratios, $\delta^{13}C$ and $\delta^{15}N$ decreased at SA_{14} and SA_{18} relative to SA_2 suggesting the progressive restoration of the SOM quality within the active layer at decadal time scales consistent with greater productivity and contributions from root-derived C (which in Arctic tussock tundra extend into mineral horizons), and enhanced transport of dissolved organic matter and dissolved inorganic carbon at depth within increasingly saturated soils (Fig. 9) (Loya *et al.*, 2002). Additional results from our experimental site indicate that long-term snow additions stimulated GPP above increases in ecosystem respiration, the reduced C source strength being largely attributed to a constraint of the apparent temperature sensitivity of microbial respiration, as the progressive saturation of the active layer suppressed aerobic decomposition when soil warming would otherwise drive higher rates of SOC mineralization (*see* Chapters 3 and 4) (Blanc-Betes *et al.*, 2016). Moreover, greater N availability under deeper winter snow has been shown to suppress decomposition of relatively recalcitrant C contributing to the stabilization of deep SOC in the long run (Berg, 2000; Schimel *et al.*, 2004; Lavoie *et al.*, 2011; Semenchuk *et al.*, 2015). This is further supported by additional research from our experimental plots showing reduced abundance of genes associated with SOC mineralization after 18 consecutive years of snow additions at our experimental site (Ricketts *et al.*, 2016).

Importantly, while the slow anaerobic metabolism may favor SOC accumulation within increasingly anoxic soils, enhanced methanogenesis with deeper snow may result in a positive climate forcing feedback due to the amplified global warming potential of CH_4 (*see* Chapters 3 and 4) (Myhre *et al.*, 2013; Blanc-Betes *et al.*, 2016). The net climate forcing derived from altered precipitation patterns is therefore contingent upon the form as much as the strength of resulting C emissions (*see* Chapters 3 and 4) (Deng *et al.*, 2014; Blanc-Betes *et al.*, 2016).

Consistent with trends of permafrost warming and thawing recorded across Arctic regions over the last decades (Elberling, 2007; Hayes *et al.*, 2014), our results showed warmer (+0.4±0.1ºC; $P<0.05$) and deeper (+1.9±0.4cm; $P<0.05$) active layer in CTL_{2012} compared to CTL_{2008}, suggesting an ongoing environmental change underlying the snow treatment effect. Thaw-induced consolidation led to a 1.2% compaction of the active layer at CTL_{2102} relative to CTL_{2008}, yielding 0.5±0.1cm subsidence of the ground surface in Arctic tundra (Fig. 7; Table V). Considering physical alterations of the soil column, CTL_{2012} showed an 8% (+2.3±0.6cm; $P<0.05$) increase in the ALT with respect to CTL_{2008} and exposed 0.8±0.1 kgC m^{-2} of additional SOC to decomposition between 2008 and 2012 (Fig. 7; Table V). The mobilization of previously frozen C together with observed warming trends in the area resulted in a 15% loss of SOC at CTL_{2012} relative to CTL_{2008} (Fig. 7; Table V) supporting reports of a recent shift of terrestrial Arctic systems from C sinks to C sources (Hicks Pries *et al.*, 2011; Hayes *et al.*, 2014). Long-term snow additions reduced SOC losses derived from current warming trends at SA_{18} (–4% relative to CTL_{2008}) indicating that predicted increases in snow fall and accumulation could mitigate C losses from Arctic systems (Fig. 7; Table V).

It is important to note that disregarding the physical disturbance of the soil column derived from thaw-induced settlement and consolidation of the active layer underestimated the rate of permafrost thaw by 20–70%, resulting in a 25–65% underestimation of associated increases in recently thawed SOC pools, biases increasing with the intensity of the disturbance. These results imply that permafrost degradation may be occurring at a faster rate than previously anticipated, particularly in areas with subject to greater level of disturbance, and reconcile Arctic system-wide records of recent permafrost warming with reports of an apparent stability of the ALT (Streletskiy *et al.*, 2012; Shiklomanov *et al.*, 2013). Prior studies indicate that the extent of near surface permafrost degradation could differ dramatically as a result of model deficiencies in physical representations (McGuire *et al.*, 2016). We provide evidence that physical distortion due to changes in winter precipitation patterns occur at time and spatial scales well below those resolved in regional and global models (Biesinger *et al.*, 2007), and hence the impacts on SOC vulnerability that directly result from these processes may be underestimated.

2.5 CONCLUSIONS

Predicted increases in winter precipitation accelerated soil warming and permafrost thawing above climate-driven trends in the area of study, and increased the vulnerable SOC pool over time, critically defining the stability of SOC in Arctic tundra in future climate scenarios. We propose that the Arctic tundra SOC budget responded to non-stationary physical and biological processes that unfolded over the course of progressive permafrost degradation, reflecting a non-linear response of SOC pools over time. As such, deeper winter snow led to a fast depletion of the SOC pool at an annual scale and to a gradual recovery of the SOC pool at a decadal time scales, indicating a shift from short-term C source to a long-term C sink that contradicts the previously suggested resistance of the Arctic tundra SOC budget to warming (Lamb *et al.*, 2011;

Sistla *et al.*, 2013). Our results further indicate that enhanced winter precipitation could reduce climate-driven increases of the C source strength of Arctic tundra, thereby playing a relevant role in the regulation of the annual to decadal radiative forcing from Arctic regions. From the intensification of the impacts of deeper snow on permafrost degradation over time, we infer that the system is unlikely to have reached equilibrium. If sustained, enhanced winter precipitation could further impact Arctic tundra C balance towards a new threshold in which new conditions (e.g. enhanced drainage with severe permafrost degradation, substrate quality) may stimulate decomposer activity above primary productivity ultimately offsetting ecosystem C inputs at multi-decadal time scales (Gouttevin *et al.*, 2012; Sistla *et al.*, 2013). Although permafrost degradation and associated increases of the vulnerable SOC pool with deeper snow are widely reported, we note an important underestimation bias with neglections of thaw-induced physical alterations, and an amplification of derived errors with the severity of the disturbance. We suggest that an improved representation of the time-hierarchical response of the Arctic tundra C budget and the physical processes associated with environmental disturbances will probably help reconcile observation- and model-based discrepancies and reduce uncertainties on climate-forcing feedbacks from Arctic systems. Overall, our results show that winter precipitation is a non-trivial driver of the Arctic tundra C budget over time-spans relevant for near-future climate scenarios, adding an important nuance to the well-known coupling between climate warming and SOC dynamics.

2.6 Acknowledgements

We gratefully acknowledge financial support from Department of Energy, Terrestrial Ecosystem Science Program to MAG-M (DE-SC 0006607), the University of Illinois at Chicago, Hadley award (to EB-B), NSF AON grants (0119279 and 0612384 to JMW), the International

Tundra Experiment (ITEX), and the International Polar Year. Special thanks to L. Heraty and J. Rucks for their technical support. Additionally, we would like to thank A. Williams, R Bartolomeo and S. Przybylo for their assistance with sample processing throughout the course of this project. Support from the Toolik Lake Field Station staff is greatly appreciated, as it is the logistical support of CH2MHill Polar Services.

2.7 CITED LITERATURE

Belshe EF, Schuur E a. G, Bolker BM (2013) Tundra ecosystems observed to be CO_2 sources due to differential amplification of the carbon cycle. *Ecology Letters*, **16**, 1307–1315.

Berg B (2000) Litter decomposition and organic matter turnover in northern forest soils. *Forest Ecology and Management*, **133**, 13–22.

Biasi C, Rusalimova O, Meyer H et al. (2005) Temperature-dependent shift from labile to recalcitrant carbon sources of Arctic heterotrophs. *Rapid Communications in Mass Spectrometry*, **19**, 1401–1408.

Biesinger Z, Rastetter EB, Kwiatkowski BL (2007) Hourly and daily models of active layer evolution in Arctic soils. *Ecological Modelling*, **206**, 131–146.

Blanc-Betes E, Welker JM, Sturchio NC, Chanton JP, Gonzalez-Meler MA (2016) Winter precipitation and snow accumulation drive the methane sink or source strength of Arctic tussock tundra. *Global Change Biology*, **22**, 2818–2833.

Bockheim JG, Hinkel KM (2007) The Importance of "Deep" Organic Carbon in Permafrost-Affected Soils of Arctic Alaska. *Soil Science Society of America Journal*, **71**, 1889.

Bockheim JG, Hinkel KM, Nelson FE (2003) Predicting carbon storage in Tundra soils of Arctic Alaska. *Soil Science Society of America journal*, **67**, 948–950.

Boström B, Comstedt D, Ekblad A (2007) Isotope fractionation and 13C enrichment in soil profiles during the decomposition of soil organic matter. *Oecologia*, **153**, 89–98.

Burke EJ, Hartley IP, Jones CD (2012) Uncertainties in the global temperature change caused by carbon release from permafrost thawing. *The Cryosphere*, **6**, 1063–1076.

Cooper LW, Olsen CR, Solomon DK, Larsen IL, Cook RB, Grebmeier JM (1991) Stable Isotopes of Oxygen and Natural and Fallout Radionuclides Used for Tracing Runoff During Snowmelt in an Arctic Watershed. *Water Resources Research*, **27**, 2171–2179.

Crichton KA, Bouttes N, Roche DM, Chappellaz J, Krinner G (2016) Permafrost carbon as a missing link to explain CO_2 changes during the last deglaciation. *Nature Geoscience*, **9**, 683–686.

Deng J, Li C, Frolking S, Zhang Y, Bäckstrand K, Crill P (2014) Assessing effects of permafrost thaw on C fluxes based on multiyear modeling across a permafrost thaw gradient at Stordalen, Sweden. *Biogeosciences*, **11**, 4753–4770.

Deslippe JR, Simard SW (2011) Below-ground carbon transfer among Betula nana may increase with warming in Arctic tundra. *New Phytologist*, **192**, 689–698.

Elberling B (2007) Annual soil CO_2 effluxes in the High Arctic: The role of snow thickness and vegetation type. *Soil Biology and Biochemistry*, **39**, 646–654.

Fan Z, Neff JC, Harden JW et al. (2011) Water and heat transport in boreal soils: Implications for soil response to climate change. *Science of The Total Environment*, **409**, 1836–1842.

Gifford RM, Roderick ML (2003) Soil carbon stocks and bulk density: spatial or cumulative mass coordinates as a basis of expression? *Global Change Biology*, **9**, 1507–1514.

Gomez-Casanovas N, Matamala R, Cook DR, Gonzalez-Meler MA (2012) Net ecosystem exchange modifies the relationship between the autotrophic and heterotrophic components of soil respiration with abiotic factors in prairie grasslands. *Global Change Biology*, **18**, 2532–2545.

Gouttevin I, Menegoz M, Dominé F et al. (2012) How the insulating properties of snow affect soil carbon distribution in the continental pan-Arctic area. *Journal of Geophysical Research: Biogeosciences*, **117**, G02020.

Harden JW, Fuller CC, Wilmking M, Myers-Smith I, Trumbore SE, Bubier J (2008) The Fate of Terrestrial Carbon Following Permafrost Degradation: Detecting Changes Over Recent Decades. *Proceedings of Ninth International Conference on Permafrost*, 649–654.

Hayes DJ, Kicklighter DW, McGuire AD et al. (2014) The impacts of recent permafrost thaw on land–atmosphere greenhouse gas exchange. *Environmental Research Letters*, **9**, 045005.

Heuscher SA, Brandt CC, Jardine PM (2005) Using soil physical and chemical properties to estimate bulk density. *Soil Science Society of America Journal*, **69**, 51–56.

Hicks Pries CE, Schuur EAG, Crummer KG (2011) Holocene Carbon Stocks and Carbon Accumulation Rates Altered in Soils Undergoing Permafrost Thaw. *Ecosystems*, **15**, 162–173.

Hicks Pries CE, Schuur EAG, Natali SM, Crummer KG (2016) Old soil carbon losses increase with ecosystem respiration in experimentally thawed tundra. *Nature Climate Change*, **6**, 214–218.

Hobbie EA, Ouimette AP (2009) Controls of nitrogen isotope patterns in soil profiles. *Biogeochemistry*, **95**, 355–371.

Hodgkins SB, Tfaily MM, McCalley CK et al. (2014) Changes in peat chemistry associated with permafrost thaw increase greenhouse gas production. *Proceedings of the National Academy of Sciences*, 201314641.

Hua Q, Barbetti M, Rakowski AZ (2013) Atmospheric radiocarbon for the period 1950–2010. *Radiocarbon*, **55**, 2059–2072.

Johansson M, Callaghan TV, Bosiö J, Åkerman HJ, Jackowicz-Korczynski M, Christensen TR (2013) Rapid responses of permafrost and vegetation to experimentally increased snow cover in sub-arctic Sweden. *Environmental Research Letters*, **8**, 035025.

Jones MH, Fahnestock JT, Walker DA, Walker MD, Welker JM (1998) Carbon dioxide fluxes in moist and dry Arctic tundra during the snow-free season: responses to increases in summer temperature and winter snow accumulation. *Arctic and alpine research*, 373–380.

Jorgenson MT, Shur YL, Pullman ER (2006) Abrupt increase in permafrost degradation in Arctic Alaska. *Geophysical Research Letters*, **33**, L02503.

Kattsov VM, Källén E, Cattle HP et al. (2005) Future climate change: modeling and scenarios for the Arctic. In: *Arctic Climate Impact Assessment (ACIA)*. Cambridge University Press, Cambridge, UK, pp. 99–150.

Kimble JM, Follett RF, Stewart BA (2000) *Assessment Methods for Soil Carbon*. CRC Press, 698 pp.

Klaminder J, Yoo K, Giesler R (2009) Soil carbon accumulation in the dry tundra: Important role played by precipitation. *Journal of Geophysical Research: Biogeosciences*, **114**, G04005.

Klaminder J, Yoo K, Olid C, Ramebäck H, Vesterlund A (2014) Using Short-lived Radionuclides to Estimate Rates of Soil Motion in Frost Boils. *Permafrost and Periglacial Processes*, **25**, 184–193.

Koven CD, Riley WJ, Stern A (2012) Analysis of Permafrost Thermal Dynamics and Response to Climate Change in the CMIP5 Earth System Models. *Journal of Climate*, **26**, 1877–1900.

Kuhry P, Vitt DH (1996) Fossil Carbon/Nitrogen Ratios as a Measure of Peat Decomposition. *Ecology*, **77**, 271–275.

Lamb EG, Han S, Lanoil BD, Henry GHR, Brummell ME, Banerjee S, Siciliano SD (2011) A High Arctic soil ecosystem resists long-term environmental manipulations. *Global Change Biology*, **17**, 3187–3194.

Lavoie M, Mack MC, Schuur E a. G (2011) Effects of elevated nitrogen and temperature on carbon and nitrogen dynamics in Alaskan Arctic and boreal soils. *Journal of Geophysical Research: Biogeosciences*, **116**, G03013.

Lawrence DM, Slater AG (2010) The contribution of snow condition trends to future ground climate. *Climate Dynamics*, **34**, 969–981.

Lee J, Hopmans JW, Rolston DE, Baer SG, Six J (2009) Determining soil carbon stock changes: Simple bulk density corrections fail. *Agriculture, Ecosystems & Environment*, **134**, 251–256.

Leffler AJ, Klein ES, Oberbauer SF, Welker JM (2016) Coupled long-term summer warming and deeper snow alters species composition and stimulates gross primary productivity in tussock tundra. *Oecologia*, **181**, 287–297.

Loya WM, Johnson LC, Kling GW, King JY, Reeburgh WS, Nadelhoffer KJ (2002) Pulse-labeling studies of carbon cycling in Arctic tundra ecosystems: Contribution of photosynthates to soil organic matter. *Global Biogeochemical Cycles*, **16**, 1101.

Mackelprang R, Waldrop MP, DeAngelis KM et al. (2011) Metagenomic analysis of a permafrost microbial community reveals a rapid response to thaw. *Nature*, **480**, 368–371.

McGuire AD, Koven C, Lawrence DM et al. (2016) Variability in the sensitivity among model simulations of permafrost and carbon dynamics in the permafrost region between 1960 and 2009. *Global Biogeochemical Cycles*, 2016GB005405.

Michaelson GJ, Ping CL (2003) Soil organic carbon and CO_2 respiration at subzero temperature in soils of Arctic Alaska. *Journal of Geophysical Research: Atmospheres*, **108**, 8164.

Michaelson GJ, Ping CL, Kimble JM (1996) Carbon Storage and Distribution in Tundra Soils of Arctic Alaska, U.S.A. *Arctic and Alpine Research*, **28**, 414–424.

Myhre G, Shindell D, Bréon FM et al. (2013) Anthropogenic and natural radiative forcing. *Climate change*, 658–740.

Natali SM, Schuur E a. G, Trucco C, Hicks Pries CE, Crummer KG, Baron Lopez AF (2011) Effects of experimental warming of air, soil and permafrost on carbon balance in Alaskan tundra. *Global Change Biology*, **17**, 1394–1407.

Natali SM, Schuur EAG, Webb EE, Pries CEH, Crummer KG (2014) Permafrost degradation stimulates carbon loss from experimentally warmed tundra. *Ecology*, **95**, 602–608.

Nobrega S, Grogan P (2007) Deeper Snow Enhances Winter Respiration from Both Plant-associated and Bulk Soil Carbon Pools in Birch Hummock Tundra. *Ecosystems*, **10**, 419–431.

Nowinski NS, Taneva L, Trumbore SE, Welker JM (2010) Decomposition of old organic matter as a result of deeper active layers in a snow depth manipulation experiment. *Oecologia*, **163**, 785–792.

Oechel WC, Laskowski CA, Burba G, Gioli B, Kalhori AAM (2014) Annual patterns and budget of CO_2 flux in an Arctic tussock tundra ecosystem. *Journal of Geophysical Research: Biogeosciences*, **119**, 2013JG002431.

Osterkamp TE (2007) Causes of warming and thawing permafrost in Alaska. *Eos, Transactions American Geophysical Union*, **88**, 522–523.

Osterkamp TE, Jorgenson MT, Schuur E a. G, Shur YL, Kanevskiy MZ, Vogel JG, Tumskoy VE (2009) Physical and ecological changes associated with warming permafrost and thermokarst in Interior Alaska. *Permafrost and Periglacial Processes*, **20**, 235–256.

Pattison RR, Welker JM (2014) Differential ecophysiological response of deciduous shrubs and a graminoid to long-term experimental snow reductions and additions in moist acidic tundra, Northern Alaska. *Oecologia*, **174**, 339–350.

Piñeiro G, Perelman S, Guerschman JP, Paruelo JM (2008) How to evaluate models: Observed vs. predicted or predicted vs. observed? *Ecological Modelling*, **216**, 316–322.

Ping CL, Michaelson GJ, Kimble JM (1997) Carbon storage along a latitudinal transect in Alaska. *Nutrient Cycling in Agroecosystems*, **49**, 235–242.

Ricketts MP, Poretsky RS, Welker JM, Gonzalez-Meler MA (2016) Soil bacterial community and functional shifts in response to altered snowpack in moist acidic tundra of northern Alaska. *SOIL*, **2**, 459–474.

Ruehlmann J, Körschens M (2009) Calculating the effect of soil organic matter concentration on soil bulk density. *Soil Science Society of America Journal*, **73**, 876–885.

Saini GR (1966) Organic Matter as a Measure of Bulk Density of Soil. *Nature*, **210**, 1295–1296.

Schaefer K, Lantuit H, Romanovsky VE, Schuur EAG, Witt R (2014) The impact of the permafrost carbon feedback on global climate. *Environmental Research Letters*, **9**, 085003.

Schimel JP, Bilbrough C, Welker JM (2004) Increased snow depth affects microbial activity and nitrogen mineralization in two Arctic tundra communities. *Soil Biology and Biochemistry*, **36**, 217–227.

Schuur E a. G, Abbott BW, Bowden WB et al. (2013) Expert assessment of vulnerability of permafrost carbon to climate change. *Climatic Change*, **119**, 359–374.

Semenchuk PR, Elberling B, Amtorp C, Winkler J, Rumpf S, Michelsen A, Cooper EJ (2015) Deeper snow alters soil nutrient availability and leaf nutrient status in high Arctic tundra. *Biogeochemistry*, **124**, 81–94.

Shiklomanov NI, Streletskiy DA, Little JD, Nelson FE (2013) Isotropic thaw subsidence in undisturbed permafrost landscapes. *Geophysical Research Letters*, **40**, 2013GL058295.

Sistla SA, Moore JC, Simpson RT, Gough L, Shaver GR, Schimel JP (2013) Long-term warming restructures Arctic tundra without changing net soil carbon storage. *Nature*, **497**, 615–618.

Staunton S, Dumat C, Zsolnay A (2002) Possible role of organic matter in radiocaesium adsorption in soils. *Journal of Environmental Radioactivity*, **58**, 163–173.

Steller RM, Jelinski NA, Kucharik CJ (2008) Developing models to predict soil bulk density in southern Wisconsin using soil chemical properties. *J Int Biosci*, **6**, 53–63.

Streletskiy DA, Shiklomanov NI, Nelson FE (2012) Spatial variability of permafrost active-layer thickness under contemporary and projected climate in Northern Alaska. *Polar Geography*, **35**, 95–116.

Sturm M, Schimel J, Michaelson G et al. (2005) Winter Biological Processes Could Help Convert Arctic Tundra to Shrubland. *BioScience*, **55**, 17–26.

Subin ZM, Koven CD, Riley WJ, Torn MS, Lawrence DM, Swenson SC (2013) Effects of Soil Moisture on the Responses of Soil Temperatures to Climate Change in Cold Regions. *Journal of Climate*, **26**, 3139–3158.

Vogel JS, Southon JR, Nelson DE, Brown TA (1984) Performance of catalytically condensed carbon for use in accelerator mass spectrometry. *Nuclear Instruments and Methods in Physics Research Section B: Beam Interactions with Materials and Atoms*, **5**, 289–293.

Wahren C-H, Walker MD, Bret-Harte MS (2005) Vegetation responses in Alaskan Arctic tundra after 8 years of a summer warming and winter snow manipulation experiment. *Global Change Biology*, **11**, 537–552.

Waldrop MP, Wickland KP, White Iii R, Berhe AA, Harden JW, Romanovsky VE (2010) Molecular investigations into a globally important carbon pool: permafrost-protected carbon in Alaskan soils. *Global Change Biology*, **16**, 2543–2554.

Walker MD, Walker DA, Auerbach NA (1994) Plant Communities of a Tussock Tundra Landscape in the Brooks Range Foothills, Alaska. *Journal of Vegetation Science*, **5**, 843–866.

Walker MD, Walker DA, Welker JM et al. (1999) Long-term experimental manipulation of winter snow regime and summer temperature in Arctic and alpine tundra. *Hydrological Processes*, **13**, 2315–2330.

Welker JM, Fahnestock JT, Jones MH (2000) Annual CO_2 Flux in Dry and Moist Arctic Tundra: Field Responses to Increases in Summer Temperatures and Winter Snow Depth. *Climatic Change*, **44**, 139–150.

Wendt JW, Hauser S (2013) An equivalent soil mass procedure for monitoring soil organic carbon in multiple soil layers. *European Journal of Soil Science*, **64**, 58–65.

White DJ, Take WA, Bolton MD (2003) Soil deformation measurement using particle image velocimetry (PIV) and photogrammetry. *Geotechnique*, **53**, 619–632.

Wild B, Schnecker J, Alves RJE et al. (2014) Input of easily available organic C and N stimulates microbial decomposition of soil organic matter in Arctic permafrost soil. *Soil Biology and Biochemistry*, **75**, 143–151.

Xue K, M. Yuan M, J. Shi Z et al. (2016) Tundra soil carbon is vulnerable to rapid microbial decomposition under climate warming. *Nature Climate Change*, **6**, 595–600.

3. DEEPER WINTER SNOW REDUCES ECOSYSTEM CARBON LOSSES BUT INCREASES THE GLOBAL WARMING POTENTIAL OF ARCTIC TUSSOCK TUNDRA OVER THE GROWING SEASON

3.1 ABSTRACT

Projected changes in winter precipitation accompanying future warming may lead to major climate/C-cycle feedbacks from Arctic regions. However, the sign, magnitude and form (CO_2 and CH_4) of C fluxes and derived climate forcing (i.e. GWP, global warming potential) from Arctic tundra under future precipitation scenarios remain unresolved. We investigated how 18-yrs of experimental snow depth increases and decreases affects ecosystem C fluxes and modulates the GWP of moist acidic tundra over the growing season. The response of Arctic tundra C fluxes to deeper winter snow was markedly non-linear. Both reduced- (RS, –15–30%) and increased- (MS, +20–45%; HS, +70–100%) winter snow decreased the Arctic tundra CO_2 source strength relative to Ambient, reducing net ecosystem C losses over the growing season. Decreases in the ecosystem CO_2 source strength responded mostly to constraints on SOC mineralization (R_{het}), by temperature limitation within colder soils at RS and by snow- and thaw-induced increases in soil moisture that promoted the anaerobic metabolism and dampened the temperature sensitivity of R_{het} at MS and HS, with thaw-induced changes in SOC availability and decomposability likely exerting a secondary control. However, enhanced CH_4 emissions within wetter soils increased the GWP of Arctic tundra at MS and HS despite observed decreases in Arctic tundra C losses. Notably, our results suggest certain resistance of the net ecosystem productivity to long-term alterations of snow accumulation regimes, and that this resistance responds to metabolic adjustments at the canopy level mediated by shifts in plant community structure rather than by the acclimation of physiological processes. Our results indicate that projected precipitation scenarios in Arctic regions will largely determine the Arctic tundra C

budget and critically shape climate/C-cycle forcing feedbacks from Arctic regions.

3.2 INTRODUCTION

Permanently frozen soils (permafrost) contain up to 50% of the global terrestrial soil organic carbon (SOC) (Hugelius *et al.*, 2014). Current and projected Arctic warming and associated changes in precipitation are likely to increase the vulnerability of permafrost C but the magnitude, direction and form (CO_2 and CH_4) of climate/carbon-cycle feedbacks from Arctic regions remain uncertain (Burke *et al.*, 2012a; Fisher *et al.*, 2014; Schaefer *et al.*, 2014; Schuur *et al.*, 2015).

Climate models robustly predict 25–50% more precipitation in Arctic regions by the end of the century, mostly as fall and winter snowfall (Kattsov *et al.*, 2005; Zhang *et al.*, 2013; Bintanja & Selten, 2014). However, spatial heterogeneity is expected, with some areas experiencing snow accumulation beyond predictions and others receiving less snow than current values (Callaghan *et al.*, 2011; Stocker *et al.*, 2013). Deeper snow promotes soil warming directly through the insulating effect of snow over the snow-covered season (Leffler & Welker, 2013; Pattison & Welker, 2014), and indirectly over the growing season through enhanced soil thermal conductivity and latent heat with snow- and thaw-induced increases in soil moisture (Fig. 1) (Qian et al., 2011; Subin et al., 2013; Zhang et al., 2013; Yi et al., 2015). Associated thermal and hydrological changes result in cascading effects on permafrost degradation (Osterkamp et al., 2009; Fan et al., 2011; Yi et al., 2015), soil C and N mineralization (Schimel *et al.*, 2004) and plant community structure, phenology and productivity (Welker *et al.*, 2000; Leffler *et al.*, 2016), critically shaping the ecosystem C balance in Arctic tundra under future climate scenarios (Fig. 1) (Cassidy *et al.*, 2015; Blanc-Betes *et al.*, 2016; Zona *et al.*, 2016). The potential magnitude of derived climate/C-cycle feedbacks suggests that projected changes in

winter precipitation may be as relevant climate forcing elements as climate warming in Arctic regions (Carvalhais *et al.*, 2014; Yi *et al.*, 2015; Blanc-Betes *et al.*, 2016).

Predictions of climate/C-cycle feedbacks from Arctic systems under future climate scenarios build on two major competing processes. Warmer soils and thaw-induced increases in SOC availability under deeper snow may accelerate SOC decomposition and hence ecosystem respiration, resulting in a positive feedback to climate change (Schaefer *et al.*, 2011; Mishra & Riley, 2012; Xue *et al.*, 2016). In turn, enhanced mineralization could increase nutrient availability and stimulate shrub expansion and plant productivity, partly compensating or offsetting ecosystem C losses (Elmendorf *et al.*, 2012a; DeMarco *et al.*, 2014; Salmon *et al.*, 2016).

Much effort has been invested into investigating the impacts of changes in precipitation on the C balance of tundra ecosystems within this conceptual framework. However, results are inconclusive. Experimental manipulations with snow accumulation, and soil warming and/or nutrient additions consistent with deeper snow have shown enhancing, constraining and neutral effects on microbial activity (Buckeridge & Grogan, 2008; Brooks *et al.*, 2011; Lamb *et al.*, 2011; Ricketts *et al.*, 2016; Semenchuk *et al.*, 2016), nutrient assimilation and uptake (Shaver *et al.*, 2001; Craine *et al.*, 2009; Natali *et al.*, 2012; Pattison & Welker, 2014; Semenchuk *et al.*, 2015; Leffler *et al.*, 2016) and physiological responses of the supported vegetation (Heskel *et al.*, 2012; Leffler & Welker, 2013; Weg *et al.*, 2013; Leffler *et al.*, 2016). Discrepancies persist at the ecosystem level, with the CO_2 sink or source strength of both Arctic and subarctic tussock tundra displaying an equally wide array of responses (Welker *et al.*, 2000; Natali *et al.*, 2011; Lund *et al.*, 2012; Li *et al.*, 2014; Abbott *et al.*, 2016; Leffler *et al.*, 2016).

The robustness of predictions of climate/C-cycle feedbacks from Arctic tundra is particularly sensitive to snow accumulation, as enhanced soil wetness, by reducing the proportion of aerobic to anaerobic decomposition slows down SOC mineralization but increases CH_4 emissions (Blanc-Betes *et al.*, 2016). Given the disproportional contributions of CO_2 and CH_4 to the global warming potential (GWP) of ecosystem C fluxes (33 CO_2-eq; Shindell et al., 2009; Myhre et al., 2013), snow- and thaw-induced changes in soil hydrology may introduce to up to 50% divergence in model predictions of the resulting radiative forcing (McGuire *et al.*, 2012; Schneider von Deimling *et al.*, 2012; Lawrence *et al.*, 2015).

The complexity of Arctic tundra responses to changes in climate lies largely on the fact that the ecosystem C balance results from the integration of all contributing processes (i.e. ecosystem productivity, auto- and heterotrophic respiration, and net ecosystem CH_4 fluxes), which may differ in lag-times and sensitivities to disturbances (Weg *et al.*, 2013). As such, there is growing evidence of non-linearity in the response of Arctic C dynamics to changes in the environment over time, where long-term (decades or longer) impacts differ from or even oppose short-term (years) impacts (Mack *et al.*, 2004; Weg *et al.*, 2013; Semenchuk *et al.*, 2016). For example, although warmer soils under deeper winter snow may initially accelerate SOC decomposition rates (Morgner *et al.*, 2010; Nowinski *et al.*, 2010; Xue *et al.*, 2016), SOC losses may decrease over time (*see* Chapter 2). The decline of the labile C pool (Semenchuk *et al.*, 2016), the greater recalcitrance of litter inputs with transitions towards shrub-dominated communities (Hobbie, 1996; Cornelissen *et al.*, 2007), the thermal acclimation and adaptation of microbial communities and plant respiration with persistent soil warming (Craine *et al.*, 2012; McLaughlin *et al.*, 2014; Wallenstein, 2014), and the development of anoxic soils (Blanc-Betes *et al.*, 2016) are some of the mechanisms suggested to contribute to the long-term attenuation of

the ecosystem C source strength. In addition, previous studies have also reported a non-linear response of the Arctic tundra C balance to level warming (Sharp *et al.*, 2013) or nutrient additions (Arens *et al.*, 2008) consistent with deeper winter snow. Together, these observations suggest that the impacts of changes in winter precipitation on Arctic tundra C dynamics may be contingent upon the duration and intensity of the disturbance (*see* Chapter 2).

Here we investigated the mechanisms underlying the long-term responses (decadal or longer) of the ecosystem C sink or source strength and associated climate forcing from Arctic tundra to projected changes in winter precipitation. We combined periodic measurements of ecosystem, soil and heterotrophic CO_2 fluxes over the growing season with seasonal ecosystem CH_4 budgets from Arctic tussock tundra after 18 years of multi-level snow depth increases and decreases. We coupled alterations of the soil environment and plant community structure to examine causality in the observed changes, and used plot and period specific response curves to develop empirical models to estimate growing season C budgets and GWP from Arctic tundra in response to different levels of disturbance. We hypothesized that a deeper and warmer active layer would result in increases in SOC decomposition, but that C losses would be partly or fully compensated by increases in gross primary productivity associated with greater abundance of woody species. We further anticipated that enhanced CH_4 emissions from increasingly wetter soils with deeper winter snow would strongly influence the radiative forcing of C emissions from our moist tussock tundra site in northern Alaska, representative of 40% of the Alaskan tundra and 20% of the Arctic tundra, globally (Walker et al., 2005; Forbes, 2015).

3.3 METHODS

3.3.1 Site description

The research was conducted in moist acidic tussock tundra near Toolik Lake (68°38'N, 149°38'W; 760 m) at the long-term US ITEX (International Tundra Experiment) in the northern foothills of the Brooks Range, Alaska (Fig. 2) (Walker *et al.*, 1999). Annual air temperature averages –8°C, with monthly mean summer temperatures ranging from 7 to 12°C. Mean annual precipitation is 350 mm, with approximately 50% falling during winter as snow (Deslippe & Simard, 2011). Winter snow accumulation is typically 45–80 cm, and the area becomes snow-free by late-May setting the beginning of the growing season. Soils are classified as coarse-loamy, mixed, acidic, Ruptic-Histic Pergelic Cryaquept (Romanovsky et al., 2011). The experimental area is characterized by poorly drained soils and shallow organic horizons (10–15cm). The active layer typically reaches a maximum thaw depth of 45–50 cm by the end of August. The vegetation is dominated by tussock forming sedges (*Eriophorum vaginatum*) and mosses (*Sphagnum spp.*, *Hylocomium splendens*), with scattered distribution of deciduous (*Betula nana, Salix pulchra*) and evergreen shrubs (*Cassiope tetragona*, *Ledum Palustra*) (Walker *et al.*, 1994; Wahren *et al.*, 2005).

3.3.2 Experimental design

The experimental 2.8 x 60 m snow fence was installed in 1994 perpendicular to prevailing winter winds to create a snow drift that extends 60 m downwind (Walker *et al.*, 1999). In 2012, we established five sampling plots in each of the following distinct snow accumulation regimes (n=5): i) ambient snow accumulation (Ambient), ii) Medium Snow addition (MS) with 20–45% more snow than Ambient, iii) High Snow addition (HS) with 70–100% more snow than Ambient, and iv) Reduce Snow (RS) with 15–30% less snow than Ambient (Jones *et al.*, 1998;

Walker *et al.*, 1999; Pattison & Welker, 2014). The onset of the growing season was delayed by 5–7 days at MS and 15–20 days at HS compared to Ambient, whereas RS becomes snow-free 3–5 days before Ambient.

Measurements of ecosystem, soil and heterotrophic CO_2 fluxes and soil environmental variables (i.e. soil temperature and moisture, and thawing depth) were taken at biweekly intervals from May 30 to Aug 31, 2012, adding a total of six sampling periods. At each sampling period, measurements were made between 10 am and 3 pm over 3 days. To minimize potential confounding effects from day to day variability, measurements were randomly alternated among plots. To minimize disturbance, plots were accessed from permanently installed boardwalks.

3.3.3 Microclimate measurements

Hourly Photosynthetically Active Radiation (PAR) and air temperature data, were obtained from the micrometeorological station located 500 m from our site (Arctic LTER, Toolik Lake Field Station; http://www.lternet.edu/sites/arc). Point PAR and air temperature measurements were collected daily at the experimental site and agreed well with climate readings from the meteorological station (r^2=98.6; P<0.05).

Soil temperature (10 cm depth) was measured continuously (0.5 h intervals) over the growing season in each treatment using iButton temperature dataloggers to a precision of ±0.5°C (Maxim Integrated Products, Sunnyvale, CA, USA) (n=3). In addition, during each sampling session, handheld sensors were used to measure soil temperature (10 cm depth; OMEGA Engineering Inc., CT, USA) and 0–12 cm depth-integrated volumetric water content (HydroSense II, Campbell Scientific Inc., UT, USA), and thaw depth was measured using a metal depth rod. Replicates (n=5) were averaged values of 8 point measurements per plot and sampling session.

3.3.4 Vegetation cover characterization

Vegetation cover was characterized at each treatment (n=5) with a 100-point 0.7 x 0.7 m frame following methods described by Walker (1996). Plant species, litter and standing dead biomass, and canopy height were recorded for each point measurement. These point-frame data provided percentage cover estimates for the most common species comprising more than 80% of biomass of Alaskan tussock tundra. Vegetation cover characterization was conducted at the peak of the growing season, between late July (RS, Ambient and MS treatments) and early August (HS treatment).

3.3.5 Ecosystem CO_2 flux measurements

Net ecosystem CO_2 exchange (NEE) represents the balance between gross primary productivity (GPP) and ecosystem respiration (R_{eco}). Each of these components was directly measured (NEE, R_{eco}) or indirectly estimated (GPP) at all treatments over the growing season.

Midday NEE was measured following procedures described in Shaver *et al.*, (2007). Briefly, we used a Li-6400 (Li-Cor Inc, Lincoln, NE, USA) fitted to a custom-designed 0.7x0.7x0.4 m clear acrylic chamber equipped with temperature and PAR sensors, and two internal chamber fans. At each plot and sampling period, we conducted a light response curve of NEE with six point NEE measurements corresponding to full ambient light, four levels of shade (ca. 15%, 30%, 50% and 70%), and one dark chamber measurement of R_{eco}. The chamber volume was corrected for plot-level microtopography by measuring the distance between ground level and the base over a 100-point 0.7x0.7 m grid.

NEE is intrinsically linked to a given set of environmental conditions (i.e. air temperature and PAR) that may vary between measurements. To allow inter-comparison of CO_2 exchange between treatments and sampling periods excluding differences associated to environmental

conditions we generated plot- and period-specific light response curves by fitting rectangular hyperbolas to measured values of NEE and PAR using Sigmaplot v10 (Systat, Richmond, CA, USA).

(Eq. 3.1) $$NEE = \hat{R}_{eco} + \frac{Amax \times I}{Ks+I}$$

where $\hat{R}_{eco}$ is a fitted estimate of R_{eco} (μmol CO_2 m^{-2} s^{-1}), A_{max} is the rate of light-saturated photosynthesis (μmol CO_2 m^{-2} s^{-1}), K_s is the half-saturation constant (μmol photons m^{-2} s^{-1}), and I is the incident PAR (μmol photons m^{-2} s^{-1}) (Williams *et al.*, 2006; Shaver *et al.*, 2007; Street *et al.*, 2007). The goodness-of-fit fit of the rectangular hyperbola was evaluated using the coefficient of determination (r^2) of each the light-response curve. Data with r^2 below the 95% confidence limit (r^2<0.80) were rejected (< 3% of the data).

Midday NEE fluxes were then normalized to 600 μmol photons m^{-2} s^{-2} (i.e. NEE_{600}) using treatment- and period-specific fitted photosynthetic parameters (A_{max} and K_s). Normalized GPP (GPP_{600}) was calculated as the difference between NEE_{600} and R_{eco} values (GPP_{600} = NEE_{600} – R_{eco}). The accuracy of NEE and GPP standardizations is contingent upon the fitness of model-fitted parameters. Therefore, derived errors were further examined by regressing predicted against observed NEE from randomly selected measurements excluded from model parameterizations. The strong linear relationship (r^2=0.96; *P*<0.0001) and negligible deviations from the 1:1 line (slope=0.97±0.1; intercept=–0.09±0.08) indicated the robustness of model-fitted parameters. Similarly, model-fitted $\hat{R}_{eco}$ and observed R_{eco} showed no evidence of a bias (r^2=0.99, *P*<0.001).

3.3.6 Effective leaf area index

Effective leaf area index (i.e. Effective LAI) was estimated from the linear relationship that describes GPP_{600} as a function of leaf area index developed by Street *et al.* (2007) for moist acidic tussock tundra near the area of study (slope=6.7842; intercept=0.732).

3.3.7 Soil and heterotrophic respiration measurements

Soil CO_2 fluxes were measured with a Li-6400 infrared gas analyzer equipped with a 6400-09 soil flux chamber (Li-Cor Inc, Lincoln, NE, USA). At each plot and sampling period, soil respiration (R_{soil}) was measured from PVC collars (10 cm diameter) inserted into the soil to the average depth of the Oe horizon (5–7 cm depth) upon snowmelt (n=5). Measurements of R_{soil} were conducted two weeks after insertion to minimize the impact of disturbance.

At each sampling period, heterotrophic respiration (R_{het}) was measured using the root exclusion method. Root exclusion PVC collars (50-cm long) were installed by late Aug in 2011 (before the first snow of the previous year) (n=3). We note that root exclusions for R_{het} are problematic (Hopkins *et al.*, 2013) but the large amount of SOC and relative low root density are likely to minimize the impacts of rhizosphere on R_{het} when compared to other ecosystems (Chen *et al.*, 2013). All soil CO_2 fluxes were calculated considering chamber volume corrections accounting for plot specific depths of insertion. Replicates are averaged values of 2 pseudo-replicates of three cycles each (30 and 10 μmol mol^{-1} for R_{soil} and R_{het} measurements respectively) per plot.

3.3.8 Modeling seasonal gross primary productivity, ecosystem respiration and net ecosystem exchange.

Seasonal ecosystem CO_2 fluxes (GPP, R_{eco} and NEE) at each treatment were estimated from gap filling methods considering response functions to environmental factors (PAR and atmospheric temperature). Previous studies show that model parameterizations with midday values accurately predict daily CO_2 fluxes in Arctic systems (Sharp *et al.*, 2013). Therefore, we used midday model-fitted parameters to estimate seasonal NEE using the Photosynthetic Irradiance-Response and Temperature-sensitive respiration model (PIRT model; Williams et al., 2006). The PIRT model is a two-term algorithm that integrates ecosystem photosynthetic irradiance-response (i.e. GPP') and develops the R_{eco} term as a function of the ecosystem respiration-temperature response (i.e. R'_{eco}) (*Supp. Info.* 3.9.1).

We estimated hourly GPP' by fitting the photosynthetic irradiance-response term to daily treatment-specific model-fitted parameters ($Amax_d$ and Ks_d), and PAR hourly records.

(Eq. 3.2) $$GPP' = \frac{Amax_d \times I}{Ks_d + I}$$

To integrate phenology that may be cause of divergence in the photosynthetic response among treatments, we used mean A_{max} and K_s at each treatment and sampling period (n=5) to calculate mean quantum efficiency (E_0; μmol CO_2 μmol^{-1} PAR) using the following equation (Street *et al.*, 2007):

(Eq. 3.3) $$E_0 = \frac{Amax}{Ks}$$

Then, daily A_{max} ($Amax_d$) was calculated by linearly interpolating between sampling periods, and daily Ks (Ks_d) was calculated assuming constant E_0 over the interpolated period. The uncertainty associated to each individual curve fit for A_{max} and K_s was propagated within treatment and over time, and therefore the error term integrated both model fitness and spatial heterogeneity.

Alternative models estimate GPP' using an adaptation of the aggregated canopy photosynthesis model that considers the hyperbolic photosynthesis-light equation at the leaf level and light extinction through the canopy to reflect the seasonality of plant development (Shaver *et al.*, 2007; Ives *et al.*, 2013; Sharp *et al.*, 2013). To gauge confidence in our predictions, we tested for discrepancies between both model predictions (*Supp. Info.* 3.9.2). The strong agreement between model estimates (r^2=0.97, *P*<0.0001; slope=0.93, intercept=0.4) suggested that the photosynthetic irradiance-response term of the PIRT model was a useful tool for predicting GPP, and that the interpolation of period-specific parameterizations successfully integrated seasonality in our model outputs (*Supp. Info.* 3.9.2).

We estimated hourly R'_{eco} by fitting the ecosystem respiration-temperature response to treatment-specific parameterizations of the exponential regression that describes the temperature sensitivity of R_{eco} and hourly records of air temperature (Vogel *et al.*, 2009; Natali *et al.*, 2011).

(Eq. 3.4) $$R'_{eco} = R_b \times e^{\beta T_{air}}$$

where R'_{eco} is the modeled estimate of R_{eco} (μmol CO_2 m^{-2} s^{-1}), R_b represents basal ecosystem respiration (i.e. μmol CO_2 m^{-2} s^{-1} at 0°C), and β quantifies the relative increase in R_{eco} with air temperature, T_{air} (1/°C).

We used dark chamber measurements and corresponding air temperature values to determine treatment-specific R_b and β. The regression of predicted against observed R_{eco} values of two randomly selected measurements per plot and sampling period excluded from model parameterizations revealed unbiased relationships at all treatments (r^2=0.83, *P*<0.0001; slope=1.01±0.1, intercept=0.5±0.7) (*Supp. Info.* 3.9.1).

Hourly GPP' and R'_{eco} were combined to estimate hourly NEE (i.e. hourly NEE') for each treatment (*Supp. Info.* 3.9.1).

(Eq. 3.5) $$NEE' = \left[R_b \times e^{\beta T_{air}}\right] + \frac{Amax \times I}{Ks+I}$$

Hourly estimates were summed to calculate daily and seasonal GPP', R'_{eco} and NEE' for each treatment.

3.3.9 Modeling soil, heterotrophic and autotrophic respiration

Daily values of soil respiration (R'_{soil}) at each treatment were estimated by linearly interpolating R_{soil} between sampling periods. Previous research showed high performance of linear interpolation methods for R_{soil} records with low sampling frequency (Gomez-Casanovas *et al.*, 2013). Alternatively, to evaluate the robustness of our estimates, we applied gap filling methods considering the temperature sensitivity of R_{soil}. Results from treatment-specific temperature-dependent functions showed good agreement with linearly interpolated values (r^2=0.92; *P*<0.0001) (*Supp. Info.* 3.9.3). Therefore, linear interpolation was used to avoid additional self-correlation with other variables using temperature-dependent model estimates. Daily estimates were summed to calculate seasonal R'_{soil} at each treatment.

Given the strong correlation of R_{het} with changes in soil temperature (Table IX), daily values of R_{het} at each treatment were estimated from treatment-specific temperature-dependent functions:

(Eq. 3.6) $$R'_{het} = R_0 \times e^{\varphi T_{soil}}$$

where R'_{het} is a temperature-dependent estimate of R_{het}, R_0 represents basal heterotrophic respiration (μmol CO_2 m^{-2} s^{-1} at 0°C), and φ quantifies the relative increase in R_{het} with soil temperature, T_{soil} (1/°C). We used daily records of soil temperature and treatment-specific parameterizations of the temperature-response function of R_{het} to predict daily R'_{het} for each treatment. Robust predictions resulted when treatment-specific parameters were used to predict R_{het} for point measurements not included in the parameter development, indicating that the gap filling methods applied were successful in interpolating daily values (r^2=0.82; Slope 0.98±0.08, Intercept 0.09±0.08) (*Supp. Info.* 3.9.3). Daily estimates were summed to calculate seasonal R'_{het} at each treatment.

For each treatment, we estimated the temperature sensitivity of R_{het} (Q_{10}) by using model fit parameters from temperature-dependent functions (Eq. 3.4) into the following equation:

(Eq. 3.7) $$Q_{10} = e^{10\varphi}$$

Soil moisture and substrate quality and quantity may exert a major control over temperature sensitivity of R_h (Davidson *et al.*, 2006). Therefore, Q_{10} is referred to as apparent temperature sensitivity of R_{het} hereafter.

Daily estimates of autotrophic respiration (R'_{aut}; above- and below-ground plant respiration) were calculated as the difference between R'_{eco} and R'_{het}, and daily estimates were summed to calculate seasonal R'_{aut} at each treatment.

3.3.10 Seasonal ecosystem carbon budgets and Global Warming Potential

Seasonal ecosystem C budgets at each treatment were calculated from the sum of the net seasonal ecosystem CO_2 and CH_4 balance, accounting for the mass difference between CO_2 and CH_4 gas and expressed in gCO_2-C and gCH_4-C. We used model estimates of NEE to calculate the seasonal ecosystem CO_2 budget. Seasonal net ecosystem CH_4 budget was estimated from the direct CH_4 flux determination from the same sampling plots and periods taken in parallel to CO_2 flux measurements (Blanc-Betes *et al.*, 2016). Details on CH_4 flux sampling procedures, data analyses and calculations are provided in Blanc-Betes *et al.* (2016). Briefly, seasonal CH_4 budgets were calculated for each treatment as the sum of the daily ecosystem CH_4 flux using linear interpolation gap-fill methods. Ecosystem CH_4 fluxes, and CH_4 seasonal dynamics and budgets of each treatment are available in Fig.3 and Table 4 of Blanc-Betes *et al.* (2016) (*see* Chapter 4; Fig. 27, Table XV).

To calculate the ecosystem global warming potential (GWP) resulting from ecosystem C fluxes over the growing season, the net seasonal ecosystem C flux from each treatment was expressed in CO_2 equivalents (CO_2-eq) by multiplying the seasonal CH_4 budget of each treatment by its 100-year GWP (33 CO_2-eq; Shindell *et al.*, 2009; Myhre *et al.*, 2013), and adding that value to its corresponding seasonal CO_2 budget.

3.3.11 Statistical analyses

All statistical analyses were performed using Statgraphics Centurion XVI (Statistical Graphics Corp., MD, USA) software. We investigated the effect of snow treatment on abiotic factors (air and soil temperature, volumetric water content, and thaw depth), biotic variables (NEE_{600}, GPP_{600}, R_{eco}, and R_{het}), model-fitted parameters (A_{max}, K_s), and derived variables (Effective LAI) using repeated measures analysis of variance (repeated ANOVA), with treatment (RS, Ambient, MS, and HS) and sampling period (1 to 6) as main effects, and plot within treatment (n=5, except for R_{het} where n=3) as a random effect. Treatment effects on CO_2 fluxes within period were examined with simple analysis of variance (ANOVA). Simple regression analyses (SRA) were conducted to describe ecosystem, soil and heterotrophic CO_2 flux responses to single environmental variables. Multiple regression analyses were performed to investigate the combined effect of abiotic variables on CO_2 fluxes. Normalized GPP_{600}, R_{eco}, and R_{het} were independently measured, thus avoiding overestimation of regression coefficients derived from the calculation of auto-correlated variables (DeLucia et al., 2007). However, given the inherent codependency between estimates of ecosystem CO_2 assimilation and respiration, we subtracted self-correlation by estimating the fraction attributed to shared variables (r_{SC}; Vickers *et al.*, 2009; Gomez-Casanovas *et al.*, 2012). All residuals were checked for normality and homogeneity of variances to ensure that the assumptions of ANOVA and regressions were met, and the statistical significance was determined at the $P<0.05$ level. For seasonal budgets of ecosystem CO_2 and CH_4 fluxes, and soil and heterotrophic CO_2 fluxes the error term was propagated considering daily variance as the main parameter representing the uncertainty associated with spatial heterogeneity within treatment (Davidson *et al.*, 2008).

3.4 RESULTS

3.4.1 Environmental parameters

Seasonal mean temperature was 12.1°C, with highest monthly mean occurring in July (14.4 °C) (*Supp. Info.,* Fig. 18a). Over the growing season, (PAR) was above 600 μmol photon m^{-2} s^{-1} for more than 30% of the time. PAR was highest in June and decreased thereafter, being below 600 μmol photon m^{-2} s^{-1} over 90% of August (*Supp. Info.,* Fig. 18a).

Soil temperature increased and differences among treatments intensified as the season progressed ($P<0.05$). Soils were colder in RS than in Ambient (1.8±0.07 and 2.4±0.1 °C at RS and Ambient respectively; $P<0.05$), and increasingly warmer with snow additions (3.5±0.08 and 4.1±0.04 °C at MS and HS respectively; $P<0.05$) (Fig. 10a).

Soil volumetric water content (0–12 depth integrated) increased over the growing season at all treatments except for HS that maintained water-saturation conditions throughout the season. Soils were drier at RS (0.63±cm^3 cm^{-3}; $P<0.05$), and wetter with snow additions (0.88±0.02 and 0.96±0.03 cm^3 cm^{-3} at MS and HS respectively; $P<0.05$) than at Ambient (0.71±0.03 cm^3 cm^{-3}) (Fig. 10b).

Thaw depth and differences among treatments increased as the season progressed. Maximum thaw depth was similar in RS and Ambient (49.3±1.1 and 51.1±1.6 cm in RS and Ambient; $P>0.1$), and increased with snow additions (56.7±1.4 and 65.8±2.3 cm at MS and HS respectively; $P<0.05$) (Fig. 10c).

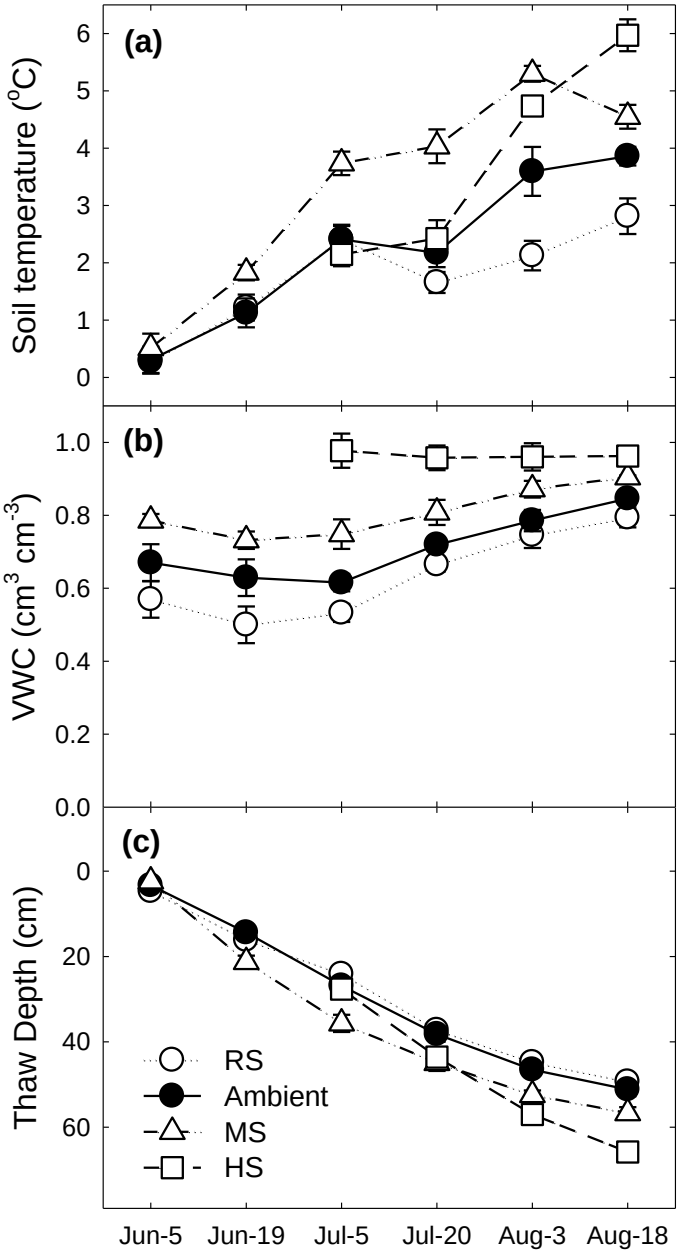

Figure 10: Seasonal variation from point measurements of **(a)** soil temperature, **(b)** volumetric water content and **(c)** thaw depth at Reduced Snow (RS), Ambient, Medium Snow addition (MS) and High Snow addition (HS) treatments. Error bars correspond to Standard Error of the Mean (±SE). Mean values within the same sampling period with different letter indicate statistical differences between treatment sites within sampling period (ANOVA; $P<0.05$).

3.4.2 Vegetation cover

The relative abundance of shrubs increased with deeper winter snow from RS to Ambient to MS, but decreased with further snow additions at HS (Fig. 11). RS lowered the presence of deciduous (–56%) and increased the presence of evergreen (+10%) shrubs, decreasing the relative abundance of shrubs by 18% compared to Ambient (Fig. 11). At MS, deciduous shrubs increased (87%) and evergreen shrubs decreased (–36%), increasing the relative abundance of shrubs relative to Ambient by +17% (Fig. 11). In contrast, HS decreased both deciduous (–25%) and evergreen (–97%) shrubs, reducing the presence of shrubs by 66% relative to Ambient (Fig. 11). The relative abundance of total graminoids decreased at RS (–14%) and increased at MS (+21%) and HS (+54%) compared to Ambient, mostly driven by changes in tall graminoids (Fig. 11). The relative abundance of mosses was similar in RS, Ambient and MS, and increased by 600% at HS (Fig. 11).

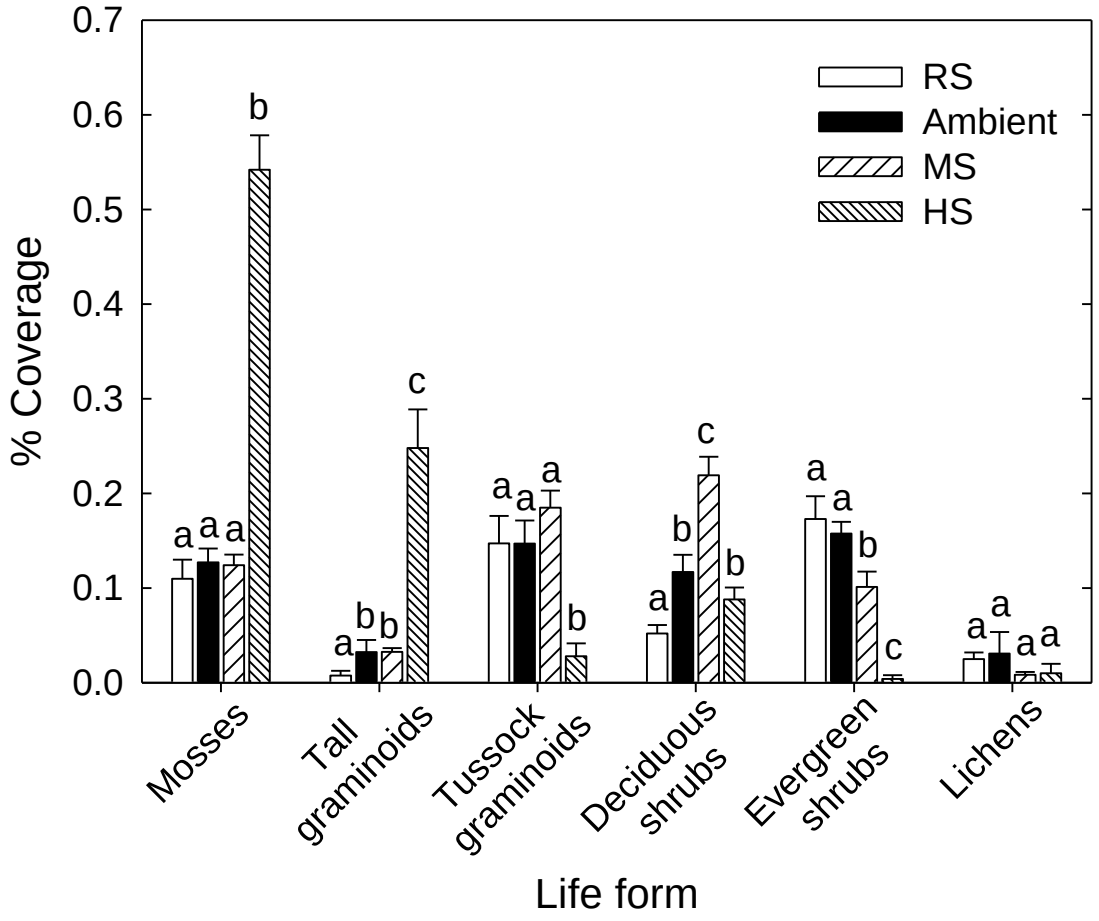

Figure 11: Percentage coverage of main life forms at Reduced Snow (RS), Ambient, Medium Snow addition (MS) and High Snow addition (HS) treatments. Mosses include *Spagnum sp*. and *Hylocomium splendens*; Tall graminoids are dominated by *Carex bigelowii*; Tussock forming graminoids refer to *Eriophorum vaginatum*; Deciduous shrubs are dominated by *Betula nana*, *Salix pulchra* and *Vaccinum ulginosum*; Evergreen shrubs include *Vaccinum vitis-ideae*, *Ledum decumbens* and *Cassiope tetragona*; Lichens are dominated by *Peltigera sp.* and *Cladina sp*. Values shown are mean percentage coverage (n=5). Mean values within the same sampling period with different letter indicate statistical differences among sites within sampling period (ANOVA; $P<0.05$). Error bars correspond to Standard Error of the Mean (±SE).

3.4.3 Ecosystem, soil and heterotrophic CO_2 fluxes

Mean GPP_{600} was similar in RS and Ambient despite lower A_{max} due to smaller Ks (Figs. 12 and 13a; Tables VI and VII). Over the growing season, GPP_{600} was consistently higher in MS than in Ambient due to a greater A_{max} despite increased Ks (Figs. 12 and 13a; Tables VI and VII). However, further snow additions reduced GPP_{600} due to lower A_{max} and higher Ks in HS compared to Ambient (Figs. 12 and 13a; Tables VI and VII). Co-variation of A_{max} and Ks across treatments yielded relatively constant E_0, although E_0 increased slightly from RS and Ambient to MS ($P<0.1$), and decreased at HS below Ambient values ($P<0.05$) (Tables VI and VII).

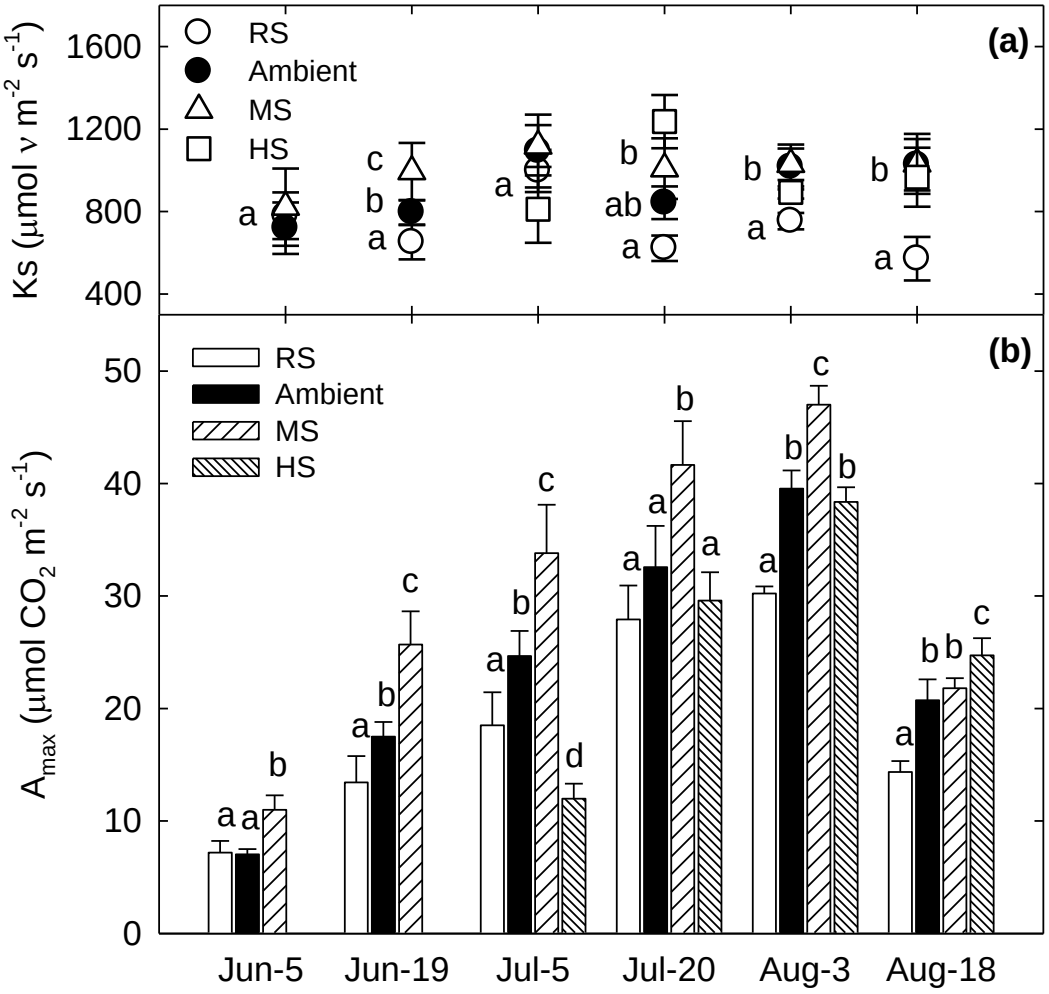

Figure 12: Seasonal variation of estimated values of **(a)** half-saturation constant (K_s; µmol photons m^{-2} s^{-1}) and **(b)** light-saturated photosynthesis (A_{max}; µmol CO_2 m^{-2} s^{-1}) at Reduced Snow (RS), Ambient, Medium Snow addition (MS) and High Snow addition (HS) treatments. Mean values within the same sampling period with different letter indicate statistical differences among sites within sampling period (ANOVA; $P<0.05$; n=5). Error bars correspond to Standard Error of the Mean (±SE).

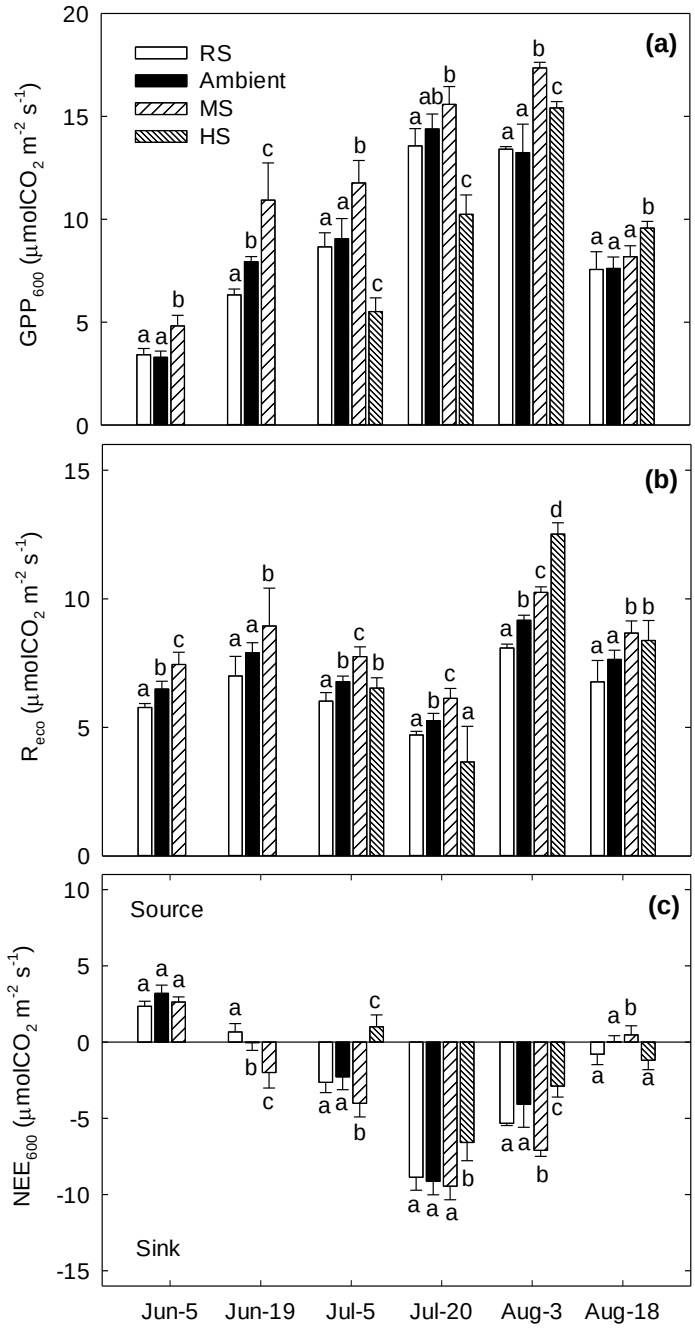

Figure 13: Seasonal variation of **(a)** GPP_{600}, **(b)** R_{eco} and **(c)** NEE_{600} rates at Reduced Snow (RS), Ambient, Medium Snow addition (MS) and High Snow addition (HS) treatments (µmol CO_2 m^{-2} s^{-1}). Mean values within the same sampling period with different letter indicate statistical differences among sites within sampling period (ANOVA; $P<0.05$; n=5). Error bars correspond to Standard Error of the Mean (±SE).

TABLE VI

Results of the PIRT model parameterization. Section **(A)** shows model parameters and statistics for each treatment developed from treatment specific period averages. Values reported are seasonal mean ± Standard Error of the Mean (±SE). Values with different letter denote statistical differences between snow treatment (P<0.05). Section **(B)** shows statistics of the fit when treatment specific parameters are used to predict NEE in the whole data set. Section **(C)** shows statistics of fit when treatment specific parameters are used to predict NEE in a subset of data not included in the parameterization of the model.

	RS	Ambient	MS	HS
(A) PIRT model parameterization				
A_{max}	18.2 ± 1.1^{a}	22.0 ± 1.4^{b}	28.2 ± 1.1^{c}	20.4 ± 0.9^{ab}
Ks	711.3 ± 74.7^{a}	870.1 ± 80.3^{ab}	1019.4 ± 98.0^{b}	976.2 ± 77.8^{ab}
E_0	0.026 ± 0.003^{a}	0.025 ± 0.002^{a}	0.028 ± 0.002^{a}	0.021 ± 0.003^{b}
Effective LAI	1.08 ± 0.02^{a}	1.19 ± 0.02^{b}	1.42 ± 0.03^{c}	1.05 ± 0.02^{d}
R_b	1.57	1.72	2.17	0.31
β	0.078	0.080	0.075	0.177
Q_{10}	2.2	2.2	2.1	5.9
r^2	0.41	0.57	0.59	0.79
(B) Model evaluation				
Slope	0.954	0.968	0.972	0.965
Intercept	– 0.068	– 0.209	– 0.247	0.037
R^2	0.970	0.951	0.953	0.974
RMSE	0.960	1.298	1.342	0.877
n	180	180	180	120
(C) Model validation				
Slope	0.922	0.949	0.936	0.945
Intercept	0.166	– 0.452	– 0.407	0.336
R^2	0.974	0.919	0.936	0.968
RMSE	0.883	1.213	1.253	1.028
n	36	36	36	24

TABLE VII

Results from repeated ANOVA. Evaluation of the single and combined effects of treatment and period on the parameters defining **(A)** ecosystem photosynthetic activity, **(B)** normalized ecosystem CO_2 fluxes, and **(C)** soil and heterotrophic respiration.

	Effect	df (res)	F		*P*
(A) Photosynthetic activity parameters					
A_{max}	Period	5 (85)	55.4	<	0.0001
	Treatment	3 (85)	15.4	<	0.0001
	Period x Treatment	9 (48)	7.3	<	0.0001
Ks	Period	5 (85)	0.4		0.8375
	Treatment	3 (85)	3.0		0.0523
	Period x Treatment	9 (48)	2.5		0.1223
E_0	Period	5 (85)	32.2	<	0.0001
	Treatment	3 (85)	3.5		0.0392
	Period x Treatment	9 (48)	3.9		0.0012
Effective LAI	Period	5 (85)	53.9	<	0.0001
	Treatment	3 (85)	10.3		0.0002
	Period x Treatment	9 (48)	4.2		0.0001
(B) Ecosystem CO_2 Fluxes					
GPP_{600}	Period	5 (85)	54.0	<	0.0001
	Treatment	3 (85)	10.6		0.0004
	Period x Treatment	9 (48)	4.6		0.0002
R_{eco}	Period	5 (85)	65.6	<	0.0001
	Treatment	3 (85)	46.7	<	0.0001
	Period x Treatment	9 (48)	16.6	<	0.0001
NEE_{600}	Period	5 (85)	18.3	<	0.0001
	Treatment	3 (85)	4.2		0.0198
	Period x Treatment	9 (48)	13.0	<	0.0001

TABLE VII (continued)

	Effect	df (res)	F		*P*
(C) Soil and heterotrophic respiration					
R_{soil}	Period	5 (264)	14.2	<	0.0001
	Treatment	3 (264)	54.0	<	0.0001
	Period x Treatment	9 (202)	8.9	<	0.0001
R_{het}	Period	5 (51)	31.0	<	0.0001
	Treatment	3 (51)	47.0		0.0198
	Period x Treatment	9 (26)	21.6	<	0.0001

R_{eco} was lower at RS and higher with snow additions than in Ambient plots, although it was greater at MS than at HS (Fig. 13b; Table VII). Although seasonal variation of R_{eco} was mainly driven by air temperature (r^2=0.51; P<0.05), differences in R_{eco} among treatments were mostly explained by changes in GPP_{600} (Table VIII). The correlation between R_{eco} and GPP_{600} varied among treatments, increasing from RS to Ambient to MS, but decreasing at HS (Table VIII).

TABLE VIII

Results from simple regression analyses. Evaluation of the relationship between GPP_{600} and ecosystem and soil respiration[1]. Coefficients of determination considering raw regression (r^2), estimated self-correlation between co-dependent variables (r^2sc), and estimated real correlation between variables subtracting inherent co-dependency ($\hat{r}_2$) are reported.

Dependent		r^2	r^2_{sc}	$\hat{r}^2$	F	*P*
R_{eco}	All treatments	0.16	0.12	0.04	18.8	< 0.0001
	RS	0.42	0.08	0.34	15.9	0.0006
	Ambient	0.50	0.08	0.42	23.4	0.0001
	MS	0.74	0.08	0.66	64.6	< 0.0001
	HS	0.48	0.26	0.23	12.2	0.004
R_{soil}	All treatments	0.29	0.01	0.28	40.4	< 0.0001
	RS	0.32	0.00	0.32	12.8	0.0013
	Ambient	0.51	0.01	0.50	29.2	< 0.0001
	MS	0.66	0.01	0.65	53.7	< 0.0001
	HS	0.28	0.01	0.27	6.5	0.0207

[1] Units are in μmol CO_2 m^{-2} s^{-1}. Normalized GPP_{600} were ln-transformed.

Snow treatments altered R_{soil} and R_{het} (Fig. 14; Table VII). R_{soil} increased from RS to Ambient to MS, but decreased at HS relative to Ambient (Fig. 14a; Table VII) and was positively correlated with GPP_{600}, but correlation coefficients varied among treatments, increasing from RS to Ambient to MS, but decreasing at HS (Table VIII).

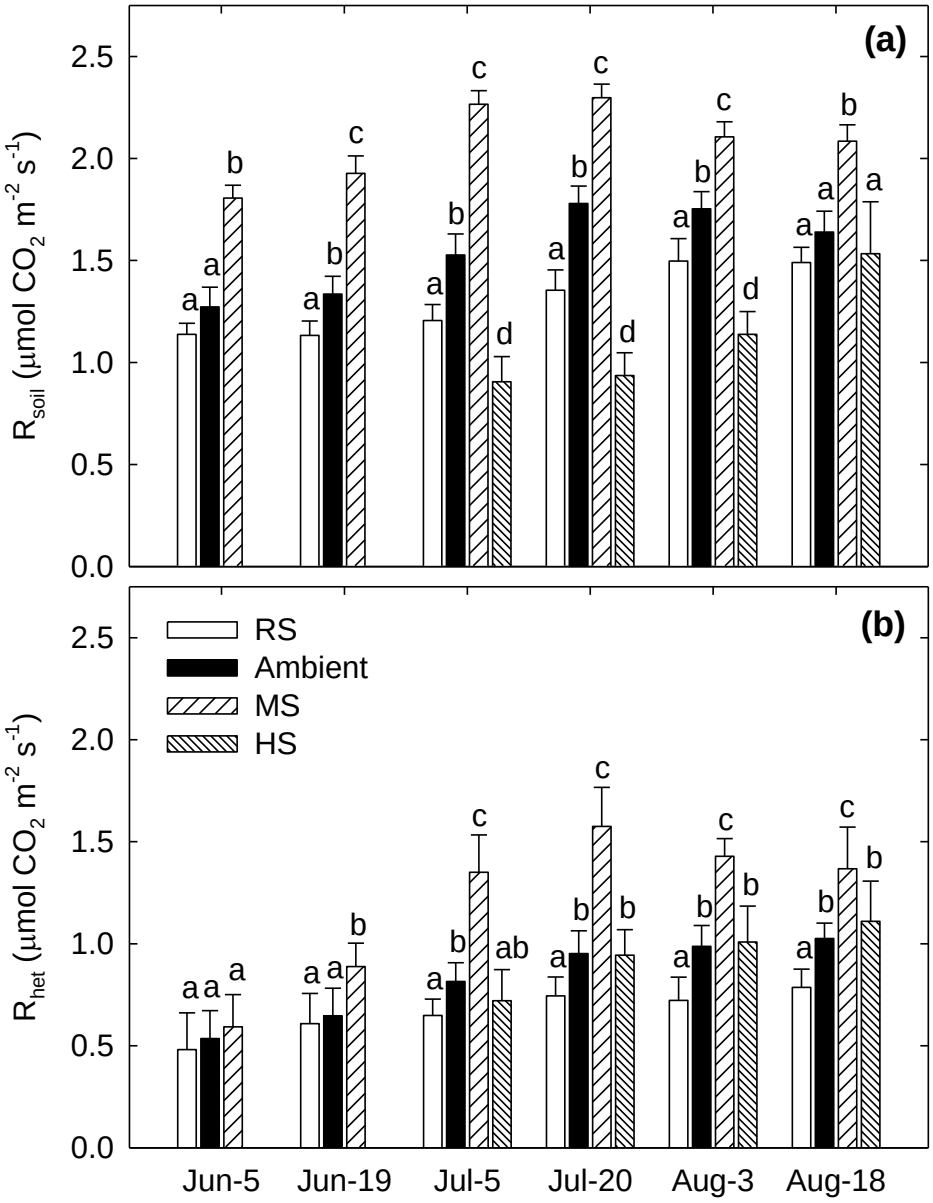

Figure 14: Seasonal variation of **(a)** R_{soil} and **(b)** R_{het} rates at Reduced Snow (RS), Ambient, Medium Snow addition (MS) and High Snow addition (HS) treatments (µmol CO_2 m^{-2} s^{-1}). Mean values within the same sampling period with different letter indicate statistical differences among sites within sampling period (ANOVA; $P<0.05$; n=5). Error bars correspond to Standard Error of the Mean (±SE).

Over the growing season, R_{het} was consistently lower at RS and higher at MS than in Ambient (Fig. 14b; Table VII). However, R_{het} was similar in HS and Ambient (Fig. 14b; Table VII). Soil temperature and moisture explained variations in R_{het} (Fig. 15; Table IX). Seasonal Q_{10} decreased slightly from RS to Ambient to MS, and substantially at HS (Table IX). Basal R_{het} (R_0; R_{het} at 0°C) was unaffected by snow treatment (Table IX). Increases in soil moisture increased R_{het}, reaching maximum rates between 0.65–0.77 cm^3 cm^{-3}, but decreased with further increases in VWC (Fig. 15). The relative importance of soil temperature and moisture in explaining R_{het} differed among treatments, with soil temperature losing leverage as soil moisture gained control with deeper snow (Table IX).

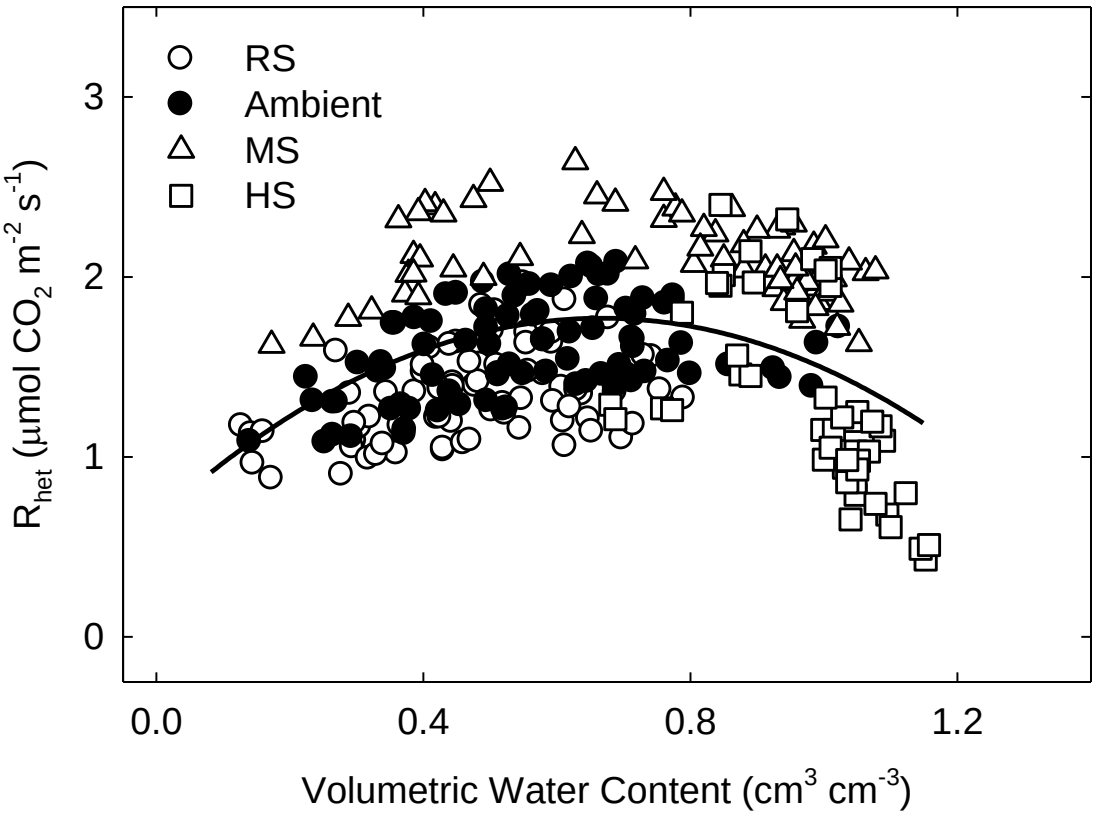

Figure 15: Results from simple regression analysis. Evaluation of the relationship between soil moisture (volumetric water content, VWC; cm^3 cm^{-3}) and heterotrophic respiration (R_{het}; µmol CO_2 m^{-2} s^{-1}) during the growing season including Reduced Snow (RS), Ambient, Medium Snow addition (MS) and High Snow addition (HS) plots.

TABLE IX

Results from simple regression analyses. Evaluation of the relationship between heterotrophic respiration (R_{het}; μmol CO_2 m^{-2} s^{-1}) and **(A)** soil volumetric water content, **(B)** soil temperature, and **(C)** thaw depth. Coefficients of determination (r^2) and statistics across and within treatments are reported. Section (B) includes model parameters describing the apparent temperature sensitivity of R_{het}. Values with different letter denote statistical differences between snow treatment (P<0.05).

	All treatments	RS	Ambient	MS	HS
(A) Volumetric water content (cm^3 cm^{-3}). Best fit: Polynomial					
r^2	0.31	0.48	0.50	0.64	0.88
RMSE	0.078	0.141	0.045	0.143	0.047
F-value	13.4	5.9	4.5	11.8	41.2
P	<0.0001	0.0147	0.0441	0.0012	<0.0001
(B) Soil temperature (ºC). Best fit: Exponential					
R_0	0.602	0.429[a]	0.478[a]	0.494[a]	0.490[a]
φ	0.142	0.237[a]	0.220[a]	0.247[a]	0.158[b]
Q_{10}	4.1 ± 1.5	10.7 ± 1.3[a]	9.0 ± 1.2[a]	8.6 ± 1.3[a]	4.8 ± 1.3[b]
r^2	0.56	0.87	0.85	0.81	0.77
RMSE	0.142	0.074	0.053	0.070	0.076
F-value	77.1	89.7	100.2	80.2	41.2
P	<0.0001	<0.0001	<0.0001	<0.0001	<0.0001
(C) Thaw depth (cm). Best fit: Linear					
r^2	0.00	0.14	0.15	0.01	0.07
RMSE	0.223	0.210	0.131	0.233	0.159
F-value	0.2	1.3	1.4	0.1	1.0
P	0.6391	0.2835	0.2645	0.7928	0.3466

3.4.4 Effective Leaf Area Index

Snow treatment altered Effective LAI (Tables VI and VII). Estimates of Effective LAI increased from RS to Ambient to MS, but decreased with further snow additions at HS below those in Ambient (Tables VI and VII).

3.4.5 Seasonal CO_2-C budgets

Both cumulative GPP and R_{eco} were lower in RS and higher in MS than in Ambient. However, further increases in snow accumulation at HS decreased both GPP and R_{eco} compared to Ambient (Figs. 16a and 16b). The contribution of R_{het} to R_{eco} was 15±1.5% in RS, 20±1.2% in Ambient, 21±1.0% in MS and 26±1.7% in HS. The contribution of R_{het} to R_{soil} was 50.7±4.5% in RS, 51.2±3.2% in Ambient, 58.2±3.0% in MS and 87.3±7.9% in HS.

Snow treatment altered seasonal sums and patterns of NEE (Figs. 16c; Table VII). Over the growing season, Arctic tundra was a net CO_2 source at Ambient and a net CO_2 sink at RS (Figs. 16c). Snow additions reduced the CO_2 source strength at MS compared to Ambient, and switched the system into a weak CO_2 sink at HS (Figs. 16c). At Ambient, Arctic tundra transitioned from a CO_2 source into a sink by mid-July (Fig. 16c). RS and MS anticipated by 5 and 12 days the transition into a net sink for CO_2, and HS delayed the transition by 19 days (Fig. 16c). By late August, Arctic tundra became a net CO_2 source at Ambient and MS, whereas RS and HS remained net CO_2 sinks until the first snow (Fig. 16c).

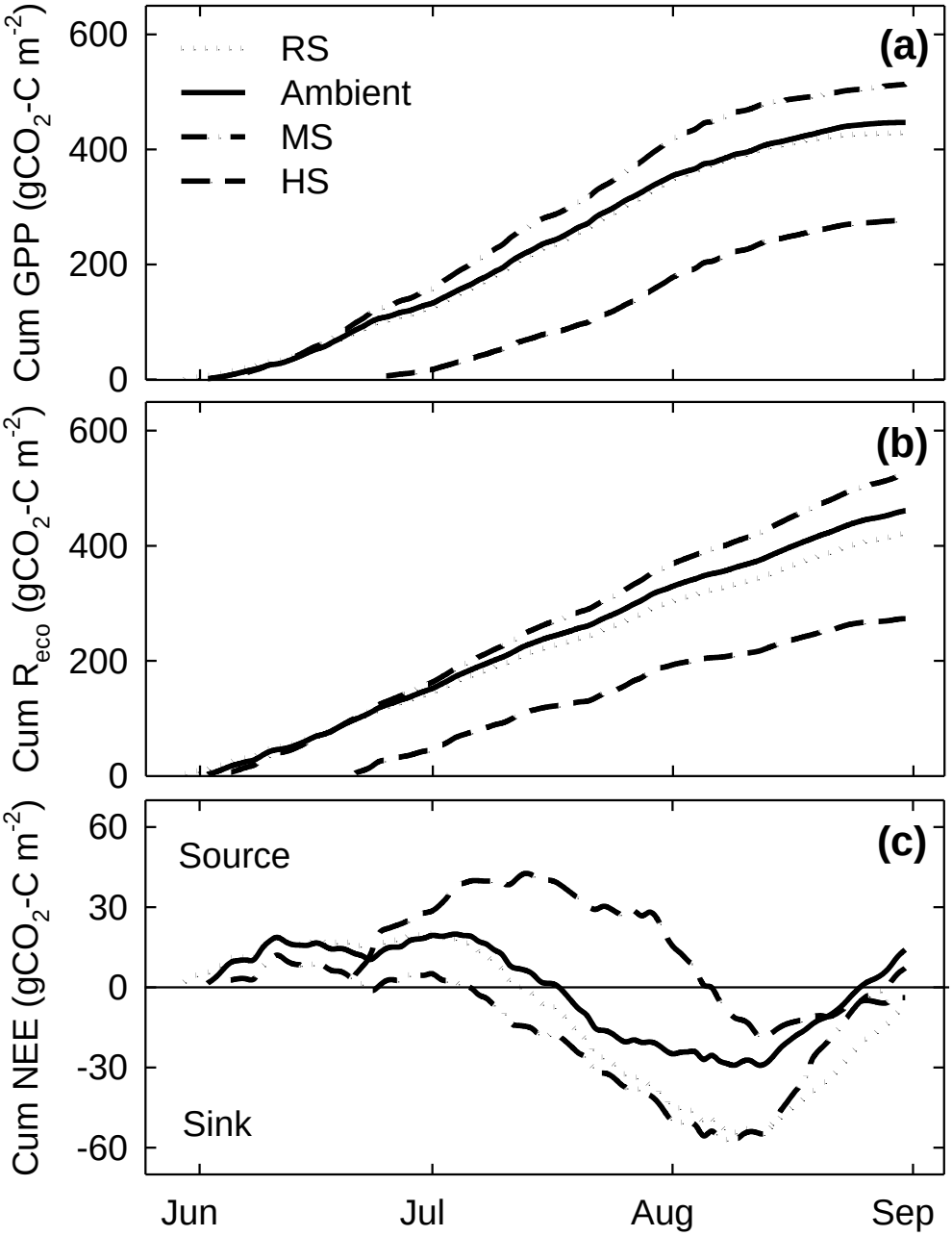

Figure 16: Seasonal cumulative of **(a)** GPP, **(b)** R_{eco} and **(c)** NEE at Reduced Snow (RS), Ambient, Medium Snow addition (MS) and High Snow addition (HS) treatments over the growing season (gCO_2-C m^{-2}).

3.4.6 Seasonal ecosystem carbon budget and Global Warming Potential

Incorporating CH_4 emissions into the C budget, Ambient Arctic tundra was a net source of C and GWP (Fig. 17). RS converted Arctic tundra into a net sink of both C and GWP (Fig. 17). MS reduced net C losses by 30%, but did not affect the GWP compared to Ambient when accounting for the radiative forcing of a 20-fold increase in ecosystem CH_4 source strength (*see* Chapter 4) (Fig. 17). However, further snow additions at HS switched the system into a small net C sink, but increased the GWP source strength of Arctic tundra by 130% as a result of a 150-fold increase in the ecosystem CH_4 source strength compared to Ambient (*see* Chapter 4) (Fig. 17).

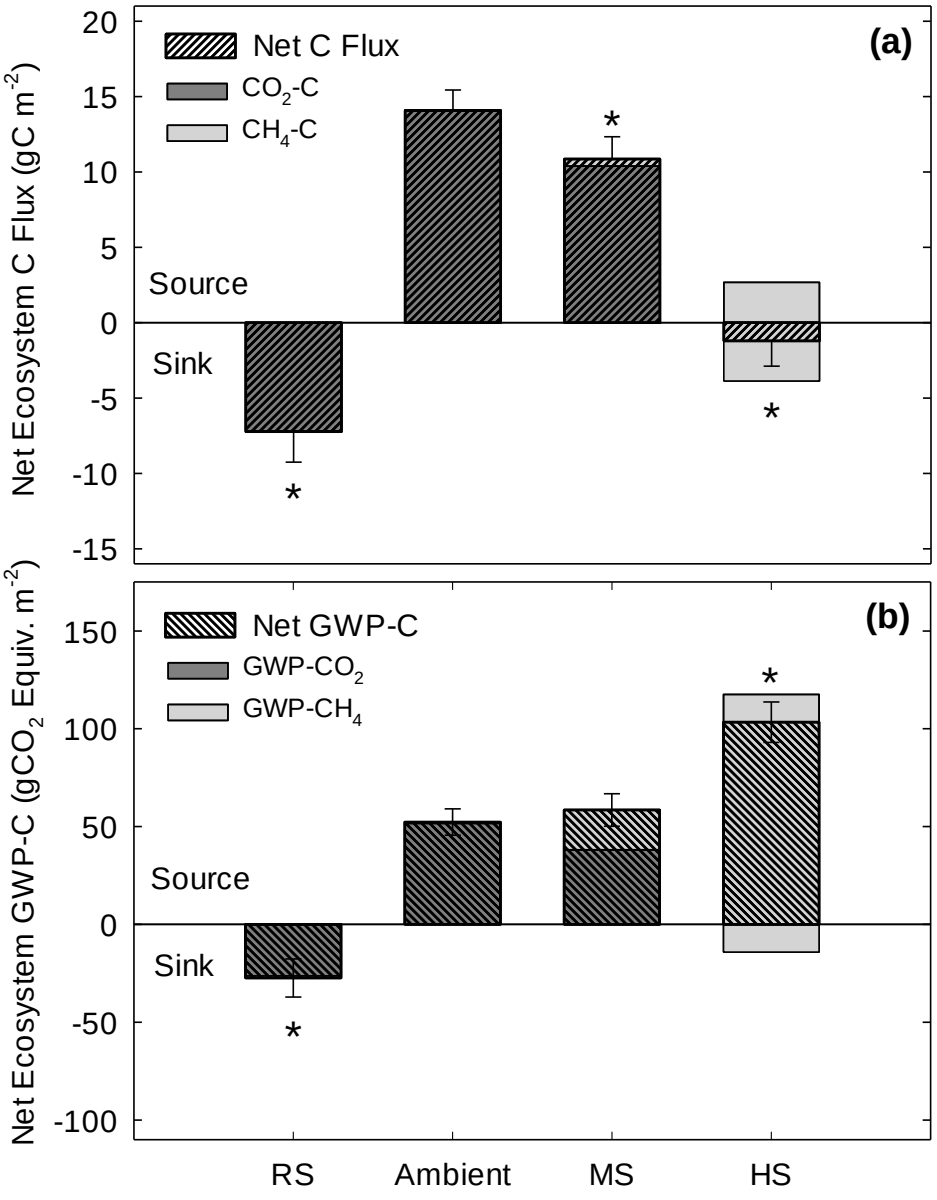

Figure 17: Seasonal estimates of **(a)** net ecosystem C fluxes (gC m^{-2}), and **(b)** net C global warming potential (GWP-C, patterned; gCO_2 Equiv. m^{-2}) derived from net ecosystem CO_2 (solid dark grey) and CH_4 (solid light grey) budgets at Reduced Snow (RS), Ambient, Medium Snow addition (MS) and High Snow addition (HS) treatments. Error bars correspond to Standard Error of the Mean (±SE). (*) Denotes significant difference between treatment and Ambient sites (P<0.05).

3.5 DISCUSSION

Our results indicate a marked nonlinearity in the response of the Arctic tundra C budget to changes in winter precipitation. Both reduced- (RS) and high- (HS) snow accumulation switched the system into a C sink, whereas medium snow additions (MS) reduced the C source strength of Arctic tundra relative to Ambient over the growing season (Fig. 17a). An evaluation of the components of Arctic tundra C balance (i.e. CO_2 and CH_4 budgets) revealed that this nonlinearity was a consequence of the nonlinear response of NEE to increasing levels of winter snow, and could be traced to shifts in plant community structure, and a strong control on R_{het} (Fig. 17a). Parallel work at the site showed enhanced CH_4 emissions with deeper winter snow (Blanc-Betes *et al.*, 2016), which increased the GWP of Arctic tundra relative to Ambient despite decreases in the ecosystem C source strength (Fig. 17b). Our results indicate that by reshaping soil thermal and hydrological regimes and supported vegetation, projected precipitation scenarios in Arctic regions will drive the Arctic tundra C budget and climate/C-cycle forcing feedbacks beyond the impacts of winter warming alone.

3.5.1 Snow accumulation effects on plant community structure

Snow additions favored the expansion of deciduous shrubs to the detriment of evergreen shrubs and sedges from RS to Ambient to MS likely due to thaw- and warming- induced nutrient availability (Schimel *et al.*, 2004; Salmon *et al.*, 2016), and improved rates of N uptake and developmental plasticity of deciduous species above that of evergreen shrubs or non-woody species (Chapin & Shaver, 1996; Oechel *et al.*, 2000; Bret-Harte *et al.*, 2001; Shaver *et al.*, 2001; Bret-Harte *et al.*, 2002) (Figs. 10 and 11). This is in agreement with changes in plant community structure observed at our experimental site after 8 years of 1-3 fold snow increases (Wahren *et al.*, 2005), and supports observations of recent shrub expansion into Arctic tundra accompanying

climate warming (Tape *et al.*, 2006; Walker *et al.*, 2006; Elmendorf *et al.*, 2012a, 2012b; Tape *et al.*, 2012). However, with further snow additions at HS both deciduous and evergreen shrubs were replaced by tall sedges and mosses (Fig. 11). Similar transitions towards wet sedge tundra have been reported associated with severe permafrost degradation (Jorgenson *et al.*, 2001; Christensen *et al.*, 2004; Osterkamp *et al.*, 2009).

3.5.2 Snow accumulation controls on Arctic tundra CO_2 sink or source strength

Under Ambient conditions, Arctic tundra was a net CO_2 source over the growing season, similar in magnitude to that reported across the Alaskan Arctic tundra over the last decades (Figs. 16c and 17a) (Jones *et al.*, 1998; Grogan & Chapin III, 1999, 2000, Welker *et al.*, 2000, 2004; Kwon *et al.*, 2006; Biasi *et al.*, 2013; Leffler *et al.*, 2016).

Moderate snow additions reduced the Arctic tundra CO_2 source strength at MS relative to Ambient, whereas both reduced and high snow additions switched Arctic tundra into a CO_2 sink at RS and HS respectively (Figs. 16c and 17a). The observed nonlinearities resulted from the individual responses of all contributing fluxes (i.e. GPP, R_{eco}, and R_{het}) to greater soil wetness, warming and deepening of the active layer (Fig. 10), and alterations of the plant community structure with deeper winter snow (Fig. 11).

Seasonal GPP was not affected at RS, but increased at MS and decreased with further snow additions at HS relative to Ambient (Fig. 16a). These results contrast with measures of leaf-level photosynthesis across our experimental site, which decreased at RS (Pattison & Welker, 2014) and were not affected by MS or HS (Leffler *et al.*, 2016). The apparent discrepancy suggests that changes in A_{max} and GPP resulted from changes in Effective LAI rather than in leaf-level physiology (Street *et al.*, 2007; Starr *et al.*, 2008; Sharp *et al.*, 2013). Both Effective LAI and ecosystem A_{max} increased with deeper snow from RS to Ambient to MS

but decreased at HS in close correspondence with patterns of relative abundance of deciduous shrubs (Fig 12; Tables VI and VII). These results agree with greater LAI, branching and secondary growth of deciduous shrubs in response to experimental warming and fertilization (Bret-Harte *et al.*, 2001; Shaver *et al.*, 2001; Bret-Harte *et al.*, 2002; Miller & Smith, 2012).

The denser canopy of a deciduous shrub-dominated overstory however, comes to the detriment of shaded understory vegetation (Bret-Harte *et al.*, 2001; Miller & Smith, 2012), leading to greater A_{max}, but also increasing Ks (Table VI; Fig 12) (Sweet *et al.*, 2015). Consistently, Ks increased proportionally with A_{max} from RS to Ambient to MS yielding relatively conservative A_{max}-to-Ks values (E_0), and hence limiting the GPP response to moderate changes in snow depth (Table VI). As such, at RS, lower Ks, by allowing greater GPP at low PAR, compensated decreases in A_{max}, yielding similar seasonal GPP than Ambient (Figs. 12, 13a and 16a; Table VI). On the other hand, MS increased A_{max} and enhanced GPP early in the growing season likely by accelerated green-up rates and early leaf expansion of deciduous shrubs (Bosiö *et al.*, 2014; Sweet *et al.*, 2015). This hastened the transition from CO_2 source to sink by 12 days with respect to Ambient despite the 7-day delay in the onset of the growing season (Figs. 12, 13a and 16a; Table VI). However, greater Ks, particularly by the end of the growing season due to the earlier senescence of deciduous shrubs, along with low PAR by mid-late Aug partly limited increases in seasonal GPP at MS (Figs. 12, 13a and 16a; Table VI). In contrast, the drastic shortening of the growing season and the succession towards wet sedge-dominated tundra at HS reduced E_0 and seasonal GPP compared to Ambient (Figs. 12, 13a and 16a; Table VI). Together, these observations indicate the resistance of ecosystem productivity to moderate long-term changes in climate (Oechel *et al.*, 2000; Bosiö *et al.*, 2014), and suggest that correlations between plant productivity and the length of the growing season (Groendahl *et al.*, 2007; Lund *et*

al., 2010; Wipf & Rixen, 2010) are mediated by shifts in vegetation structure and contingent upon the severity of the disturbance.

GPP_{600} and R_{eco} were positively correlated across treatments suggesting important contributions from autotrophic respiration (R_{aut}; above- and below-ground pant respiration) to R_{eco} (Table VIII) (Hobbie & Chapin, 1998; Gonzalez-Meler *et al.*, 2004; La Puma *et al.*, 2007). Consistently, GPP_{600} explained and increasing portion of the R_{eco} variability from RS to Ambient to MS but lose leverage at HS, showing greater uncoupling between ecosystem productivity and respiration at RS and HS (Table VIII). This uncoupling can be traced to differences in the fraction of GPP lost through R_{aut}, and R_{het}.

Across treatments, variations in GPP were largely compensated by proportional changes in R_{aut}, suggesting that the uncoupling between GPP_{600} and R_{eco} determining the ecosystem CO_2 sink or source strength was mostly attributable to the direct impact of winter snow on R_{het}.

R_{het} and GPP have been shown to be linked (Gomez-Casanovas *et al.*, 2012; Hopkins *et al.*, 2013). Consistently, R_{soil} was positively correlated with GPP_{600}, as greater plant productivity likely increased root respiration and provided additional labile substrates for microbial decomposition (Table VIII) (Raich & Schlesinger, 1992; Christiansen *et al.*, 2012; Gomez-Casanovas *et al.*, 2012). However, GPP_{600} and R_{soil} lost correlation at RS and HS (Tables VIII), suggesting that additional parameters drove R_{soil} responses to snow accumulation possibly through impacts on R_{het}. Soil temperature was a key driver of R_{het} across treatments (Table IX), which exhibited apparent seasonal Q_{10} values of ~10 at RS, Ambient and MS, and ~5 at HS (Table IX), similar to those reported for tussock and wet-sedge Arctic tundra soils respectively and hence, in agreement with observed changes in plant community structure across treatments (Fig. 11) (Mikan *et al.*, 2002).

Values of Q_{10} above 2.5 however, suggest that other variables such as soil moisture and substrate supply may co-vary with soil temperature to explain changes in R_{het} (Davidson *et al.*, 2006; Davidson & Janssens, 2006). Soil moisture explained an increasing fraction of R_{het} variability from RS to Ambient to MS, and became the main driver at HS (Table IX), where near water-saturation conditions likely limited the aerobic metabolism within anoxic soils (Fig. 15) (*see* Chapter 4; Fig. 29) (Blanc-Betes *et al.*, 2016). Consistently, Q_{10} decreased at HS, explaining similar R_{het} values at HS and Ambient despite substantial increases in soil temperature (Fig. 14; Table IX). This is consistent with the negative relationship between water table position and ecosystem Q_{10} reported from subarctic and Arctic regions (Huemmrich *et al.*, 2010; McConnell *et al.*, 2013).

In addition, high Q_{10} of Arctic soils has been suggested to integrate temperature responses to SOC decomposability (Mikan *et al.*, 2002). However, contrary to recent studies that propose that litter quantity (Myers-Smith & Hik, 2013) and quality (DeMarco *et al.*, 2014) are more important than environmental variables in determining decomposition rates, similar R_0 (i.e. R_{het} at 0^oC) suggests comparable substrate utilization across snow treatments despite the greater decomposability of graminoid-derived litter than that of deciduous shrubs (Fig. 11; Table IX) (Hobbie, 1996; Mikan *et al.*, 2002; Mack *et al.*, 2004). Similarly, R_0 did not respond to deeper and warmer active layer contravening arguments of thaw-induced shifts in substrate utilization (Biasi *et al.*, 2005; Uhlířová *et al.*, 2007; Abbott *et al.*, 2014). This is further supported by the negligible effect of thawing depth on R_{het} (Table IX). Unaltered R_0 despite substantial changes in plant community structure and deepening of the active layer with deeper winter snow suggests that microbial activity responded to soil thermal and hydrological constraints rather than plant-derived or thaw-induced changes in C availability and decomposability.

3.5.3 Impacts of snow accumulation on Arctic tundra carbon balance and Global Warming Potential

Both reduced snow and snow additions increased the strength of the net C sink of Arctic tundra, a response primarily driven by impacts on ecosystem CO_2 dynamics (Fig. 17a). However, greater CH_4 emissions increased the GWP of Arctic tundra with increases in winter snow accumulation (Fig. 17b). These results agree with model predictions of climate/C-cycle forcing feedbacks from Arctic regions including the prognostic dynamics of incomplete permafrost degradation (Grant, 2015), but contrast with model projections considering scenarios of dramatic losses of permafrost area by the end of the century (Koven *et al.*, 2011; Schaefer *et al.*, 2011; Burke *et al.*, 2012b; Koven *et al.*, 2015). Severe permafrost degradation under projected increases in winter precipitation over time spans longer than considered in this study, by promoting soil drainage could accelerate R_{het} and suppress ecosystem CH_4 emissions, increasing ecosystem C losses but reducing the GWP of Arctic tundra (Romanovsky *et al.*, 2010; Avis *et al.*, 2011; Lawrence *et al.*, 2015).

3.6 CONCLUSIONS

In summary, deeper winter snow reduced the C source strength but increased the GWP of Arctic tundra over the growing season. Our results further indicate that increases in the Arctic tundra C sink strength resulted from impacts on the predominant microbial function and activity rather than from enhanced nutrient availability and plant productivity, and variations in microbial activity responded to changes in soil thermal and hydrological regimes rather than on plant-derived or thaw-induced changes in C availability or decomposability. Notably, our results suggested certain resistance of net plant productivity to long-term changes in winter precipitation that responded to metabolic adjustments at the canopy level mediated by shifts in plant

community structure rather than the acclimation of physiological processes. Overall, our findings suggest the capacity of Arctic tundra to dampen C flux responses to long-term changes in climate but significantly contribute to the ecosystem GWP. However, the sign and magnitude of these feedbacks hinge on intensity of the disturbance and operating time spans. Predictions of climate/C-cycle feedbacks from Arctic regions would greatly benefit from improved representations of the timing and intensity of changes in precipitation and impacts on soil hydrology.

3.7 Acknowledgements

This study was made possible by the field assistance of N. Van Hoey and B. Thurnhoffer. We thank A. Anderson-Smith and M. Rogers for their technical support and the assistance by the UIC isotope lab. Support from the Toolik Lake Field Station staff is greatly appreciated, as it is the logistical support of CH2MHill Polar Services. This research was funded by the Department of Energy, Terrestrial Ecosystem Science Program (DE-SC 0006607), and by NSF OPP grants (0119279 and 0612384) awarded to J.M. Welker and the International Tundra Experiment and the International Polar Year.

3.8 Cited Literature

Abbott BW, Larouche JR, Jones JB, Bowden WB, Balser AW (2014) Elevated dissolved organic carbon biodegradability from thawing and collapsing permafrost. *Journal of Geophysical Research: Biogeosciences*, **119**, 2014JG002678.

Abbott BW, Jones JB, Schuur EAG et al. (2016) Biomass offsets little or none of permafrost carbon release from soils, streams, and wildfire: an expert assessment. *Environmental Research Letters*, **11**, 034014.

Arens SJT, Sullivan PF, Welker JM (2008) Nonlinear responses to nitrogen and strong interactions with nitrogen and phosphorus additions drastically alter the structure and function of a high Arctic ecosystem. *Journal of Geophysical Research: Biogeosciences*, **113**, G03S09.

Avis CA, Weaver AJ, Meissner KJ (2011) Reduction in areal extent of high-latitude wetlands in response to permafrost thaw. *Nature Geoscience*, **4**, 444–448.

Biasi C, Rusalimova O, Meyer H et al. (2005) Temperature-dependent shift from labile to recalcitrant carbon sources of Arctic heterotrophs. *Rapid Communications in Mass Spectrometry*, **19**, 1401–1408.

Biasi C, Jokinen S, Marushchak ME, Hämäläinen K, Trubnikova T, Oinonen M, Martikainen PJ (2013) Microbial Respiration in Arctic Upland and Peat Soils as a Source of Atmospheric Carbon Dioxide. *Ecosystems*, **17**, 112–126.

Bintanja R, Selten FM (2014) Future increases in Arctic precipitation linked to local evaporation and sea-ice retreat. *Nature*, **509**, 479–482.

Blanc-Betes E, Welker JM, Sturchio NC, Chanton JP, Gonzalez-Meler MA (2016) Winter precipitation and snow accumulation drive the methane sink or source strength of Arctic tussock tundra. *Global Change Biology*, **22**, 2818–2833.

Bosiö J, Stiegler C, Johansson M, Mbufong HN, Christensen TR (2014) Increased photosynthesis compensates for shorter growing season in subarctic tundra—8 years of snow accumulation manipulations. *Climatic Change*, **127**, 321–334.

Bret-Harte MS, Shaver GR, Zoerner JP et al. (2001) Developmental plasticity allows Betula nana to dominate tundra subjected to an altered environment. *Ecology*, **82**, 18–32.

Bret-Harte MS, Shaver GR, Chapin FS (2002) Primary and secondary stem growth in Arctic shrubs: implications for community response to environmental change. *Journal of Ecology*, **90**, 251–267.

Brooks PD, Grogan P, Templer PH, Groffman P, Öquist MG, Schimel J (2011) Carbon and Nitrogen Cycling in Snow-Covered Environments. *Geography Compass*, **5**, 682–699.

Buckeridge KM, Grogan P (2008) Deepened snow alters soil microbial nutrient limitations in Arctic birch hummock tundra. *Applied Soil Ecology*, **39**, 210–222.

Burke EJ, Hartley IP, Jones CD (2012a) Uncertainties in the global temperature change caused by carbon release from permafrost thawing. *The Cryosphere*, **6**, 1063–1076.

Burke EJ, Jones CD, Koven CD (2012b) Estimating the Permafrost-Carbon Climate Response in the CMIP5 Climate Models Using a Simplified Approach. *Journal of Climate*, **26**, 4897–4909.

Callaghan TV, Johansson M, Brown RD et al. (2011) The Changing Face of Arctic Snow Cover: A Synthesis of Observed and Projected Changes. *AMBIO*, **40**, 17–31.

Carvalhais N, Forkel M, Khomik M et al. (2014) Global covariation of carbon turnover times with climate in terrestrial ecosystems. *Nature*, **514**, 213–217.

Cassidy AE, Christen A, Henry GHR (2015) The effect of a permafrost disturbance on growing-season carbon-dioxide fluxes in a high Arctic tundra ecosystem. *Biogeosciences Discussions*, **12**.

Chapin FS, Shaver GR (1996) Physiological and Growth Responses of Arctic Plants to a Field Experiment Simulating Climatic Change. *Ecology*, **77**, 822–840.

Chen G, Yang Y, Robinson D (2013) Allocation of gross primary production in forest ecosystems: allometric constraints and environmental responses. *New Phytologist*, **200**, 1176–1186.

Christensen TR, Johansson T, Åkerman HJ et al. (2004) Thawing sub-arctic permafrost: Effects on vegetation and methane emissions. *Geophysical Research Letters*, **31**, L04501.

Christiansen CT, Svendsen SH, Schmidt NM, Michelsen A (2012) High Arctic heath soil respiration and biogeochemical dynamics during summer and autumn freeze-in – effects of long-term enhanced water and nutrient supply. *Global Change Biology*, **18**, 3224–3236.

Cornelissen JHC, Van Bodegom PM, Aerts R et al. (2007) Global negative vegetation feedback to climate warming responses of leaf litter decomposition rates in cold biomes. *Ecology Letters*, **10**, 619–627.

Craine JM, Elmore AJ, Aidar MPM et al. (2009) Global patterns of foliar nitrogen isotopes and their relationships with climate, mycorrhizal fungi, foliar nutrient concentrations, and nitrogen availability. *New Phytologist*, **183**, 980–992.

Craine JM, Fierer N, McLauchlan KK, Elmore AJ (2012) Reduction of the temperature sensitivity of soil organic matter decomposition with sustained temperature increase. *Biogeochemistry*, **113**, 359–368.

Davidson EA, Janssens IA (2006) Temperature sensitivity of soil carbon decomposition and feedbacks to climate change. *Nature*, **440**, 165–173.

Davidson EA, Janssens IA, Luo Y (2006) On the variability of respiration in terrestrial ecosystems: moving beyond Q10. *Global Change Biology*, **12**, 154–164.

Davidson EA, Nepstad DC, Ishida FY, Brando PM (2008) Effects of an experimental drought and recovery on soil emissions of carbon dioxide, methane, nitrous oxide, and nitric oxide in a moist tropical forest. *Global Change Biology*, **14**, 2582–2590.

DeMarco J, Mack MC, Bret-Harte MS, Burton M, Shaver GR (2014) Long-term experimental warming and nutrient additions increase productivity in tall deciduous shrub tundra. *Ecosphere*, **5**, 1–22.

Deslippe JR, Simard SW (2011) Below-ground carbon transfer among Betula nana may increase with warming in Arctic tundra. *New Phytologist*, **192**, 689–698.

Elmendorf SC, Henry GHR, Hollister RD et al. (2012a) Global assessment of experimental climate warming on tundra vegetation: heterogeneity over space and time. *Ecology Letters*, **15**, 164–175.

Elmendorf SC, Henry GHR, Hollister RD et al. (2012b) Plot-scale evidence of tundra vegetation change and links to recent summer warming. *Nature Climate Change*, **2**, 453–457.

Fan Z, Neff JC, Harden JW et al. (2011) Water and heat transport in boreal soils: Implications for soil response to climate change. *Science of The Total Environment*, **409**, 1836–1842.

Fisher JB, Sikka M, Oechel WC et al. (2014) Carbon cycle uncertainty in the Alaskan Arctic. *Biogeosciences Discuss.*, **11**, 2887–2932.

Gomez-Casanovas N, Matamala R, Cook DR, Gonzalez-Meler MA (2012) Net ecosystem exchange modifies the relationship between the autotrophic and heterotrophic components of soil respiration with abiotic factors in prairie grasslands. *Global Change Biology*, **18**, 2532–2545.

Gomez-Casanovas N, Anderson-Teixeira K, Zeri M, Bernacchi CJ, DeLucia EH (2013) Gap filling strategies and error in estimating annual soil respiration. *Global Change Biology*, **19**, 1941–1952.

Gonzalez-Meler MA, Taneva L, Trueman RJ (2004) Plant Respiration and Elevated Atmospheric CO_2 Concentration: Cellular Responses and Global Significance. *Annals of Botany*, **94**, 647–656.

Grant RF (2015) Ecosystem CO_2 and CH_4 exchange in a mixed tundra and a fen within a hydrologically diverse Arctic landscape: 2. Modeled impacts of climate change. *Journal of Geophysical Research: Biogeosciences*, **120**, 2014JG002889.

Groendahl L, Friborg T, Soegaard H (2007) Temperature and snow-melt controls on interannual variability in carbon exchange in the high Arctic. *Theoretical and Applied Climatology*, **88**, 111–125.

Grogan P, Chapin III FS (1999) Arctic Soil Respiration: Effects of Climate and Vegetation Depend on Season. *Ecosystems*, **2**, 451–459.

Grogan P, Chapin III FS (2000) Initial effects of experimental warming on above- and belowground components of net ecosystem CO_2 exchange in Arctic tundra. *Oecologia*, **125**, 512–520.

Heskel MA, Anderson OR, Atkin OK, Turnbull MH, Griffin KL (2012) Leaf-and cell-level carbon cycling responses to a nitrogen and phosphorus gradient in two Arctic tundra species. *American Journal of Botany*, **99**, 1702–1714.

Hobbie SE (1996) Temperature and Plant Species Control Over Litter Decomposition in Alaskan Tundra. *Ecological Monographs*, **66**, 503–522.

Hobbie SE, Chapin FS (1998) The response of tundra plant biomass, aboveground production, nitrogen, and CO_2 flux to experimental warming. *Ecology*, **79**, 1526–1544.

Hopkins F, Gonzalez-Meler MA, Flower CE, Lynch DJ, Czimczik C, Tang J, Subke J-A (2013) Ecosystem-level controls on root-rhizosphere respiration. *New Phytologist*, **199**, 339–351.

Huemmrich KF, Kinoshita G, Gamon JA, Houston S, Kwon H, Oechel WC (2010) Tundra carbon balance under varying temperature and moisture regimes. *Journal of Geophysical Research: Biogeosciences*, **115**, G00I02.

Ives SL, Sullivan PF, Dial R, Berg EE, Welker JM (2013) CO_2 exchange along a hydrologic gradient in the Kenai Lowlands, AK: feedback implications of wetland drying and vegetation succession. *Ecohydrology*, **6**, 38–50.

Jones MH, Fahnestock JT, Walker DA, Walker MD, Welker JM (1998) Carbon dioxide fluxes in moist and dry Arctic tundra during the snow-free season: responses to increases in summer temperature and winter snow accumulation. *Arctic and alpine research*, 373–380.

Jorgenson MT, Racine CH, Walters JC, Osterkamp TE (2001) Permafrost Degradation and Ecological Changes Associated with a Warming Climate in Central Alaska. *Climatic Change*, **48**, 551–579.

Kattsov VM, Källén E, Cattle HP et al. (2005) Future climate change: modeling and scenarios for the Arctic. In: *Arctic Climate Impact Assessment (ACIA)*. Cambridge University Press, Cambridge, UK, pp. 99–150.

Koven CD, Ringeval B, Friedlingstein P et al. (2011) Permafrost carbon-climate feedbacks accelerate global warming. *Proceedings of the National Academy of Sciences*, **108**, 14769–14774.

Koven CD, Schuur E a. G, Schädel C et al. (2015) A simplified, data-constrained approach to estimate the permafrost carbon–climate feedback. *Phil. Trans. R. Soc. A*, **373**, 20140423.

Kwon H-J, Oechel WC, Zulueta RC, Hastings SJ (2006) Effects of climate variability on carbon sequestration among adjacent wet sedge tundra and moist tussock tundra ecosystems. *Journal of Geophysical Research: Biogeosciences*, **111**, G03014.

La Puma IP, Philippi TE, Oberbauer SF (2007) Relating NDVI to ecosystem CO_2 exchange patterns in response to season length and soil warming manipulations in Arctic Alaska. *Remote Sensing of Environment*, **109**, 225–236.

Lamb EG, Han S, Lanoil BD, Henry GHR, Brummell ME, Banerjee S, Siciliano SD (2011) A High Arctic soil ecosystem resists long-term environmental manipulations. *Global Change Biology*, **17**, 3187–3194.

Lawrence DM, Koven CD, Swenson SC, Riley WJ, Slater AG (2015) Permafrost thaw and resulting soil moisture changes regulate projected high-latitude CO_2 and CH_4 emissions. *Environmental Research Letters*, **10**, 094011.

Leffler AJ, Welker JM (2013) Long-term increases in snow pack elevate leaf N and photosynthesis in Salix arctica: responses to a snow fence experiment in the High Arctic of NW Greenland. *Environmental Research Letters*, **8**, 025023.

Leffler AJ, Klein ES, Oberbauer SF, Welker JM (2016) Coupled long-term summer warming and deeper snow alters species composition and stimulates gross primary productivity in tussock tundra. *Oecologia*, **181**, 287–297.

Li J, Luo Y, Natali S, Schuur EAG, Xia J, Kowalczyk E, Wang Y (2014) Modeling permafrost thaw and ecosystem carbon cycle under annual and seasonal warming at an Arctic tundra site in Alaska. *Journal of Geophysical Research: Biogeosciences*, **119**, 2013JG002569.

Lund M, Lafleur PM, Roulet NT et al. (2010) Variability in exchange of CO_2 across 12 northern peatland and tundra sites. *Global Change Biology*, **16**, 2436–2448.

Lund M, Falk JM, Friborg T, Mbufong HN, Sigsgaard C, Soegaard H, Tamstorf MP (2012) Trends in CO_2 exchange in a high Arctic tundra heath, 2000–2010. *Journal of Geophysical Research: Biogeosciences*, **117**, G02001.

Mack MC, Schuur EAG, Bret-Harte MS, Shaver GR, Chapin FS (2004) Ecosystem carbon storage in Arctic tundra reduced by long-term nutrient fertilization. *Nature*, **431**, 440–443.

McConnell NA, Turetsky MR, McGuire AD, Kane ES, Waldrop MP, Harden JW (2013) Controls on ecosystem and root respiration across a permafrost and wetland gradient in interior Alaska. *Environmental Research Letters*, **8**, 045029.

McGuire AD, Christensen TR, Hayes D et al. (2012) An assessment of the carbon balance of Arctic tundra: comparisons among observations, process models, and atmospheric inversions. *Biogeosciences Discuss.*, **9**, 4543–4594.

McLaughlin BC, Xu C-Y, Rastetter EB, Griffin KL (2014) Predicting ecosystem carbon balance in a warming Arctic: the importance of long-term thermal acclimation potential and inhibitory effects of light on respiration. *Global Change Biology*, **20**, 1901–1912.

Mikan CJ, Schimel JP, Doyle AP (2002) Temperature controls of microbial respiration in Arctic tundra soils above and below freezing. *Soil Biology and Biochemistry*, **34**, 1785–1795.

Miller PA, Smith B (2012) Modelling Tundra Vegetation Response to Recent Arctic Warming. *Ambio*, **41**, 281–291.

Mishra U, Riley WJ (2012) Alaskan soil carbon stocks: spatial variability and dependence on environmental factors. *Biogeosciences*, **9**, 3637–3645.

Morgner E, Elberling B, Strebel D, Cooper EJ (2010) The importance of winter in annual ecosystem respiration in the High Arctic: effects of snow depth in two vegetation types. *Polar Research*, **29**, 58–74.

Myers-Smith IH, Hik DS (2013) Shrub canopies influence soil temperatures but not nutrient dynamics: An experimental test of tundra snow–shrub interactions. *Ecology and Evolution*, **3**, 3683–3700.

Myhre G, Shindell D, Bréon FM et al. (2013) Anthropogenic and natural radiative forcing. *Climate change*, 658–740.

Natali SM, Schuur E a. G, Trucco C, Hicks Pries CE, Crummer KG, Baron Lopez AF (2011) Effects of experimental warming of air, soil and permafrost on carbon balance in Alaskan tundra. *Global Change Biology*, **17**, 1394–1407.

Natali SM, Schuur EAG, Rubin RL (2012) Increased plant productivity in Alaskan tundra as a result of experimental warming of soil and permafrost. *Journal of Ecology*, **100**, 488–498.

Nowinski NS, Taneva L, Trumbore SE, Welker JM (2010) Decomposition of old organic matter as a result of deeper active layers in a snow depth manipulation experiment. *Oecologia*, **163**, 785–792.

Oechel WC, Vourlitis GL, Hastings SJ, Zulueta RC, Hinzman L, Kane D (2000) Acclimation of ecosystem CO_2 exchange in the Alaskan Arctic in response to decadal climate warming. *Nature*, **406**, 978–981.

Osterkamp TE, Jorgenson MT, Schuur E a. G, Shur YL, Kanevskiy MZ, Vogel JG, Tumskoy VE (2009) Physical and ecological changes associated with warming permafrost and thermokarst in Interior Alaska. *Permafrost and Periglacial Processes*, **20**, 235–256.

Pattison RR, Welker JM (2014) Differential ecophysiological response of deciduous shrubs and a graminoid to long-term experimental snow reductions and additions in moist acidic tundra, Northern Alaska. *Oecologia*, **174**, 339–350.

Qian B, Gregorich EG, Gameda S, Hopkins DW, Wang XL (2011) Observed soil temperature trends associated with climate change in Canada. *Journal of Geophysical Research: Atmospheres*, **116**, D02106.

Raich JW, Schlesinger WH (1992) The global carbon dioxide flux in soil respiration and its relationship to vegetation and climate. *Tellus B*, **44**, 81–99.

Ricketts MP, Poretsky RS, Welker JM, Gonzalez-Meler MA (2016) Soil bacterial community and functional shifts in response to thermal insulation in moist acidic tundra of Northern Alaska. *SOIL Discussions*, 1–32.

Romanovsky VE, Smith SL, Christiansen HH (2010) Permafrost thermal state in the polar Northern Hemisphere during the international polar year 2007–2009: a synthesis. *Permafrost and Periglacial Processes*, **21**, 106–116.

Salmon VG, Soucy P, Mauritz M, Celis G, Natali SM, Mack MC, Schuur EAG (2016) Nitrogen availability increases in a tundra ecosystem during five years of experimental permafrost thaw. *Global Change Biology*, **22**, 1927–1941.

Schaefer K, Zhang T, Bruhwiler L, Barrett AP (2011) Amount and timing of permafrost carbon release in response to climate warming. *Tellus B*, **63**, 165–180.

Schaefer K, Lantuit H, Romanovsky VE, Schuur EAG, Witt R (2014) The impact of the permafrost carbon feedback on global climate. *Environmental Research Letters*, **9**, 085003.

Schimel JP, Bilbrough C, Welker JM (2004) Increased snow depth affects microbial activity and nitrogen mineralization in two Arctic tundra communities. *Soil Biology and Biochemistry*, **36**, 217–227.

Schneider von Deimling T, Meinshausen M, Levermann A, Huber V, Frieler K, Lawrence DM, Brovkin V (2012) Estimating the near-surface permafrost-carbon feedback on global warming. *Biogeosciences*, **9**, 649–665.

Schuur E a. G, McGuire AD, Schädel C et al. (2015) Climate change and the permafrost carbon feedback. *Nature*, **520**, 171–179.

Semenchuk PR, Elberling B, Amtorp C, Winkler J, Rumpf S, Michelsen A, Cooper EJ (2015) Deeper snow alters soil nutrient availability and leaf nutrient status in high Arctic tundra. *Biogeochemistry*, **124**, 81–94.

Semenchuk PR, Christiansen CT, Grogan P, Elberling B, Cooper EJ (2016) Long-term experimentally deepened snow decreases growing season respiration in a low and high Arctic tundra ecosystem. *Journal of Geophysical Research: Biogeosciences*, 2015JG003251.

Sharp ED, Sullivan PF, Steltzer H, Csank AZ, Welker JM (2013) Complex carbon cycle responses to multi-level warming and supplemental summer rain in the high Arctic. *Global Change Biology*, **19**, 1780–1792.

Shaver GR, Bret-Harte MS, Jones MH, Johnstone J, Gough L, Laundre J, Chapin FS (2001) Species Composition Interacts with Fertilizer to Control Long-Term Change in Tundra Productivity. *Ecology*, **82**, 3163–3181.

Shaver GR, Street LE, Rastetter EB, Van Wijk MT, Williams M (2007) Functional convergence in regulation of net CO_2 flux in heterogeneous tundra landscapes in Alaska and Sweden. *Journal of Ecology*, **95**, 802–817.

Shindell DT, Faluvegi G, Koch DM, Schmidt GA, Unger N, Bauer SE (2009) Improved Attribution of Climate Forcing to Emissions. *Science*, **326**, 716–718.

Starr G, Oberbauer SF, Ahlquist LE (2008) The Photosynthetic Response of Alaskan Tundra Plants to Increased Season Length and Soil Warming. *Arctic, Antarctic, and Alpine Research*, **40**, 181–191.

Stocker TF, Qin D, Plattner G-K et al. (2013) Long-term Climate Change: Projections, Commitments and Irreversibility. In: *Climate Change 2013: The Physical Science Basis. Contribution of Working Group I to the Fifth Assessment Report of the Intergovernmental Panel on Climate Change.*

Street LE, Shaver GR, Williams M, Van Wijk MT (2007) What is the relationship between changes in canopy leaf area and changes in photosynthetic CO_2 flux in Arctic ecosystems? *Journal of Ecology*, **95**, 139–150.

Subin ZM, Koven CD, Riley WJ, Torn MS, Lawrence DM, Swenson SC (2013) Effects of Soil Moisture on the Responses of Soil Temperatures to Climate Change in Cold Regions. *Journal of Climate*, **26**, 3139–3158.

Sweet SK, Griffin KL, Steltzer H, Gough L, Boelman NT (2015) Greater deciduous shrub abundance extends tundra peak season and increases modeled net CO_2 uptake. *Global Change Biology*, **21**, 2394–2409.

Tape K, Sturm M, Racine C (2006) The evidence for shrub expansion in Northern Alaska and the Pan-Arctic. *Global Change Biology*, **12**, 686–702.

Tape KD, Hallinger M, Welker JM, Ruess RW (2012) Landscape Heterogeneity of Shrub Expansion in Arctic Alaska. *Ecosystems*, **15**, 711–724.

Uhlířová E, Šantrůčková H, Davidov SP (2007) Quality and potential biodegradability of soil organic matter preserved in permafrost of Siberian tussock tundra. *Soil Biology and Biochemistry*, **39**, 1978–1989.

Vickers D, Thomas CK, Martin JG, Law B (2009) Self-correlation between assimilation and respiration resulting from flux partitioning of eddy-covariance CO_2 fluxes. *Agricultural and Forest Meteorology*, **149**, 1552–1555.

Vogel J, Schuur EAG, Trucco C, Lee H (2009) Response of CO_2 exchange in a tussock tundra ecosystem to permafrost thaw and thermokarst development. *Journal of Geophysical Research: Biogeosciences*, **114**, G04018.

Wahren C-HA, Walker MD, Bret-Harte MS (2005) Vegetation responses in Alaskan Arctic tundra after 8 years of a summer warming and winter snow manipulation experiment. *Global Change Biology*, **11**, 537–552.

Walker MD, Walker DA, Auerbach NA (1994) Plant Communities of a Tussock Tundra Landscape in the Brooks Range Foothills, Alaska. *Journal of Vegetation Science*, **5**, 843–866.

Walker MD (1996) Community baseline measurements for ITEX studies. In: *ITEX Manual* (eds MolauU, MølgaardP), Danish Polar Center, Copenhagen, Denmark.

Walker MD, Walker DA, Welker JM et al. (1999) Long-term experimental manipulation of winter snow regime and summer temperature in Arctic and alpine tundra. *Hydrological Processes*, **13**, 2315–2330.

Walker MD, Wahren CH, Hollister RD et al. (2006) Plant Community Responses to Experimental Warming across the Tundra Biome. *Proceedings of the National Academy of Sciences of the United States of America*, **103**, 1342–1346.

Wallenstein MD (2014) Microbial Community-Level Responses to Warming and Altered Precipitation Patterns Determine Terrestrial Carbon-Climate Feedbacks. In: *Global Environmental Change* (ed Freedman B), pp. 349–354. Springer Netherlands.

Weg MJ van de, Shaver GR, Salmon VG (2013) Contrasting effects of long term versus short-term nitrogen addition on photosynthesis and respiration in the Arctic. *Plant Ecology*, **214**, 1273–1286.

Welker JM, Fahnestock JT, Jones MH (2000) Annual CO_2 Flux in Dry and Moist Arctic Tundra: Field Responses to Increases in Summer Temperatures and Winter Snow Depth. *Climatic Change*, **44**, 139–150.

Welker JM, Fahnestock JT, Henry GHR, O'Dea KW, Chimner RA (2004) CO_2 exchange in three Canadian High Arctic ecosystems: response to long-term experimental warming. *Global Change Biology*, **10**, 1981–1995.

Williams M, Street LE, Wijk MT van, Shaver GR (2006) Identifying Differences in Carbon Exchange among Arctic Ecosystem Types. *Ecosystems*, **9**, 288–304.

Wipf S, Rixen C (2010) A review of snow manipulation experiments in Arctic and alpine tundra ecosystems. *Polar Research*, **29**, 95–109.

Xue K, M. Yuan M, J. Shi Z et al. (2016) Tundra soil carbon is vulnerable to rapid microbial decomposition under climate warming. *Nature Climate Change*, **6**, 595–600.

Yi Y, Kimball JS, Rawlins MA, Moghaddam M, Euskirchen ES (2015) The role of snow cover affecting boreal-arctic soil freeze–thaw and carbon dynamics. *Biogeosciences*, **12**, 5811–5829.

Zhang X, He J, Zhang J, Polyakov I, Gerdes R, Inoue J, Wu P (2013) Enhanced poleward moisture transport and amplified northern high-latitude wetting trend. *Nature Climate Change*, **3**, 47–51.

Zona D, Gioli B, Commane R et al. (2016) Cold season emissions dominate the Arctic tundra methane budget. *Proceedings of the National Academy of Sciences*, **113**, 40–45.

3.9 SUPPLEMENTARY INFORMATION

3.9.1 Photosynthetic Irradiance-Response and Temperature-sensitive respiration model. Model parameterization, validation and evaluation

The Photosynthetic Irradiance-Response and Temperature-sensitive respiration model (PIRT model; Williams et al., 2006) estimates NEE (NEE') using a two-term algorithm that integrates ecosystem photosynthetic irradiance-response (i.e. GPP) and develops the R_{eco} term as a function of the ecosystem respiration-temperature response.

(Eq. S3.1) $$NEE' = \left[R_b \times e^{\beta T_{air}}\right] + \frac{Amax \times I}{Ks+I}$$

where R_b represents basal ecosystem respiration (μmol CO_2 m^{-2} s^{-1} at 0ºC), β quantifies the relative increase in respiration with air temperature, T_{air} (1/ºC), A_{max} is the rate of light-saturated photosynthesis (μmol CO_2 m^{-2} s^{-1}), K_s is the half-saturation constant (μmol photons m^{-2} s^{-1}), and I is the incident PAR (μmol photons m^{-2} s^{-1}) (Williams *et al.*, 2006; Shaver *et al.*, 2007; Street *et al.*, 2007).

We used 30 individual measurements per treatment and period, adding a total of 720 observations over the growing season, and their corresponding air temperature and PAR values. Model-fitted parameters were A_{max} (rate of light-saturated photosynthesis; μmol CO_2 m^{-2} s^{-1}), Ks (half-saturation constant; μmol photons m^{-2} s^{-1}), R_b (basal ecosystem respiration; μmol CO_2 m^{-2} s^{-1}), and β (sensitivity of R_{eco} to changes in air temperature; 1/ºC) (Fig. 12; Table VI).

Treatment- and period- specific model-fitted parameters were used to simulate the NEE and R_{eco} within each treatment and to predict NEE and R_{eco} for the reminder of the data set (Fig. 18).

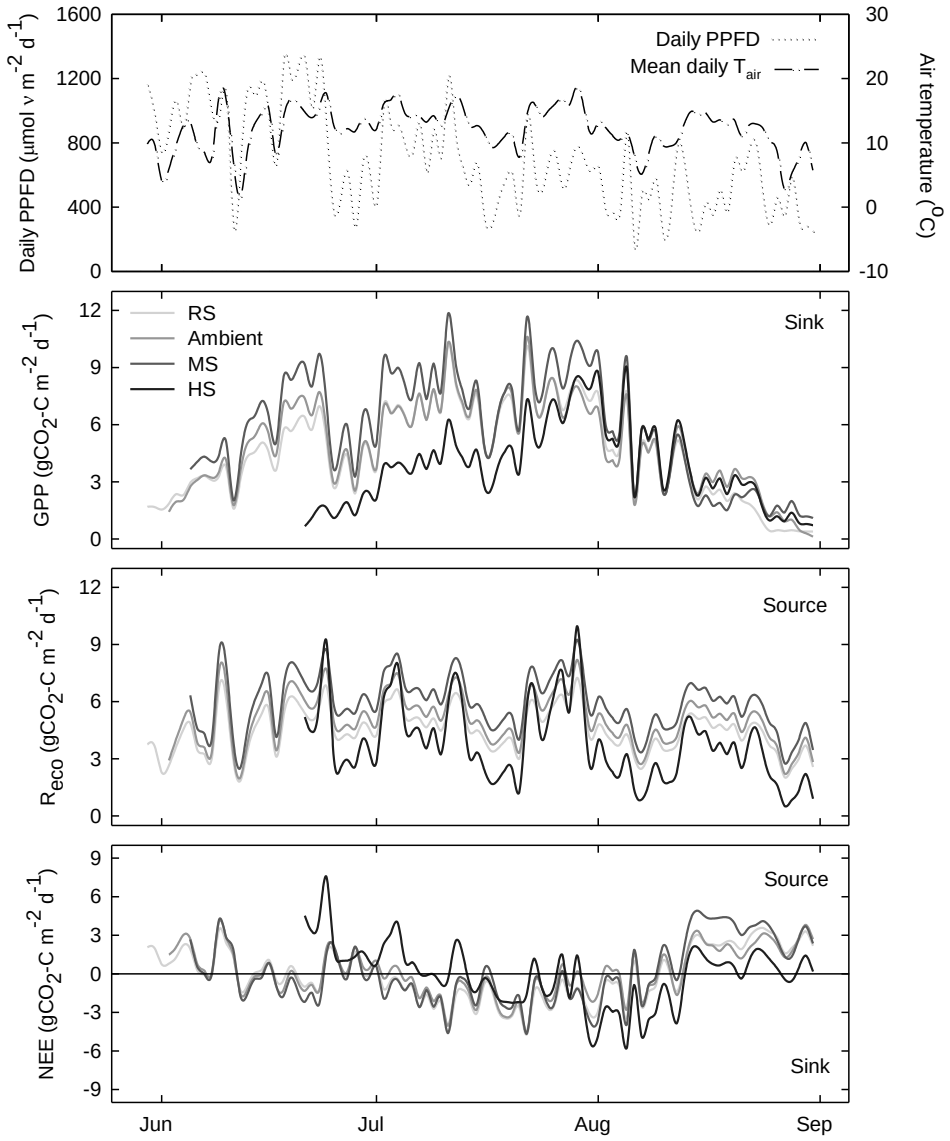

Figure 18: Mean daily records of **(a)** PPFD (µmol photon m^{-2} s^{-1}) and T_{air} (°C), and **(b)** daily estimates of GPP, **(c)** R_{eco} and **(d)** NEE (gCO_2-C m^{-2} d^{-1}) at Reduced Snow (RS), Ambient, Medium Snow addition (MS) and High Snow addition (HS) treatments over the growing season. Daily NEE values are PIRT model estimates (Williams et al., 2006). Daily GPP corresponds to the photosynthetic irradiance-response term of the PIRT model fitted to site- and period-specific A_{max} and K_s estimates (n=5), and hourly PAR records (Fig. 12; Table VI). Daily R_{eco} corresponds to the temperature-response term of the PIRT model fitted to site-specific R_b and β estimates, and hourly T_{air} records (n=5) (Table VI). Daily flux estimates correspond to the sum of hourly values over each day.

Model performance was evaluated by regressing observed vs. modelled values of NEE and R_{eco} based on r^2, RMSE, and slope and intercept deviations from the 1:1 line considering the entire data set within each treatment, and randomly selected measurements excluded from model parameterizations (Figs. 19 and 20; Table VI).

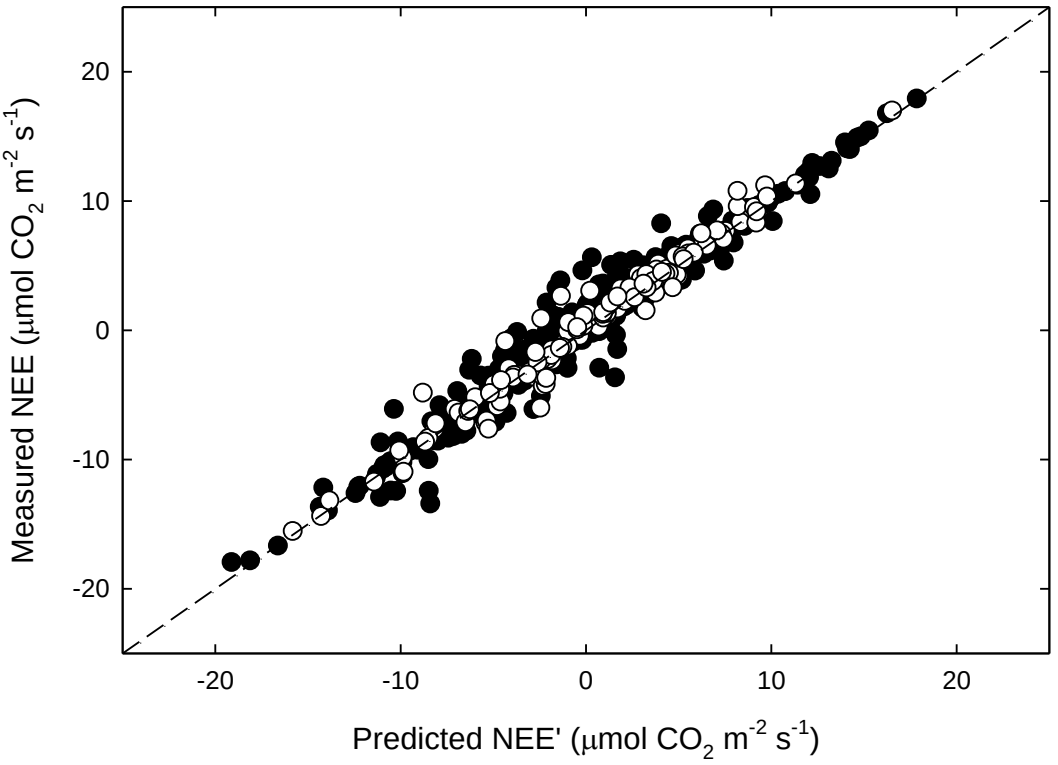

Figure 19: Validation of modelled net ecosystem exchange (NEE'). Measured NEE versus modelled NEE' for all plot measurements (closed symbol), and for one randomly selected measurement per plot and period not included in the model parameterization (open symbol). Statistics of the fit are shown in Table VI. The dashed line represents the ideal relationship (slope=1, intercept=0).

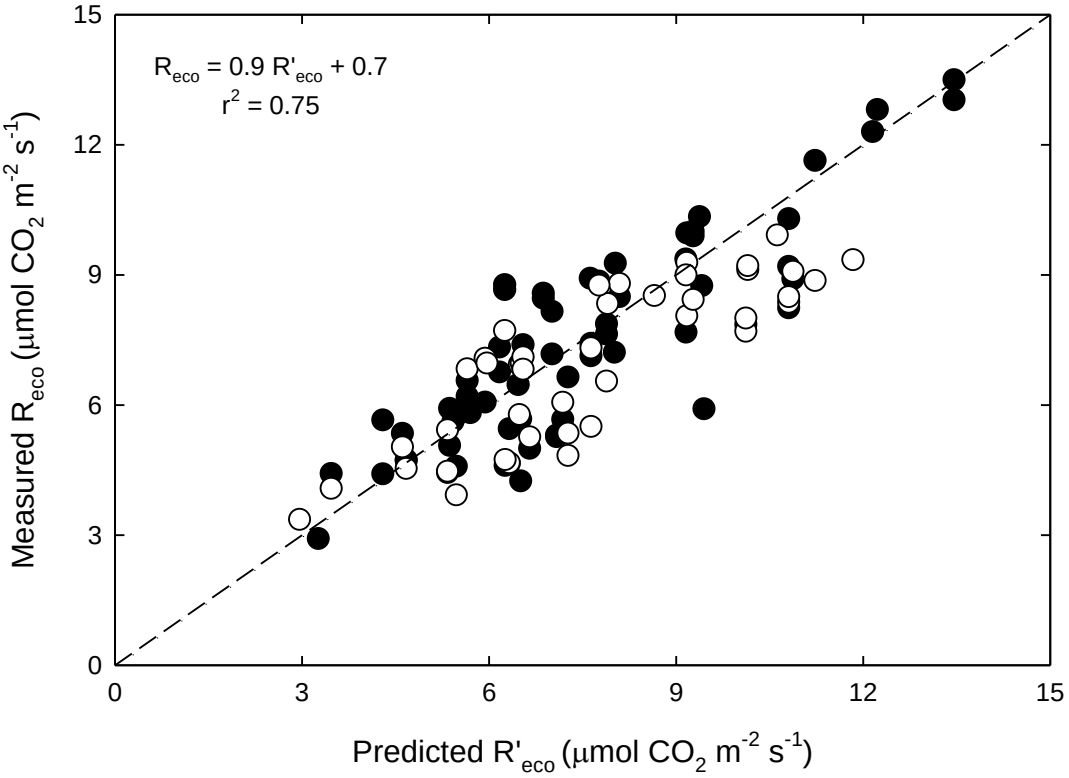

Figure 20: Validation of modelled ecosystem respiration (R'_{eco}). Measured R_{eco} versus modelled R'_{eco} for all plot measurements (closed symbol), and for one randomly selected measurement per plot and period not included in the model parameterization (open symbol). The dashed line represents the ideal relationship (slope=1, intercept=0).

Model-fitted parameters were similar to those reported for moist acidic tundra in the proximities of the area of study. Mean A_{max} and Ks values at our Ambient and treatment plots ranged within values reported by Williams *et al.*, (2006) across the area of study (6.6–30.0 μmol CO_2 m^{-2} s^{-1} and 281–1000 μmol PAR m^{-2} s^{-1} respectively) (Table VI). Accordingly, peak season values of quantum efficiency (E_0; Eq. 3.3) ranged between 0.031–0.035 μmol CO_2 μmol^{-1} PAR across our Ambient and treatment plots, agreeing with those reported for Alaskan tussock tundra (0.035 μmol CO_2 μmol^{-1} PAR; Shaver *et al.*, 2007; Street *et al.*, 2007). Mean R_b at RS, Ambient and MS plots were consistent with values reported for moist acidic tundra (0.25–1.98 μmol CO_2 m^{-2} s^{-1}; Williams *et al.*, 2006; Shaver *et al.*, 2007), whereas HS showed values within those observed in sedge-dominated areas (0.1–0.6 μmol CO_2 m^{-2} s^{-1}; Williams *et al.*, 2006; Shaver *et al.*, 2007) (Table VI). Similarly, model-fitted respiration-temperature coefficients (β) under Reduced snow (RS), Ambient and Medium Snow addition (MS) conditions ranged within values expected for moist acidic tundra (0.01–0.09; Williams *et al.*, 2006; Shaver *et al.*, 2007) but increased with High Snow additions (HS) to values similar to those reported for wet-sedge areas (0.08–0.189; Williams *et al.*, 2006; Shaver *et al.*, 2007) (Table VI).

3.9.2 Leaf Area Index – dependent model for Gross Primary Productivity. Evaluation of modelled GPP′

Daily GPP was estimated by applying the photosynthetic irradiance-response term from the PIRT model to daily treatment-specific A_{max} and Ks. However, while phonologic development is inherently integrated within the seasonal variation of these model-fitted parameters, considerations of seasonal patterns of gross productivity are indirect in this approach. In addition, GPP is a variable estimated from the direct determination of NEE and R_{eco}, direct validations being therefore impossible.

Therefore, to gauge confidence in our GPP predictions we applied an alternative model to estimate GPP′ using an adaptation of the aggregated canopy photosynthesis model that considers the hyperbolic photosynthesis-light equation at the leaf level and light extinction through the canopy to integrate the seasonality of plant development (Shaver *et al.*, 2007; Ives *et al.*, 2013; Sharp *et al.*, 2013).

(Eq. S3.2) $$GPP' = \frac{Amax_L}{k} \times Ln \frac{Amax_L + (E_0 \times PAR)}{Amax_L + (E_0 \times PAR \times e^{-k \times LAI_{Eff}})}$$

where $Amax_L$ is the light-saturated photosynthetic rate per unit of leaf area (μmol CO_2 m^{-2} leaf s^{-1}), k is the Beer's law light extinction coefficient (m^{-2} ground m^{-2} leaf), E_0 is the initial slope of the light response curve (μmol CO_2 μmol^{-1} photons), PAR is the light level at the top of the canopy, and LAI_{Eff} is the effective leaf area index (m^2 leaf m^{-2} ground).

Treatment- and period- specific LAI_{Eff} was estimated from the linear relationship between leaf area index and GPP_{600} described by Street et al. (2007) for moist acidic tussock tundra in the proximities of our experimental site, and $Amax_L$ was calculated as the light-saturated photosynthetic rate per unit of effective leaf area index:

(Eq. S3.3) $$Amax_L = \frac{Amax}{LAI_{Eff}}$$

Estimated values of LAI_{Eff} at our Ambient plots (1.2±0.1 m^2 m^{-2}) were within the range expected for moist acidic tundra with similar vegetation cover and equivalent phonologic development (0.8–1.2 m^2 m^{-2}; Street *et al.*, 2007), and increased at MS (2.3±0.2 m^2 m^{-2}) to values comparable to those in response to experimental fertilization (2.2–2.8 m^2 m^{-2}; Street *et al.*, 2007). This is consistent with observed increases in the area cover of deciduous shrubs. Similarly, $Amax_L$ across our Ambient and treatment plots (19.2±0.1 μmol CO_2 m^{-2} leaf s^{-1}) agreed well with those reported for tussock-dominated tundra in the vicinities of Toolik Lake (19.8 μmol CO_2 m^{-2} leaf s^{-1}; Shaver *et al.*, 2007).

Regression of PIRT against LAI-dependent model predictions showed a strong agreement of in hourly GPP' estimates for all treatments, suggesting that the photosynthetic irradiance-response term of the PIRT model was a useful tool for interpolating GPP, and that the interpolation of period-specific parameterizations successfully integrated seasonality in our model outputs (Fig. 21).

While the LAI-dependent approach integrates unquantified parameters that are likely to affect photosynthesis (e.g. leaf nitrogen concentrations, stomatal conductance), it may create circularity in the parameters used and the model output. Therefore, reported daily GPP' and GPP seasonal budgets at our Ambient and treatment plots were estimated from PIRT model outputs, using the LAI-dependent model for validation purposes only.

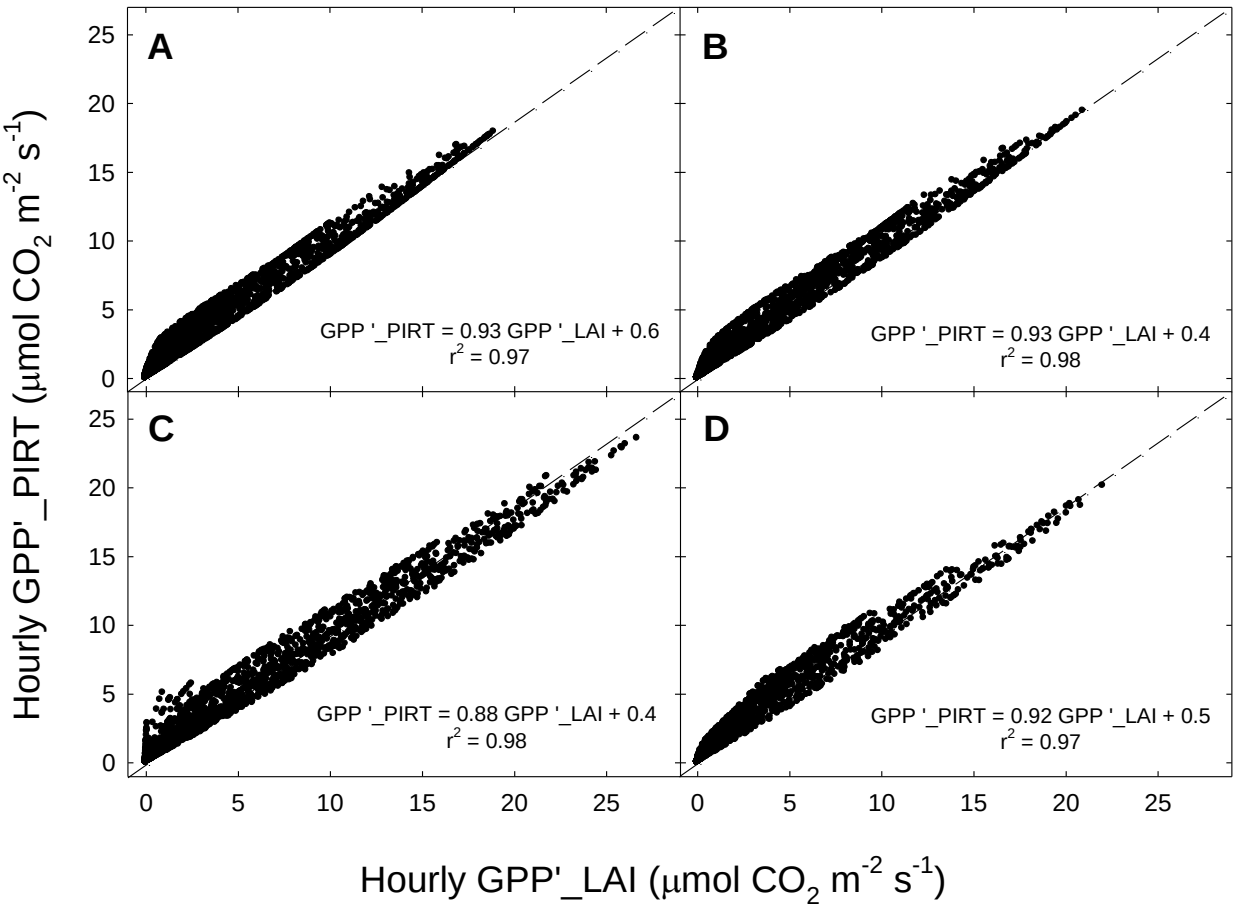

Figure 21: Evaluation of modelled Gross Primary Productivity (GPP'). Linear regression of hourly GPP' predicted by the photosynthetic irradiance-response term of the PIRT model against hourly GPP' predicted by the LAI-dependent model for **(a)** Reduced Snow (RS), **(b)** Ambient, **(c)** Medium Snow addition (MS), and **(d)** High Snow addition (HS) treatments. Regressions were significant (P<0.05), and the slope and intercept terms were not significantly different from 1 and 0 respectively for all treatments and Ambient plots. Dashed lines represent ideal relationships (slope=1, intercept=0).

3.9.3 Evaluation of model estimates of seasonal soil and heterotrophic respiration

To evaluate the robustness of daily soil respiration estimates (R'_{soil}), we applied both linear interpolation and temperature sensitivity gap filling methods of R_{soil}. Results from treatment-specific temperature-dependent functions showed good agreement with linearly interpolated values of R'_{soil} (r^2=0.92; P<0.0001) (Fig 22).

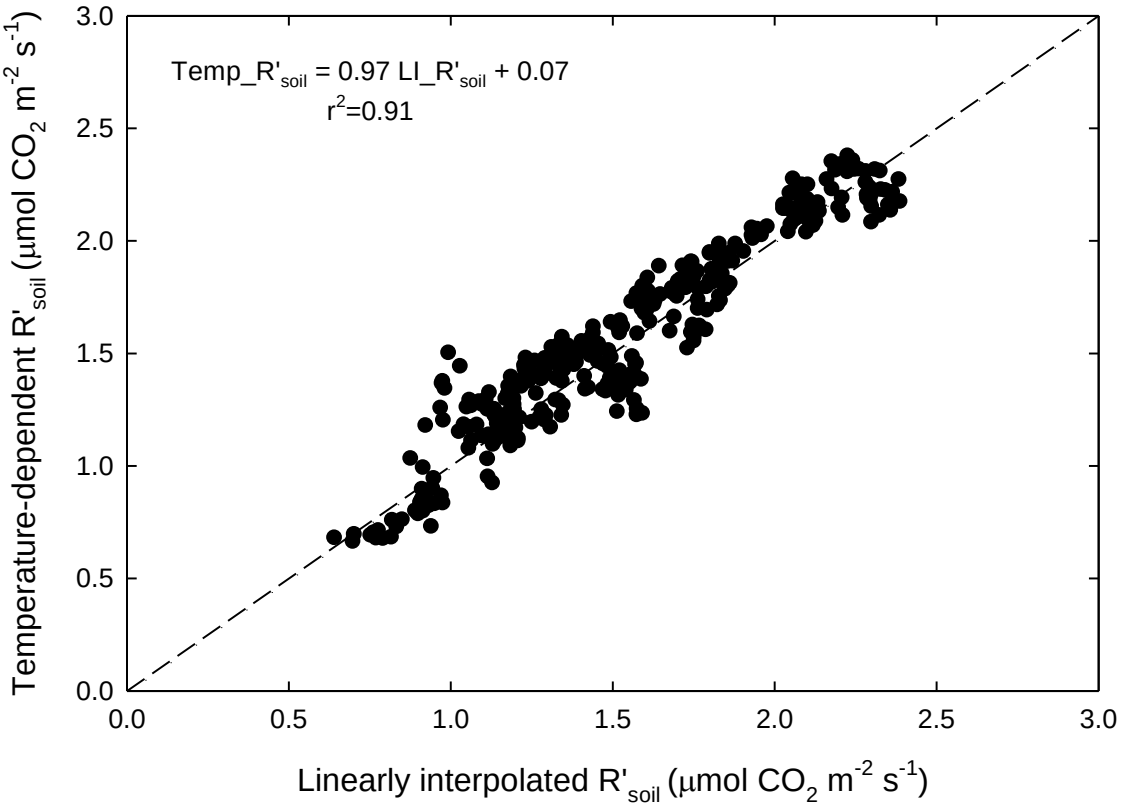

Figure 22: Evaluation of modelled daily soil respiration (R'_{soil}). Linear regression of daily R'_{soil} predicted by soil temperature dependent functions against daily R'_{soil} predicted by linear interpolation. Regression was significant (P<0.05), and the slope and intercept terms were not significantly different from 1 and 0 respectively. The dashed line represents ideal relationships (slope=1, intercept=0).

We used treatment-specific model parameters (R_0 and φ) to predict daily R_{het} (R'_{het}) for point measurements not included in parameter determinations. The strong robustness of predicted values indicated that the gap filling methods applied were successful in interpolating daily values (Slope 0.98±0.08, Intercept 0.09±0.08; r^2=0.82; Fig. 23).

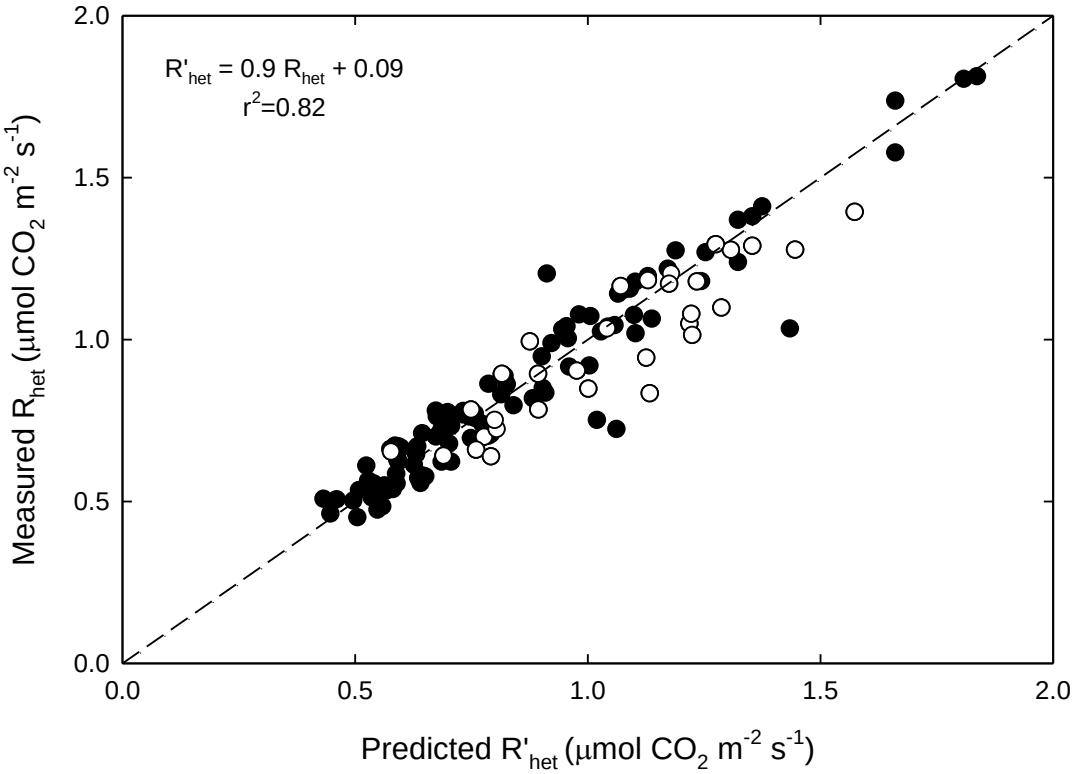

Figure 23: Validation of modelled heterotrophic respiration (R'_{het}). Measured versus modelled heterotrophic respiration for all plot measurements (closed symbol), and for two randomly selected measurements per plot and period not included in model parameterizations (open symbol). Statistics of the fit are shown in Table VIII. The dashed line represents the ideal relationship (slope=1, intercept=0).

3.9.4 Supplementary information. Cited literature

Ives SL, Sullivan PF, Dial R, Berg EE, Welker JM (2013) CO_2 exchange along a hydrologic gradient in the Kenai Lowlands, AK: feedback implications of wetland drying and vegetation succession. *Ecohydrology*, **6**, 38–50.

Sharp ED, Sullivan PF, Steltzer H, Csank AZ, Welker JM (2013) Complex carbon cycle responses to multi-level warming and supplemental summer rain in the high Arctic. *Global Change Biology*, **19**, 1780–1792.

Shaver GR, Street LE, Rastetter EB, Van Wijk MT, Williams M (2007) Functional convergence in regulation of net CO_2 flux in heterogeneous tundra landscapes in Alaska and Sweden. *Journal of Ecology*, **95**, 802–817.

Street LE, Shaver GR, Williams M, Van Wijk MT (2007) What is the relationship between changes in canopy leaf area and changes in photosynthetic CO_2 flux in Arctic ecosystems? *Journal of Ecology*, **95**, 139–150.

Williams M, Street LE, van Wijk MT, Shaver GR (2006) Identifying Differences in Carbon Exchange among Arctic Ecosystem Types. *Ecosystems*, **9**, 288–304.

4. WINTER PRECIPITATION AND SNOW ACCUMULATION DRIVE THE METHANE SINK OR SOURCE STRENGTH OF ARCTIC TUSSOCK TUNDRA

Reprinted in its entirety with permission from: **Blanc-Betes, E.**, Welker, J. M., Sturchio, N. C., Chanton, J. P. and Gonzalez-Meler, M. A. (2016) Winter precipitation and snow accumulation drive the methane sink or source strength of Arctic tussock tundra. *Glob Change Biol*, **22**, 2818–2833. doi:10.1111/gcb.13242

(*See* Appendix A, Copyright clearance statement from publisher)

4.1 ABSTRACT

Arctic winter precipitation is projected to increase with global warming, but some areas will experience decreased snow accumulation. Although Arctic CH_4 emissions may represent a significant climate forcing feedback, long-term impacts of changes in snow accumulation on CH_4 fluxes remain uncertain. We measured ecosystem fluxes, and soil CH_4 and CO_2 concentration and ^{13}C composition to investigate changes in emission and the predominant metabolic pathways and transport mechanisms driving moist acidic tundra CH_4 fluxes over the growing season (Jun–Aug) after 18 years of experimental snow depth increases and decreases. Deeper snow promoted soil wetness and warming, which reduced soil $\%O_2$ saturation and increased thaw depth. Soil moisture, through changes in soil $\%O_2$, determined predominance of methanotrophy or methanogenesis, with soil temperature regulating the ecosystem CH_4 sink or source strength. Reduced snow (RS) increased the fraction of oxidized CH_4 (F_{ox}) by 75–120% compared to Ambient, switching the system from a small source to a net CH_4 sink (21±2 and –31±1 mg CH_4 m^{-2} $season^{-1}$ at Ambient and RS). Deeper snow reduced F_{ox} by 35–40% and 90–100% in medium- (MS) and high- (HS) snow additions relative to Ambient, largely contributing to increased CH_4 source strength (464±15 and 3,561±97 mg CH_4 m^{-2} $season^{-1}$ at MS and HS). Decreases in F_{ox} with deeper snow were partly explained by increased plant-mediated CH_4 transport associated with the expansion of tall graminoids. Deeper snow stimulated CH_4

production within newly thawed soils responding mainly to warming rather than to increases in acetate fermentation expected with thaw-induced increases in SOC availability. Our results suggest that increased winter precipitation will increase the CH_4 source strength of Arctic tundra, but the resulting positive feedback on climate change will depend on the balance between areas with more or less snow accumulation than they are currently facing.

4.2 INTRODUCTION

In a changing climate, Arctic warming and associated precipitation increases may largely exceed global trends (Kattsov & Walsh, 2000; Miller *et al.*, 2010; Christensen *et al.*, 2013; Cohen *et al.*, 2014). Because Arctic regions contain up to 50% of the global soil organic carbon (SOC) within frozen soils (permafrost), climate change may induce soil C losses as CO_2 and CH_4 causing a positive feedback on permafrost degradation and climate change (Hugelius *et al.*, 2014; Ping *et al.*, 2014; Schaefer *et al.*, 2014). While the vulnerabilities of Arctic SOC to rising temperatures are identified (Schuur *et al.*, 2013, 2015), the sensitivity of ecosystem C dynamics to changes in precipitation has only recently been appraised (Hicks Pries *et al.*, 2013; Sharp *et al.*, 2013; Carvalhais *et al.*, 2014).

Climate models robustly predict 25–50% more precipitation globally in Arctic regions by the end of the century, mostly as fall and winter snow (Kattsov *et al.*, 2005; Zhang *et al.*, 2013; Bintanja & Selten, 2014). However, subject to regional and local heterogeneity in winter precipitation and snow accumulation, some areas will experience snow accumulations beyond predictions or reduced below current values across the Arctic region (Callaghan *et al.*, 2011; Stocker *et al.*, 2013a). Changes in winter precipitation strongly influence soil hydrological and thermal conditions (Fan *et al.*, 2011; Subin *et al.*, 2013; Zhang *et al.*, 2013), with cascading effects on permafrost degradation (Osterkamp, 2007; Johansson *et al.*, 2013), soil C and N

mineralization (Schimel *et al.*, 2004), and associated changes in plant community composition (Fig. 1) (Elmendorf *et al.*, 2012; Tape *et al.*, 2012). Moreover, derived changes in microrelief and vegetation cover could further alter snow accumulation locally (Liston *et al.*, 2002; Seppälä, 2011; Johansson *et al.*, 2013), triggering a feedback loop that amplifies the impacts of changes in snow accumulation over time (Fig. 1) (Sturm *et al.*, 2005; Osterkamp *et al.*, 2009). These effects combine to influence the magnitude and timing of C fluxes from Arctic ecosystems (Fig. 1). However, research on the effects of changes in Arctic winter precipitation has primarily focused on CO_2 rather than CH_4 fluxes, leaving a large portion of the C cycle climate feedback unresolved (Elberling, 2007; Morgner *et al.*, 2010; Nowinski *et al.*, 2010; Lupascu *et al.*, 2014a, 2014b, 2014c; Schuur *et al.*, 2015).

Current models estimate that CH_4 emissions will be responsible for 20–30% of the radiative forcing from Arctic regions over the course of this century (Schneider von Deimling *et al.*, 2012; Myhre *et al.*, 2013; Deng *et al.*, 2014). At present, Arctic tundra contributes to about 45% of all Arctic CH_4 sources and 7% of global CH_4 emissions (McGuire *et al.*, 2012; Kirschke *et al.*, 2013; Turner *et al.*, 2015). Changes in CH_4 emissions from Arctic tundra could substantially alter climate forcing feedbacks from the Arctic region.

Changes in snow fall and accumulation influence CH_4 emissions in Arctic tundra through complex controls on CH_4 production (methanogenesis), oxidation (methanotrophy), and transport, all processes intimately linked to soil hydrology, temperature, and substrate availability (Elberling *et al.*, 2008; Chowdhury & Dick, 2013; Treat *et al.*, 2014, 2015). Limited drainage of permafrost soils increases soil wetness upon snowmelt, altering the zonation of prevalent methanogenesis and methanotrophy and hence the potential of the ecosystem to produce and oxidize CH_4. Increased soil water content also favors heat transfer within the soil

column (Lunardini, 1991; Romanovsky & Osterkamp, 2000; Subin *et al.*, 2013) with synergistic effects on CH_4 production, as warmer soils may promote both metabolic activity (Wallenstein *et al.*, 2009; Inglett *et al.*, 2012; Tveit *et al.*, 2015) and permafrost thaw, exposing previously frozen SOC to methanogens (Fig. 1) (McCalley *et al.*, 2014). In addition, transitions in dominant vegetation associated with changes in snow accumulation may further alter SOC quality and availability through changes in root exudation and litter inputs (Fig. 1) (Ström *et al.*, 2003, 2012; Dorrepaal *et al.*, 2005). Understanding how long-term changes in winter precipitation affect CH_4 dynamics in Arctic tundra is therefore critical for accurate predictions of the fate of permafrost SOC and climate forcing from the Arctic region.

Methanogens utilize two major metabolic pathways, acetate fermentation and CO_2 reduction. Acetate is the main substrate under anaerobic conditions accounting for up to 70% of the produced CH_4, and is generally associated with decomposition of relatively labile SOC (Avery *et al.*, 2003; Metje & Frenzel, 2007). Thus, vegetation- and permafrost thaw- induced changes in substrate availability and decomposability could greatly alter CH_4 production and emission (Hodgkins *et al.*, 2014; McCalley *et al.*, 2014). Moreover, shifts in plant communities may further influence net ecosystem CH_4 uptake or emission by influencing gas diffusivity, promoting both rhizospheric CH_4 oxidation by the oxygenation of shallow horizons, and CH_4 efflux through plant mediated transport (Kelker & Chanton, 1997; King *et al.*, 1998; Ström *et al.*, 2005).

The carbon isotopic composition of CH_4 and CO_2 in pore water and surface emissions provides insight into ecosystem CH_4 dynamics, as $\delta^{13}C\text{-}CH_4$ and $\delta^{13}C\text{-}CO_2$ values integrate the effects of CH_4 production, oxidation and transport (Whiticar & Faber, 1986; Chanton *et al.*, 1992; Hornibrook *et al.*, 1997). While the intricacy of these codependent processes makes it

difficult to estimate the absolute magnitude of each process, shifts in the $\delta^{13}C$ and distribution of co-existing CO_2 and CH_4 within the soil profile and emissions reflect changes in the relative predominance of the metabolic pathways and transport mechanisms contributing to ecosystem CH_4 fluxes (Corbett *et al.*, 2013; Throckmorton *et al.*, 2015).

The objective of this study was to determine the long-term effect of projected changes in snow accumulation (increase and decrease) on ecosystem CH_4 fluxes in moist acidic tundra, which represents over 25% of the Alaskan Arctic and globally over 15% of the circum-Arctic vegetated landscapes (Walker *et al.*, 2005). We combined $\delta^{13}C$-CH_4 and $\delta^{13}C$-CO_2 measurements from the soil profile and ecosystem fluxes to evaluate changes CH_4 production, oxidation and transport through the soil column in response to 18 years of snow depth increase and decrease predicted by climate models. We coupled alterations of the soil climate and vegetation cover to shifts in the predominant metabolic and transport pathways to further investigate the control mechanisms ultimately driving changes in ecosystem CH_4 fluxes. We hypothesized that increases in snow accumulation would result in wetter and warmer soils, greater thaw depth and increases in the relative abundance of shrubs and tall sedges. We predicted that wetter and warmer soils would lead to increases of CH_4 production and would suppress CH_4 oxidation, overall increasing ecosystem CH_4 emissions. We further predicted that increases in ecosystem CH_4 emissions would be partly fueled by increases in the relative contribution of acetate fermentation to CH_4 production as a result of vegetation- and thaw-induced increases in substrate availability, and by increases in plant mediated transport associated to increases in the relative abundance of tall graminoids.

4.3 METHODS

4.3.1 Site description

The experimental site is located in moist acidic tussock tundra near Toolik Lake (68°38'N, 149°38'W; 760 m) at the Long Term Ecological Research Site in the northern foothills of the Brooks Range, Alaska (Fig. 2) (Jones *et al.*, 1998; Welker *et al.*, 2000; Pattison & Welker, 2014). Mean annual air temperature is –8°C, with summer temperatures averaging 10.5°C. The soil active layer typically reaches a maximum thaw depth of 45–50 cm by late August (Welker, Arctic LTER). Annual precipitation is around 350 mm, 50% of which falls as snow (Deslippe & Simard, 2011). Winter snow accumulation is 45–80 cm, and the area becomes snow-free by late-May setting the beginning of the growing season. Soils are classified as coarse-loamy, mixed, acidic, Ruptic-Histic Pergelic Cryaquept (Romanovsky et al., 2011). Soils in the area are generally poorly drained, with shallow organic horizons (10–15cm; 20–45 %C) grading into increasingly mineral horizons at depth within the active layer (1–3 %C; Ping *et al.*, 1997). Vegetation is dominated by tussock forming sedges (*Eriophorum vaginatum*), and interspaced shrubs (*Betula nana*, *Salix pulchra*) and mosses (*Sphagnum sp.*) characteristic of moist acidic tundra across the Alaskan North Slope (Walker *et al.*, 1994; Wahren *et al.*, 2005).

4.3.2 Experimental design

The experimental setup consists of a 2.8 x 60 m snow fence erected in 1994 perpendicular to prevailing winter winds to create a snow drift that extends 60 m downwind. In 2012, 4 plots were established in each of the following distinct snow accumulation regimes (n=4): i) ambient snow accumulation (Ambient), ii) Medium Snow addition (MS) with 20–45% more snow than Ambient, iii) High Snow addition (HS) with snow increase 70–100% over Ambient, and iv) Reduced Snow (RS) with 15–30% less snow than Ambient (Jones *et al.*, 1998;

Walker *et al.*, 1999; Pattison & Welker, 2014). After 18 years, snow addition treatments showed soil consolidation consistent with first stages of thermokarst development (*see* Chapter 2).

Measurements and samples were taken concurrently from permanently installed boardwalks, at biweekly intervals during the growing season (May 30 to Aug 31, 2012). At each sampling period, measurements were taken between 10am and 3pm over four days, and plot order was randomized during the sampling.

4.3.3 Soil environmental variables

Soil temperature at 10, 20, 35 and 50 cm depth was measured in each plot using a portable profile temperature probe (OMEGA Engineering Inc., CT, USA). Volumetric water content (VWC; 12-cm depth-integrated) was measured with a soil moisture meter (HydroSense II, Campbell Scientific Inc., UT, USA). Thaw depth (thickness of unfrozen ground) was monitored using a metal depth rod. Replicates (n=4) are averaged values of 8 pseudo-replicates per plot.

4.3.4 Vegetation cover characterization

Vegetation cover was characterized at each treatment (n=5) with a 100-point 0.7 x 0.7 m frame following methods described by Walker (1996). Plant species were recorded for each point measurement providing relative % cover and grouped according to growth form. Vegetation characterization was conducted at peak season, between late July (RS, Ambient and MS treatments) and early August (HS treatment).

4.3.5 Soil sampling and $\delta^{13}C$ determination

Soil cores (5 cm diameter) to the frost table (depth to the thawing front) were collected in mid-August at all treatments (n=5). Cores were sectioned into 2-cm depth intervals and kept frozen at –20ºC for the later determination of C isotopic composition (δ^{13}C-OM) using a continuous flow ThermoFinnigan Delta Plus XL equipped with Conflo III, and zero-blank Elemental Analyzer (Costech Analytical, ECS 4010).

4.3.6 Ecosystem CH_4 flux measurements

At each plot, ecosystem CH_4 fluxes and δ^{13}C values were measured using the static chamber approach (Bubier *et al.*, 1995) with a 25-cm-diameter PVC collars inserted 15 cm into the soil (average depth to the mineral horizon) (n=4). Collar insertion had no effect on plant development, species composition, or soil moisture or temperature, and provided a gas-tight chamber-soil system. From each chamber, five gas samples were taken at 15-min intervals over a 75-min period and analyzed for CH_4 and CO_2 concentrations (pCH_4, pCO_2) and δ^{13}C-CH_4 and δ^{13}C-CO_2 within 4–6 hr after collection using a Picarro G2201-*i* cavity ring-down spectrometer (CRDS) (*Supp. Info. 4.9.1*). A standard mix of 2.5 ppm CH_4 (δ^{13}C-CH_4 = –40.2 ‰) and 396 ppm CO_2 (δ^{13}C-CO_2 = –35.7 ‰) was run every five samples to account for instrument drift. The accuracy for pCH_4 and δ^{13}C-CH_4 was better than 90 ppb and 0.1‰. The accuracy of pCO_2 and δ^{13}C-CO_2 was better than 1ppm and 0.06 ‰. Ecosystem CH_4 flux was calculated as the slope of the linear regression of pCH_4 versus time. The δ^{13}C value of emitted CH_4 (δ_{eco}) was calculated as the intercept of δ^{13}C-CH_4 against the inverse of pCH_4 in the chamber headspace over time (Keeling, 1958; Chanton *et al.*, 2008a). Slopes with correlation coefficients below 0.9 (P<0.05; n=5) were rejected (< 5% of data).

(Eq. 4.1) $\delta_{eco} = [(\delta_{(f)} \cdot pCH_{4\,(f)}) - (\delta_{(i)} \cdot pCH_{4\,(i)})] / pCH_{4\,(f)} - pCH_{4\,(i)}$

4.3.7 Soil gas concentration and carbon isotopic composition

Soil interstitial gas and pore water were collected from soil probes progressively installed at each plot at 10, 20, 35 and 50-cm depth as the thaw depth increased over the growing season. Two samples were taken at each depth, plot and sampling period, and values were averaged for a total of 4 replicates per treatment, depth and period. All samples were analyzed within 4–6 hr after collection for the direct determination of pCH_4, pCO_2, $\delta^{13}C\text{-}CH_4$ and $\delta^{13}C\text{-}CO_2$ using a Picarro G2201-*i* CRDS (*Supp. Info.* 4.9.1). The percent saturation of O_2 ($\%O_2$) was determined using a fiber-optic oxygen meter on 20mL sample aliquots (Firesting O_2; Pyroscience, Germany). Dissolved gas concentrations were calculated by applying Henry's Law and the solubility coefficient for O_2, CH_4 and CO_2 considering the temperature and atmospheric pressure at the depth and time of collection (Sander, 1999). Values from non-water-saturated zones correspond to the calculated dissolved concentration in equilibrium with measured concentrations in the air-filled space (Sander, 1999; Whalen & Reeburgh, 2000).

4.3.8 Apparent carbon isotope fractionation

At each plot, depth and sampling period, values of coexisting $\delta^{13}C\text{-}CH_4$ and $\delta^{13}C\text{-}CO_2$ from soil interstitial gas and pore water were used to calculate the apparent C isotope fractionation factor (α_C) using the following equation (Whiticar *et al.*, 1986):

(Eq. 4.2) $\alpha_C = (\delta^{13}C\text{-}CO_2 + 1000) / (\delta^{13}C\text{-}CH_4 + 1000)$

where α_C represents the magnitude of the kinetic isotopic separation effects between CO_2 and CH_4 during methanogenesis (Whiticar *et al.*, 1986). Values of α_C are indicative of the relative

predominance of acetate fermentation versus CO_2 reduction methanogenic pathways, which are responsible for 95% of total CH_4 produced (Segers, 1998; Chowdhury & Dick, 2013). Lines of constant α_C delineate regions of predominant acetate fermentation (α_C ~ 1.040 to 1.055) or CO_2 reduction (α_C ~ 1.055 to 1.090) (Whiticar *et al.*, 1986). Conversely, methanotrophy is associated with a gradual enrichment of residual $\delta^{13}C$-CH_4, yielding lower α_C in zones with prevailing oxidation (α_C ~ 1.005 to 1.03; Barker & Fritz, 1981; Whiticar & Faber, 1986). α_C values reflect the combined isotope fractionation effects of methanogenesis, methanotrophy and CH_4 transport. Therefore, α_C is used as an indication of the predominant metabolic process in response to treatment rather than a measure of the absolute contribution of each individual process.

4.3.9 Fraction of oxidized CH_4

The fraction of oxidized CH_4 (F_{ox}; CH_4 oxidation efficiency) was estimated from the $\delta^{13}C$ value of emitted CH_4 and the $\delta^{13}C$ value of dissolved CH_4 sampled in pore water at the production zone using an isotope mass balance approach (Liptay *et al.*, 1998).

(Eq. 4.3) $$F_{ox} = (\delta_{eco} - \delta_{anox}) / [(\alpha_{ox} - \alpha_{trans}) \cdot 1000]$$

where δ_{eco} is the $\delta^{13}C$ value of emitted CH_4 (Eq. 4.1), δ_{anox} is the $\delta^{13}C$ value of dissolved CH_4 at the production zone, α_{ox} is the isotopic fractionation for CH_4 oxidation, and α_{trans} is the isotope fractionation for diffusive soil/plant transport of CH_4.

This approach considers the soil profile as an open system, where deep horizons dominate CH_4 production and assumes no significant methanogenic pathway shift along the soil profile. A shift from CO_2 reduction to acetate fermentation up the soil profile would enrich the $\delta^{13}C$ of produced CH_4, overestimating F_{ox}. While we observed a depth effect in the distribution of dominant methanogenic pathways (Fig. 32), more than 80% of the produced CH_4 originated

below 35 cm predominantly by CO_2 reduction across all treatments and sampling periods (Figs. 32 and 33). Therefore, our data indicates this is a reasonable assumption within the constraints of the F_{ox} model.

Because CH_4 isotope fractionation during oxidation and transport near the frost table has been shown to be negligible (Popp *et al.*, 1999; Hines *et al.*, 2008), δ_{anox} is approximated to the $\delta^{13}C$-CH_4 value at the bottom of the thawed soil layer. α_{ox} was determined at plots with net ecosystem CH_4 oxidation. Temperature corrections were made to estimate period- and treatment-specific α_{ox} accounting for the temperature sensitivity of the fractionation factor (*Supp. Info.* 4.9.2; King *et al.*, 1989; Chanton *et al.*, 2008b).

The α_{trans} coefficient is contingent upon the transport mechanism dominating upward transport of CH_4 through the soil profile. Transport of CH_4 may occur via non-fractionating mechanisms (i.e. diffusion through water-saturated soils, plant-mediated transport or ebullition), or via fractionating mechanisms (i.e. molecular diffusion within the plant aerenchyma or through unsaturated soils) (Chanton *et al.*, 1992; Chanton, 2005). Near water-saturation conditions across our study site (VWC=0.70–1.12 cm^3 cm^{-3}) suggest the predominance of non-fractionating transport mechanisms through the soil column (Preuss *et al.*, 2013). However, plant-mediated transport may account for a substantial portion of emitted CH_4 (King *et al.*, 1998) yielding depleted δ_{eco}, and hence, underestimating F_{ox}. A sensitivity analysis on estimates of F_{ox} considering predominant non-fractionating (α_{trans} = 1.0013; Chasar *et al.*, 2000; Teh *et al.*, 2005; Preuss *et al.*, 2013) and predominant fractionating transport mechanisms (α_{trans} = 1.012; Chanton *et al.*, 1992) showed that changes in α_{trans} alter F_{ox} by 17.2% across treatments. Therefore, the reported F_{ox} values incorporate this uncertainty as in Chanton *et al.*, (2011).

4.3.10 Methane produced, oxidized and transported within the soil column

At each treatment and sampling period, the CH_4 produced within the soil column was estimated as in Corbett *et al.* (2013). Assuming that both methanogenic pathways produce an equimolar amount of CO_2 and CH_4 as expected from the decomposition of cellulose or hemicellulose (Chanton *et al.*, 2004), we can estimate the $\delta^{13}C\text{-}CO_2$ derived from methanogenesis ($\delta^{13}C\text{-}CO_2$-meth) as follows (Corbett *et al*., 2013):

(Eq. 4.4) $$\delta^{13}C\text{-OM} = ½\ (\delta^{13}C\text{-}CH_4) + ½\ (\delta^{13}C\text{-}CO_2\text{-meth})$$

where $\delta^{13}C$-OM is the $\delta^{13}C$ of the starting organic matter and $\delta^{13}C\text{-}CH_4$ is the $\delta^{13}C$ of pore water dissolved CH_4. This approach assumes that measured $\delta^{13}C\text{-}CH_4$ approximate that of produced CH_4. This assumption implies negligible contribution of CO_2 from CH_4 oxidation, and that the upward transport of CH_4 is dominated by non-fractionating mechanisms. In our study site, the profile distribution of pCH_4, $\%O_2$ and α_C values suggest minimal oxidation at depth (Figs. 28, 30, 32) (Popp *et al.*, 1999). However, α_C values reveal substantial oxidation and shallow depths, especially at RS and Ambient plots (Fig. 32b). We estimated the potential error introduced from contributions of oxidized CH_4 to shallow pCO_2 to be negligible (*Supp. Info.* 4.9.3). While plant-mediated transport may potentially result in substantial contributions to ecosystem CH_4 emissions, associated fractionation is primarily attributed to diffusion processes within the plant aerenchyma rather than to root uptake in the rhizosphere (Chanton, 2005; Throckmorton *et al.*, 2015). Therefore, we considered that diffusion through water and bulk flow (plant mediated and ebullition) dominated transport mechanisms operating within the soil column, with negligible effects on belowground $\delta^{13}C\text{-}CH_4$.

Methanogenesis, either by acetate fermentation or CO_2 reduction, results in considerably enriched $\delta^{13}C\text{-}CO_2$ relative to $\delta^{13}C$-OM, but alternative decay processes (i.e. respiration and

fermentation) yield $\delta^{13}C\text{-}CO_2$ similar to $\delta^{13}C$-OM (Whiticar *et al.*, 1986; Zetsche *et al.*, 2011). Hence, we can calculate the fraction pCO_2 from methanogenesis ($f\,CO_2$-meth) using the following mass balance equations (Corbett *et al.*, 2013):

(Eq. 4.5) $\delta^{13}C\text{-}CO_2 = (\delta^{13}C\text{-OM} \times f\,CO_2\text{-OM}) + (\delta^{13}C\text{-}CO_2\text{-meth} \times f\,CO_2\text{-meth})$

(Eq. 4.6) $f\,CO_2\text{-OM} + f\,CO_2\text{-meth} = 1$

where $f\,CO_2$-meth is the fraction of CO_2 from methanogenic pathways and $f\,CO_2$-OM is the fraction derived from alternative decay processes of OM.

The amount of CO_2 formed from methanogenesis (CO_2-meth) was determined using the following equation (Corbett *et al.*, 2013):

(Eq. 4.7) $f\,CO_2\text{-meth} \times pCO_2 = CO_2\text{-meth}$

Based on the equimolarity of CO_2 and CH_4 formed from methanogenesis, we assume equal amounts of CO_2-meth and CH_4 (CH_4-Prod). Differences between estimated CH_4-Prod and observed pCH_4 at a given depth (CH_4-Measured) reflects the fraction of CH_4 lost from the system ($f\,CH_4$-Lost; Corbett *et al.*, 2013; Throckmorton *et al.*, 2015) by oxidation (CH_4-Ox) or plant-mediated transport and/or ebullition (CH_4-Trans):

(Eq. 4.8) $f\,CH_4\text{-Lost} = (CH_4\text{-Prod} - CH_4\text{-Measured}) / CH_4\text{-Prod}$

Given that calculations of F_{ox} integrate the entire soil column, we estimated CH_4-Ox within the soil column combining estimates of F_{ox} (Eq. 4.3) and CH_4-Prod (Eq. 4.7). Differences between CH_4-Lost and CH_4-Ox will therefore provide a measure of the fraction of produced CH_4 lost by transport towards the atmosphere ($f\,CH_4$-Trans).

(Eq. 4.9) $CH_4\text{-Ox} = F_{ox} \times CH_4\text{-Prod}$

(Eq. 4.10) $CH_4\text{-Trans} = CH_4\text{-Lost} - CH_4\text{-Ox}$

(Eq. 4.11) $f\,CH_4\text{-Trans} = CH_4\text{-Trans} / CH_4\text{-Prod}$

It should be noted that CH_4 production, oxidation and transport are codependent processes occurring simultaneously within the soil column. The fraction of CH_4 subject to each process is therefore uncertain. Hence, we reiterate that our goal was not to test the model or provide absolute values for CH_4 production, oxidation and transport, but to use it as a tool to identify the relative effect of changes in snow accumulation on the mechanisms affecting CH_4 dynamics.

4.3.11 Gross ecosystem CH_4 production and oxidation, and net ecosystem CH_4 flux

Gross ecosystem CH_4 production and oxidation over the growing season was calculated using the following equations (Teh *et al.*, 2005):

(Eq. 4.12) $CH_{4\ Prod} = CH_{4\ Net} \times 1/(1-F_{ox})$

(Eq. 4.13) $CH_{4\ Ox} = CH_{4\ Prod} - CH_{4\ Net}$

where $CH_{4\ Net}$ is the net ecosystem CH_4 flux (mg CH_4 m^{-2} d^{-1}), $CH_{4\ Prod}$ is the gross ecosystem CH_4 production (mg CH_4 m^{-2} d^{-1}), $CH_{4\ Ox}$ is the gross ecosystem CH_4 oxidation (mg CH_4 m^{-2} d^{-1}), and F_{ox} is the fraction of oxidized CH_4 (Eq. 4.3). Seasonal $CH_{4\ Net}$, $CH_{4\ Prod}$ and $CH_{4\ Ox}$ were estimated from linear interpolation procedures between sampling periods over the growing season (Teh *et al.*, 2005, 2011).

4.3.12 Statistical analyses

Statistical analyses were performed using Statgraphics Centurion XVI software (Statistical Graphics Corp., MD, USA). Repeated measures analysis of variance were used to investigate the effect of snow treatment and sampling period and all interactions among these independent variables on soil environmental variables (i.e. soil moisture, temperature and

thawing depth), ecosystem CH_4 fluxes and δ_{eco} with replicates (n=4) as a random effect. For seasonal and treatment effects on soil interstitial parameters ($\%O_2$, dissolved pCH_4, $\delta^{13}C\text{-}CH_4$, $\delta^{13}C\text{-}CO_2$, α_C, and CH_4 production, oxidation and transport), depth was included as an additional fixed within treatment factor. Differences among treatments, within period and/or depth were examined with simple analysis of variance (ANOVA). We used the coefficient of determination (R^2) from simple regression analyses to explore codependence between single variables. Separate analyses for each depth and/or treatment were used to evaluate changes in codependency with depth and/or treatment. Multiple regression analyses that included soil environmental parameters as independent variables and net ecosystem CH_4 flux, production and oxidation separately as dependent variables were used to assess the mechanisms driving CH_4 dynamics across treatments. Stepwise removal of independent variables based on changes in likelihood was used to evaluate individual contributions to the model. Paired t-tests were used to determine significant differences between δ_{eco}, $\delta_{shallow}$ and δ_{anox} within treatments. Data was transformed to ensure normality. A fixed integer was added to all CH_4 fluxes to make all values positive prior to transformations (Davidson *et al.*, 2008). All seasonal means were calculated from linearly interpolated data and error propagation for seasonal averages and budgets were determined by linear interpolation of the variance as the main parameter representing the uncertainty associated with spatial heterogeneity (Davidson *et al.*, 2008).

4.4 RESULTS

4.4.1 Soil environmental variables

Snow regimes substantially altered soil environmental variables over the growing season (Fig. 24). Soil volumetric water content (0–12 cm depth) increased over the growing season at all

treatments except for HS (High Snow) (P=0.01; Fig. 24a). Soil volumetric water content at RS (Reduced Snow) (0.66±0.03 cm^3 cm^{-3}) was consistently lower than that of Ambient (0.75±0.02 cm^3 cm^{-3}) (P=0.07) (Fig. 24a). Snow additions increased volumetric water content compared to Ambient (0.83±0.007 and 0.96±0.004 cm^3 cm^{-3} at MS (Medium Snow) and HS respectively; P<0.05) (Fig. 24a). Soil was water-saturated below 15 cm at all treatments and sampling periods.

Soil temperature at 10-cm depth at the beginning of the growing season was similar across treatments, increasing over the growing season at all treatments, with significantly stronger treatment effect as the season progressed (P=0.0001; Fig. 24b). Soil temperature at 10-cm depth increased at a rate of 0.045±0.001 ^oC d^{-1} at Ambient, averaging 2.6±0.06 ^oC over the growing season. RS reduced soil warming rate (0.043±0.001 ^oC d^{-1}; P<0.05) yielding lower mean soil temperatures compared to Ambient (2.0±0.06 ^oC; P<0.05) (Fig. 24b). Seasonal warming rate was faster at MS and HS (0.05±0.002 and 0.10±0.002 ^oC d^{-1} respectively; P<0.05), averaging higher mean soil temperatures relative to Ambient (3.9±0.07 and 4.3±0.11 ^oC at MS and HS respectively; P<0.05) (Fig. 24b). Soil temperature decreased with depth at all treatments (P<0.05), but differences among treatments persisted (P<0.05).

Thaw depth deepened over the growing season, with differences among treatments intensifying throughout the season (P=0.0001; Fig. 24c). Thaw depth reached a maximum of 50.5cm at Ambient, increasing by +6.5 and +11.7 cm at MS and HS, respectively (P<0.05; Fig. 24c). RS had no significant effect on thaw depth (P=0.21; Fig. 24c). Changes in volumetric water content explained 83% of the seasonal warming recorded across treatments (P<0.0001; Table X), which explained 77% of the seasonal deepening of thaw depth (P<0.0001; Table X).

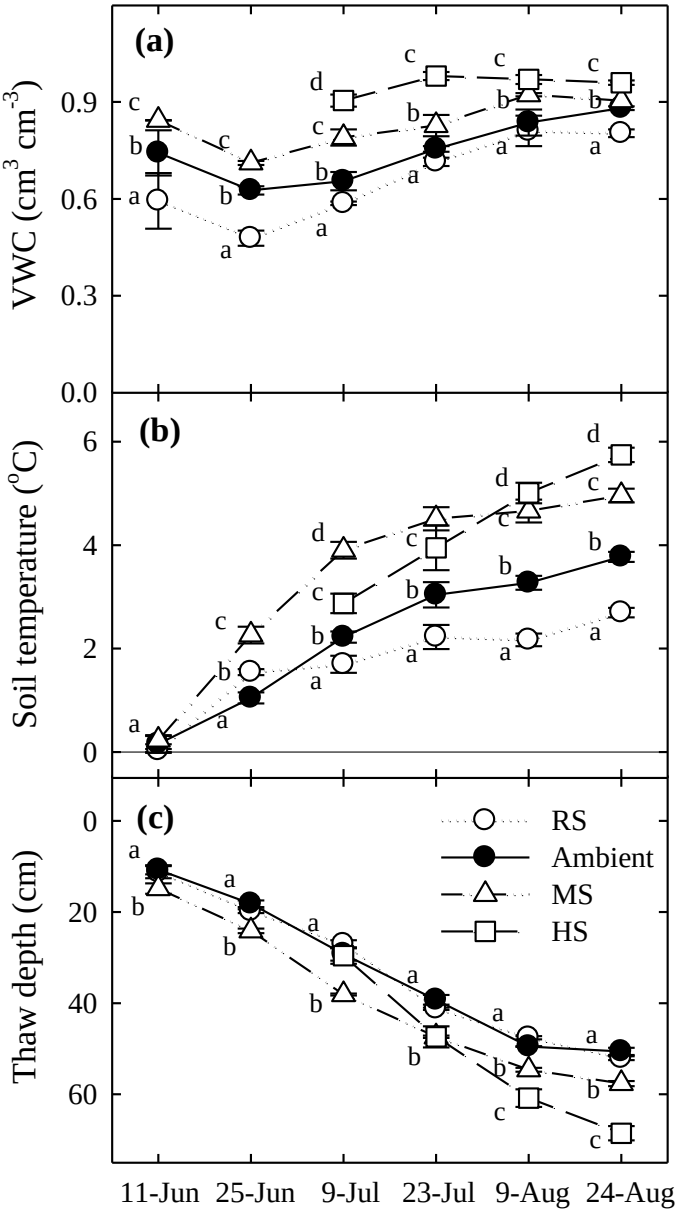

.

Figure 24: Seasonal variation of **(a)** volumetric water content (VWC; 0–12 cm), **(b)** soil temperature (10 cm) and **(c)** thaw depth at Reduced Snow (RS), Ambient, Medium Snow (MS) and High Snow (HS) addition treatments over the growing season. Error bars correspond to Standard Error of the Mean (±SE). Mean values within the same sampling period with different letter indicate statistical differences among treatments at a given sampling period (P<0.05) *(Reprinted with permission from: Blanc-Betes et al., 2016).*

TABLE X

Results from simple regression analyses among soil environmental variables and between the soil profile distribution of O_2 saturation (%) and volumetric water content (VWC), dissolved CH_4 concentration (Log[CH_4]) and apparent isotopic fractionation (α_C). Soil profile dissolved CH_4 concentrations were log-transformed to meet the requirements of parametric correlations *(Reprinted with permission from: Blanc-Betes et al., 2016).*

Variables		Curve fit	Coef. Corr.	R^2	F	*P*
Independent	Dependent					
VWC (cm^3 cm^{-3}) *	Seasonal warming (^oC d^{-1}) [1]	Quadratic	0.93	0.83	28.81	0.0001
Soil temperature (^oC) *	Thaw depth (cm)	Linear	0.88	0.77	308.35	<0.0001
	VWC (cm^3 cm^{-3}) [1]	Sigmoidal	– 0.92	0.84	186.63	<0.0001
O_2 Saturation (%)	Log[CH_4] (μmol L^{-1})	Linear	– 0.98	0.97	7059.14	<0.0001
	α_C	Exponential	– 0.83	0.69	611.47	<0.0001

[1] Values correspond to shallow soil layers (0–10 cm depth).

4.4.2 Vegetation cover characterization

After 18 years of experimental snow accumulation, we observe changes in the relative abundance of the main vegetation life forms in response to treatment. RS did not show significant shifts in vegetation cover compared to Ambient (Fig. 25; $P>0.05$). MS increased the presence of shrubs but further snow additions at HS drastically decreased the relative abundance of shrubs and tussock forming species, and increased the % cover of tall sedges and mosses compared to Ambient (Fig. 25; $P<0.05$).

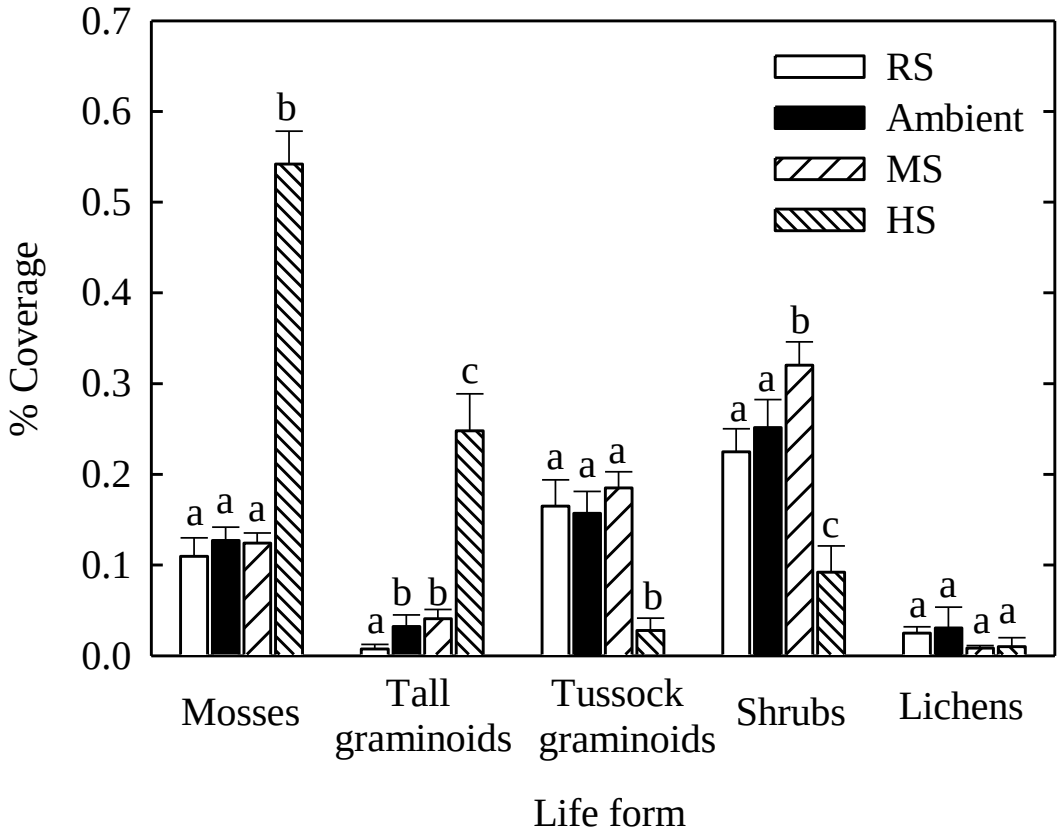

Figure 25: Percentage coverage of main life forms at Reduced Snow (RS), Ambient, Medium Snow addition (MS) and High Snow addition (HS) treatments. Values shown are mean percentage coverage from point-frame estimates taken at each site over peak season in 2012 and 2013. Error bars correspond to Standard Error of the Mean (±SE). Mosses include *Sphagnum sp*. and feather mosses; Tall graminoids are dominated by *Carex sp*.; Tussock forming graminoids refer to *Eriophorum vaginatum*; Shrubs include *Betula nana*, *Salix pulchra*, *Vaccinum vitis-ideae*, *Vaccinum ulginosum*, *Ledum decumbens* and *Cassiope tetragona*; Lichens are dominated by *Peltigera sp.* and *Cladina sp*. Different letter superscript denotes significant differences in the percentage coverage among treatments for a given life form ($P<0.05$) *(Reprinted with permission from: Blanc-Betes et al., 2016).*

4.4.3 Carbon isotopic signature of bulk soil

The $\delta^{13}C$ of bulk soil was not statistically different among treatments (P=0.62) and no depth effect was detected (P=0.18), although an enrichment trend was observed down the soil profile, $\delta^{13}C$ varying between –27‰ and –25.5‰ from soil surface to the permafrost table (Fig. 26).

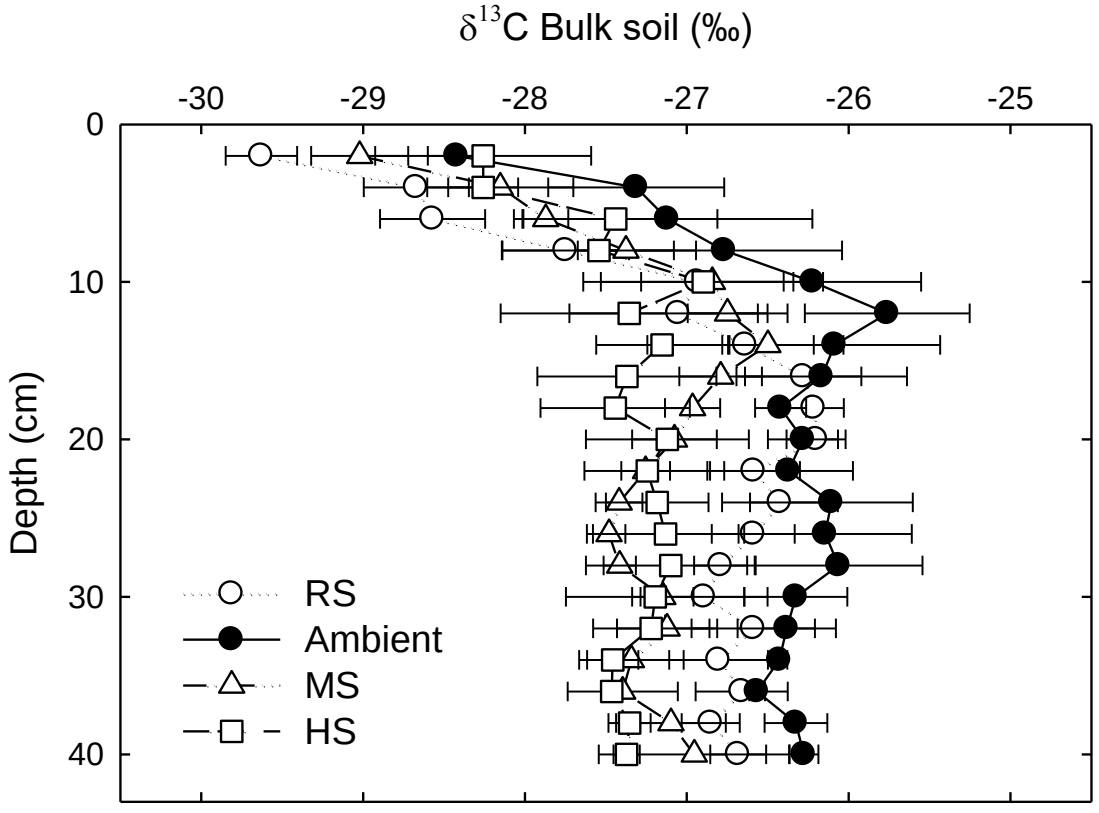

Figure 26: Soil profile distribution of $\delta^{13}C$ of the bulk soil at Reduced Snow (RS), Ambient, Medium Snow addition (MS) and High Snow addition (HS) treatments. Values shown are mean $\delta^{13}C$ of bulk soil (n=5) collected at each site at the end of the growing season. Error bars correspond to Standard Error of the Mean (±SE) *(Reprinted with permission from: Blanc-Betes et al., 2016).*

4.4.4 Ecosystem CH_4 fluxes

Ecosystem CH_4 fluxes showed treatment and seasonal effects with a significantly stronger treatment effect as the growing season progressed (P=0.02; Fig. 27). Under Ambient conditions, tussock tundra shifted from a CH_4 sink to a source as the season progressed, with a seasonal mean of 0.14±0.11 mg CH_4 m^{-2} d^{-1} (greater than zero, P<0.01). Reduced snow increased the CH_4 sink strength, averaging –0.32±0.07 mg CH_4 m^{-2} d^{-1} over the growing season (smaller than zero, P<0.05; Fig. 27). Snow additions converted tundra into increasingly stronger CH_4 sources (5.8±1.8 and 58±16 mg CH_4 m^{-2} d^{-1} at MS and HS respectively; Fig. 27). The CH_4 sink or source strength increased as the growing season progressed (P<0.05).

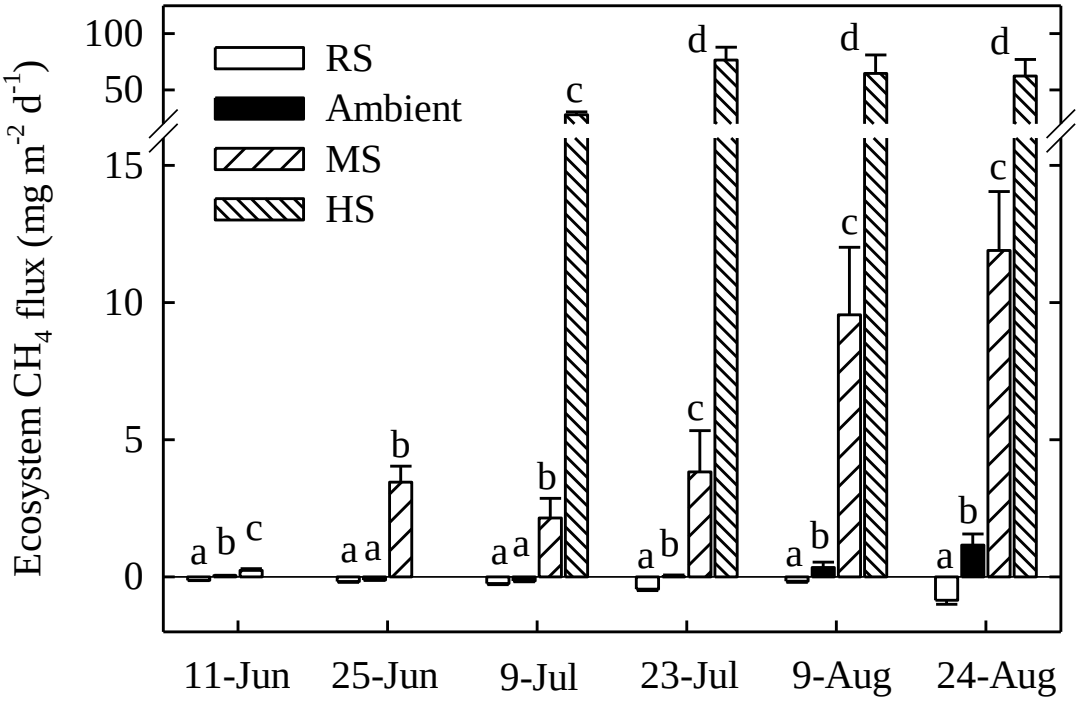

Figure 27: Seasonal dynamics of net ecosystem daily CH_4 flux at Reduced Snow (RS), Ambient, Medium Snow addition (MS) and High Snow addition (HS) treatments over the growing season. Negative values indicate net ecosystem CH_4 uptake, whereas positive values indicate net ecosystem CH_4 emission. Mean values within the same sampling period with different letter indicate statistical differences among treatments at a given sampling period (P<0.05). Error bars correspond to Standard Error of the Mean (±SE) *(Reprinted with permission from: Blanc-Betes et al., 2016).*

Volumetric water content, followed by soil temperature and thaw depth, explained about 50% of variability in net ecosystem CH_4 flux across treatments (Table XI). Variability in net ecosystem CH_4 production and oxidation was mostly explained by soil temperature, with volumetric water content exerting a significant control only on net CH_4 production (Table XI). Thaw depth showed no correlation with net ecosystem CH_4 flux, net ecosystem CH_4 production, or net ecosystem CH_4 oxidation rates (Table XI).

TABLE XI

Results from multiple regression analyses. Evaluation of the relationship between soil environmental variables and net ecosystem CH_4 flux, production and oxidation[1]. Model coefficients of determination (R^2) considering all independent variables and individual contributions from single environmental parameters to the model are reported. Values in bold denote statistical significance ($P<0.05$) *(Reprinted with permission from: Blanc-Betes et al., 2016).*

Variables		df	Type III	F	R^2	*P*
Dependent	Independent	(res)	SS			
Net CH_4 Flux	Model	3 (88)	71.6	24.9	**0.46**	**<0.0001**
	VWC (cm^3 cm^{-3})	1	66.6	23.6	**0.35**	**<0.0001**
	Soil temperature (^oC)	1	7.9	2.8	0.10	0.113
	Thaw depth (cm)	1	1.1	0.4	0.01	0.545
Net CH_4 Production	Model	3 (44)	178.7	19.4	**0.57**	**<0.0001**
	VWC (cm^3 cm^{-3})	1	69.0	22.5	**0.50**	**<0.0001**
	Soil temperature (^oC)	1	14.6	4.8	**0.07**	**0.035**
	Thaw depth (cm)	1	1.0	0.3	0.00	0.570
Net CH_4 Oxidation	Model	3 (41)	14.7	9.5	**0.42**	**0.0001**
	VWC (cm^3 cm^{-3})	1	0.4	0.8	0.02	0.421
	Soil temperature (^oC)	1	3.7	7.3	**0.40**	**0.010**
	Thaw depth (cm)	1	0.0	0.0	0.00	0.999

[1] Units are mg CH_4 m^{-2} d^{-1}. Net ecosystem CH_4 flux, production and oxidation rates were ln-transformed.

The $\delta^{13}C$ values of emitted CH_4 (δ_{eco}) were depleted over the growing season (P=0.03) and varied with treatment, yielding gradually $\delta^{13}C$ depleted values with increases in snow accumulation (P=0.003) (Fig. 28; Table XII).

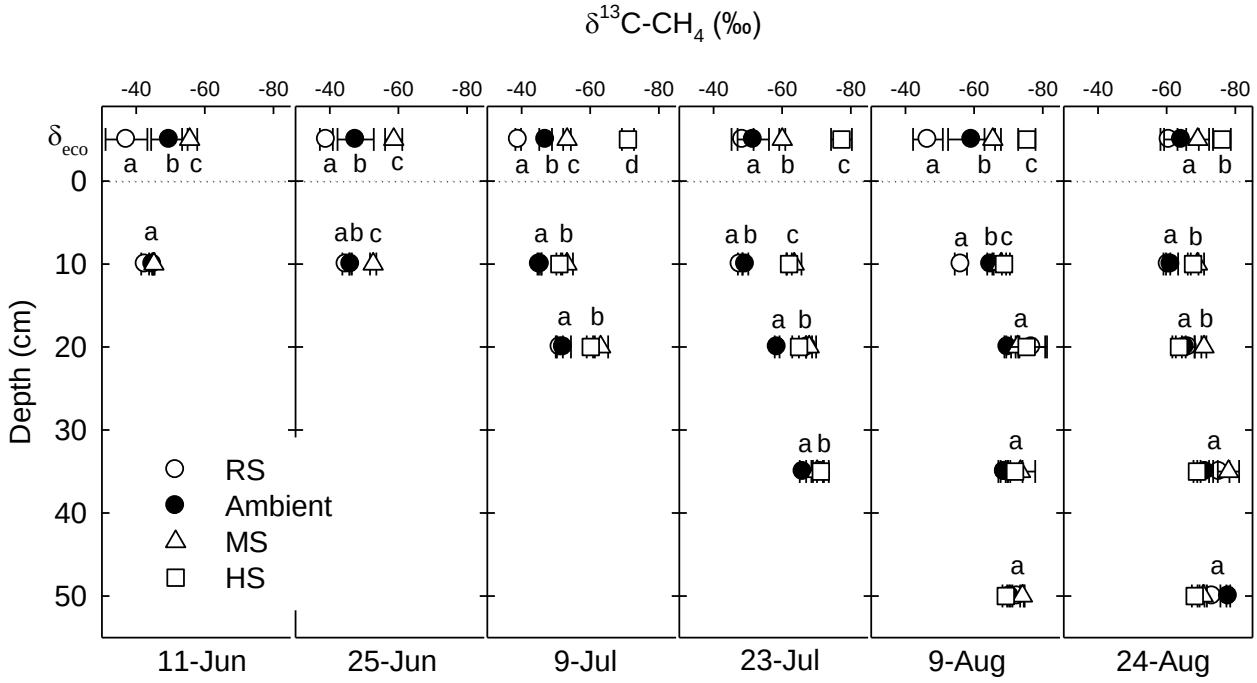

Figure 28: $\delta^{13}C$ of emitted CH_4 (δ_{eco}) and soil profile distribution of $\delta^{13}C$ of dissolved CH_4 at Reduced Snow (RS), Ambient, Medium Snow addition (MS) and High Snow addition (HS) treatments over the growing season. Error bars correspond to Standard Error of the Mean (±SE). Mean values within the same sampling period and depth with different letter indicate statistical differences among treatments at a given sampling period (P<0.05) *(Reprinted with permission from: Blanc-Betes et al., 2016).*

TABLE XII

Carbon isotope ratios ($\delta^{13}C$ values) of CH_4 efflux (δ_{eco}), soil CH_4 at shallow depths ($\delta_{shallow}$; 10-cm depth), and soil CH_4 near the frost table (δ_{anox}) at Reduced Snow (RS), Ambient, Medium Snow (MS) and High Snow (HS) treatments. The F_{ox} term refers to the calculated fraction of oxidized CH_4 considering predominant diffusion within water-saturated soils (α_{trans} = 1.0013) or through the plant aerenchyma (α_{trans} = 1.012). Values reported are seasonal averages and Standard Error of the Mean (±SE). (*) Denotes statistical significance between δ_{eco} and $\delta_{shallow}$ or δ_{anox} within site (P<0.05) *(Reprinted with permission from: Blanc-Betes et al., 2016).*

	δ_{eco}	$\delta_{shallow}$	δ_{anox}	F_{ox}	
				α_{trans} = 1.0013	α_{trans} = 1.0120
RS	–45.1 ± 1.4 ‰	–49.7 ± 0.5 ‰ *	–59.3 ± 0.6 ‰ *	72.2 ± 8.0 %	119.4 ± 13.3 %
Ambient	–53.6 ± 2.0 ‰	–52.9 ± 0.3 ‰	–60.1 ± 0.4 ‰ *	41.3 ± 8.9 %	54.7 ± 18.5 %
MS	–60.3 ± 0.9 ‰	–58.6 ± 0.7 ‰ *	–62.6 ± 0.5 ‰ *	26.9 ± 4.7 %	33.4 ± 12.6 %
HS	–74.9 ± 0.8 ‰	–62.4 ± 0.3 ‰ *	–67.2 ± 0.5 ‰ *	0.0 ± 0.0 %	5.6 ± 8.8 %

4.4.5 Soil gas concentration and carbon isotopic composition

Soil O_2 saturation ($\%O_2$) decreased with snow additions and over the growing season (P<0.0001; Fig. 29a). At 0–10 cm depth, $\%O_2$ was consistently higher at RS than at Ambient but decreased at MS and HS (Fig. 29b). Below 10-cm depth, $\%O_2$ decreased with depth in all treatments (P<0.05), except for HS where $\%O_2$ was consistently low throughout the soil column resulting in hypoxia/anoxia below 10-cm depth (P=0.4) (Fig. 29a). Roughly, 85% of the depth distribution of $\%O_2$ was explained by volumetric water content (P<0.0001; Table X). In turn, $\%O_2$ explained 96.6% of pCH_4 depth distribution and seasonal dynamics (P<0.0001; Table X).

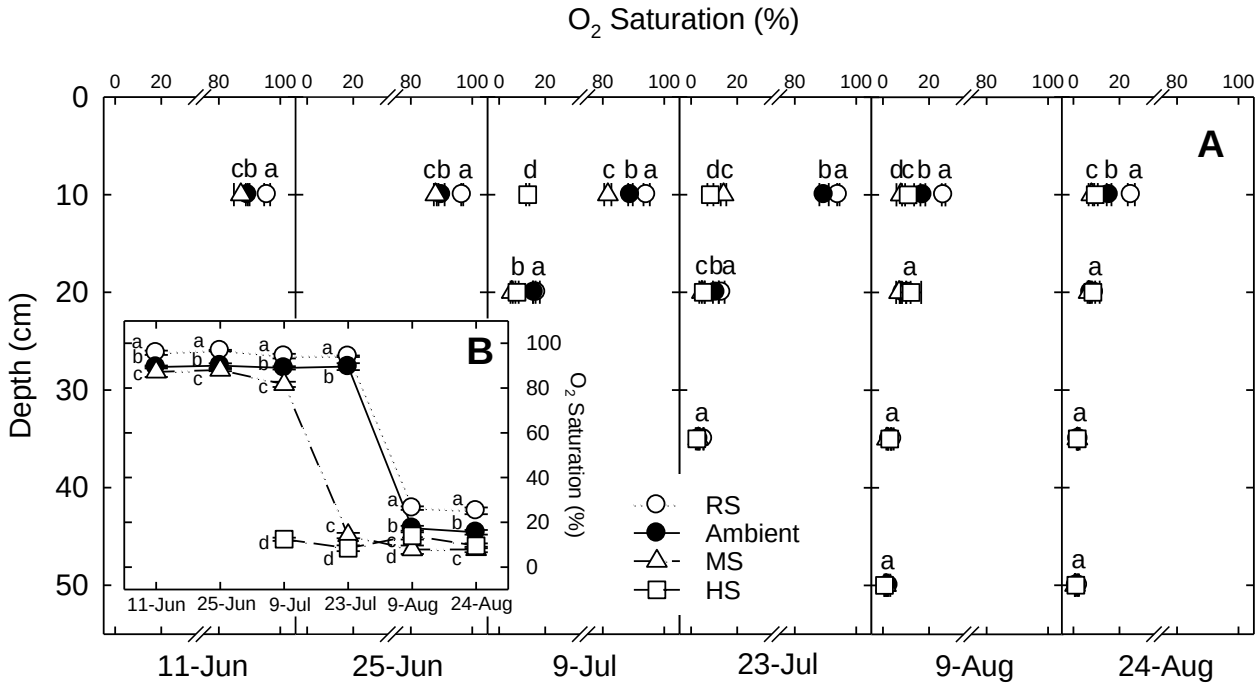

Figure 29: O_2 Saturation **(a)** throughout the soil profile and **(b)** at shallow depths (10-cm depth) at Reduced Snow (RS), Ambient, Medium Snow addition (MS) and High Snow addition (HS) treatments over the growing season. Error bars correspond to Standard Error of the Mean (±SE). Mean values within the same sampling period and depth with different letter indicate statistical differences among treatments at a given depth and sampling period (P<0.05) *(Reprinted with permission from: Blanc-Betes et al., 2016).*

Dissolved CH_4 concentration (pCH_4) increased over the growing season at all treatments and depths (P=0.002; Fig. 30a). At 0–10cm, snow additions consistently increased dissolved pCH_4 compared to Ambient and RS (P<0.05; Fig. 30b). Dissolved pCH_4 increased with depth at all treatments (P<0.0001; Fig. 30a).

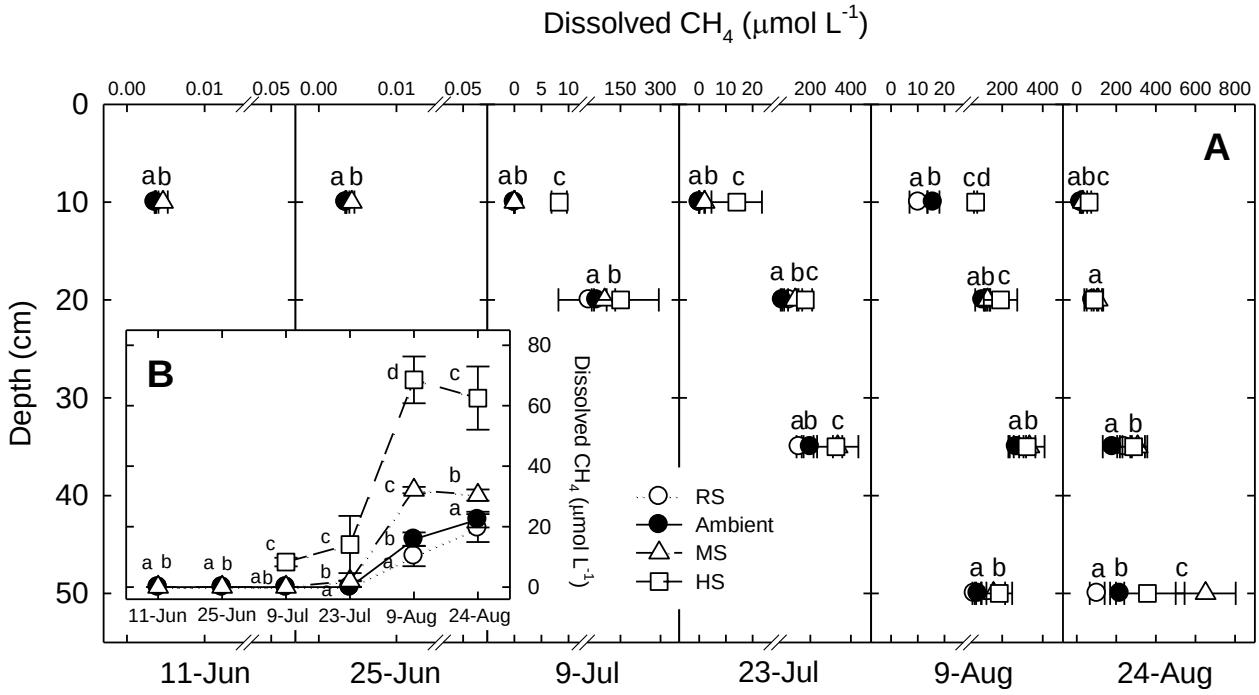

Figure 30: Dissolved CH_4 concentration **(a)** throughout the soil profile and **(b)** at shallow depths (10-cm) at Reduced Snow (RS), Ambient, Medium Snow addition (MS) and High Snow addition (HS) treatments over the growing season. Error bars correspond to Standard Error of the Mean (±SE). Mean values within the same sampling period and depth with different letter indicate statistical differences among treatments at a given depth and period (P<0.05) *(Reprinted with permission from: Blanc-Betes et al., 2016).*

The $\delta^{13}C$ value of dissolved CH_4 ($\delta^{13}C$-CH_4) varied with treatment (P=0.002), sampling period (P<0.0001) and depth (P<0.0001). Values of $\delta^{13}C$-CH_4 became more $\delta^{13}C$ depleted as the growing season progressed (P=0.07; Fig. 28). The $\delta^{13}C$-CH_4 value at 0–10cm ($\delta_{shallow}$) was consistently $\delta^{13}C$ enriched at RS but depleted at MS and HS relative to Ambient (P<0.0001; Fig. 28). Values of $\delta_{shallow}$ were $\delta^{13}C$ depleted relative to δ_{eco} at RS (P<0.05; Table XII; Fig. 28). No significant differences between $\delta_{shallow}$ and δ_{eco} were observed at Ambient (P=0.12; Table XII; Fig. 28), but $\delta_{shallow}$ was increasingly $\delta^{13}C$ enriched relative to δ_{eco} with snow additions (P<0.05; Table XII; Fig. 28). Across treatments, $\delta^{13}C$-CH_4 was increasingly $\delta^{13}C$ depleted with increasing depth (P<0.0001), and converged at 50 cm depth by the end of the growing season (ranging from –67 to –73‰) (Fig. 28). Deep $\delta^{13}C$-CH_4 (δ_{anox}; permafrost surface depth) at RS was consistently $\delta^{13}C$ enriched, whereas snow additions resulted in increasingly $\delta^{13}C$ depleted δ_{anox} relative to Ambient (P<0.0001; Table XII; Fig. 28).

The $\delta^{13}C$ value of dissolved CO_2 ($\delta^{13}C$-CO_2) varied with treatment (P=0.003) and depth (P<0.0001). Values of $\delta^{13}C$-CO_2 became more $\delta^{13}C$ enriched with snow additions and with increasing depth (Fig. 31).

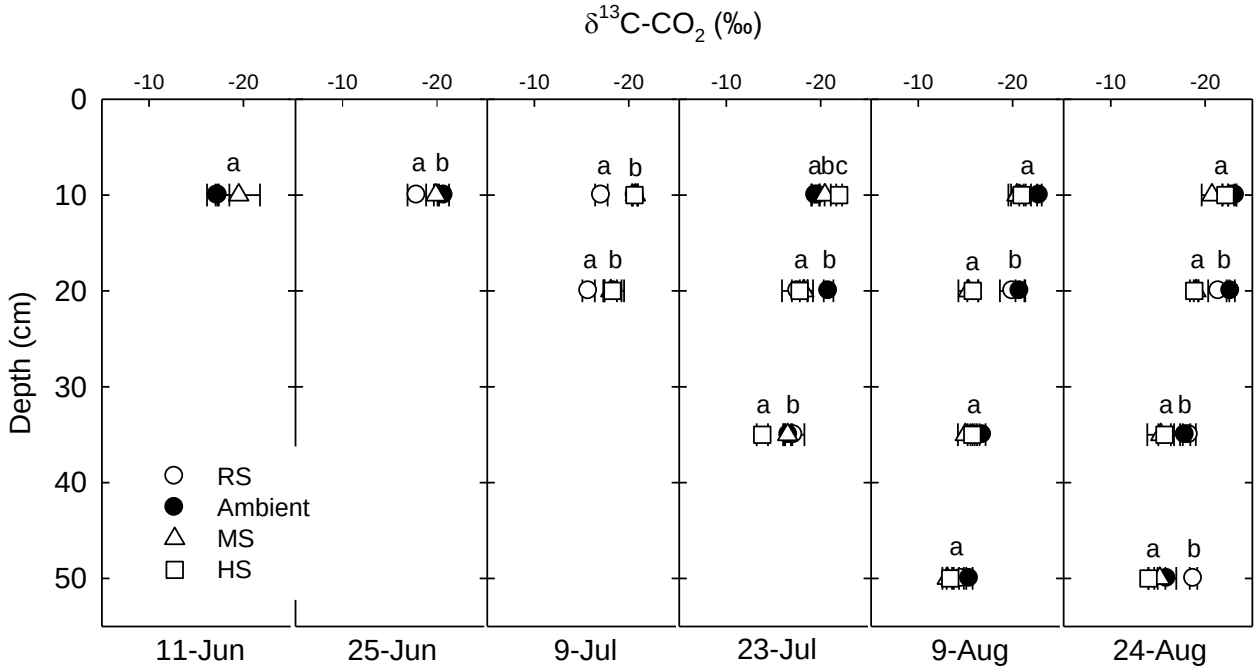

Figure 31: Soil profile distribution of $\delta^{13}C$ of dissolved CO_2 at Reduced Snow (RS), Ambient, Medium Snow addition (MS) and High Snow addition (HS) treatments over the growing season. Error bars correspond to Standard Error of the Mean (±SE). Mean values within the same sampling period and depth with different letter indicate statistical differences among treatments at a given sampling period (P<0.05) *(Reprinted with permission from: Blanc-Betes et al., 2016).*

4.4.6 Apparent carbon isotopic fractionation and oxidation efficiency

The apparent C isotopic fractionation (α_C) within the soil profile increased at all treatments over the growing season, showing stronger treatment effect on the relative dominance of the CH_4 metabolic pathways as the season progressed (P<0.05; Fig. 32a). Soil $\%O_2$ explained 70% of the distribution of α_C within the soil profile and across treatments (P<0.0001; Table X). At 10-cm depth (i.e. shallow depths), lower α_C values were observed at RS and Ambient, increasing with snow additions and over the growing season (P<0.0001; Fig. 32b). At RS, shallow α_C remained below the 1.040 line of constant fractionation indicative of prevailing methanotrophy (α_C <1.040; Fig. 32b). At Ambient, shallow α_C increased over the growing indicating a shift from predominant methanotrophy to predominant methanogenesis by acetate fermentation (1.040 < α_C <1.055; Fig. 32b). At MS and HS, shallow α_C indicated predominant acetate fermentation throughout the growing season (Fig. 32b). The value of α_C increased with depth at all treatments and over the growing season displaying relatively more fractionation in the methanogenic CO_2 reduction zone (1.055 < α_C < 1.090) with increasing snow, depth and sampling period (P<0.0001; Fig. 32a).

Estimates of the oxidized fraction of CH_4 produced within the soil column (F_{ox}; oxidation efficiency) was highest at RS and gradually decreased with snow accumulation reaching negligible values at HS (Table XII).

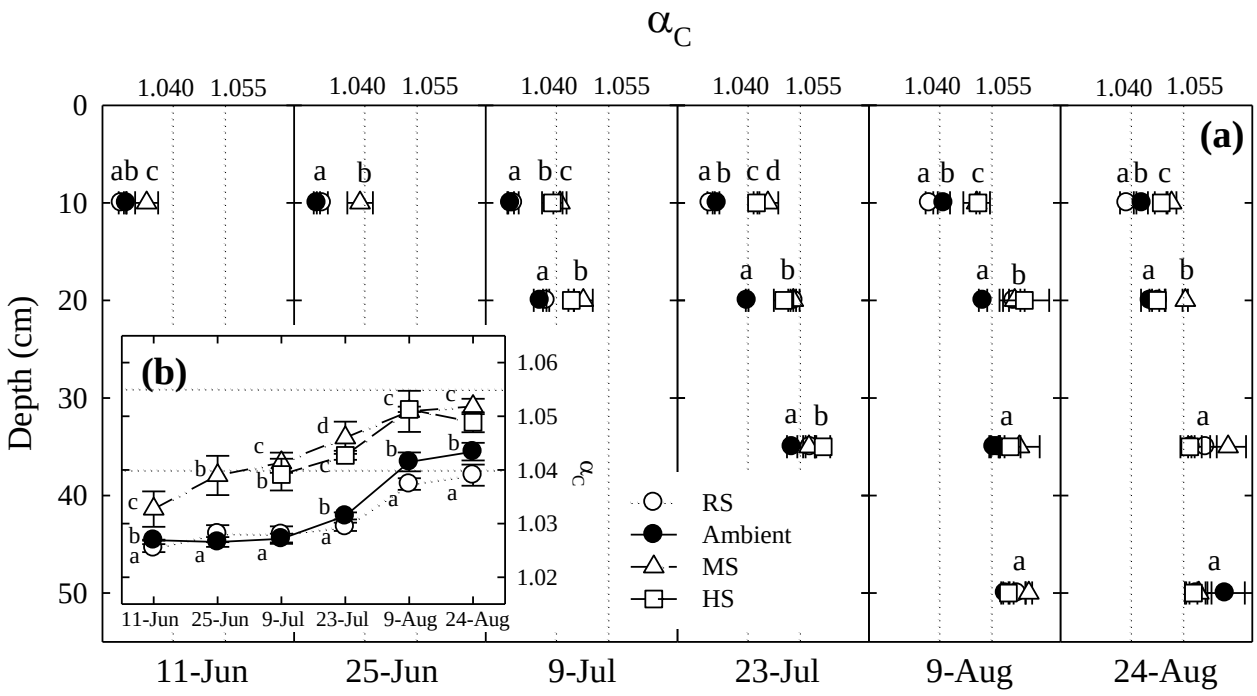

Figure 32: Apparent isotopic fractionation of coexisting pairs of $\delta^{13}C\text{-}CO_2$: $\delta^{13}C\text{-}CH_4$ (α_C) **(a)** throughout the soil profile and **(b)** at shallow depths (10-cm) at Reduced Snow (RS), Ambient, Medium Snow addition (MS) and High Snow addition (HS) treatments over the growing season. Error bars correspond to Standard Error of the Mean (±SE). Mean values within the same sampling period and depth with different letter indicate statistical differences among treatments at a given sampling period (P<0.05). Lines of constant fractionation show ranges of α_C for coexisting CO_2 and CH_4 as reported by Whiticar et al. (1986) to be characteristic of predominant CH_4 oxidation (α_C <1.040), and production by the acetate fermentation (α_C ~ 1.040 to 1.055) and CO_2 reduction (α_C ~ 1.055 to 1.090) pathways *(Reprinted with permission from: Blanc-Betes et al., 2016).*

4.4.7 Methane produced, oxidized and transported within the soil column

Produced CH_4 increased with depth and over the growing season at all treatments, with 83–86% being produced below 35-cm depth (P<0.05; Fig. 33a). At 0–10 cm, snow additions increased produced CH_4 compared to Ambient and RS (P<0.05; Fig. 33b), and differences among treatments increased with depth (P<0.05; Fig. 33a).

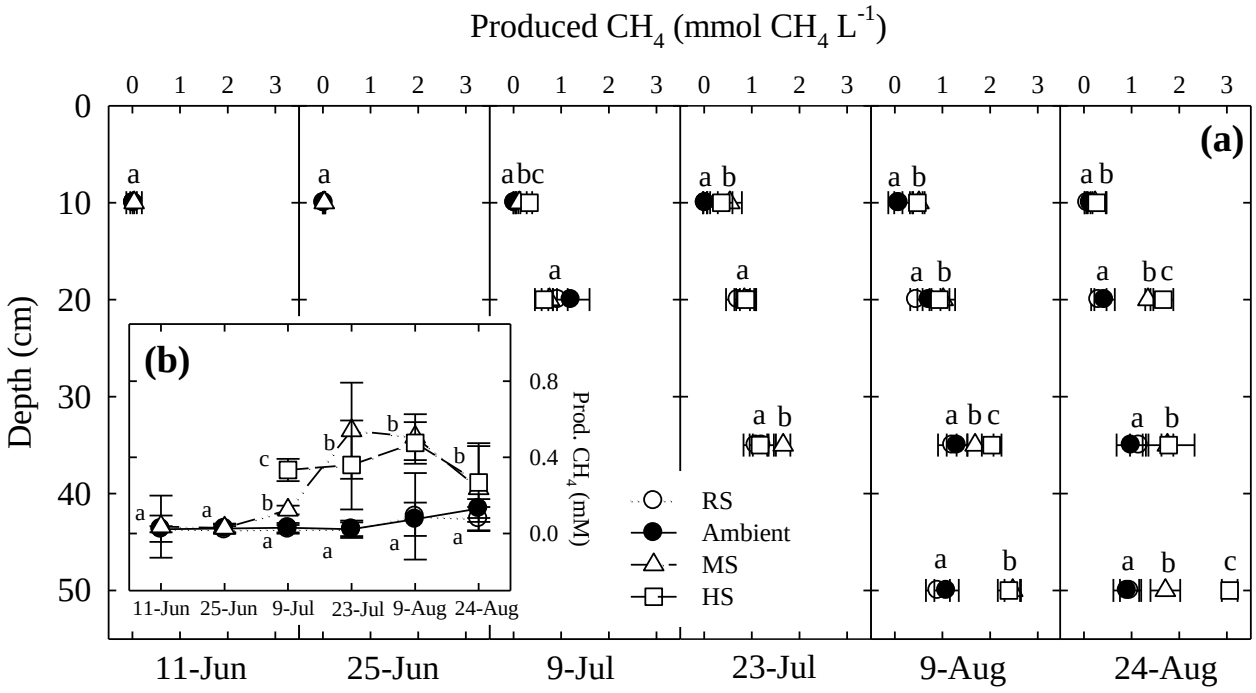

Figure 33: Estimates of produced CH_4 **(a)** throughout the soil profile and **(b)** at shallow depths (10-cm) at Reduced Snow (RS), Ambient, Medium Snow addition (MS) and High Snow addition (HS) treatments over the growing season. Error bars correspond to Standard Error of the Mean (±SE). Mean values within the same sampling period and depth with different letter indicate statistical differences among treatments at a given sampling period (P<0.05) *(Reprinted with permission from: Blanc-Betes et al., 2016).*

Accordingly, gross CH_4 production was on average slightly lower at RS than Ambient (P>0.1; Table XIII), and significantly increased with snow additions (P<0.05; Table XIII). Variations in produced CH_4 estimates across treatments was correlated to soil $\%O_2$ (R^2=0.83; P<0.05) (Table XIV). However, while $\%O_2$ controlled CH_4 production at shallow depths (R^2=0.88; P<0.05) (Table XIV), soil temperature gained leverage with depth, governing CH_4 production near the frost table (R^2=0.86; P<0.05) (Table XIV).

Only 10–15% of the CH_4 produced remained dissolved in pore water, with no significant differences in the fraction of CH_4 lost among treatments (Table XIII). Contribution of oxidation to ecosystem CH_4 losses increased at RS but decreased with snow additions relative to Ambient (Table XIII). Conversely, the estimated fraction of produced CH_4 lost via ebullition or plant mediated transport was lowest at RS, and increased with increasing snow accumulation (Table XIII).

TABLE XIII

Estimates of gross CH_4 production within the soil column (CH_4-Prod), CH_4 lost from the soil column (CH_4-Lost), and the fraction of CH_4-Lost by oxidation (CH_4-Ox) or via plant-mediated transport to the atmosphere (CH_4-Trans) at Reduced Snow (RS), Ambient, Medium Snow (MS) and High Snow (HS) treatments. Values of CH_4-Prod and CH_4-Lost are seasonal averages and Standard Error of the Mean (±SE). (*) Denotes statistical significance relative to Ambient (P<0.05). Values for CH_4-Ox and CH_4-Trans correspond to % of CH_4-Lost calculated considering predominant diffusion within water-saturated soils (α_{trans} = 1.0013) or through the plant aerenchyma (α_{trans} = 1.012) *(Reprinted with permission from: Blanc-Betes et al., 2016).*

	RS	Ambient	MS	HS
CH_4-Prod (mM)	0.75 ± 0.1	0.79 ± 0.1	1.4 ± 0.1 *	1.5 ± 0.1 *
CH_4-Lost (mM)	0.65 ± 0.1	0.66 ± 0.1	1.1 ± 0.1 *	1.3 ± 0.1 *
CH_4-Ox (%CH_4-Lost)	84 – 139	47 – 65	32 – 40	0 – 6
CH_4-Trans (%CH_4-Lost)	0.1 – 16	35 – 53	60 – 68	94 – 100

TABLE XIV

Results from linear regression analyses between estimates of CH_4 produced considering the entire soil profile and at a given depth against %O_2 saturation (%) and soil temperature (ºC). Estimated values of produced CH_4 were log-transformed to meet the requirements of parametric correlations. Values in bold denote statistical significance (P<0.05) *(Reprinted with permission from: Blanc-Betes et al., 2016).*

	O_2 Saturation (%)				Soil temperature (ºC)			
DEPTH	Coef Corr	R^2	F	*P*	Coef Corr	R^2	F	*P*
ALL DEPTHS	–0.91	**0.83**	273.1	**<0.0001**	0.08	0.01	0.4	0.5310
10	–0.94	**0.88**	150.2	**<0.0001**	0.63	**0.41**	13.6	**0.0015**
20	–0.49	0.24	4.3	0.0566	0.61	**0.37**	8.5	**0.0112**
35	–0.41	0.16	2.0	0.1887	0.72	**0.52**	10.8	**0.0083**
50	–0.60	0.36	3.3	0.2123	0.92	**0.86**	37.8	**0.0008**

4.4.8 Cumulative gross ecosystem CH_4 production and oxidation, and net CH_4 flux

At Ambient, gross ecosystem CH_4 production was slightly higher than gross ecosystem CH_4 oxidation, resulting in a small net CH_4 source over the growing season (Table XV). RS did not affect gross ecosystem CH_4 production (P>0.1; Table XV) but increased gross ecosystem CH_4 oxidation compared to Ambient (P<0.05; Table XV), resulting in a net CH_4 sink over the growing season (Table XV). Snow additions significantly increased both gross ecosystem CH_4 production and oxidation at MS and HS compared to Ambient over the growing season (P<0.05; Table XV). Increases in snow accumulation increased gross ecosystem CH_4 production above increases in gross ecosystem CH_4 oxidation resulting in increasingly stronger net CH_4 sources with snow additions over the growing season (P<0.05; Table XV).

TABLE XV

Cumulative seasonal net CH_4 fluxes, and cumulative seasonal gross CH_4 production and oxidation at Reduced Snow (RS), Ambient, Medium Snow (MS) and High Snow (HS) treatments. Values of gross CH_4 production and oxidation correspond to seasonal budgets calculated considering predominant diffusion within water-saturated soils (α_{trans} = 1.0013) or through the plant aerenchyma (α_{trans} = 1.012). All values reported are in mg CH_4 m^{-2} ± Standard Error of the Mean (±SE). Values with different letter denote statistical differences between snow treatment (P<0.05) *(Reprinted with permission from: Blanc-Betes et al., 2016).*

	Net CH_4 Flux	Gross CH_4 Production		Gross CH_4 Oxidation	
		α_{trans} = 1.0013	α_{trans} = 1.0120	α_{trans} = 1.0013	α_{trans} = 1.0120
RS	–31 ± 0.6 [a]	93 ± 9.9 [a]	116 ± 6.6 [a]	–123 ± 9.9 [a]	–147 ± 6.6 [a]
Ambient	21 ± 1.7 [b]	72 ± 16 [a]	113 ± 10 [a]	–52 ± 16 [b]	–93 ± 10 [b]
MS	464 ± 15 [c]	719 ± 34 [b]	837 ± 50 [b]	–256 ± 37 [c]	–373 ± 52 [c]
HS	3,561 ± 97 [d]	3,561 ± 97 [c]	3,838 ± 149 [c]	–7.4 ± 137 [d]	–284 ± 177 [d]

4.5 DISCUSSION

Arctic tundra switched from a small source to a sustained CH_4 sink under reduced winter snow, and to an increasingly stronger CH_4 source with increases in winter snow depth (Table XV). Ecosystem CH_4 fluxes at Ambient conditions agreed with those reported for Alaskan tussock tundra (0.2–1.3 mg CH_4 m^{-2} d^{-1}; Morrissey & Livingston, 1992; Torn & Chapin III, 1993). Our results showed that increases in snow accumulation, by promoting soil wetness and warming, and favoring the expansion of tall graminoids stimulated CH_4 production and transport while suppressing CH_4 oxidation, ultimately increasing the ecosystem CH_4 source strength over the growing season.

4.5.1 Snow accumulation and soil microclimate and vegetation

Snow accumulation, through variations in soil water content and winter thermal insulation influenced soil warming and thawing trends over the growing season likely as a result of changes in soil thermal conductivity and latent heat (Table X; Subin *et al.*, 2013). This suggests that winter precipitation plays a prominent role on governing ecosystem processes beyond the impacts of winter warming alone (Lupascu *et al.*, 2014c). Snow additions were accompanied by successional shifts plant communities, from tussock-dominated to wet-meadow vegetation dominated by tall graminoids (Fig. 25). Similar transitions have been reported with thermokarst development (Jorgenson *et al.*, 2001; Christensen *et al.*, 2004; Johansson *et al.*, 2006; Osterkamp *et al.*, 2009).

4.5.2 Snow accumulation and ecosystem CH_4 fluxes

Soil climatic variables influenced ecosystem CH_4 fluxes over the growing season (Table XI). Soil water content defined the predominant CH_4 metabolism (aerobic vs anaerobic; Whalen & Reeburgh, 1990b; Yavitt *et al.*, 1990; Bartlett *et al.*, 1992), whereas soil temperature enhanced methanogenic or methanotrophic activity under prevailing anoxic or oxic soil conditions (Blankinship *et al.*, 2010; Tveit *et al.*, 2015). This is supported by seasonal patterns of ecosystem CH_4 fluxes, as both net production and oxidation increased with seasonal warming (Table XI; Fig. 27). The strengthening effect of soil temperature on net CH_4 production and oxidation is consistent with previous research from northern peatlands, where soil warming increased the CH_4 source strength by 75 to 80% above the effects of flooding alone (Updegraff *et al.*, 2001; Turetsky *et al.*, 2008). Similarly, a recent study showed enhanced CH_4 sink strength of non-water-saturated soils with progressive Arctic warming (Juncher Jørgensen *et al.*, 2015). The synergistic effect that snow accumulation exerts on CH_4 fluxes by influencing both soil moisture and temperature emphasizes the importance of winter precipitation on modulating climate forcing feedbacks from Arctic tundra, especially under a climate warming scenario.

Net ecosystem CH_4 oxidation showed relatively higher correlation with soil temperature than net ecosystem CH_4 production, despite the higher temperature sensitivity to methanogenesis compared to methanotrophy (Table XI) (Dunfield *et al.*, 1993). This may be explained by soil $\%O_2$ limiting the methanotrophic community to the near-surface, where changes in soil temperature are more pronounced. In addition, soil warming indirectly stimulates methanotrophy by increasing CH_4 availability owing to the strong temperature sensitivity of the methanogenic community (West & Schmidt, 2002; Shukla *et al.*, 2013). This agrees with seasonal increases of pCH_4 and produced CH_4 at RS despite increases in net ecosystem CH_4 oxidation (Fig. 33).

4.5.3 Snow accumulation and methane metabolism and transport

Soil water content was a major driver of soil $\%O_2$ distribution within the soil profile, which in turn determined the zonation for prevailing methanogenesis and methanotrophy (α_C) over the growing season (Table X).

Methane oxidation dominated shallow depths at Ambient and RS (mean $\alpha_C < 1.040$ over most or all the growing season; Fig. 32b), as supported by relatively enriched δ_{eco} over $\delta_{shallow}$ (Table XII; Fig. 28) (Hornibrook *et al.*, 1997; Popp *et al.*, 1999). Accordingly, 41–55% and 72–119% of produced CH_4 was oxidized (F_{ox}) at Ambient and RS respectively, total oxidation mitigating or even offsetting CH_4 production (Table XII). The F_{ox} observed at Ambient and RS agree with values reported for tussock-dominated tundra (55–90%; Reeburgh *et al.*, 1993; Ström *et al.*, 2005). Notably, RS maintained gross CH_4 production but increased gross CH_4 oxidation relative to Ambient, shifting to a net CH_4 sink despite negligible decreases in volumetric water content (Tables XIII and XV). These results indicate a strong sensitivity of methanotrophy to soil wetness and suggest the potential of Arctic tundra to rapidly shift into a CH_4 sink under favorable conditions, with important implications in climate forcing feedbacks (Stocker *et al.*, 2013b).

With snow additions, F_{ox} dropped to 27–33% at MS and to negligible values at HS (Table XII). Accordingly, α_C values indicate predominant methanogenesis with increased snow even at shallow depths (mean $\alpha_C > 1.040$ over most or all the growing season; Fig. 32b). This is consistent with observed increases in estimates of produced CH_4, lower $\%O_2$ and higher soil temperature under increased snow accumulation (Figs. 24, 29 and 33; Table XIV), which partly contributed to greater net CH_4 emissions with deeper winter snow (Fig. 27, Table XIII). Moreover, snow additions resulted in depleted δ_{eco} relative to $\delta_{shallow}$ (Table XII) suggesting the

increasingly important role of plant-mediated CH_4 transport with snow accumulation (Chanton *et al.*, 1992; King *et al.*, 1998; Chanton, 2005). In agreement with these results, while the fraction of CH_4 lost from the system was unaffected by winter snow depth, the relative contribution of CH_4 lost by plant-mediated transport increased with snow accumulation following the expansion of tall graminoids (Table XIII; Fig. 25). The estimated fractions of CH_4 emitted by plant-mediated transport at Ambient (35–53%) and HS (94–100%) are consistent with values reported for tussock-dominated (0–50%; Torn & Chapin III, 1993; Greenup *et al.*, 2000; Dorodnikov *et al.*, 2011) and tall-graminoid dominated systems (>90%; Torn & Chapin III, 1993; Kelker & Chanton, 1997) (Table XIII). Plant transport bypasses shallow methanotrophic zones limiting CH_4 oxidation (Table XIII) (Torn & Chapin III, 1993; Joabsson & Christensen, 2001), and hence contributing to increase the ecosystem CH_4 source strength with deeper snow.

Within predominantly methanogenic zones, values of α_C indicated that acetate fermentation dominated at depths roughly corresponding with the rhizosphere (0–20 cm), where root exudates, rapid root turnover and litter inputs likely fueled methanogenesis (Popp *et al.*, 1999; Greenup *et al.*, 2000), whereas CO_2 reduction dominated at deeper zones (Fig. 32). At shallow depths, α_C is susceptible to oxidation, which could potentially explain lower values near the surface. However, higher α_C with snow additions relative to Ambient matched parallel increases in produced CH_4 (Figs. 32b and 33b) and plant-mediated transport (Table XIII), suggesting that methanogenesis dominated at shallow depths, and that the upward decrease in α_C can be mostly attributed to shifts from CO_2 reduction to acetate fermentation. This is consistent with previous research linking acetate fermentation with high SOC decomposability, and CO_2 reduction with greater recalcitrance of the organic substrate (Hornibrook *et al.*, 1997, 2000; Avery *et al.*, 2003).

Permafrost SOC is labile (Uhlířová *et al.*, 2007; Waldrop *et al.*, 2010; Wild *et al.*, 2014; Abbott *et al.*, 2014). However, consistent with other studies, deeper active layer with snow additions (10% and 28% at MS and HS, respectively) did not stimulate acetate fermentation (Fig. 32b) (Prater *et al.*, 2007; Lee *et al.*, 2012). Instead, we observed an increasing correlation between produced CH_4 estimates and soil temperature with depth, which suggests that warming rather than thaw-induced increases in SOC availability drove increases in CH_4 production within newly thawed horizons (Table XIV).

4.5.4 Implications of projected changes in winter precipitation for CH_4 emissions

A major concern associated with permafrost degradation in a changing climate is the vulnerability of previously frozen SOC to rapidly decompose (MacDougall *et al.*, 2012; O'Donnell *et al.*, 2012; Schneider von Deimling *et al.*, 2012; Schuur *et al.*, 2013, 2015). Our results suggest that CH_4 fluxes responded primarily to changes in vegetation, and soil hydrology and temperature rather than increases in SOC availability with deeper active layer (Table XI, Fig. 32b). The lack of response of the acetoclastic community could be explained by low presence and activities of acetate fermenters relative to CO_2 reducers in newly thawed soils (Waldrop *et al.*, 2010; Mondav *et al.*, 2014). In our study site, low pH (~5.4) and temperatures likely limited acetate fermentation at permafrost surface (Horn *et al.*, 2003; Kotsyurbenko *et al.*, 2007). However, given that acetate fermentation accounts for approximately 70% of the produced CH_4, any climate-induced shift in the ability of acetate to act as a CH_4 precursor could greatly stimulate CH_4 production and emission rates (Hines *et al.*, 2001, 2008; Metje & Frenzel, 2007).

Recent research has shown substantial increases in CH_4 production rates coupled to thaw-induced shifts towards acetate fermentation with severe permafrost degradation (Hodgkins *et al.*, 2014; McCalley *et al.*, 2014). Increased snowfall and accumulation, by promoting progressive

permafrost degradation, could facilitate the development of an acetoclastic community, thereby triggering CH_4 production and emission over time spans longer than considered in this study (Sistla *et al.*, 2013; McCalley *et al.*, 2014; Tveit *et al.*, 2015). Alternatively, the extensive permafrost degradation projected under future scenarios could promote the gradual drainage of permafrost supported soils (Romanovsky *et al.*, 2010; Avis *et al.*, 2011). Given the strong sensitivity of CH_4 oxidation to soil moisture and temperature, drier soils together with Arctic warming could potentially convert extended areas of upland tundra from net CH_4 sources to net CH_4 sinks (Juncher Jørgensen *et al.*, 2015; Lawrence *et al.*, 2015).

4.6 CONCLUSIONS

In summary, changes in winter precipitation, by regulating soil water content, influence soil $\%O_2$, temperature and thawing over the growing season, affecting ecosystem CH_4 fluxes beyond the direct effects of snow insulation on winter processes. Moreover, our results reveal a synergistic effect of soil moisture and temperature on net ecosystem CH_4 production and oxidation under near water-saturated (more anoxic) and drier (more oxic) soil conditions respectively. Thus, changes in winter precipitation, by influencing both soil wetness and temperature impact ecosystem CH_4 fluxes beyond what may be predicted by Arctic warming alone. Shifts in vegetation cover derived from changes in snow accumulation define the predominant CH_4 transport mechanism within the soil profile and largely contribute to the ecosystem CH_4 sink or source strength. Contrary to our expectations, our results suggest that thaw-induced changes in SOC availability play a minor role on CH_4 forcing from Arctic tundra under the studied scenarios and time spans, and that increases in CH_4 production within newly thawed horizons under deeper snow were mostly driven by soil warming. Progressive permafrost degradation under projected increases in winter precipitation has the potential to further

exacerbate (if anoxia is maintained) or mitigate (if degradation results in drier, more oxic soils) the radiative forcing of CH_4 emissions from Arctic tundra over longer time-scales. Whether Arctic tundra will act as a significant source or sink of CH_4 over the 21st century will largely depend on soil moisture-temperature interactions associated to changes in winter precipitation.

4.7 Acknowledgements

This study was made possible by the field assistance of N. Van Hoey and B. Thurnhoffer. We thank N. Gomez-Casanovas and J. Bogner for their helpful comments and guidance on the manuscript. Support from the Toolik Lake Field Station staff is greatly appreciated, as it is the logistical support of CH2MHill Polar Services. We thank Dr. C. Treat and two anonymous reviewers for their helpful comments. This research was funded by the Department of Energy, Terrestrial Ecosystem Science Program (DE-SC 0006607), and by NSF OPP grants (0119279 and 0612384) awarded to J.M. Welker and the International Tundra Experiment and the International Polar Year.

4.8 Cited Literature

Abbott BW, Larouche JR, Jones JB, Bowden WB, Balser AW (2014) Elevated dissolved organic carbon biodegradability from thawing and collapsing permafrost. *Journal of Geophysical Research: Biogeosciences*, **119**, 2014JG002678.

Avery GB, Shannon RD, White JR, Martens CS, Alperin MJ (2003) Controls on methane production in a tidal freshwater estuary and a peatland: methane production via acetate fermentation and CO_2 reduction. *Biogeochemistry*, **62**, 19–37.

Avis CA, Weaver AJ, Meissner KJ (2011) Reduction in areal extent of high-latitude wetlands in response to permafrost thaw. *Nature Geoscience*, **4**, 444–448.

Barker JF, Fritz P (1981) Carbon isotope fractionation during microbial methane oxidation. *Nature*, **293**, 289–291.

Bartlett KB, Crill PM, Sass RL, Harriss RC, Dise NB (1992) Methane emissions from tundra environments in the Yukon-Kuskokwim delta, Alaska. *Journal of Geophysical Research: Atmospheres*, **97**, 16645–16660.

Bintanja R, Selten FM (2014) Future increases in Arctic precipitation linked to local evaporation and sea-ice retreat. *Nature*, **509**, 479–482.

Blankinship JC, Brown JR, Dijkstra P, Allwright MC, Hungate BA (2010) Response of Terrestrial CH_4 Uptake to Interactive Changes in Precipitation and Temperature Along a Climatic Gradient. *Ecosystems*, **13**, 1157–1170.

Bubier JL, Moore TR, Bellisario L, Comer NT, Crill PM (1995) Ecological controls on methane emissions from a Northern Peatland Complex in the zone of discontinuous permafrost, Manitoba, Canada. *Global Biogeochemical Cycles*, **9**, 455–470.

Callaghan TV, Johansson M, Brown RD et al. (2011) The Changing Face of Arctic Snow Cover: A Synthesis of Observed and Projected Changes. *Ambio*, **40**, 17–31.

Carvalhais N, Forkel M, Khomik M et al. (2014) Global covariation of carbon turnover times with climate in terrestrial ecosystems. *Nature*, **514**, 213–217.

Chanton JP (2005) The effect of gas transport on the isotope signature of methane in wetlands. *Organic Geochemistry*, **36**, 753–768.

Chanton JP, Martens CS, Kelley CA, Crill PM, Showers WJ (1992) Methane transport mechanisms and isotopic fractionation in emergent macrophytes of an Alaskan tundra lake. *Journal of Geophysical Research: Atmospheres*, **97**, 16681–16688.

Chanton J, Chaser L, Glasser P, Siegel D (2004) Carbon and hydrogen isotopic effects in microbial methane from terrestrial environments. *Stable isotopes and biosphere-atmosphere interactions, physiological ecology series*, 85–105.

Chanton JP, Powelson DK, Abichou T, Hater G (2008a) Improved Field Methods to Quantify Methane Oxidation in Landfill Cover Materials Using Stable Carbon Isotopes. *Environmental Science & Technology*, **42**, 665–670.

Chanton JP, Powelson DK, Abichou T, Fields D, Green R (2008b) Effect of Temperature and Oxidation Rate on Carbon-isotope Fractionation during Methane Oxidation by Landfill Cover Materials. *Environmental Science & Technology*, **42**, 7818–7823.

Chanton J, Abichou T, Langford C, Hater G, Green R, Goldsmith D, Swan N (2011) Landfill Methane Oxidation Across Climate Types in the U.S. *Environmental Science & Technology*, **45**, 313–319.

Chasar LS, Chanton JP, Glaser PH, Siegel DI (2000) Methane Concentration and Stable Isotope Distribution as Evidence of Rhizospheric Processes: Comparison of a Fen and Bog in the Glacial Lake Agassiz Peatland Complex. *Annals of Botany*, **86**, 655–663.

Chowdhury TR, Dick RP (2013) Ecology of aerobic methanotrophs in controlling methane fluxes from wetlands. *Applied Soil Ecology*, **65**, 8–22.

Christensen TR, Johansson T, Åkerman HJ et al. (2004) Thawing sub-arctic permafrost: Effects on vegetation and methane emissions. *Geophysical Research Letters*, **31**, L04501.

Christensen JH, Kanikicharla KK, Marshall GJ, Turner J (2013) Climate phenomena and their relevance for future regional climate change. In: *Climate Change 2013: The physical science basis. Contribution of Working Group I to the fifth Assessment of the Intergovernmental Panel on Climate Change* (eds Stocker TF, Qin D, Plattner G-K, Tignor MMB, Allen SK, Boschung J, Nauels A, Xia Y, Bex V, Midgley PM), pp. 1217–1308. Cambridge University Press, Cambridge.

Cohen J, Screen JA, Furtado JC et al. (2014) Recent Arctic amplification and extreme mid-latitude weather. *Nature Geoscience*, **7**, 627–637.

Corbett JE, Tfaily MM, Burdige DJ, Cooper WT, Glaser PH, Chanton JP (2013) Partitioning pathways of CO_2 production in peatlands with stable carbon isotopes. *Biogeochemistry*, **114**, 327–340.

Davidson EA, Nepstad DC, Ishida FY, Brando PM (2008) Effects of an experimental drought and recovery on soil emissions of carbon dioxide, methane, nitrous oxide, and nitric oxide in a moist tropical forest. *Global Change Biology*, **14**, 2582–2590.

Deng J, Li C, Frolking S, Zhang Y, Bäckstrand K, Crill P (2014) Assessing effects of permafrost thaw on C fluxes based on multiyear modeling across a permafrost thaw gradient at Stordalen, Sweden. *Biogeosciences*, **11**, 4753–4770.

Deslippe JR, Simard SW (2011) Below-ground carbon transfer among Betula nana may increase with warming in Arctic tundra. *New Phytologist*, **192**, 689–698.

Dorodnikov M, Knorr K-H, Kuzyakov Y, Wilmking M (2011) Plant-mediated CH_4 transport and contribution of photosynthates to methanogenesis at a boreal mire: a ^{14}C pulse-labeling study. *Biogeosciences*, **8**, 2365–2375.

Dorrepaal E, Cornelissen JH c., Aerts R, Wallén B, Van Logtestijn RS p. (2005) Are growth forms consistent predictors of leaf litter quality and decomposability across peatlands along a latitudinal gradient? *Journal of Ecology*, **93**, 817–828.

Dunfield P, knowles R, Dumont R, Moore TR (1993) Methane production and consumption in temperate and subarctic peat soils: Response to temperature and pH. *Soil Biology and Biochemistry*, **25**, 321–326.

Elberling B (2007) Annual soil CO_2 effluxes in the High Arctic: The role of snow thickness and vegetation type. *Soil Biology and Biochemistry*, **39**, 646–654.

Elberling B, Nordstrøm C, Grøndahl L et al. (2008) High‐Arctic Soil CO_2 and CH_4 Production Controlled by Temperature, Water, Freezing and Snow. In: *Advances in Ecological Research*, Vol. 40 (ed Hans Meltofte TRC Bo Elberling, Mads C. Forchhammer and Morten Rasch), pp. 441–472. Academic Press.

Elmendorf SC, Henry GHR, Hollister RD et al. (2012) Plot-scale evidence of tundra vegetation change and links to recent summer warming. *Nature Climate Change*, **2**, 453–457.

Fan Z, Neff JC, Harden JW et al. (2011) Water and heat transport in boreal soils: Implications for soil response to climate change. *Science of The Total Environment*, **409**, 1836–1842.

Greenup AL, Bradford MA, McNamara NP, Ineson P, Lee JA (2000) The role of Eriophorum vaginatum in CH_4 flux from an ombrotrophic peatland. *Plant and Soil*, **227**, 265–272.

Hicks Pries CE, Schuur E a. G, Vogel JG, Natali SM (2013) Moisture drives surface decomposition in thawing tundra. *Journal of Geophysical Research: Biogeosciences*, **118**, 1133–1143.

Hines ME, Duddleston KN, Kiene RP (2001) Carbon flow to acetate and C1 compounds in northern wetlands. *Geophysical Research Letters*, **28**, 4251–4254.

Hines ME, Duddleston KN, Rooney-Varga JN, Fields D, Chanton JP (2008) Uncoupling of acetate degradation from methane formation in Alaskan wetlands: Connections to vegetation distribution. *Global Biogeochemical Cycles*, **22**, GB2017.

Hodgkins SB, Tfaily MM, McCalley CK et al. (2014) Changes in peat chemistry associated with permafrost thaw increase greenhouse gas production. *Proceedings of the National Academy of Sciences*, 201314641.

Horn MA, Matthies C, Küsel K, Schramm A, Drake HL (2003) Hydrogenotrophic Methanogenesis by Moderately Acid-Tolerant Methanogens of a Methane-Emitting Acidic Peat. *Applied and Environmental Microbiology*, **69**, 74–83.

Hornibrook ERC, Longstaffe FJ, Fyfe WS (1997) Spatial distribution of microbial methane production pathways in temperate zone wetland soils: Stable carbon and hydrogen isotope evidence. *Geochimica et Cosmochimica Acta*, **61**, 745–753.

Hornibrook ERC, Longstaffe FJ, Fyfe WS (2000) Factors Influencing Stable Isotope Ratios in CH_4 and CO_2 within Subenvironments of Freshwater Wetlands: Implications for δ-Signatures of Emissions. *Isotopes in Environmental and Health Studies*, **36**, 151–176.

Hugelius G, Strauss J, Zubrzycki S et al. (2014) Improved estimates show large circumpolar stocks of permafrost carbon while quantifying substantial uncertainty ranges and identifying remaining data gaps. *Biogeosciences Discussions*, **11**, 4771–4822.

Inglett KS, Inglett PW, Reddy KR, Osborne TZ (2012) Temperature sensitivity of greenhouse gas production in wetland soils of different vegetation. *Biogeochemistry*, **108**, 77–90.

Joabsson A, Christensen TR (2001) Methane emissions from wetlands and their relationship with vascular plants: an Arctic example. *Global Change Biology*, **7**, 919–932.

Johansson T, Malmer N, Crill PM, Friborg T, Åkerman JH, Mastepanov M, Christensen TR (2006) Decadal vegetation changes in a northern peatland, greenhouse gas fluxes and net radiative forcing. *Global Change Biology*, **12**, 2352–2369.

Johansson M, Callaghan TV, Bosiö J, Åkerman HJ, Jackowicz-Korczynski M, Christensen TR (2013) Rapid responses of permafrost and vegetation to experimentally increased snow cover in sub-arctic Sweden. *Environmental Research Letters*, **8**, 035025.

Jones MH, Fahnestock JT, Walker DA, Walker MD, Welker JM (1998) Carbon dioxide fluxes in moist and dry Arctic tundra during the snow-free season: responses to increases in summer temperature and winter snow accumulation. *Arctic and alpine research*, 373–380.

Jorgenson MT, Racine CH, Walters JC, Osterkamp TE (2001) Permafrost Degradation and Ecological Changes Associated with a WarmingClimate in Central Alaska. *Climatic Change*, **48**, 551–579.

Juncher Jørgensen C, Lund Johansen KM, Westergaard-Nielsen A, Elberling B (2015) Net regional methane sink in High Arctic soils of northeast Greenland. *Nature Geoscience*, **8**, 20–23.

Kattsov VM, Walsh JE (2000) Twentieth-Century Trends of Arctic Precipitation from Observational Data and a Climate Model Simulation. *Journal of Climate*, **13**, 1362–1370.

Kattsov VM, Källén E, Cattle HP et al. (2005) Future climate change: modeling and scenarios for the Arctic. In: *Arctic Climate Impact Assessment (ACIA)*. Cambridge University Press, Cambridge, UK, pp. 99–150.

Keeling CD (1958) The concentration and isotopic abundances of atmospheric carbon dioxide in rural areas. *Geochimica et Cosmochimica Acta*, **13**, 322–334.

Kelker D, Chanton J (1997) The effect of clipping on methane emissions from Carex. *Biogeochemistry*, **39**, 37–44.

King SL, Quay PD, Lansdown JM (1989) The $^{13}C/^{12}C$ kinetic isotope effect for soil oxidation of methane at ambient atmospheric concentrations. *Journal of Geophysical Research: Atmospheres*, **94**, 18273–18277.

King JY, Reeburgh WS, Regli SK (1998) Methane emission and transport by Arctic sedges in Alaska: Results of a vegetation removal experiment. *Journal of Geophysical Research: Atmospheres*, **103**, 29083–29092.

Kirschke S, Bousquet P, Ciais P et al. (2013) Three decades of global methane sources and sinks. *Nature Geoscience*, **6**, 813–823.

Kotsyurbenko OR, Friedrich MW, Simankova MV, Nozhevnikova AN, Golyshin PN, Timmis KN, Conrad R (2007) Shift from Acetoclastic to H_2-Dependent Methanogenesis in a West Siberian Peat Bog at Low pH Values and Isolation of an Acidophilic Methanobacterium Strain. *Applied and Environmental Microbiology*, **73**, 2344–2348.

Lawrence DM, Koven CD, Swenson SC, Riley WJ, Slater AG (2015) Permafrost thaw and resulting soil moisture changes regulate projected high-latitude CO_2 and CH_4 emissions. *Environmental Research Letters*, **10**, 094011.

Lee H, Schuur EA, Inglett KS, Lavoie M, Chanton JP (2012) The rate of permafrost carbon release under aerobic and anaerobic conditions and its potential effects on climate. *Global Change Biology*, **18**, 515–527.

Liptay K, Chanton J, Czepiel P, Mosher B (1998) Use of stable isotopes to determine methane oxidation in landfill cover soils. *Journal of Geophysical Research: Atmospheres*, **103**, 8243–8250.

Liston GE, Mcfadden JP, Sturm M, Pielke RA (2002) Modelled changes in Arctic tundra snow, energy and moisture fluxes due to increased shrubs. *Global Change Biology*, **8**, 17–32.

Lunardini VJ (1991) Heat transfer with freezing and thawing. In: *Developments in Geotechnical Engineering* 65, Department of the Army, CRREL, Corps of Engineers, Hanover, USA. Elsevier, Amsterdam.

Lupascu M, Welker JM, Seibt U, Maseyk K, Xu X, Czimczik CI (2014a) High Arctic wetting reduces permafrost carbon feedbacks to climate warming. *Nature Climate Change*, **4**, 51–55.

Lupascu M, Welker JM, Xu X, Czimczik CI (2014b) Rates and radiocarbon content of summer ecosystem respiration in response to long-term deeper snow in the High Arctic of NW Greenland. *Journal of Geophysical Research: Biogeosciences*, **119**, 2013JG002494.

Lupascu M, Welker JM, Seibt U, Xu X, Velicogna I, Lindsey DS, Czimczik CI (2014c) The amount and timing of precipitation control the magnitude, seasonality and sources (^{14}C) of ecosystem respiration in a polar semi-desert, northwestern Greenland. *Biogeosciences*, **11**, 4289–4304.

MacDougall AH, Avis CA, Weaver AJ (2012) Significant contribution to climate warming from the permafrost carbon feedback. *Nature Geoscience*, **5**, 719–721.

McCalley CK, Woodcroft BJ, Hodgkins SB et al. (2014) Methane dynamics regulated by microbial community response to permafrost thaw. *Nature*, **514**, 478–481.

McGuire AD, Christensen TR, Hayes D et al. (2012) An assessment of the carbon balance of Arctic tundra: comparisons among observations, process models, and atmospheric inversions. *Biogeosciences Discuss.*, **9**, 4543–4594.

Metje M, Frenzel P (2007) Methanogenesis and methanogenic pathways in a peat from subarctic permafrost. *Environmental Microbiology*, **9**, 954–964.

Miller GH, Alley RB, Brigham-Grette J, Fitzpatrick JJ, Polyak L, Serreze MC, White JWC (2010) Arctic amplification: can the past constrain the future? *Quaternary Science Reviews*, **29**, 1779–1790.

Mondav R, Woodcroft BJ, Kim E-H et al. (2014) Discovery of a novel methanogen prevalent in thawing permafrost. *Nature Communications*, **5**.

Morgner E, Elberling B, Strebel D, Cooper EJ (2010) The importance of winter in annual ecosystem respiration in the High Arctic: effects of snow depth in two vegetation types. *Polar Research*, **29**, 58–74.

Morrissey LA, Livingston GP (1992) Methane emissions from Alaska Arctic tundra: An assessment of local spatial variability. *Journal of Geophysical Research: Atmospheres*, **97**, 16661–16670.

Myhre G, Shindell D, Bréon FM et al. (2013) Anthropogenic and natural radiative forcing. *Climate change*, 658–740.

Nowinski NS, Taneva L, Trumbore SE, Welker JM (2010) Decomposition of old organic matter as a result of deeper active layers in a snow depth manipulation experiment. *Oecologia*, **163**, 785–792.

O'Donnell JA, Jorgenson MT, Harden JW, McGuire AD, Kanevskiy MZ, Wickland KP (2012) The Effects of Permafrost Thaw on Soil Hydrologic, Thermal, and Carbon Dynamics in an Alaskan Peatland. *Ecosystems*, **15**, 213–229.

Osterkamp TE (2007) Causes of warming and thawing permafrost in Alaska. *Eos, Transactions American Geophysical Union*, **88**, 522–523.

Osterkamp TE, Jorgenson MT, Schuur E a. G, Shur YL, Kanevskiy MZ, Vogel JG, Tumskoy VE (2009) Physical and ecological changes associated with warming permafrost and thermokarst in Interior Alaska. *Permafrost and Periglacial Processes*, **20**, 235–256.

Pattison RR, Welker JM (2014) Differential ecophysiological response of deciduous shrubs and a graminoid to long-term experimental snow reductions and additions in moist acidic tundra, Northern Alaska. *Oecologia*, **174**, 339–350.

Ping CL, Michaelson GJ, Kimble JM (1997) Carbon storage along a latitudinal transect in Alaska. *Nutrient Cycling in Agroecosystems*, **49**, 235–242.

Ping CL, Jastrow JD, Jorgenson MT, Michaelson GJ, Shur YL (2014) Permafrost soils and carbon cycling. *SOIL Discussions*, **1**, 709–756.

Popp TJ, Chanton JP, Whiting GJ, Grant N (1999) Methane stable isotope distribution at a Carex dominated fen in north central Alberta. *Global Biogeochemical Cycles*, **13**, 1063–1077.

Prater JL, Chanton JP, Whiting GJ (2007) Variation in methane production pathways associated with permafrost decomposition in collapse scar bogs of Alberta, Canada. *Global Biogeochemical Cycles*, **21**, GB4004.

Preuss I, Knoblauch C, Gebert J, Pfeiffer E-M (2013) Improved quantification of microbial CH_4 oxidation efficiency in Arctic wetland soils using carbon isotope fractionation. *Biogeosciences*, **10**, 2539–2552.

Reeburgh WS, Whalen SC, Alperin MJ (1993) The role of methylotrophy in the global methane budget. *Microbial growth on C1 compounds*, 1–14.

Romanovsky VE, Osterkamp TE (2000) Effects of unfrozen water on heat and mass transport processes in the active layer and permafrost. *Permafrost and Periglacial Processes*, **11**, 219–239.

Romanovsky VE, Smith SL, Christiansen HH (2010) Permafrost thermal state in the polar Northern Hemisphere during the international polar year 2007–2009: a synthesis. *Permafrost and Periglacial Processes*, **21**, 106–116.

Sander R (1999) *Compilation of Henry's law constants for inorganic and organic species of potential importance in environmental chemistry*. Max-Planck Institute of Chemistry, Air Chemistry Department Mainz, Germany.

Schaefer K, Lantuit H, Romanovsky VE, Schuur EAG, Witt R (2014) The impact of the permafrost carbon feedback on global climate. *Environmental Research Letters*, **9**, 085003.

Schimel JP, Bilbrough C, Welker JM (2004) Increased snow depth affects microbial activity and nitrogen mineralization in two Arctic tundra communities. *Soil Biology and Biochemistry*, **36**, 217–227.

Schneider von Deimling T, Meinshausen M, Levermann A, Huber V, Frieler K, Lawrence DM, Brovkin V (2012) Estimating the near-surface permafrost-carbon feedback on global warming. *Biogeosciences*, **9**, 649–665.

Schuur E a. G, Abbott BW, Bowden WB et al. (2013) Expert assessment of vulnerability of permafrost carbon to climate change. *Climatic Change*, **119**, 359–374.

Schuur E a. G, McGuire AD, Schädel C et al. (2015) Climate change and the permafrost carbon feedback. *Nature*, **520**, 171–179.

Segers R (1998) Methane production and methane consumption: a review of processes underlying wetland methane fluxes. *Biogeochemistry*, **41**, 23–51.

Seppälä M (2011) Synthesis of studies of palsa formation underlining the importance of local environmental and physical characteristics. *Quaternary Research*, **75**, 366–370.

Sharp ED, Sullivan PF, Steltzer H, Csank AZ, Welker JM (2013) Complex carbon cycle responses to multi-level warming and supplemental summer rain in the high Arctic. *Global Change Biology*, **19**, 1780–1792.

Shukla PN, Pandey KD, Mishra VK (2013) Environmental Determinants of Soil Methane Oxidation and Methanotrophs. *Critical Reviews in Environmental Science and Technology*, **43**, 1945–2011.

Sistla SA, Moore JC, Simpson RT, Gough L, Shaver GR, Schimel JP (2013) Long-term warming restructures Arctic tundra without changing net soil carbon storage. *Nature*, **497**, 615–618.

Stocker TF, Qin D, Plattner G-K et al. (2013a) Long-term Climate Change: Projections, Commitments and Irreversibility. In: *Climate Change 2013 : The Physical Science Basis. Contribution of Working Group I to the Fifth Assessment Report of the Intergovernmental Panel on Climate Change.*

Stocker BD, Roth R, Joos F et al. (2013b) Multiple greenhouse-gas feedbacks from the land biosphere under future climate change scenarios. *Nature Climate Change*, **3**, 666–672.

Ström L, Ekberg A, Mastepanov M, Røjle Christensen T (2003) The effect of vascular plants on carbon turnover and methane emissions from a tundra wetland. *Global Change Biology*, **9**, 1185–1192.

Ström L, Mastepanov M, Christensen TR (2005) Species-specific Effects of Vascular Plants on Carbon Turnover and Methane Emissions from Wetlands. *Biogeochemistry*, **75**, 65–82.

Ström L, Tagesson T, Mastepanov M, Christensen TR (2012) Presence of Eriophorum scheuchzeri enhances substrate availability and methane emission in an Arctic wetland. *Soil Biology and Biochemistry*, **45**, 61–70.

Sturm M, Schimel J, Michaelson G et al. (2005) Winter biological processes could help convert Arctic tundra to shrubland. *Bioscience*, **55**, 17–26.

Subin ZM, Koven CD, Riley WJ, Torn MS, Lawrence DM, Swenson SC (2013) Effects of Soil Moisture on the Responses of Soil Temperatures to Climate Change in Cold Regions. *Journal of Climate*, **26**, 3139–3158.

Tape KD, Hallinger M, Welker JM, Ruess RW (2012) Landscape Heterogeneity of Shrub Expansion in Arctic Alaska. *Ecosystems*, **15**, 711–724.

Teh YA, Silver WL, Conrad ME (2005) Oxygen effects on methane production and oxidation in humid tropical forest soils. *Global Change Biology*, **11**, 1283–1297.

Teh YA, Silver WL, Sonnentag O, Detto M, Kelly M, Baldocchi DD (2011) Large Greenhouse Gas Emissions from a Temperate Peatland Pasture. *Ecosystems*, **14**, 311–325.

Throckmorton HM, Heikoop JM, Newman BD et al. (2015) Pathways and transformations of dissolved methane and dissolved inorganic carbon in Arctic tundra watersheds: Evidence from analysis of stable isotopes. *Global Biogeochemical Cycles*, 2014GB005044.

Torn MS, Chapin III FS (1993) Environmental and biotic controls over methane flux from Arctic tundra. *Chemosphere*, **26**, 357–368.

Treat CC, Wollheim WM, Varner RK, Grandy AS, Talbot J, Frolking S (2014) Temperature and peat type control CO_2 and CH_4 production in Alaskan permafrost peats. *Global Change Biology*, **20**, 2674–2686.

Treat CC, Natali SM, Ernakovich J et al. (2015) A pan-Arctic synthesis of CH_4 and CO_2 production from anoxic soil incubations. *Global Change Biology*, **21**, 2787–2803.

Turetsky MR, Treat CC, Waldrop MP, Waddington JM, Harden JW, McGuire AD (2008) Short-term response of methane fluxes and methanogen activity to water table and soil warming manipulations in an Alaskan peatland. *Journal of Geophysical Research: Biogeosciences*, **113**, G00A10.

Turner AJ, Jacob DJ, Wecht KJ et al. (2015) Estimating global and North American methane emissions with high spatial resolution using GOSAT satellite data. *Atmos. Chem. Phys. Discuss.*, **15**, 4495–4536.

Tveit AT, Urich T, Frenzel P, Svenning MM (2015) Metabolic and trophic interactions modulate methane production by Arctic peat microbiota in response to warming. *Proceedings of the National Academy of Sciences*, 201420797.

Uhlířová E, Šantrůčková H, Davidov SP (2007) Quality and potential biodegradability of soil organic matter preserved in permafrost of Siberian tussock tundra. *Soil Biology and Biochemistry*, **39**, 1978–1989.

Updegraff K, Bridgham SD, Pastor J, Weishampel P, Harth C (2001) Response of CO_2 and CH_4 emissions from peatlands to warming and water table manipulation. *Ecological Applications*, **11**, 311–326.

Wahren C-H, Walker MD, Bret-Harte MS (2005) Vegetation responses in Alaskan Arctic tundra after 8 years of a summer warming and winter snow manipulation experiment. *Global Change Biology*, **11**, 537–552.

Waldrop MP, Wickland KP, White Iii R, Berhe AA, Harden JW, Romanovsky VE (2010) Molecular investigations into a globally important carbon pool: Permafrost-protected carbon in Alaskan soils. *Global Change Biology*, **16**, 2543–2554.

Walker DA, Raynolds MK, Daniëls FJA et al. (2005) The Circumpolar Arctic vegetation map. *Journal of Vegetation Science*, **16**, 267–282.

Walker MD, Walker DA, Auerbach NA (1994) Plant Communities of a Tussock Tundra Landscape in the Brooks Range Foothills, Alaska. *Journal of Vegetation Science*, **5**, 843–866.

Walker MD (1996) Community baseline measurements for ITEX studies. In: *ITEX Manual* (eds MolauU, MølgaardP), Danish Polar Center, Copenhagen, Denmark.

Walker MD, Walker DA, Welker JM et al. (1999) Long-term experimental manipulation of winter snow regime and summer temperature in Arctic and alpine tundra. *Hydrological Processes*, **13**, 2315–2330.

Wallenstein MD, Mcmahon SK, Schimel JP (2009) Seasonal variation in enzyme activities and temperature sensitivities in Arctic tundra soils. *Global Change Biology*, **15**, 1631–1639.

Welker JM, Fahnestock JT, Jones MH (2000) Annual CO_2 flux in dry and moist Arctic tundra: field responses to increases in summer temperatures and winter snow depth. *Climatic Change*, **44**, 139–150.

West AE, Schmidt SK (2002) Endogenous Methanogenesis Stimulates Oxidation of Atmospheric CH_4 in Alpine Tundra Soil. *Microbial Ecology*, **43**, 408–415.

Whalen SC, Reeburgh WS (1990) Consumption of atmospheric methane by tundra soils. *Nature*, **346**, 160–162.

Whalen SC, Reeburgh WS (2000) Methane Oxidation, Production, and Emission at Contrasting Sites in a Boreal Bog. *Geomicrobiology Journal*, **17**, 237–251.

Whiticar MJ, Faber E (1986) Methane oxidation in sediment and water column environments—Isotope evidence. *Organic Geochemistry*, **10**, 759–768.

Whiticar MJ, Faber E, Schoell M (1986) Biogenic methane formation in marine and freshwater environments: CO_2 reduction vs. acetate fermentation—Isotope evidence. *Geochimica et Cosmochimica Acta*, **50**, 693–709.

Wild B, Schnecker J, Alves RJE et al. (2014) Input of easily available organic C and N stimulates microbial decomposition of soil organic matter in Arctic permafrost soil. *Soil Biology and Biochemistry*, **75**, 143–151.

Yavitt JB, Downey DM, Lancaster E, Lang GE (1990) Methane consumption in decomposing Sphagnum-derived peat. *Soil Biology and Biochemistry*, **22**, 441–447.

Zetsche E, Thornton B, Midwood AJ, Witte U (2011) Utilization of different carbon sources in a shallow estuary identified through stable isotope techniques. *Continental Shelf Research*, **31**, 832–840.

Zhang X, He J, Zhang J, Polyakov I, Gerdes R, Inoue J, Wu P (2013) Enhanced poleward moisture transport and amplified northern high-latitude wetting trend. *Nature Climate Change*, **3**, 47–51.

4.9 SUPPLEMENTARY INFORMATION

4.9.1 Ecosystem CH_4 emissions and soil profile sampling and analyses

4.10.1.1 Field sampling

4.10.1.1.1 Ecosystem CH_4 emissions

Ecosystem CH_4 fluxes and $\delta^{13}C$ values of emitted CH_4 were measured using the static chamber approach (Bubier *et al.*, 1995). At each plot, we installed a fixed 25-cm-diameter PVC collar inserted 15 cm into the soil (average depth of the mineral horizon) to ensure a good seal at the bottom of the chamber. Collar insertion had no effect on plant development, species composition, soil water content or soil temperature, indicating that the collar diameter was enough to minimize disturbance. At the moment of the sampling, collars were capped with opaque lids fitted with a rubber closed cell foam gasket, resulting in an average chamber volume of 12L. Chamber lids were equipped with a stainless-steel sampling port (Swagelok Corporation, OH, USA) fitted with a PTFE/butyl septum (Restek Corporation, PA, USA). From each chamber, five 90 mL samples were taken at 15-min intervals over a 75-min period with 60 mL syringes equipped with 3-way stopcocks. Gas samples were injected into pre-evacuated sampling bags equipped with Luer-Lock valve fittings (Cali-5-Bond™, Calibrated Instruments Inc., NY, USA).

4.10.1.1.2 Soil profile

Soil interstitial gas and pore water were collected from soil probes progressively installed at each plot at 10, 20, 35 and 50-cm depth as the thaw depth increased over the growing season. Two pseudo-replicates were taken at each depth, plot and sampling period, and values were averaged for a total of 4 replicates per treatment, depth and period. Soil probes consisted of ¼”

OD stainless-steel tubing fitted with stainless-steel Swagelok unions and PTFE/butyl septum creating a gas tight unit. The bottoms of the probes were crimped and small holes were drilled 2-cm above the bottom to allow sample collection. Interstitial gas samples were extracted from non-water-saturated soil depths with a 60mL plastic syringe equipped with 3-way stopcock and injected into pre-evacuated sampling bags. At water-saturated soil depths, bubble-free pore water samples were extracted with a 60mL syringe and injected into sampling bags filled with a known volume of N_2 (i.e., water:N_2 ratio was 70:30) and equilibrated by vigorously agitating for 5-min following procedures described in Lewin et al., 1990. The headspace was subsequently extracted and injected into a pre-evacuated bag.

4.10.1.2 Sample analyses

All samples were analyzed within 4–6 hr after collection for the direct determination of pCH_4, pCO_2, $\delta^{13}C\text{-}CH_4$ and $\delta^{13}C\text{-}CO_2$ using a Picarro G2201-*i* cavity ring-down spectrometer (CRDS) equipped with a 16-port distribution manifold (Picarro Inc., CA, USA). The inlets of the distribution manifold were adapted with stainless-steel Luer-Lock valve fittings for a gas tight connection with the sampling bags. Samples were run in continuous flow for 5 min in High Dynamic Range mode. For each measurement, the signal was allowed to stabilize for 30 secs, and the result integrated 4.5 min of data at measurement intervals of 3 secs for manufacturer guaranteed precision of <0.05% of the reading for pCH_4 and pCO_2 values, and <0.55‰ and <0.16‰ for $\delta^{13}C\text{-}CH_4$ and $\delta^{13}C\text{-}CO_2$ values respectively. A standard mix of 2.5 ppm CH_4 ($\delta^{13}C\text{-}CH_4$ = –40.2 ‰) and 396 ppm CO_2 ($\delta^{13}C\text{-}CO_2$ = –35.7 ‰) was run every five samples from both sampling bags and directly from the tank with no sign of drift or bias. The accuracy for pCH_4 and $\delta^{13}C\text{-}CH_4$ was better than 90 ppb and 0.1‰. The accuracy of pCO_2 and $\delta^{13}C\text{-}CO_2$ was better than 1ppm and 0.6 ‰. All pCH_4 data were pressure and temperature corrected.

4.9.2 Calculation of the oxidation fractionation factor

The oxidation fractionation factor (α_{ox}) was described as a Rayleigh fractionation process (1896) and calculated as in King *et al.*, (1989):

(Eq. S4.1) $$1/\alpha_{ox} = \{Ln [(\delta_{(f)}+1000) / (\delta_{(i)}+1000)] / Ln (pCH_{4(f)} / pCH_{4(i)})\} + 1$$

where $\delta_{(i)}$ and $\delta_{(f)}$ are $\delta^{13}C$ of the initial and final CH_4 in the chamber headspace, and $pCH_{4(i)}$ and $pCH_{4(f)}$ are the initial and final pCH_4 in the chamber headspace (Tyler *et al.*, 1994; Reeburgh *et al.*, 1997). α_{ox} was determined at plots where net CH_4 oxidation was observed through part or the entire growing season. Calculated α_{ox} averaged 1.0206±0.0003 and 1.0209±0.0004 at Ambient and RS respectively and were within those reported for Arctic tundra ecosystems (1.009–1.031; Tyler *et al.*, 1994; Reeburgh *et al.*, 1997; Preuss *et al.*, 2013).

Given the temperature sensitivity of α_{ox} (Tyler *et al.*, 1994; Chanton *et al.*, 2008), calculations were additionally conducted with a temperature-dependent correction of the average α_{ox} reported at the RS (sustained net CH_4 oxidation over the growing season) to allow common ground calculations of ecosystem oxidation efficiency for treatments where no net CH_4 oxidation was observed using the following relationship:

(Eq. S4.2) $$\alpha_{ox,(I)} = \alpha_{ox,measured} - 0.00039 (T_{(I)} - T_{measured})$$

where $\alpha_{ox,(I)}$ represents the oxidation fractionation factor at the temperature of interest, $T_{(I)}$ in ^{o}C, and $\alpha_{ox,measured}$ is the fractionation factor at $T_{measured}$ in ^{o}C (Chanton *et al.*, 2008).

α_{ox} at Ambient was used to test the predictability of α_{ox} at our experimental treatments, with a 98% agreement. Comparisons between F_{ox} calculated from treatment specific α_{ox} and F_{ox} calculated from the theoretical α_{ox} reported for Arctic tundra soils (1.020; Tyler *et al.*, 1994; Reeburgh *et al.*, 1997) revealed a 0.6% bias on F_{ox} estimates, which was considered an

acceptable uncertainty for the purpose of this paper.

4.9.3 Error introduced by contributions from oxidized CH_4 to total pCO_2

Using calculated estimates of the oxidation efficiency (F_{ox}; Methods, Eq. 4.2), we estimated that 0.6–0.8% of the pCO_2 within the soil column originated from oxidized CH_4, which was considered an acceptable uncertainty for the purpose of the paper (Throckmorton et al., 2015).

4.9.4 Supplementary information. Cited Literature

Bubier JL, Moore TR, Bellisario L, Comer NT, Crill PM (1995) Ecological controls on methane emissions from a Northern Peatland Complex in the zone of discontinuous permafrost, Manitoba, Canada. *Global Biogeochemical Cycles*, **9**, 455–470.

Chanton JP, Powelson DK, Abichou T, Fields D, Green R (2008) Effect of Temperature and Oxidation Rate on Carbon-isotope Fractionation during Methane Oxidation by Landfill Cover Materials. *Environmental Science & Technology*, **42**, 7818–7823.

King SL, Quay PD, Lansdown JM (1989) The $^{13}C/^{12}C$ kinetic isotope effect for soil oxidation of methane at ambient atmospheric concentrations. *Journal of Geophysical Research: Atmospheres*, **94**, 18273–18277.

Lewin K, Blakey NC, Cooke DA, Britain G (1990) *The Validation of Methodology in the Determination of Methane in Water: Final Report*. Great Britain, Health and Safety Executive.

Preuss I, Knoblauch C, Gebert J, Pfeiffer E-M (2013) Improved quantification of microbial CH_4 oxidation efficiency in Arctic wetland soils using carbon isotope fractionation. *Biogeosciences*, **10**, 2539–2552.

Rayleigh, Lord (1896) L. Theoretical considerations respecting the separation of gases by diffusion and similar processes. *The London, Edinburgh, and Dublin Philosophical Magazine and Journal of Science*, **42**, 493–498.

Reeburgh WS, Hirsch AI, Sansone FJ, Popp BN, Rust TM (1997) Carbon kinetic isotope effect accompanying microbial oxidation of methane in boreal forest soils. *Geochimica et Cosmochimica Acta*, **61**, 4761–4767.

Throckmorton HM, Heikoop JM, Newman BD et al. (2015) Pathways and transformations of dissolved methane and dissolved inorganic carbon in Arctic tundra watersheds: Evidence from analysis of stable isotopes. *Global Biogeochemical Cycles*, 2014GB005044.

Tyler SC, Crill PM, Brailsford GW (1994) 13C12C Fractionation of methane during oxidation in a temperate forested soil. *Geochimica et Cosmochimica Acta*, **58**, 1625–1633.

5. DISCUSSION: RESHAPING OUR UNDERSTANDING OF THE ARCTIC TUNDRA CARBON DYNAMICS

Climate (i.e. atmospheric temperatures and precipitation patterns) is changing at a rate that is unprecedented in the last 1300 years (Serreze *et al.*, 2000; Miller *et al.*, 2010; Serreze & Barry, 2011; Mudryk *et al.*, 2014), reshaping Arctic tundra structure and functioning (Schuur *et al.*, 2013, 2015; Abbott *et al.*, 2016). The Arctic tundra has been responsible for a substantial portion of the global land-based sink for atmospheric CO_2 throughout the 20th century (McGuire *et al.*, 2009, 2012). However, paleo-reconstruction studies indicate large losses of permafrost C during past warming episodes that largely contributed to increases in GHGs concentrations in the atmosphere, raising great concern about the fate of the large permafrost SOC pool and derived feedbacks on the climate system (DeConto *et al.*, 2012; Crichton *et al.*, 2016; Tesi *et al.*, 2016). At present, model predictions vary widely among studies suggesting the incomplete or inaccurate representation of the mechanisms driving the C sink or source strength of Arctic tundra and radiative forcing on future climate (Schaefer *et al.*, 2011; Burke *et al.*, 2012).

Deeper winter snow results in cascading effects on many key system drivers including winter and summer warming, enhanced soil wetness, accelerated permafrost thaw, increased nutrient availability, and changes in plant community structure and plant productivity (Fig. 1). The complex interactions among these variables difficult the assessment of the full impacts of progressive degradation on Arctic tundra C cycle from single factor responses. With multiple, and often contrasting, lines of evidence emerging on the response of Arctic tundra C dynamics to changes in individual driving factors, a comprehensive and integrated view of the overall impact of changes in climate is needed (Hicks Pries *et al.*, 2011; Bosiö *et al.*, 2012; Elmendorf *et al.*, 2012a; Trucco *et al.*, 2012; Elberling *et al.*, 2013; DeMarco *et al.*, 2014; Leffler *et al.*, 2016;

Webb *et al.*, 2016). The research presented here, by using a holistic approach in a system-wide, multi-year and multi-level snow manipulation experiment provides a unique opportunity to reconcile discrepancies, and identify and constrain the mechanisms driving the response of the Arctic tundra C cycle to future climate scenarios.

5.1 Helping reconcile predictions of the impacts of changes in climate on Arctic tundra carbon budget and feedbacks to the global climate system

The depth of the active layer is a major determinant of the Arctic tundra C cycle, as it determines the amount and rate at which permafrost C becomes vulnerable for decomposition (Grosse *et al.*, 2011; Koven *et al.*, 2011; Burke *et al.*, 2012; Harden *et al.*, 2012; Schuur *et al.*, 2015), influences soil thermal and hydrological regimes thereby regulating microbial activity and decomposition rates (Kuhry *et al.*, 2010; Lee *et al.*, 2012), and determines rooting depth of tundra vegetation and access to nutrients influencing plant community structure and productivity (Bret-Harte *et al.*, 2001; Iversen *et al.*, 2015). Therefore, an adequate assessment of permafrost dynamics and active layer thickness (ALT) under future climate scenarios is a critical step towards accurately predicting C-cycle/climate feedbacks from Arctic regions.

Long-term climatic records from northern Alaska indicate an increase in atmospheric and near-surface permafrost temperatures since the 1970s (Osterkamp, 2007; Solomon, 2007), a trend that has intensified over the last decades (Shiklomanov *et al.*, 2010). However, data from the Circumpolar Active Layer Monitoring (CALM) network show no clear indication of a deepening of the active layer accompanying warming trends (Shiklomanov *et al.*, 2010; Streletskiy *et al.*, 2012). This contradicts model reconstructions that estimate significant permafrost degradation and deepening of the active layer across the Arctic region over the considered period (Hayes *et al.*, 2014). Our results provide evidence of a significant thaw-

induced soil consolidation of the active layer and subsidence of the ground surface in the area of study between 2008 and 2012, which led to a 20% underestimation in the rate of permafrost thaw resulting in the apparent stability of the ALT (*see* Chapter 2). Accounting for physical alterations of the soil column, the depth of active layer increased at a mean rate of 0.4 cm yr^{-1}, which exposed 0.2 kgC m^{-2} yr^{-1} to decomposition over the 4-yr period considered (*see* Chapter 2). These values are comparable to model-estimated rates of increases in ALT and the vulnerable SOC pool across the Arctic region over the last decades (Hayes *et al.*, 2014). Therefore, our findings bridge the gap between empirical observations and model simulations of permafrost dynamics in recent decades, and suggest that failing to adequately reproduce climate-driven alterations of the physical properties of the active layer, the full impacts of Arctic warming could go unnoticed until long after the onset of permafrost thaw.

Arctic C dynamics are defined by the integration of the constraining, saturating or accelerating effects of driving variables on all contributing C fluxes, which may differ in lag-times and sensitivities to disturbance. As such, the response of the Arctic tundra C budget to climate change is unlikely to be neither permanent nor fixed, but rather to evolve over the course of progressive permafrost degradation, initial responses not necessarily being maintained in the long run. Given the paucity of direct measurements of long-term responses of the Arctic tundra SOC pool and C fluxes to changes in climate, climate/C-cycle coupled models must rely heavily on the linear extrapolation of short-term responses to infer long-term changes in Arctic tundra C stocks and fluxes (Luo *et al.*, 2011; Koven *et al.*, 2015a, 2015b).

We show that the response of C fluxes and budget from Arctic tundra to changes in winter precipitation are markedly nonlinear with both time and treatment intensity (*see* Chapters 2 and 3). These results help reconcile discrepancies among empirical and model reports of the

impacts of warming on the Arctic C balance (Hicks Pries *et al.*, 2011; Lamb *et al.*, 2011; Lund *et al.*, 2012; Sistla *et al.*, 2013; Li *et al.*, 2014; Natali *et al.*, 2014). Our findings are consistent with studies showing similar non-linearities in other ecosystems under a changing environment over time and treatment intensity (Burkett *et al.*, 2005; Gomez-Casanovas *et al.*, 2016). Taken together, our results and those from other studies suggest that assumptions of linearity could lead to substantial inaccuracies in both the magnitude and direction of the response of the C budget to changes in climate of terrestrial ecosystems, including the Arctic tundra.

Overall, we show that the response of Arctic tundra C balance to altered winter precipitation patterns is defined by thresholds and tipping points beyond which the ecosystem shifts to alternative states. Therefore, the short-term effects of changes in climate on the ecosystem physical and biological parameters should be understood as the dynamic foundation shaping long-term ecosystem responses to climate change. Designing multi-year and multi-level field manipulation experiments that integrate the interactions among all variables driving ecosystem C fluxes over time will improve predictions of the C cycle of Arctic tundra.

5.2 Reconsidering the mechanisms driving the Arctic tundra carbon sink or source strength and radiative forcing on future climate.

At present, predictions of climate forcing from Arctic regions build upon a conceptual framework based on two competing hypotheses. The first hypothesis states that under future climate scenarios, projected warming will increase primary productivity above ecosystem C losses, enhancing the Arctic C sink strength. Alternatively, the second hypothesis states that the combined effect of warming and thaw-induced increases in the availability of permafrost SOC to decomposers will stimulate C mineralization and emission rates, offsetting photosynthetic CO_2 uptake and turning the Arctic region into a C source. Whether plant productivity or microbial

decomposition will drive the Arctic tundra C sink or source strength in future climate scenarios is a long-lasting question with important implications on predictions of climate forcing feedbacks from the Arctic region. Our results suggest that the overall behavior of Arctic tundra C dynamics in response to changes in climate may diverge in some important ways from these conceptual hypotheses.

Remote sensing data indicate a warming-driven increase in vegetation greenness and productivity of 15% in northern high latitudes over the last 50 years (Elmendorf *et al.*, 2012b; Forkel *et al.*, 2016; Zhu *et al.*, 2016), primarily associated to widespread shrub expansion into Arctic tundra (Tape *et al.*, 2006, 2012; Myers-Smith *et al.*, 2011). The cumulative effects of long-term warming on shrub expansion have been used as indication of the potential of enhanced photosynthetic CO_2 uptake to act as a significant mitigating agent of climate change (Schuur *et al.*, 2013; Koven *et al.*, 2015a; Abbott *et al.*, 2016).

Our results indicate that enhanced Gross Primary Productivity (GPP) associated to increases in the relative abundance of shrubs with moderate permafrost thaw under medium snow additions was largely compensated with increases in plant respiration (R_{aut}). The observed decreases in the Arctic tundra C source strength relative to ambient conditions were mostly explained by constraints on the aerobic decomposition of SOC (*see* Chapter 3). However, transitions towards wet-sedge tundra with severe permafrost thaw under high snow reduced plant respiration below photosynthetic CO_2 uptake, increasing the ecosystem C sink strength despite substantial decreases in GPP relative to ambient conditions (*see* Chapter 3). Together, these results suggest that the ability of Arctic tundra to mitigate climate forcing feedbacks through the changes in supported vegetation is determined by changes of plant respiration relative to GPP rather than by enhanced greenness or GPP alone.

In contrast with model estimates predicting a large attenuating effect of the Arctic radiative forcing from enhanced plant productivity (Qian *et al.*, 2010; Schuur *et al.*, 2013; Koven *et al.*, 2015a), our results indicate a tight coupling between R_{aut} and GPP. These observations suggest a limited role of supported vegetation in driving the ecosystem C sink or source strength, and that changes are primarily explained by impacts on microbial activity and function (*see* Chapter 3). These results agree with studies suggesting a predominant role of ecosystem respiration (R_{eco}) in driving responses of Arctic tundra C fluxes to warming (Cahoon *et al.*, 2012; Lund *et al.*, 2012; Trucco *et al.*, 2012; Belshe *et al.*, 2013). Our findings provide empirical support to recent modelling studies that suggest a limited ability of increases in biomass to offset C losses under future climate scenarios (Hayes *et al.*, 2011; Abbott *et al.*, 2016).

The impacts of climate change on plant community structure however, could be critical to the regulation of climate forcing feedbacks from Arctic tundra. We show that the increased abundance of tall sedges with transitions towards wed-sedge tundra with severe permafrost degradation favors the transport of CH_4 through the plant aerenchyma. By bypassing the oxidation zone, enhanced plant-mediated transport reduces CH_4 oxidation subsidizing ecosystem CH_4 emissions, and hence contributes to increases in the GWP of C emissions from Arctic tundra (*see* Chapter 4).

The permafrost C feedback on climate (i.e. amplification of climate warming due to warming-induced release of C currently frozen in permafrost) represents a critical potential for climate change amplification from the Arctic region. Model estimates of the permafrost C feedback is generally assumed proportional to thaw-induced increases in the SOC pool available to decomposers (Harden *et al.*, 2012; Schaefer *et al.*, 2014; Koven *et al.*, 2015a; Lawrence *et al.*, 2015). Radiocarbon studies consistently report the release of old C accompanying permafrost

thaw further supporting this assumption (Schuur *et al.*, 2009; Vogel *et al.*, 2009; Nowinski *et al.*, 2010; Lupascu *et al.*, 2014). However, our results suggest little contributions of newly thawed permafrost SOC to either CO_2 or CH_4 emissions despite significant thaw-induced increases in the vulnerable SOC pool with deeper snow (*see* Chapters 3 and 4). Rather, our results suggest that the release of old C following thaw responded to the increased vulnerability of the SOC contained within the organic-mineral horizon (*see* Chapter 2).

We propose that the fate of permafrost SOC is closely tied not only to temperature but also to hydrology, which may add an additional constraint in permafrost C mobilization following thaw. As such, permafrost SOC may be rapidly released or long-term protected. Therefore, predictions of permafrost C feedback from thaw-induced increases in the vulnerable SOC pool may result in large biases in the magnitude and timing of the radiative forcing from terrestrial Arctic systems to global climate.

In summary, based in our findings from a multi-year and multi-level field manipulation experiment, we suggest that an integrative conceptualization of both physical and biological processes driving changes in the Arctic tundra C budget and emissions over time is likely to reshape our understanding of Arctic C dynamics in a changing environment, and help improving predictions of the contribution of the Arctic region to future climate.

5.3 CITED LITERATURE

Abbott BW, Jones JB, Schuur EAG et al. (2016) Biomass offsets little or none of permafrost carbon release from soils, streams, and wildfire: an expert assessment. *Environmental Research Letters*, **11**, 034014.

Belshe EF, Schuur E a. G, Bolker BM (2013) Tundra ecosystems observed to be CO_2 sources due to differential amplification of the carbon cycle. *Ecology Letters*, **16**, 1307–1315.

Bosiö J, Johansson M, Callaghan TV, Johansen B, Christensen TR (2012) Future vegetation changes in thawing subarctic mires and implications for greenhouse gas exchange—a regional assessment. *Climatic Change*, **115**, 379–398.

Bret-Harte MS, Shaver GR, Zoerner JP et al. (2001) Developmental Plasticity Allows Betula Nana to Dominate Tundra Subjected to an Altered Environment. *Ecology*, **82**, 18–32.

Burke EJ, Jones CD, Koven CD (2012) Estimating the Permafrost-Carbon Climate Response in the CMIP5 Climate Models Using a Simplified Approach. *Journal of Climate*, **26**, 4897–4909.

Burkett VR, Wilcox DA, Stottlemyer R et al. (2005) Nonlinear dynamics in ecosystem response to climatic change: Case studies and policy implications. *Ecological Complexity*, **2**, 357–394.

Cahoon SMP, Sullivan PF, Shaver GR, Welker JM, Post E (2012) Interactions among shrub cover and the soil microclimate may determine future Arctic carbon budgets. *Ecology Letters*, **15**, 1415–1422.

Crichton KA, Bouttes N, Roche DM, Chappellaz J, Krinner G (2016) Permafrost carbon as a missing link to explain CO_2 changes during the last deglaciation. *Nature Geoscience*, **9**, 683–686.

DeConto RM, Galeotti S, Pagani M et al. (2012) Past extreme warming events linked to massive carbon release from thawing permafrost. *Nature*, **484**, 87–91.

DeMarco J, Mack MC, Bret-Harte MS, Burton M, Shaver GR (2014) Long-term experimental warming and nutrient additions increase productivity in tall deciduous shrub tundra. *Ecosphere*, **5**, 1–22.

Elberling B, Michelsen A, Schädel C et al. (2013) Long-term CO_2 production following permafrost thaw. *Nature Climate Change*, **3**, 890–894.

Elmendorf SC, Henry GHR, Hollister RD et al. (2012a) Plot-scale evidence of tundra vegetation change and links to recent summer warming. *Nature Climate Change*, **2**, 453–457.

Elmendorf SC, Henry GHR, Hollister RD et al. (2012b) Global assessment of experimental climate warming on tundra vegetation: heterogeneity over space and time. *Ecology Letters*, **15**, 164–175.

Forkel M, Carvalhais N, Rödenbeck C et al. (2016) Enhanced seasonal CO_2 exchange caused by amplified plant productivity in northern ecosystems. *Science*, **351**, 696–699.

Gomez-Casanovas N, Hudiburg TW, Bernacchi CJ, Parton WJ, DeLucia EH (2016) Nitrogen deposition and greenhouse gas emissions from grasslands: uncertainties and future directions. *Global Change Biology*, **22**, 1348–1360.

Grosse G, Harden J, Turetsky M et al. (2011) Vulnerability of high-latitude soil organic carbon in North America to disturbance. *Journal of Geophysical Research: Biogeosciences*, **116**, G00K06.

Harden JW, Koven CD, Ping C-L et al. (2012) Field information links permafrost carbon to physical vulnerabilities of thawing. *Geophysical Research Letters*, **39**, L15704.

Hayes DJ, McGuire AD, Kicklighter DW, Gurney KR, Burnside TJ, Melillo JM (2011) Is the northern high-latitude land-based CO_2 sink weakening? *Global Biogeochemical Cycles*, **25**, GB3018.

Hayes DJ, Kicklighter DW, McGuire AD et al. (2014) The impacts of recent permafrost thaw on land–atmosphere greenhouse gas exchange. *Environmental Research Letters*, **9**, 045005.

Hicks Pries CE, Schuur EAG, Crummer KG (2011) Holocene Carbon Stocks and Carbon Accumulation Rates Altered in Soils Undergoing Permafrost Thaw. *Ecosystems*, **15**, 162–173.

Iversen CM, Sloan VL, Sullivan PF et al. (2015) The unseen iceberg: plant roots in Arctic tundra. *New Phytologist*, **205**, 34–58.

Koven CD, Ringeval B, Friedlingstein P et al. (2011) Permafrost carbon-climate feedbacks accelerate global warming. *Proceedings of the National Academy of Sciences*, **108**, 14769–14774.

Koven CD, Schuur E a. G, Schädel C et al. (2015a) A simplified, data-constrained approach to estimate the permafrost carbon–climate feedback. *Phil. Trans. R. Soc. A*, **373**, 20140423.

Koven CD, Lawrence DM, Riley WJ (2015b) Permafrost carbon−climate feedback is sensitive to deep soil carbon decomposability but not deep soil nitrogen dynamics. *Proceedings of the National Academy of Sciences*, **112**, 3752–3757.

Kuhry P, Dorrepaal E, Hugelius G, Schuur EAG, Tarnocai C (2010) Potential remobilization of belowground permafrost carbon under future global warming. *Permafrost and Periglacial Processes*, **21**, 208–214.

Lamb EG, Han S, Lanoil BD, Henry GHR, Brummell ME, Banerjee S, Siciliano SD (2011) A High Arctic soil ecosystem resists long-term environmental manipulations. *Global Change Biology*, **17**, 3187–3194.

Lawrence DM, Koven CD, Swenson SC, Riley WJ, Slater AG (2015) Permafrost thaw and resulting soil moisture changes regulate projected high-latitude CO_2 and CH_4 emissions. *Environmental Research Letters*, **10**, 094011.

Lee H, Schuur EA, Inglett KS, Lavoie M, Chanton JP (2012) The rate of permafrost carbon release under aerobic and anaerobic conditions and its potential effects on climate. *Global Change Biology*, **18**, 515–527.

Leffler AJ, Klein ES, Oberbauer SF, Welker JM (2016) Coupled long-term summer warming and deeper snow alters species composition and stimulates gross primary productivity in tussock tundra. *Oecologia*, **181**, 287–297.

Li J, Luo Y, Natali S, Schuur EAG, Xia J, Kowalczyk E, Wang Y (2014) Modeling permafrost thaw and ecosystem carbon cycle under annual and seasonal warming at an Arctic tundra site in Alaska. *Journal of Geophysical Research: Biogeosciences*, **119**, 2013JG002569.

Lund M, Falk JM, Friborg T, Mbufong HN, Sigsgaard C, Soegaard H, Tamstorf MP (2012) Trends in CO_2 exchange in a high Arctic tundra heath, 2000–2010. *Journal of Geophysical Research: Biogeosciences*, **117**, G02001.

Luo Y, Melillo J, Niu S et al. (2011) Coordinated approaches to quantify long-term ecosystem dynamics in response to global change. *Global Change Biology*, **17**, 843–854.

Lupascu M, Welker JM, Xu X, Czimczik CI (2014) Rates and radiocarbon content of summer ecosystem respiration in response to long-term deeper snow in the High Arctic of NW Greenland. *Journal of Geophysical Research: Biogeosciences*, **119**, 2013JG002494.

McGuire AD, Anderson LG, Christensen TR et al. (2009) Sensitivity of the carbon cycle in the Arctic to climate change. *Ecological Monographs*, **79**, 523–555.

McGuire AD, Christensen TR, Hayes D et al. (2012) An assessment of the carbon balance of Arctic tundra: comparisons among observations, process models, and atmospheric inversions. *Biogeosciences Discuss.*, **9**, 4543–4594.

Miller GH, Brigham-Grette J, Alley RB et al. (2010) Temperature and precipitation history of the Arctic. *Quaternary Science Reviews*, **29**, 1679–1715.

Mudryk LR, Kushner PJ, Derksen C (2014) Interpreting observed northern hemisphere snow trends with large ensembles of climate simulations. *Climate Dynamics*, **43**, 345–359.

Myers-Smith IH, Forbes BC, Wilmking M et al. (2011) Shrub expansion in tundra ecosystems: dynamics, impacts and research priorities. *Environmental Research Letters*, **6**, 045509.

Natali SM, Schuur EAG, Webb EE, Pries CEH, Crummer KG (2014) Permafrost degradation stimulates carbon loss from experimentally warmed tundra. *Ecology*, **95**, 602–608.

Nowinski NS, Taneva L, Trumbore SE, Welker JM (2010) Decomposition of old organic matter as a result of deeper active layers in a snow depth manipulation experiment. *Oecologia*, **163**, 785–792.

Osterkamp TE (2007) Characteristics of the recent warming of permafrost in Alaska. *Journal of Geophysical Research: Earth Surface*, **112**, F02S02.

Qian H, Joseph R, Zeng N (2010) Enhanced terrestrial carbon uptake in the Northern High Latitudes in the 21st century from the Coupled Carbon Cycle Climate Model Intercomparison Project model projections. *Global Change Biology*, **16**, 641–656.

Schaefer K, Zhang T, Bruhwiler L, Barrett AP (2011) Amount and timing of permafrost carbon release in response to climate warming. *Tellus B*, **63**, 165–180.

Schaefer K, Lantuit H, Romanovsky VE, Schuur EAG, Witt R (2014) The impact of the permafrost carbon feedback on global climate. *Environmental Research Letters*, **9**, 085003.

Schuur EAG, Vogel JG, Crummer KG, Lee H, Sickman JO, Osterkamp TE (2009) The effect of permafrost thaw on old carbon release and net carbon exchange from tundra. *Nature*, **459**, 556–559.

Schuur E a. G, Abbott BW, Bowden WB et al. (2013) Expert assessment of vulnerability of permafrost carbon to climate change. *Climatic Change*, **119**, 359–374.

Schuur E a. G, McGuire AD, Schädel C et al. (2015) Climate change and the permafrost carbon feedback. *Nature*, **520**, 171–179.

Serreze MC, Barry RG (2011) Processes and impacts of Arctic amplification: A research synthesis. *Global and Planetary Change*, **77**, 85–96.

Serreze MC, Walsh JE, Chapin FS et al. (2000) Observational Evidence of Recent Change in the Northern High-Latitude Environment. *Climatic Change*, **46**, 159–207.

Shiklomanov NI, Streletskiy DA, Nelson FE et al. (2010) Decadal variations of active-layer thickness in moisture-controlled landscapes, Barrow, Alaska. *Journal of Geophysical Research: Biogeosciences*, **115**, G00I04.

Sistla SA, Moore JC, Simpson RT, Gough L, Shaver GR, Schimel JP (2013) Long-term warming restructures Arctic tundra without changing net soil carbon storage. *Nature*, **497**, 615–618.

Solomon S (2007) *Climate change 2007-the physical science basis: Working group I contribution to the fourth assessment report of the IPCC*, Vol. 4. Cambridge University Press.

Streletskiy DA, Shiklomanov NI, Nelson FE (2012) Spatial variability of permafrost active-layer thickness under contemporary and projected climate in Northern Alaska. *Polar Geography*, **35**, 95–116.

Tape K, Sturm M, Racine C (2006) The evidence for shrub expansion in Northern Alaska and the Pan-Arctic. *Global Change Biology*, **12**, 686–702.

Tape KD, Hallinger M, Welker JM, Ruess RW (2012) Landscape Heterogeneity of Shrub Expansion in Arctic Alaska. *Ecosystems*, **15**, 711–724.

Tesi T, Muschitiello F, Smittenberg RH et al. (2016) Massive remobilization of permafrost carbon during post-glacial warming. *Nature Communications*, **7**.

Trucco C, Schuur EAG, Natali SM, Belshe EF, Bracho R, Vogel J (2012) Seven-year trends of CO_2 exchange in a tundra ecosystem affected by long-term permafrost thaw. *Journal of Geophysical Research: Biogeosciences*, **117**, G02031.

Vogel J, Schuur EAG, Trucco C, Lee H (2009) Response of CO_2 exchange in a tussock tundra ecosystem to permafrost thaw and thermokarst development. *Journal of Geophysical Research: Biogeosciences*, **114**, G04018.

Webb EE, Schuur EAG, Natali SM et al. (2016) Increased wintertime CO_2 loss as a result of sustained tundra warming. *Journal of Geophysical Research: Biogeosciences*, **121**, 2014JG002795.

Zhu Z, Piao S, Myneni RB et al. (2016) Greening of the Earth and its drivers. *Nature Climate Change*, **6**, 791–795.

6. BROADER IMPACTS

Findings presented herein add to a growing body of evidence suggesting the potential of projected changes in precipitation to derive in a significant radiative forcing from Arctic regions, critically affecting future climate. At present, the lack of an accurate process-based, all-encompassing assessment of Arctic C dynamics under future precipitation scenarios is a major gap in our ability to estimate climate/C-cycle feedbacks from the Arctic region. Our results emphasize the potential of Arctic tundra to become a transient C source under future precipitation scenarios contributing to reduce the overall global terrestrial C sink, but also to act as an additional long-term C sink with persistent increases in winter precipitation, as SOC may remain largely immobilized over decades under thaw-induced near-water saturated conditions. This additional C sink however, may come at the cost of a substantial positive feedback on climate, as near-surface hydrological conditions may stimulate CH_4 production and emission, further subsidized by transitions in plant community structure over the course of progressive permafrost degradation. We suspect that much of current divergence among predictive models stem from inaccurate representations of the sensitivity of both physical and biotic processes to changes in precipitation at different time-scales. If such projections are used to establish meaningful GHGs emission targets, climate targets are likely to be uncertain. Improving predictions of Arctic climate/C-cycle feedbacks will require conceptualizing and adequately parameterizing the magnitude and evolution of key processes such as permafrost dynamics, the potential of plant productivity to offset ecosystem C emissions, and the ability of Arctic tundra to act as a significant source of CH_4 under future precipitation scenarios.

VITA

NAME:	Maria Elena Blanc Betes
EDUCATION:	B.A., Biological Sciences, University of Barcelona, Barcelona, Spain, 2003
	M.S. Environmental Management and Engineering, Catalan Institute of Technology, Barcelona, Spain, 2004
	Ph.D. candidate: Ecology and Evolution, University of Illinois at Chicago, Chicago, Illinois, 2017
PROFESIONAL EXPERIENCE:	Graduate Assistant; University of Illinois at Chicago (2007–present)
	Research Technician 2; University of Illinois at Chicago (2005–2006)
	Graduate Assistant; University of Barcelona (2003–2005)
	Laboratory Manager; Mediterranean Marine and Environmental Center (2002–2004)
	Research Assistant; Mediterranean Marine and Environmental Center (2001–2002)
TEACHING:	Graduate Teaching Assistant, University of Illinois at Chicago, Department of Ecology and Evolution 2007–2016:
	BIOS 240b: Animal Physiology
	BIOS 240a: Homeostasis of Plants and Animals
	BIOS 230: Ecology and Evolution
	BIOS 222: Cell Biology
PUBLICATIONS:	Blanc-Betes E., Welker J.M., Sturchio N.C., Chanton J.P., Gonzalez-Meler M.A. (2016) Winter precipitation and snow accumulation drive the methane sink or source strength of Arctic tussock tundra. *Global Change Biology* **22**, 2818–2833.
	Gonzalez-Meler M.A., Lynch D.J., Blanc-Betes E. (2013) Hidden Challenges in Ecosystem Responses to Climate Change. *JSM Environmental Science Ecology* **1**, 1006.

Gonzalez-Meler M.A., Blanc-Betes E., Flower C.E., Ward J.K., Gomez-Casanovas N. (2009) Plastic and adaptive responses of plant respiration to changes in atmospheric CO_2 concentration. *Physiologia Plantarum* **137**, 473–484.

Gomez-Casanovas N., Blanc-Betes E., Azcon-Bieto J. and Gonzalez-Meler M.A. (2007) Changes in Respiratory Mitochondrial Machinery and Cytochrome and Alternative Pathway Activities in Response to Energy Demand Underlie the Acclimation of Respiration to Elevated CO_2 in the Invasive Opuntia ficus-indica. *Plant Physiology* **145**, 49–61.

Blanc-Betes E. (2004) Evaluation of the tree-line uprising in the Catalan Pyrenees due to Global Change and its effects using photointerpretation and GIS. MSc. Catalan Institute of Technology (UPC-EOI-ICT).

In review or in preparation

Blanc-Betes E., Welker J.M., Gomez-Casanovas N., Gonzalez-Meler M.A. *in prep*. Deeper winter snow reduces ecosystem C losses but increases the global warming potential of Arctic tussock tundra over the growing season. *Global Change Biology*.

Blanc-Betes E., Sturchio N.C., Taneva L., Welker J.M., Guilderson T.P., Poghosyan A., Gonzalez-Meler M.A. *in prep*. Winter snow drives transient modulations in Arctic tundra soil carbon budget. *Nature*.

HONORS AND AWARDS:

Graduate Research Award, 2016 ($100). Department of Biological Sciences, University of Illinois at Chicago

LAS Travel Award, 2015 ($250). Liberal Arts and Sciences, University of Illinois at Chicago

Biological Science Department Travel Award, 2015 ($600). University of Illinois at Chicago

Graduate College Presenters Award, 2015 ($200). Graduate Student Council, University of Illinois at Chicago

Graduate Student Council Award, 2015 ($250). Graduate Student Council, University of Illinois at Chicago

Graduate Student Council Award, 2012 ($250). Graduate Student Council, University of Illinois at Chicago

Graduate College Presenters Award, 2012 ($300). Graduate College, University of Illinois at Chicago

Graduate Teaching Award, 2011 ($100). Department of Biological Sciences, University of Illinois at Chicago

Graduate Student Council Award, 2010 ($250). Graduate Student Council, University of Illinois at Chicago

Graduate College Presenters Award, 2010 ($300). Graduate College, University of Illinois at Chicago

Elmer Hadley Award, 2009–2010 ($2,400). Department of Biological Sciences, University of Illinois at Chicago

Graduate Student Council Award, 2008 ($250). Graduate Student Council, University of Illinois at Chicago

Graduate College Presenters Award, 2008 ($300). Graduate College, University of Illinois at Chicago

Motorola Foundation Travel Grants, 2008 ($250). Women in Science and Engineering Program, University of Illinois at Chicago

PROFESSIONAL ACTIVITIES:

Manuscript Review

Global Change Biology

Workshop and Symposia Participation

Annual Meeting Permafrost Carbon Network, San Francisco, CA, December 2015

Annual Meeting Permafrost Carbon Network, San Francisco, CA, December 2012

Characterizing Soil Carbon in Permafrost Regions and Its Vulnerability to Climate Change Workshop, Argonne National Laboratory, Chicago Illinois, USA, February, 2011

Annual Meeting Permafrost Carbon Network, San Francisco, CA, December 2010

Annual Argonne Soils Workshop, Argonne National Laboratory, Chicago Illinois, USA, October, 2010

OUTREACH AND AFFILIATIONS:

Permafrost Carbon Network (member since 2009)

American Geophysical Union (member since 2008)

SCIENTIFIC MEETINGS:

Kropp H., Loranty M.M, Natali S. *et al*. Impacts of vegetation on the decoupling between ait and soil temperaturas across the Arctic. American Geophysical Union (AGU), San Francisco, CA, December 2016 *(poster presentation).*

Blanc-Betes E., Welker J.M., Gomez-Casanovas N., Gonzalez-Meler M.A. Deeper winter snow reduces ecosystem C losses but increases the global warming potential of Arctic tussock tundra over the growing season. American Geophysical Union (AGU), San Francisco, CA, December 2015 *(oral presentation).*

Blanc-Betes E., Thurnhoffer B.M., Gonzalez-Meler M.A., Sturchio N.C., Welker J.M. Increased winter precipitation makes Arctic tundra a methane source but gas diffusion modulates abiotic sensitivity of soil C efflux. American Geophysical Union (AGU), San Francisco, CA, December 2012 *(poster presentation).*

Blanc-Betes E., Sturchio N.C., Taneva L., Welker J.M., Guilderson T.P., Poghosyan A., Gonzalez-Meler M.A. Radioisotopes (^{137}Cs, ^{40}K, ^{210}Pb) indicate that cryoturbation processes in Alaskan tussock tundra are accelerated under deeper winter snow: results from short and long-term winter snow depth experiments. American Geophysical Union (AGU), San Francisco, CA, December 2010 *(poster presentation).*

Blanc-Betes E., Gomez-Casanovas N., Ward JK., Gonzalez-Meler MA. Responses of Plant Respiration to Pleistocene Changes in Atmospheric CO_2 Concentrations. American Geophysical Union (AGU), San Francisco, CA, December 2008 *(poster presentation).*

APPENDIX A: COPYRIGHT CLEARANCE STATEMENT FROM JOHN WILEY AND SONS

JOHN WILEY AND SONS LICENSE TERMS AND CONDITIONS

Feb 15, 2017

This Agreement between Elena Blanc ("You") and John Wiley and Sons ("John Wiley and Sons") consists of your license details and the terms and conditions provided by John Wiley and Sons and Copyright Clearance Center.

License Number	4041591028484
License date	
Licensed Content Publisher	John Wiley and Sons
Licensed Content Publication	Global Change Biology
Licensed Content Title	Winter precipitation and snow accumulation drive the methane sink or source strength of Arctic tussock tundra
Licensed Content Author	Elena Blanc-Betes,Jeffrey M. Welker,Neil C. Sturchio,Jeffrey P. Chanton,Miquel A. Gonzalez-Meler
Licensed Content Date	May 9, 2016
Licensed Content Pages	16
Type of use	Dissertation/Thesis
Requestor type	Author of this Wiley article
Format	Print and electronic
Portion	Full article
Will you be translating?	No
Title of your thesis / dissertation	Impacts of Changes in Winter Precipitation on C Stocks and Fluxes in Arctic Tussock Tundra
Expected completion date	Feb 2017
Expected size (number of pages)	196
Requestor Location	Elena Blanc-Betes 845 West Taylor St SES Bldg, Room 3342 CHICAGO, IL 60607 United States Attn: Elena Blanc-Betes
Publisher Tax ID	EU826007151
Billing Type	Invoice
Billing Address	Elena Blanc-Betes 845 West Taylor St SES Bldg, Room 3342 CHICAGO, IL 60607 United States Attn: Elena Blanc-Betes
Total	0.00 USD

TERMS AND CONDITIONS

and the right to reproduce the Wiley Materials pursuant to Section 2 herein during the continuance of this Agreement. You agree that you own no right, title or interest in or to the Wiley Materials or any of the intellectual property rights therein. You shall have no rights hereunder other than the license as provided for above in Section 2. No right, license or interest to any trademark, trade name, service mark or other branding ("Marks") of WILEY or its licensors is granted hereunder, and you agree that you shall not assert any such right, license or interest with respect thereto

- NEITHER WILEY NOR ITS LICENSORS MAKES ANY WARRANTY OR REPRESENTATION OF ANY KIND TO YOU OR ANY THIRD PARTY, EXPRESS, IMPLIED OR STATUTORY, WITH RESPECT TO THE MATERIALS OR THE ACCURACY OF ANY INFORMATION CONTAINED IN THE MATERIALS, INCLUDING, WITHOUT LIMITATION, ANY IMPLIED WARRANTY OF MERCHANTABILITY, ACCURACY, SATISFACTORY QUALITY, FITNESS FOR A PARTICULAR PURPOSE, USABILITY, INTEGRATION OR NON-INFRINGEMENT AND ALL SUCH WARRANTIES ARE HEREBY EXCLUDED BY WILEY AND ITS LICENSORS AND WAIVED BY YOU.

- WILEY shall have the right to terminate this Agreement immediately upon breach of this Agreement by you.

- You shall indemnify, defend and hold harmless WILEY, its Licensors and their respective directors, officers, agents and employees, from and against any actual or threatened claims, demands, causes of action or proceedings arising from any breach of this Agreement by you.

- IN NO EVENT SHALL WILEY OR ITS LICENSORS BE LIABLE TO YOU OR ANY OTHER PARTY OR ANY OTHER PERSON OR ENTITY FOR ANY SPECIAL, CONSEQUENTIAL, INCIDENTAL, INDIRECT, EXEMPLARY OR PUNITIVE DAMAGES, HOWEVER CAUSED, ARISING OUT OF OR IN CONNECTION WITH THE DOWNLOADING, PROVISIONING, VIEWING OR USE OF THE MATERIALS REGARDLESS OF THE FORM OF ACTION, WHETHER FOR BREACH OF CONTRACT, BREACH OF WARRANTY, TORT, NEGLIGENCE, INFRINGEMENT OR OTHERWISE (INCLUDING, WITHOUT LIMITATION, DAMAGES BASED ON LOSS OF PROFITS, DATA, FILES, USE, BUSINESS OPPORTUNITY OR CLAIMS OF THIRD PARTIES), AND WHETHER OR NOT THE PARTY HAS BEEN ADVISED OF THE POSSIBILITY OF SUCH DAMAGES. THIS LIMITATION SHALL APPLY NOTWITHSTANDING ANY FAILURE OF ESSENTIAL PURPOSE OF ANY LIMITED REMEDY PROVIDED HEREIN.

- Should any provision of this Agreement be held by a court of competent jurisdiction to be illegal, invalid, or unenforceable, that provision shall be deemed amended to achieve as nearly as possible the same economic effect as the original provision, and the legality, validity and enforceability of the remaining provisions of this Agreement shall not be affected or impaired thereby.

- The failure of either party to enforce any term or condition of this Agreement shall not constitute a waiver of either party's right to enforce each and every term and condition of this Agreement. No breach under this agreement shall be deemed waived or

excused by either party unless such waiver or consent is in writing signed by the party granting such waiver or consent. The waiver by or consent of a party to a breach of any provision of this Agreement shall not operate or be construed as a waiver of or consent to any other or subsequent breach by such other party.

- This Agreement may not be assigned (including by operation of law or otherwise) by you without WILEY's prior written consent.

- Any fee required for this permission shall be non-refundable after thirty (30) days from receipt by the CCC.

- These terms and conditions together with CCC's Billing and Payment terms and conditions (which are incorporated herein) form the entire agreement between you and WILEY concerning this licensing transaction and (in the absence of fraud) supersedes all prior agreements and representations of the parties, oral or written. This Agreement may not be amended except in writing signed by both parties. This Agreement shall be binding upon and inure to the benefit of the parties' successors, legal representatives, and authorized assigns.

- In the event of any conflict between your obligations established by these terms and conditions and those established by CCC's Billing and Payment terms and conditions, these terms and conditions shall prevail.

- WILEY expressly reserves all rights not specifically granted in the combination of (i) the license details provided by you and accepted in the course of this licensing transaction, (ii) these terms and conditions and (iii) CCC's Billing and Payment terms and conditions.

- This Agreement will be void if the Type of Use, Format, Circulation, or Requestor Type was misrepresented during the licensing process.

- This Agreement shall be governed by and construed in accordance with the laws of the State of New York, USA, without regards to such state's conflict of law rules. Any legal action, suit or proceeding arising out of or relating to these Terms and Conditions or the breach thereof shall be instituted in a court of competent jurisdiction in New York County in the State of New York in the United States of America and each party hereby consents and submits to the personal jurisdiction of such court, waives any objection to venue in such court and consents to service of process by registered or certified mail, return receipt requested, at the last known address of such party.

WILEY OPEN ACCESS TERMS AND CONDITIONS

Wiley Publishes Open Access Articles in fully Open Access Journals and in Subscription journals offering Online Open. Although most of the fully Open Access journals publish open access articles under the terms of the Creative Commons Attribution (CC BY) License only, the subscription journals and a few of the Open Access Journals offer a choice of Creative Commons Licenses. The license type is clearly identified on the article.

The Creative Commons Attribution License

The Creative Commons Attribution License (CC-BY) allows users to copy, distribute and transmit an article, adapt the article and make commercial use of the article. The CC-BY license permits commercial and non-

Creative Commons Attribution Non-Commercial License